THE ROLE OF OXIDATION IN THE PROTECTION OF SLIDING METAL SURFACES

by

JOHN LAWRENCE SULLIVAN

B.SC., C.ENG., C.PHY., MIEE, F.Inst.P

A thesis submitted for the degree of

DOCTOR OF PHILOSOPHY

THE UNIVERSITY OF ASTON

SEPTEMBER 1986

THE UNIVERSITY OF ASTON IN BIRMINGHAM

THE UNIVERSITY OF ASTON IN BIRMINGHAM

THE ROLE OF OXIDATION IN THE PROTECTION OF SLIDING METAL SURFACES

by
JOHN LAWRENCE SULLIVAN

A thesis submitted for the degree of:

DOCTOR OF PHILOSOPHY - 1986

SUMMARY

This study is concerned with the mechanisms of growth and wear of protective oxide films formed under various tribological conditions. In the study three different tribological systems are examined in each of which oxidational wear is the dominant equilibrium mode. These are an unlubricated steel on steel system sliding at low and elevated temperatures, a boundary lubricated aluminium bronze on steel system and an unlubricated reciprocating sliding 9% Cr steel system operated at elevated temperature, in an atmosphere of carbon dioxide.

The results of mechanical measurements of wear and friction are presented for a range of conditions of load, speed and temperature for the systems, together with the results of extensive examinations of the surfaces and sub-surfaces by various physical methods of analysis. The major part of the thesis, however, is devoted to the development and application of surface models and theoretical quantative expressions in order to explain the observed oxidational wear phenomena.

In this work, the mechanisms of formation of load bearing oxide plateaux are described and are found to be dependent on system geometry and environment. The relative importance of "in contact" and "out of contact" oxidation is identified together with growth rate constants appropriate to the two situations. Hypotheses are presented to explain the mechanisms of removal of plateaux to form wear debris. The latter hypotheses include the effects of cyclic stressing and dislocation accumulation, together with effects associated with the kinetics of growth and physical properties of the various oxides.

The proposed surface models have led to the development of quantitative expressions for contact temperature, unlubricated wear rates, boundary lubricated wear rates and the wear of material during the transition from severe to mild wear. In general theoretical predictions from these expressions are in very good agreement with experimental values.

Wear/Oxidation/Boundary Lubrication/Steels/Aluminium Bronze.

ACKNOWLEDGEMENTS

I would like to thank my many research students both past and present for providing me with a stimulus to sustain my ever growing interest in research. In this connection I particularly wish to acknowledge Sukder Athwal, Li Fah Wong and Nicholas Granville with whom I collaborated in the experimental work detailed in Chapters 2, Section 2.2; 3, Section 3.2 and 4, Section 4.2 respectively whilst these students were under my direction and supervision.

I would further like to thank our excellent technical staff, Andrew Abbot, Howard Arrowsmith and Dick Blunt for their invaluable assistance and Hazel Wright for her typing of this thesis and for all her other secretarial assistance so readily given.

I would finally like to thank Sayah Saied for coffee,sympathy and help during a difficult period.

CONTENTS PAGE

SUMMARY 1

ACKNOWLEDGEMENTS 2

CONTENTS 3

LIST OF FIGURES 7

LIST OF TABLES 19

CHAPTER 1 : INTRODUCTION 22

1.1. Classification of wear modes 22

1.2. The role of oxides in surface protection -an historical perspective 24

1.3. Severe to mild wear transitions 25

1.4. Importance of temperature in oxidational wear 30

1.5. Mechanisms of growth of tribological oxide films 34

1.6. Quantitative theories of oxidational wear 38

1.7. Oxidational wear and boundary lubrication 46

1.8. Oxidational growth rate laws and their relevance to tribological growth. 51

1.9. Formation and breakdown of compact oxide films. 57

1.10. Oxidation of iron and low alloy steels 60

1.11. Oxidation of copper 62

1.12. Research programme. 63

CHAPTER 2 : THE UNIDIRECTIONAL WEAR OF STEEL AT LOW AND ELEVATED TEMPERATURE IN AIR. 65

2.1. Experimental apparatus and procedures 65

2.2. Experimental results 73

2.2.1. Wear and friction 73

2.2.2. X-ray diffraction analysis 78

2.2.3. Scanning electron microscopy 85

2.2.4. Auger and X-ray photoelectron spectroscopy 93

2.2.5. Heat flow analysis. 103

2.3. Theoretical determination of surface parameters 103

2.4. Oxidational wear at elevated temperatures 121

2.5. Discussion. 135

CHAPTER 3 : OXIDATIONAL WEAR AND BOUNDARY LUBRICATION 152

3.1. Experimental apparatus and procedures 154

3.2. Experimental results 160

3.2.1. Wear 160

3.2.2. X-ray diffraction analysis of debris 162

3.2.3. Auger electron spectroscopy 163

3.2.4. Electron probe microanalysis and scanning electron microscopy 173

3.2.5. Contact temperature measurements 180

3.3. Boundary lubrication and oxidational wear - a surface model 182

3.4. Discussion. 189

CHAPTER 4 : RECIPROCATING WEAR OF STEEL IN CO_2 AT HIGH TEMPERATURE 206

4.1. Experimental apparatus and procedures 207

4.2. Experimental results 213

4.2.1. Wear and wear transitions 213

4.2.2. Static oxidational "dwell tests" 223

4.2.3. Microhardness measurements 225

4.2.4. X-ray diffraction analysis 227

4.2.5. Scanning electron microscopy and Auger electron spectroscopy 231

4.3. Transition from severe to mild wear - a surface model 238

4.4. Discussion. 250

CHAPTER 5 : CONCLUDING DISCUSSION - COMPARISON OF SLIDING SYSTEMS 261

CHAPTER 6 : CONCLUSIONS 271

6.1. Unidirectional sliding 271

6.2. Boundary lubricated sliding 274

6.3. Reciprocating sliding 276

6.4. General conclusions 279

6.5. Further work. 280

REFERENCES 283

PUBLICATIONS 298

LIST OF FIGURES PAGE

2.1. Detail of elevated temperature wear rig showing the loading arm with horizontal steel pin against vertical steel disc. The heater element is clamped to the rear of the disc. The slip rings on the front (pin) side of the disc are for thermocouples and those at the rear feed the heater. 66

2.2. Bulk hardness versus surface temperature curves for 52100 and BS EN8 steels. 70

2.3. Wear rate versus load curves for 52100 steel on 52100 steel at various disc temperatures. (a) Unheated disc ●, (b) 200^{0}C x, (c) 300^{0}C o and (d) 500^{0}C Δ. 74

2.4. Wear rate versus load curves for BS EN8 steel on BS EN8 steel. 76

2.5. Wear rate versus load curves for BS EN8 steel on 9% Cr steel. 77

2.6. Coefficient of friction versus load for 52100 on 52100 steel experiments at room temperature. 79

2.7. Variation of coefficient of friction with temperature for 52100 experiments. 80

2.8. Scanning electron micrographs of surfaces generated from 52100 on 52100 steel experiments with no external heating at loads of, (a) 9.8N, (b) 39N and (c) 98N. 86

2.9. Scanning electron micrographs of surfaces generated from BS EN8 on BS EN8 experiments at loads of (a) 9.8N, (b) 24.5N and (c) 59N. 88

2.10. Scanning electron micrograph of a 52100 steel pin surface worn at a load of 59N and at 400^0C. 89

2.11. Scanning electron micrographs of typical oxide plateaux edges from 52100 on 52100 experiments conducted at, (a) 39N load, room temperature, (b) 20N load, 400^0C and (c) 49N load and 300^0C. 90

2.12. Scanning electron micrographs of typical oxide plateaux edges from BS EN8 on BS EN8 experiments conducted at, (a) 9.8N load, (b) 20N load and (c) 39N load. 91

2.13. (a) Auger electron oxygen map of plateaux formed on a 52100 steel pin surface worn at 39N load and at room temperature.
(b) Corresponding secondary electron image. 94

2.14. Oxygen concentration versus depth profiles for 52100 steel surfaces generated at (a) 15N load, room temperature, o, (b) 59N load, room temperature, x and (c) 39N load and 400^{0}C ●. 96

2.15. Oxygen concentration versus depth profiles for BS EN8 pins from BS EN8 on BS EN8 experiments at loads of (a) 4.9N,o, (b) 29N, ● and (c) 49N,x. 97

2.16. Oxygen concentration versus depth profiles for BS EN8 discs from BS EN8 on BS EN8 experiments at loads of (a) 4.9N,o, (b) 29N, ● and (c) 49N,x. 98

2.17. Oxygen and chromium concentration versus depth profiles for worn surfaces from BS EN8 on 9% Cr steel experiments generated at a load of 9.8N. (a) BS EN8 pin surface, (b) 9% Cr steel disc surface. 99

2.18. Oxygen and chromium concentration versus depth profiles for worn surfaces from BS EN8 on 9% Cr steel experiments generated at a load of 19.6N. (a) BS EN8 pin surface, (b) 9% Cr steel disc surface. 100

2.19. Oxygen and chromium concentration versus depth profiles for worn surfaces from BS EN8 on 9% Cr steel experiments generated at a load of 39N. (a) BS EN8 pin surface, (b) 9% Cr steel disc surface. 101

2.20 Oxygen and chromium concentration versus depth profiles for worn surfaces from BS EN8 on 9% Cr steel experiments, generated at a load of 49N. (a) BS EN8 pin, (b) 9% Cr steel disc. 102

2.21. Calculated number of asperity contacts versus load for 52100 on 52100 experiments conducted without external heating. 112

2.22. Calculated mean contact radius versus load for 52100 on 52100 experiments conducted without external heating. 113

2.23. Calculated oxide film thickness versus load for 52100 on 52100 experiments at various disc temperatures, (a) no external heating, (b) 200^0C, (c) 500^0C. (Calculated points are represented by X; SEM measured points are represented by ●). 114

2.24 Asperity contact temperature (T_c) and general surface temperature (T_s) versus load for 52100 on 52100 experiments at various disc temperatures, (a) no external heating, (b) 200^0C, (c) 500^0C. 115

2.25 Calculated number of asperity contacts versus load for BS EN8 on BS EN8 experiments. 117

2.26. Calculated mean contact radius versus load for BS EN8 on BS EN8 experiments. 118

2.27 Calculated oxide film thickness versus load for BS EN8 on BS EN8 experiments. Calculated points are represented by x; SEM measured points are represented by ● 119

2.28 Asperity contact temperature (T_c) and general surface temperature (T_s) versus load for BS EN8 on BS EN8 experiments. 120

2.29. Wear rate versus disc temperature for 52100 on 52100 experiments conducted at a constant load of 39N. 147

3.1. Detail of pin on disc wear test rig. 155

3.2. Wear rate of aluminium bronze versus load : (a) 0.6 and $2ms^{-1}$, pure kerosene, (b) $4ms^{-1}$, pure kerosene, (c) 0.6, 2 and $4ms^{-1}$, kerosene with additive; □ $0.6ms^{-1}$, Δ $2ms^{-1}$, o $4ms^{-1}$ - pure kerosene; ■ $0.6ms^{-1}$, ▲ $2ms^{-1}$, ● $4ms^{-1}$ - kerosene with additive. 161

3.3. Auger electron spectra from an aluminium bronze pin worn under a load of 74N and speed of $0.6ms^{-1}$ in pure kerosene, before and after a period of 80 minutes of argon ion etching. 164

3.4. Auger electron spectra from an aluminium bronze pin worn under a load of 74N and speed of $0.6ms^{-1}$ in kerosene with additive, before and after a period of 80 minutes of argon ion etching. 165

3.5. Carbon differentiated Auger peak shapes from aluminium bronze surfaces, (a) worn in the presence of pure kerosene, (b) worn in kerosene with additive. 167

3.6. Oxygen and carbon concentration versus depth profiles for an aluminium bronze pin surface worn under a load of 74N at a speed of $0.6ms^{-1}$. 169

3.7. Oxygen and carbon concentration versus depth profiles for an aluminium bronze pin surface worn under a load of 74N at a speed of $2ms^{-1}$. 170

3.8. Oxygen and carbon concentration versus depth profiles for an aluminium bronze pin worn under a load of 98N at a speed of $4ms^{-1}$. 171

3.9. Mean aluminium concentration versus load for aluminium bronze pins worn at speeds of (a) $0.6ms^{-1}$, (b) $2ms^{-1}$, (c) $4ms^{-1}$. 174

3.10. Photomicrographs of a taper section of a worn pin surface; (a) secondary electron image, (b) copper X-ray distribution, (c) aluminium X-ray distribution. 176

3.11. Photomicrographs of a wear track on the steel surface; (a) secondary electron image, (b) copper X-ray distribution, (c) aluminium X-ray distribution, (d) iron X-ray distribution. 177-178

3.12. Typical scanning electron micrograph of surface of an aluminium bronze pin worn under mild conditions. 179

3.13. Scanning electron micrograph typical of aluminium bronze surfaces worn under severe conditions with no additive present in the kerosene. 179

3.14. Oscilloscope trace of output from differential thermocouple amplifier for one revolution of the disc. 181

3.15. Process of growth of a protective oxide film under conditions of boundary lubrication, where T_s is the general surface temperature, T_d the molecular desorption temperature and T_o the oxidational temperature. 184

3.16. Calculated asperity contact temperatures versus load for experiments conducted with kerosene plus additive at speeds of; (a) $0.6ms^{-1}$, (b) $2ms^{-1}$, (c) $4ms^{-1}$. 205

4.1. Schematic diagram of the reciprocating wear test machine. 208

4.2. Detail of pin and flat specimen location. 209

4.3. Coefficient of friction versus sliding distance for experiments conducted at a mean sliding speed of 36mm.s^{-1}, load of 22N and temperature 290^{0}C. 215

4.4. Distance of sliding to the transition D_T, versus ambient temperature for experiments conducted at a mean sliding speed of 36m.s^{-1} and load of 22N. 217

4.5. Distance of sliding to the transition, D_T, versus mean sliding speed at different ambient temperatures. 218

4.6. Volume removed versus time of sliding for experiments conducted at a mean sliding speed of 36mm s^{-1} and load of 22N at an ambient temperature of 290^{0}C. 221

4.7. Microhardness versus depth into the surface of a worn flat specimen from an experiment conducted at a mean sliding speed of 36mms^{-1}, load of 22N and at an ambient temperature of 290^{0}C. The test duration was 15000 s (540m). 226

4.8. Scanning electron micrograph of typical severe wear surface. 233

4.9. Scanning electron micrograph of surfaces after the establishment of mild wear conditions in this case for an experiment run at $120mms^{-1}$, 22N load and at an ambient temperature of 300^0C.
(a) oxide plateau
(b) detail of the edge of a crack visible in the plateau. 233

4.10 Scanning electron micrographs of plateaux edges; (a) sliding speed $120mms^{-1}$, load 41N and temperature 300^0C;
(b) sliding speed $36mms^{-1}$, load 22N temperature 300^0C. 234

4.11. Scanning electron micrographs of oxide debris; (a) surface debris,
(b) agglomerate debris particle. 235

4.12. Oxygen, iron and chromium concentration versus depth profiles for a flat specimen from an experiment conducted at a mean speed of $36mms^{-1}$, load 22N and temperature 300^0C. 237

4.13. Calculated pre-transition weight loss versus mean sliding speed for an ambient temperature of $450^{0}C$ and load 22N; x theoretical points, o experimentally measured values. 249

LIST OF TABLES

		PAGE
2.1	Powder X-ray diffraction observations of debris for 52100 steel, load 19.6N speed $2ms^{-1}$, no external heating.	82
2.2.	Oxides identified in the debris and on worn surfaces from 52100 steel on 52100 steel experiments.	83
2.3.	Oxides identified in the debris and on worn surfaces from BS EN8 steel on BS EN8, steel experiments.	84
2.4.	Oxides identified in the debris and on worn surfaces from 9% Cr steel on BS EN8 steel experiments.	84
2.5.	Oxide film thickness measurements on pin surfaces (with standard deviations shown in brackets)	92
2.6.	Heat flow data at a disc temperature of 500^0c.	107

2.7. Calculated values of Arrhenius constants from data taken from room temperature experiments. 131

2.8. Calculated and measured wear rates for experiments on 52100 steel at a disc temperature of 500^0C. 133

3.1. Surface concentrations of O, C and Cu_2O for experiments in kerosene and kerosene plus additive. 172

4.1. Results of dwell tests conducted to investigate the effects of static oxidation. 224

4.2. Powder X-ray diffraction observations of debris from the pre-transition region of an experiment conducted on 9% Cr steel at a speed of $36mms^{-1}$, load of 22N and temperature 290^0C. 228

4.3. Powder X-ray diffraction observations of debris from the post-transition region of an experiment conducted on 9% Cr steel at a speed of $36mms^{-1}$, load of 22N and temperature of 290^0C. 229

4.4. Glancing angle X-ray observations of a 9% Cr pin surface taken from an experiment conducted at a speed of $36 mms^{-1}$, load of 22N and temperature of $290^{0}C$. 230

CHAPTER 1

INTRODUCTION

Metals are the most commonly used engineering materials and it is therefore not surprising that the wear of these materials has been the subject of extensive study during the past five or six decades. What is surprising is that there has not been substantially more effort in this field in view of the enormous cost and resource savings possible if wear in all forms could be substantially reduced.

1.1 Classification of Wear Modes

Archard and Hirst[1] classified wear into two broad types, "severe" and "mild". Severe wear is characterised by large metallic debris, rough surfaces and low surface electrical contact resistance and mild wear by small oxide or oxidized debris, smooth surfaces and high contact resistance. This classification can lead to some confussion, for example in extreme pressure lubrication above the initial seizure load, debris consists almost

entirely of oxides plus sulphides, chlorides or phosphides (depending on the additive employed) and in general contact resistance is high, this is therefore "mild" wear, but wear rates are very high. Conversely wear rates some one or two orders of magnitude lower than those recorded for oxidational wear under similar conditions of load and speed have been observed[2] for the wear of low alloy steels in pure argon where according to the above classification we have "severe wear". Thus the categories are not necessarily an indication of the relative magnitude of attrition rates. Perhaps it is worth qualifying these broad wear types by reference to the mechanisms proposed by Burwell and Strang[3] and Burwell[4] of adhesive, abras ive, corrosive and fatigue wear, although again one must be careful not to attribute any of these mechanisms exclusively to either mild or severe wear as some workers have in the past. Other classifications, for example, due to Kragelskii[5], Bowen and Westcott[6], Tabor[7] or Peterson[8] may also be useful in characterising wear in any given set of circumstances. With regard to the classifications, this work is concerned with mild oxidational wear, where adhesion, abrasion, corrosion and fatigue all play some part and where the load range is such that deformation may be regarded as mainly plastic. The majority of the work described is concerned with steel, although other materials are included specifically in those sections dealing with lubricated wear.

1.2 The Role of Oxides in Surface Protection - an Historical Perspective

Fink[9] in 1930, published the first paper in which the importance of oxidation in the reduction of wear and friction in sliding metal surfaces was recognised. Following this Rosenberg and Jordan[10] showed that steel exhibited a wear rate in hydrogen which was 50 times that in air. They were the first to analyse wear debris using X-ray diffraction and found only Fe in the debris from experiments conducted in hydrogen, whilst in air the debris consisted mainly of the oxides α - Fe_2O_3 and Fe_3O_4. Thum and Wunderlich[11] identified α - Fe_2O_3 in debris from their small amplitude reciprocating experiments and described the process of surface oxide formation as "frictional oxidation". Mailander and Dies[12], Dies[13] and Siebel and Kobitzsch[14] similarly demonstrated the importance of oxidation and oxide film formation in experiments for a number of sliding conditions ranging from unidirectional dry sliding to reciprocating sliding in the presence of a lubricant. Dies[13] in his work also recognised the importance of dissolved oxygen in fluids. A point which will be discussed later.

Further observations of the ability of oxide films to reduce metallic contact and hence modify friction and wear were reported by Whitehead[15] sliding copper on copper and copper on steel at very low loads, Wilson[16, 17] who

confirmed the role of oxide films in preventing metallic contact by a series of contact resitance measurements and Cocks[18] who studied penetration of oxide films under static and dynamic (shearing) conditions. Cocks[19, 20] further went on to show that oxide generated due to frictional heating gave considerable protection against surface damage.

1.3 Severe to Mild Wear Transition

The beneficial effects of surface oxidation in sliding conditions were thus documented, but if the mechanisms which promote and maintain mild oxidational wear are to be understood, then the essential differences between mild and severe wear and the factors affecting the transition between these wear modes must first be established.

Archard[21] and Archard and Hirst[1] published the first work in which mild and severe wear were defined in terms of observable characteristics. In studies involving a wide range of material combinations under unlubricated conditions they found that after an initial severe wear running in stage, surfaces achieved a degree of conformity when wear rates tended to a constant value and were independent of the apparent area. In an explanation of the results the authors drew on the earlier work of Holm[22] and Bowden and Tabor[23]. Factors affecting observed transitions from severe to mild wear were studied by Hirst

and Lancaster[24] who in agreement with the observations of Moore and Tegart[25] showed that the early stages of rubbing not only produce topographical changes, but also morphological changes and that wear rate after prolonged rubbing depends on the properties of the transformed surface layer rather than the original or bulk material.

Kerridge[26] and Archard and Hirst[27] used a combination of radioactive tracer techniques and conventional methods of wear measurement to follow the history of the wear process. Kerridge's studies of soft against hard steels, showed that the initial wear mode was severe and associated with material transfer from the harder to the softer surface. The transfer fragments built up an agglomerate film of critical thickness before becoming detached to form wear particles. All the metallic debris produced during the initial stages of sliding was formed in this way. Subsequent stages of wear consisted of transformation hardening of the soft steel surface and oxidation of the metallic transfer layer to form a hard protective film. In this stage of wear, debris again originated from the now oxidized layer to be replaced by further tranferred material. The process was found to be cyclic on a local scale. In contrast to this for hard steel on hard steel[27] little transfer occurred and it was proposed that surfaces wore by oxidation and subsequent abrasive removal of the oxide film.

Rabinowicz and Tabor[28] in earlier work using similar radioactive tracer techniques also noted the importance of transfer in some sliding situations and concluded that the process of transfer is due to discrete particles. Rabinowicz[29] extended the radiographic method to estimate the size distribution of such particles and found them to be comparable to the real contact area predictions of Holm[22] and Bowden and Tabor[23] made from contact resistance measurements. The models of Green[30] and Greenwood and Tabor[31] also predicted transfer. In the light of current knowledge it might be suggested that there was over-enthusiatic application of the simple Bowden and Tabor[23] adhesive junction model in some of this work, but this does not detract from the importance of transfer in some wear situations.

Mild and severe wear modes, transfer and oxidation processes are not confined to steel on steel systems. Kerridge and Lancaster[32], Lancaster[33, 34] and Hirst and Lancaster[35] described a series of experiments in which 60/40 leaded brass was slid against tool steel where many aspects of mild wear, severe wear and mild/severe transitions were studied as functions of parameters such as load, speed and ambient temperature. The results were found to be similar in many respects to the earlier studies on the wear of steels, particularly those experiments in which soft steels were slid against hard counterfaces.

Perhaps the most definitive work in separating modes of dry wear of steel is that of Welsh[36, 37, 38]. Welsh produced a series of curves, the general pattern of which now bears his name. The curves show that large changes in wear rate can result from small changes in applied load and sliding speed. These curves are similar in many aspects to those developed by Lancaster[34] for 60/40 leaded brass on tool steel. From Welsh's curves three transision loads, T_1, T_2 and T_3 were defined. Below T_1 and above T_2 the equilbrium wear mode is oxidational mild wear. Above T_3 a further different mild wear mechanism predominates. The severe wear between T_1 and T_2 can be eliminated or supressed by hardening of the surfaces or the extent of the region altered by changing the sliding speed or the partial pressure of oxygen in the atmosphere. Transitions were explained in terms of subsurface transformations. Below the load T_1 work hardening of the surface due to plastic deformation supports a stable oxide film. In the region between $T_1$and T_2 further plastic deformation causes the oxide to break up and the temperature is not high enough to maintain the growth necessary to sustain the oxide film. Above T_2 surface temperatures are high enough to produce martensitic phase transformation and hence a hard surface region capable of supporting the oxide film. Archard and Rowntree[39] in an analysis of the frictional heating conditions between T_2 and T_3 have since concluded that many cycles of rubbing would be required to produce such transformation hardening and this could lead to either the cyclic behaviour observed in some investigations, or to very

long running in times. Although detailed studies were not undertaken above the T_3 transition Welsh stated that surface temperatures in that region are sufficient to produce rapid transformation hardening.

A further important result of this work was the establishment of two critical hardness ranges. The first being the minimum value required to support an oxide film, which lies between 340 and 425 HV and the second, a value between 550 and 775 HV, where no oxide film is necessary to produce wear rates comparable to those observed for mild oxidational wear. The work of Sullivan and Choudhury[2] confirms this latter point and Dearnley[40] has shown that for very hard surfaces such as those produced by ion implantation oxidation far from being beneficial can produce higher wear rates than if the process had been supressed.

Welsh's work on the formation of hardened surface layers prior to the establishment of mild wear conditions has been confirmed by many workers[41, 42, 43, 44, 45], in fact such layers were first reported by Trent[46] who in 1941 observed them of steel ropes subject to repeated sliding Perhaps the fact that plastic deformation and frictional heating produced during sliding contact gives rise to such layers (both Archard[47] and Quinn [48] confirmed that temperatures at the asperities were sufficient to cause the steel to change structure and harden) may mislead workers into believing that they are a necessary pre-requisite for oxidational wear. Athwal [49]

in an investigation of the mild wear of steels at elevated temperatures has shown that thick oxide films can be formed and oxidational wear maintained without a hard supportive layer if the surface temperature is high enough. It must be recognized, however, that if the mechanical properties of oxide and surface metallic layers are well matched the oxide film will be more stable.

1.4. Importance of Temperature in Oxidational Wear

It is now widely accepted that there is some form of surface modification prior to the establishment of mild oxidational wear and that temperature is of prime importance both in the initial and equilibrium stages. There is still, however, controversy over whether it is the general surface temperature or "hot-spot" or contact temperatures which govern oxide growth. Quinn[48] considered a number of experiments[27,50,51,52,53,54] in which oxidational wear debris from sliding steel systems had been analysed and attempted to correlate the results with calculated values of hot-spot temperatures determined from the curves published by Archard[47]. He concluded that the constituents of the debris were consistent with being formed at the contact rather than surface temperature. The contrary view was expressed by Clark, Pritchard and Midgely[55] and is implicit in the arguments of Lancaster[33], Razarizadeh and Eyre[56] and Sexton[57].

Opinion remains divided. Archard[58] carried out calculations using typical values of surface and contact temperatures and found that most oxidation should take place at the contact temperature. In many experiments on the mild wear of steels at low ambient temperatures a great deal of data has been collected which shows that oxidation must have taken place at temperatures well above the general surface temperature. Some of this work will be discussed later, but an example is a study reported by Sullivan, Quinn and Rowson[59] on the mild wear of low alloy steels. In this investigation FeO was found as a major constituent in the debris from experiments where surface temperatures were no greater than 100^0C. It is known that for normal atmospheric conditions FeO is only produced at temperatures greater than 570^0C, hence the oxide could not have been the result of growth at the general surface temperature. Calculations based on heat flow measurements in the experiments indicated that contact temperatures were in excess of 600^0C.

The view that contact rather than surface temperature is the most important factor determining oxide growth is supported by Tao [60] and Molgaard and Srivastava [61], although in other published work Molgaard[62] suggested that the oxidational temperature may be somewhat lower than the contact temperature even for oxidation nominally at the contact region. This latter suggestion is possibly closer to the truth, since during contact there is no free access

of oxygen to the interface. Thus oxidation under these conditions probably takes places immediately following contact at temperatures intermediate between contact and surface. Models assuming some constant oxidation temperature must, therefore, contain approximations. True oxidation kinetics for transient temperature changes of this nature would be very difficult to determine.

Whilst it is clear from the above discussion that contact temperature (or something close to this) is the major factor in low ambient temperature experiments where relatively high loads and high speeds are employed, if the ambient temperature is increased Sullivan and Athwal[63] and Sullivan and Granville[64] have shown that out of contact oxidation at the surface temperature can become the dominant mechanism. Stott, Glascott and Wood[65] produced a quantitative expression for the relative amounts of oxide generated in and out of contact and concluded that either mode could predominate. They stated that if excess contact temperature rises are significant, particularly where the number of load bearing contacts is small, the majority of the oxide is formed at the contact. Conversely if there are a large number of contacts, particularly under low speed, high temperature conditions and the excess contact temperature rise is small, then out of contact oxidation predominates.

There are two problems associated with assigning the correct oxidational temperatures to a given set of sliding

conditions and these lead to much of the confusion in current literature. The first is the lack of understanding of the kinetics of oxidation under tribological conditions. There are some workers who still uncritically employ statically derived oxidational constants to interpret tribological data. This will be addressed later in this work.

The second problem is the difficulty in obtaining reliable experimental values of contact temperatures. Attempts have been made to determine these temperatures directly using dynamic thermocouple techniques by measuring the thermoelectric voltage produced at the sliding interface of a pair of dissimilar metals. Bowden and Ridler[66], Furey[67], Glascott, Stott and Wood[68] and Sullivan and Poole[69] have all used this technique to varying degrees of sophistication. Other direct measurements using infra-red photographic methods have been employed by Meinders, Wilcock and Winer[70] and Winer and Quinn[71]. These direct methods suffer from the disadvantage that either dissimilar metals must be used or one of the sliding partners must be transparent, thus while providing useful information they are by no means universally applicable.

Less direct methods were employed by Earles and Powel[72], Earles, Hayler and Powell[73] and Powell and Earles[74] who calculated contact temperatures from a knowledge of sub-surface temperature rises measured by imbedded thermocouples. A further indirect method is

described by Rowson and Quinn[75]. This method made use of a calorimeter to hold the pin in a pin on disc wear test rig. Heat flow into the pin was thus measured and surface skin temperatures calculated. A model was developed based on the theoretical analyses of Blok[76], Jaeger[77] and Archard[47] following an approach originally employed by Grosberg and Molgaard[78] and refined by Quinn[79]. Equations were thus constructed giving contact temperatures as a function of other surface parameters such as oxide film thickness, number and size of contacts plus a number of other measureable physical properties of the surface. Parameters were determined using an iterative computer search technique and temperatures were found to be consistent with oxide structures found in the debris [59, 80, 81, 82].

1.5 Mechanisms of Growth of Tribological Oxide Films

A wide range of mechanisms have been proposed for the growth of tribological oxide films and their subsequent removal to form wear particles. Yoshimoto and Tsukizoe[83] assumed that an oxide film grows and is removed between each asperity contact and that this is the source of debris. Quinn[48] proposed two possible mechanisms. The first that the bulk of oxidation occurs at the instant that virgin metal is exposed and that further metal contact causes shearing at the metal-oxide boundary. The second is that oxidation occurs at each contact until the oxide grows to a

critical film thickness when it becomes detached to form a wear particle. Tao[60] considered two models similar to those of Quinn[48], one in which the time for oxide growth is negligible compared with the time taken to remove the oxide layer and a further model where he assumed the gradual growth of an oxide which is then removed instantaneously when a critical thickness is attained. Molgaard[62] also postulated gradual growth to a critical thickness, but suggested that this thickness is maintained by abrasive removal of the surface of the oxide film.

Models which suggest the continuous removal of thin oxide layers without the build up of a film of critical thickness are not supported by experimental evidence, which suggests that the production of relatively thick oxide or oxidized plateaux is necessary if mild wear is to ensue.

Quinn[84] in the development of his oxidational wear theory assumed that the second of his proposals[48] is most likely. The mechanism for the growth of the oxide film was not explicit in the original theory, but it is clear from subsequent work[85] that film formation and the production of wear debris can be explained in terms of the growth of homogeneous diffusion controlled oxide plateaux on one or both of the contacting surfaces. The process involves no transfer except perhaps in the "running in" severe metallic wear phase. This mechanism of oxide formation has been shown to apply in a number of studies on the unidirectional sliding wear of a range of steels at both low and elevated

temperatures[59, 80, 81, 82, 85, 86, 87]. The mechanism reponsible for removal of oxide after attainment of critical thickness is not clear, but Aranov[88] in proposing a similar model, suggested that this is due to a fatigue process at the metal-oxide interface induced by thermal and mechanical cyclic stressing.

Alternative explanations involve various models of transfer, back transfer and agglomeration and compaction of oxide and/or oxidized metal particles to form load bearing protective films.

Stott and Wood[89] Stott, Lin and Wood[90] and Wilson, Stott and Wood[91] reported the formation of oxide glazes on a number of materials under reciprocating sliding conditions. They proposed that oxide fragments are formed by an oxidation - scrape - oxidation mechanism, where the oxide grown both during the contact and out of contact is completely removed during the next or some subsequent asperity interaction. The oxide debris may then either be swept away or cause abrasive removal of the metal surface in which case severe wear will ensue or become fragmented, compacted and undergo plastic deformation to form a protective oxide glaze in which case oxidational mild wear is the result. Sasada, Norose and Mishima[92] proposed that wear debris formed under such conditions consists of a coalescence of fragmented transfer particles.

In other experiments Stott, Glascott and Wood[93] found that the rate of oxide production could not account for the rate of development of the oxide glaze film. They therefore proposed that under the conditions of their experiments, metal debris is produced, broken up and reduced in size until the surface to volume ratio is such that spontaneous oxidation occurs. The running in time relates simply to the time required to reduce the metallic particles to the required critical size. The oxidized particles then form a metallic glaze in a manner similar to that described above[89, 90, 91,]. The reduction in particle size would according to Rabinowicz, Dunn and Russell[94] reduce three body abrasion, since there is a certain critical size below which rolling is more likely than abrasion. This would aid the agglomeration process.

Skinner[95] and Smith[96] have observed "prows" or plateaux generated in high temperature reciprocating sliding experiments of thickness of about 20μm or more. They suggested that prow formation is due either to the incorporation of oxide debris into a highly plastically deformed surface layer or internal oxidation due to diffusion of gas along microcracks into the deformed material. Similar models have been proposed by Waterhouse and Wharton[97], Kostetskii and Filipchuck[98] and Toth[99].

It is thus apparent from this brief review that there are many possible mechanisms responsible for what in each

case can be legitimately described as oxidational or mild wear. The dominant mechanism will be determined by a large number of factors including surface geometry, temperature, environment, conditions of load and speed and mechanical, chemical and metallurgical properties of the sliding pair and of the type of oxide produced.

1.6 Quantitative Theories of Oxidational Wear

Oxidational wear theories which give rise to plausible quantitative expressions for wear rate expressed in measurable parameters are few.

Yoshimoto and Tsukizoe[83] produced one of the first such analytical expressions. They assumed a model which represented profile curves of two contacting metal surfaces and from this theoretically deduced the number and size of the individual areas of contact. Using this model and further assuming that the whole of the oxide produced during an encounter is removed during the next, they expressed wear rate in terms of logarithmic oxidational constants, load, speed hardness and a parameter associated with the surface profile. There was, however, no experimental validification of the expression and since that period the work has been neglected. The theory is not supported by experimental evidence and does not account for the formation of load bearing plateaux, but in the light of current knowledge it may be worth reconsidering the theory in order to develop a

quantitative description of oxidational wear when an oxidation - scrape - oxidation mechanism[65] predominates. More terms would be required to be included in order to account for the agglomoration process.

The model of Tenwick and Earles[100] leads to an expression similar to that of Yoshimoto and Tsukizoe[83], but without the mathematical complexity of the contact analysis and with oxidational growth constants expressed in Arrhenius form. Although the models produced similar expressions there is a fundamental difference in that Tenwick and Earles assumed that an asperity remains continously in contact until an oxide layer of critical thickness is generated, before becoming detached to form a wear particle. These authors considered both linear and parabolic oxidational rate laws, but failed to apply the latter to their experimental results because of the difficulties in determining critical oxide thickness.

Quinn[84] produced an expression for the oxidational wear rate based on the Archard Wear Law[101], which may be expressed as

$$w = KA_r$$

where w is the volume removed per unit distance of sliding, A_r the real area of contact and K the probability of producing a wear particle per encounter. Quinn[84] modified the interpretation of K by assuming that $1/K$ encounters are were necessary to produce an oxide of

critical thickness at the real areas of contact and obtained the following expression:

$$w = \left\{ \frac{d\, A_p \exp\left(-\frac{Q_p}{RT_o}\right)}{\xi^2 \rho_o{}^2 f^2\, U} \right\} A$$

where d is the distance of a wearing contact, A_p Arrhenius Constant and Q_p activation energy for parabolic oxidation, R the molar gas constant, ρ_o the density of the oxide, f the fraction of the oxide which is oxygen, U the speed and T_o the oxidational temperature (assumed to be equal to the contact temperature).

The real area of contact can be written, according to Bowden and Tabor[23] as

$$A_r = \frac{W}{P_m}$$

and the contact may be assumed to consist of N circular asperities of mean radius a, randomly distributed about one or more load bearing plateaux. Thus the equation becomes

$$w = \left\{ \frac{2\sqrt{W/N\pi P_m}.A_p \exp - \left(\frac{Q_p}{RT_o}\right)}{\xi^2 \rho_o{}^2\, f^2\, U} \right\} \frac{W}{P_m}$$

where W is the load and P_m the flow pressure of the metal.

Early attempts to use this equation were hampered by the lack of any independent theoretical estimates of a, ξ and T_o and by a lack of understanding of the importance of selection of the correct oxidational growth constants. By measuring the division of heat at the sliding interface and comparing this with theorectical estimates of this parameter in terms of a surface model, it was possible[79] to obtain an equation relating N, ξ and a to this division of heat. Since N is related to a, an equation with two unknowns was obtained. Analysis of the thermal aspects of sliding also gave a relationship between T_o, ξ and a. Thus using computer search techniques consistent values of these parameters could be obtained[59, 80].

Various statically derived values of the parabolic oxidational growth constants were employed in early use of the wear equation, until it was pointed out by Sullivan, Quinn and Rowson[59] that (i) the growth constants will be different depending on the predominant oxide type (Caplan and Cohen[102] showed three distinct regions in the Arrhenius curve for the oxidation of iron corresponding to regions of predominantly α - Fe_2O_3, Fe_3O_4 and FeO respectively) and (ii) the growth constants measured from static experiments are not appropriate to the tribological situation. Tribologically derived oxidational growth constants were derived from best fit computer searches for one low alloy steel and were then employed to successfully predict wear rates for a different steel[59].

Full details of the origins and developments of this oxidational wear theory for low ambient temperatures have been given by Quinn, Sullivan and Rowson[85].

A theory which has received much attention is the delamination theory of wear proposed by Suh[103]. The probable reason for the interest is the great number of situations where wear particles consist of flakes of material and some form of delamination process must have occurred. One such situation is the removal of oxide plateaux once critical thickness has been attained. One must exercise caution, however, and not assume that all processes producing laminar particles can be described as part of a single delamination mechanism.

Suh[103] assumed that during wear the surface layer of a metal is cold worked less than the sub-surface. This leads to an increase in dislocation density in the subsurface, the formation of voids and the eventual production of cracks running parallel to the surface. The material between crack and surface will then shear to and from a wear particle.

From this model Suh[104] produced an expression for total wear volume, which was re-arranged by Engel[105] in the form:

$$w = \left\{ \frac{B_1 h_1}{d_{c_1}} + \frac{B_2 h_2}{d_{c_2}} \right\} A_r$$

where w is the wear rate expressed as volume removed per unit distance of sliding, A_r the real area of contact, h the thickness of a delaminated sheet, d_c critical plastic displacement and B a parameter depending mainly on topography. the subscripts 1 and 2 refer to the separate components of a sliding pair. The quantity in the brackets in the above equation is equivalent to the Archard K factor.

Suh[103, 106] originally demonstrated delamination for experiments conducted below the T_1 transition at loads from 10 to 20N and speeds from $1 \times 10^{-2} ms^{-1}$ to $3 \times 10^{-2} ms^{-1}$ in an argon atmosphere. The wear was severe[1], although surfaces were relatively smooth and wear rates were similar to those expected for mild wear. Childs[107] preferred to classify delamination as separate from mild or severe wear in his review of sliding wear mechanisms.

In a later series of publications by Suh and his co-workers[108, 109, 110] still working below the T_1 transition in argon, delamination was reported for a wide variety of alloys and correlation between wear resistance and fatigue resistance was demonstrated. Saka, Eleiche and Suh[111] also claim a delamination mechanism for experiments on steel above the T_2 transition in air, where the wear particles produced at speeds greater than $1\ ms^{-1}$ consisted of metallic flakes.

Other supporting evidence for delamination has been presented by Hirth and Rigney[112], Rigney and Glaeser[113] and Hsu, Ahn and Rigney[114], although alternative suggestions[112] for the mechanism of delamination were presented involving crystal plasticity and stacking fault energy. This explanation may be more appropriate when explaining delamination associated with oxide films where clearly there cannot be a soft surface layer.

In the preceding paragraphs three types of wear theory have been considered, in each of which a quantitative expression for wear has been derived. It is clear that there can be no universal theory which can account for mild oxidational wear, but between them the theories discussed might be used as a basis for the evaluation of wear rates for the major mechanisms.

A theory similar to that of Yoshimoto and Tsukizoe[83] could be developed in order to explain the "oxidation - scrape - oxidation" mechanism, although account must then be taken of agglomoration. The surface model giving rise to the number and size of contacts would also require re-examination since this predicts a wear rate proportional to $(\text{load})^{1/2}$ relationship which has never been experimentally observed.

The oxidational wear theory due originally to Quinn[85] has probably been developed to a greater extent than any other. This is clearly appropriate to the situation where homogeneous diffusion controlled oxides are grown on wearing surfaces with no transfer. This type of oxide growth is also probably the dominant mechanism in lubricated conditions where reduction in surface energies by absorbed lubricant molecules makes transfer unlikely.

The Suh[103] delamination theory does not account directly for oxidational wear, but the process could be responsible for the "metal debris" mechanism[93], where metallic particles are broken up and reduced in size, before becoming oxidized and incorporated into an agglomerate film. One would argue that comminution of particles produced in flake form is more probable than for lumps. Tabor[7] observed that the delamination process frequently occurs with materials containing local inclusions, hence the theory might be applied to internal oxidation of plastically deformed layers or embedded oxide particles in those layers[95].

It is also possible that such a theory has wider implications, since the majority of oxide removed in equilibrium mild wear condition appears to be due to laminar failure at the metal oxide interface.

1.7 Oxidational Wear and Boundary Lubrication

This review has shown that there has been a substantial amount of work published on the oxidational wear of metals under dry conditions and there is some understanding of the mechanism involved in the formation of oxide films and the role played by those films in the protection of contacting surfaces. It requires only the recognition that there may be many independent processes involved in oxidational wear for further progress to be made. Far less attention however, has been paid to the role of oxidation under lubricated contact conditions.

It is known that oxidation can occur at the real areas of contact under extremely low partial pressures[115] and there is sufficient dissolved oxygen in most untreated lubricants to produce a significant reaction with the surface at the high temperatures normally attained during sliding. One would expect, therefore, that oxidation could be important under lubricated conditions when a substantial degree of asperity contact occurs, that is in boundary lubrication. It will be far less so when there is a substantial degree of fluid film support.

Prutton et al[116] working on the corrosion of metals by solutions of organic acids in hydrocarbons showed that for copper, iron zinc, cadmium and a number of other metals, reactions took place via the oxide film. Tingle[117] showed

that a 1% solution of lauric acid in paraffin was no more effective in lubricating a freshly cut metal surface then was paraffin alone, but that if the surface had an oxide film produced by exposure to oxygen and water vapour the additive acted as an effective boundary lubricant. Bowden and Young[118] reported similar findings, which they interpreted in terms of the production of a tenacious metallic soap film by reaction between the organic acid and the surface metallic oxide. Bowden, Gregory and Tabor[119] had earlier observed that such films could survive on rough surfaces to provide effective protection. From this early work, therefore, it seemed that the formation of an initial oxide film, perhaps no more than a few molecular layers thick, was a necessary prerequisite for the development of a boundary film from an organic acid additive. Later workers have shown that oxidation has a more profound effect on the development of the complete boundary film.

Hirst and Lancaster[120] showed that the rate of metal oxide formation affects friction and wear during boundary lubrication and they suggested that the protection given by the oxide complements that due to the lubricant film. The significance of dissolved oxygen in lubricated sliding contact has been studied by many investigators. Feng[121] observed the onset of severe wear of cast iron when air was removed from the lubricant. Toyoguchi and Takai[122] using a four ball test have shown that for solutions of mono - and di-sulphides in white oil, seizure occurred at a lower load when oxygen was absent from the system than when present.

Godfrey[123] observed reduction in coefficient of friction of steel using a pin on disc machine and a solution of sulphur in white oil when oil was used in the presence of oxygen. He further reported[124] that with untreated white oil mild wear was evident from the formation of surface layers of α Fe_2O_3 and Fe_3O_4 . With air removed from the oil and the system operated in a nitrogen atmosphere severe wear was observed and large metallic debris produced. Tomaru, Hironaka and Sakurai[125] have shown that the antiwear region was extended when a sulphide antiwear additive was used in the presence of oxygen. Bjerk[126] showed that for steel rollers, lubricated surfaces with high oxygen concentration suffered minimum wear and concluded that an oxide layer is developed only when sufficient oxygen is available.

Begelinger and de Gee[127] observed large decreases in both friction and wear with increased oxygen concentration in the lubricant in a steel on steel system and this they attributed to oxidation of asperities during localized breakdown. The effect is to prevent metal to metal contact during these periods. Other investigators have found the beneficial effects of oxygen to be dependent on concentration. Klaus and Bieber[128] and Fein and Kreuz[129] have shown that there is a minimum in the plot of wear against oxygen concentration in steel on steel boundary lubricated systems. It was suggested that the increase in wear at higher concentrations is due to the fact that α - Fe_2O_3 is the primary low temperature oxide formed

at high oxygen partial pressures and Fe_3O_4 when partial pressure is reduced. Fein and Kreuz[129] showed that α - Fe_2O_3 was associated with high concentrations of oxygen in the lubricant, but when the concentration was reduced Fe_3O_4 appeared in the debris. Fe_3O_4 is known to be the more wear resistant. The high wear associated with low oxygen concentrations is due to incomplete coverage. This explanation would not account for the findings of Nakayma and Okamoto[130], however, who in a study of the wear of copper under boundary conditions also found an optimum value for the concentration of dissolved oxygen at which minimum friction and wear occurred. The increased rate of wear above the optimum value was explained in terms of the formation of thicker oxide films which are more easily sheared.

Oxidation of metal surfaces under lubricated conditions may not be simply due to dissolved oxygen in the fluid. Newley, Spikes and Macpherson[131] propose that the metal surface is oxidized by reacting with peroxy radicles which form as intermediates as the lubricant oxidizes.

This author has made an extensive study of one particular boundary lubricated system[132,133,134,135], that of aluminium bronze against tool steel in the presence of kerosene. Complex surface interactions were identified, including preferential depletion of aluminium from the bronze surface and transfer of that element to the steel couterface. Under equilibrium conditions, however, the

major protecting element in the bronze surface was found to be copper oxide Cu_2O and oxidational wear was the dominant mode. The major function of a dimeric acid boundary additive included in the kerosene at a concentration of about 12 p.p.m., was to give the surface sufficient protection for a protective oxide film to develop and be maintained.

There are very few theories of boundary lubrication which give rise to plausible quantitative expressions for wear rates. A recent attempt has been made by Komvopoulos, Suh and Saka[136] who indicated that the predominant wear mechanism is abrasive ploughing. They obtained an expression for the wear coefficient from slip line field analysis and surface topography statistics. If one examines their photomicrographs of worn surfaces a degree of surface distress not typical of boundary lubrication in its conventially accepted sense is visible. This is not surprising since they used an inert, additive free, mineral oil which would produce no boundary protection. Hence their system probably consisted of metallic contacts with a minimal amount of fluid film support. The expression cannot therefore be applied to a conventional boundary system.

There is an obvious need for a complete analysis of oxidational wear under boundary conditions. This problem will be addressed later in this work.

1.8 Oxidational Growth Rate Laws and their Relevance to Tribological Growth

In order to understand the mechanisms involved in oxidational wear it is necessary to have an appreciation of the processes responsible for oxide growth on metal surfaces. It is at least necessary to know which form of oxidational growth law to employ in any given set of circumstances. Some investigators have been guilty of the indiscriminate use of a specific growth law in conditions quite outside the boundaries to which it applies.

Considering the growth of oxide on a clean metal surface[137,138]. The first stage of growth consists of adsorption of oxygen onto the surface and incorporation into some metal-oxygen structure. The second the appearance of nucleation sites due perhaps to defects on the surface or oxygen precipitation. The third stage consists of lateral growth of the oxide from the nucleation site and the forth of the vertical growth of the oxide on the surface. The initial growth is very rapid, but slows down quickly, often becoming negligibly slow.

The rate of growth with time may be governed by various rate laws all of which have been observed experimentally.

These are:

(i)	inverse logarithmic	$\frac{1}{X} = A - k \log_e t$
(ii)	direct logarithmic	$X = A \log_e (kt + 1)$
(iii)	linear	$X = k_1 t$
(iv)	parabolic	$X^2 = k_p t$
(v)	cubic	$X^3 = k_c t$

where X is the increase in a dimention (thickness, volume or mass) of the oxide in time t. A and k are growth constants.

In general the first three of the laws apply to thin films the latter two to films which are somewhat thicker and produced at higher temperatures.

Inverse logarithmic rate laws have been explained by Cabrera and Mott[139] in terms of quantum mechanical tunnelling of electrons through a thin oxide layer producing high electric fields which aid cation migration. Alternative explanations for the law have been proposed by Hauffe[140] and Fromhold and Cook[141] in terms of ionic transport through the film.

Fehlner and Mott[142] modified the theory of Cabrera and Mott[139] to include anion migration and showed that this gives rise to a direct logarithmic rate law. Other explanations for the rate determining mechanisms for this law have been proposed by Landsberg[143] and Richie and Hunt[144].

All the above work assumes uniform transport properties across the film and generally applies to films of thickness much less that 100Å, although Cabrera and Mott[139] did suggest that their basic assumptions may be applied to much thicker films, up to 2000Å, producing either cubic or parabolic rate laws. The assumptions of uniform transport have been rejected by Davies, Evans and Agar[145] since they cannot account for oxide growth in any but the lowest part of the thin film range. These workers assume instead that paths for rapid ionic transport exist, for example along grain boundaries, dislocations and surface pores. The paths are progressively blocked as growth proceeds. The theory gives rise to a direct logarithmic relationship and is probably far more appropriate to tribological oxide growth, where there is substantial surface disruption.

If a surface layer is non-protective and offers no resistance to the continued exposure of the metal surface to oxygen, the thickness of the layer has no influence on the reaction rate and this leads to a linear rate law[146]. The

two groups of metals and alloys which have been found to obey a linear relationship are those which produce porous or volatile oxide layers. There have also been suggestions that a linear rate law applies when phase boundary interactions are the rate determining factor. Linear kinetics therefore should not be applied to the majority of tribological oxidational situations, although many workers have done so.

Cubic rate laws are rare and are found only in p-type semiconductors. Engell, Hauffe and Ilschner[147] explain their existance in terms of oxide space charge layers.

For thick oxide layers and oxide produced at high temperature growth follows a parabolic rate law and is due to diffusion of metal and/or oxygen ions through the oxide. Diffusion of the ions through the oxide lattice is associated with the nature of the point defects. Wagner[148] classified different types of oxide in terms of the associated lattice defects and produced a theory predicting parabolic oxidation based on ion diffusion through the lattice under the influence of defect induced electrochemical gradients. Phase boundary reactions were considered to be very rapid, so that the diffusion of ions and transport of electrons determines the reaction rate. The theory makes it possible to predict the effect of temperature, partial pressure and impurity concentration on oxidation rates.

The temperature dependence of reaction rates is governed by the Arrhenius equation, which is a particular form of the general Botzmann relationship between temperature and the percentage of molecules having energies exceeding a certain threshold value. Dunn[149] was the first to draw attention to the fact that oxidational growth rate constants obey the Arrhenius equation and may be written in the form

$$k = A \exp - \frac{Q}{RT}$$

where

A is the Arrhenius constant

Q the activation energy

R the molar gas constant

and T the absolute temperature of oxidation.

It is now beyond doubt[146] that the equation applies to the vast majority of oxidational processes.

It is well documented, but not always appreciated that growth rates under tribological conditions can be many orders of magnitude greater that those observed with similar materials and at similar temperatures under static conditions. One example of this may be taken from the growth of oxide on steel in a carbon dioxide atmosphere. Darras, Leclarcq and Bunard[150] reported growth equivalent to an 8μm thick oxide layer in one year at a temperature of

350^0C under static conditions. In experiments to be discussed later in this work it will be shown that such a thickness of oxide may be attained in CO_2 in a matter of hours or even minutes under sliding conditions. There is much more evidence which when examined shows that statically derived rate constants cannot account for the rapid development of the tribo-oxide films.

Sullivan, Quinn and Rowson[59] explained the differences between static and tribo oxidational growth constants in terms of the Arrhenius relationship for diffusion controlled parabolic oxidation. For parabolic oxidation the rate constant k_p may be expected to be dependent on the diffusion coefficients D (where D may be written in Arrhenius form $D_o \exp(- Q/RT)$), of the various atomic species in the relevant oxide. If this is so the values of A_p and Q_p for oxide growth will depend on D_o and Q for diffusion. The activation energy for diffusion Q depends on relative barrier heights, this has been discussed for another system by Sullivan[151,152] and is not expected to differ in static and tribological conditions. The complete significance of the Arrhenius constants, D_o and hence A_p, is still not understood, but they are known to be related to the entropy of the system[153,154] and are known to vary with surface conditioning, void and dislocation density and other factors[155]. In fact Arrhenius constants measured under static conditions may vary by orders of magnitude, depending on experimental conditions. It is therefore to be expected that for highly disrupted

tribological surfaces Arrhenius constants will be much higher. Since it is proposed that activation energies will remain the same in both tribological and static conditions, the increase in Arrhenius constant results in an increase in rate constant. It is possible to construct a similar argument for other oxidational rate laws.

1.9 Formation and Breakdown of Compact Oxide Films

If an oxide is to be protective under tribological conditions it must be both compact and non-porous. The conditions for such an oxide to exist were stated by Pilling and Bedworth[156]. These are that:

$$\frac{\text{molar volume of oxide}}{\text{molar volume of metal}} \geqslant 1$$

For ratios less than one, the volume of oxide produced does not compensate for the volume of metal removed resulting in a porous film. Schottky[157] has suggested, that a ratio greater than one may not always be necessary and that the primary prerequisite is the capability of plastic flow in both metal and oxide, but examination of Pilling Bedworth ratios reveals values greater than one for all oxides commonly found on engineering surfaces.

Considering thick diffussion controlled oxide growth, the condition for the production of a compact oxide will eventually lead to its breakdown. If the Pilling Bedworth ratio is greater than one, the oxide forms in compression and the compressional stresses increase as the oxide grows in thickness. Thus at a given thickness the stresses may be sufficient for film breakdown to occur. The effect will be most pronounced when oxidation is controlled by anion diffusion since in this case oxide is formed at the metal oxide interface where expansion of the lattice has the greatest effect on the mechanical integrity of the film.

When cation diffusion predominates, vacancies may accumulate at the metal oxide interface, resulting in the formation of cavities which eventually lead to loss of adhesion. In this type of oxide laminar removal of the film is more probable than the crazing and cracking which might be expected in anion diffusion controlled oxidation.

Stresses may also be generated within an oxide film during heating or cooling due to a difference in thermal expansion coefficients between the metal and oxide. Oxx[158] expressed the magnitude of this stress as:

$$\sigma_o = \frac{E_o \, \Delta T(\alpha_o - \alpha_m)}{1 + 2 \, \frac{(E_o t_o)}{(E_m t_m)}}$$

where

σ = stress

α = coefficient of thermal expansion

E = elastic modulus

t = thickness

the subscripts o and m refer to oxide and metal.

The magnitude of the stress will be proportional to the difference in thermal expansion coefficients. Since the adhesive forces between oxide and metal are usually lower than the cohesive forces in either oxide or metal, the stresses could give rise to loss of adhesion at the interface. This is particularly true in a tribological situation where asperities are subject to very rapid heating and cooling. Thus the oxide is subject to cyclic tensional and compressional stresses which give rise to additional fatigue at the interface.

Each of the above stress producing mechanisms could account for the observation of critical film thickness and all would be exacerbated by mechanical stresses produced in a sliding system.

This argument applies to thick diffusion controlled tribological films, but not to an oxidation scrape oxidation mechanism where initial abrasive removal is more probable. In this later case other explanations may have to be found for the existance of plateaux of critical thickness.

1.10 Oxidation of Iron and Low Alloy Steels

The most commonly used materials in tribological situations are steels, it is therefore appropriate to consider oxidation of iron based alloys. Due to the economic importance of these materials there is a large amount of literature on this subject and no attempt will be made to review this here, rather the remarks will be confined to low alloy steels where the oxides formed may be regarded as wholly due to iron.

When iron or low alloy steel oxidises in air the oxide can consist of a multi-layer film of the primary oxides heamatite (α - Fe_2O_3), magnetite (Fe_3O_4) and wustite (FeO). FeO does not form at temperatures below 570^0C, thus iron oxidised below this temperature forms a two layer film of Fe_3O_4 and α - Fe_2O_3 with the Fe_3O_4 at the metal interface. Above 570^0C the sequence in the film is FeO, Fe_3O_4 and α - Fe_2O_3 with the FeO next to the metal[146]. Mills and Sullivan[159] found a further constituent in the film. In their experiments employing X-ray photoelectron spectroscopy to examine iron oxides, they found the outer layer on all oxide powder and oxidised metal surfaces examined to consist of FeOOH. The concentration of individual constituents in the oxide varies with temperature. Below 200^0C the major constituent is α-Fe_2O_3, between 200^0C and 570^0C it is Fe_3O_4 and above 570^0C it is FeO, according to Molgaard[169], although

the curves of Caplan and Cohen[102] suggest a lower temperature transition point of about 350^0C, rather than 200^0C.

Considering the oxides in turn, FeO is non-stoichiometric and contains Fe^{2+} vacant lattice sites. Growth occurs by cation diffusion. In Fe_3O_4 growth occurs by both cation and anion diffusion. Fe_2O_3 is oxygen deficient and growth proceeds by anion diffusion via vacant O^{2-} lattice sites.

Good and Godfrey[161] and Bisson, Johnson and Swibert[162] have examined a number of steel surfaces after sliding and concluded that Fe_3O_4 produces a more protective surface film than α - Fe_2O_3, resulting in lower wear rates when Fe_3O_4 predominates. Clark, Pritchard and Midgley[55] suggested that a significant factor in the fall in wear rate of steels with increase in temperature is a change in the nature of the oxide, the predominant oxide at their higher temperatures was Fe_3O_4 .

Available evidence on the protective properties of the high temperature oxide FeO is contradictory. Both Bisson, Johnson and Swibert[162] and Cornelius and Roberts[162] found FeO to be protective where Tsuji[164] and Hurricks[165] found distinct increases in wear between 500^0C and 600^0C where FeO becomes predominant.

1.11 Oxidation of Copper

The material other than steel to be considered later in this work is an aluminium bronze containing 11% aluminium. Poole and Sullivan[166,167,168] have shown that under equilbrium mild wear conditions the primary protective oxide on the surface is a copper oxide. Hence the oxidation of copper will be briefly considered here.

There is probably more literature on the oxidation kinetics of copper than any other metal including the iron based alloys. The initial stages of oxidation of copper at low temperatures and for thin films may follow direct logarithmic or possible cubic rate laws[139] (Cu_2O is a p-type semiconductor). At medium and high temperatures for relatively thick films all the evidence shows that copper ultimately follows a parabolic law[169].

Similar to iron, the oxide grown on a copper surface consists of two layers. The primary oxides are CuO and Cu_2O. Valensi[170] measured the composition of oxide films between 300^0C and 900^0C and found that the CuO concentration varied from 95% at 300^0C to 5% at 900^0C. Cruzan and Miley[171] suggested that CuO is formed from the oxidation of Cu_2O and this implies that there is a layer of Cu_2O always adjacent to the metal. In their experiments at 240^0C they found that all films less than $400\overset{0}{A}$ consisted of Cu_2O. Cruzan and Miley[171] further found that increasing the oxygen concentration increased the

proportion of CuO in the film, while decreasing the oxygen prohibited the formation of CuO entirely. This result would account for the observations of only Cu_2O by Poole and Sullivan[166,167,168] in the wear debris of their lubricated experiments where oxygen partial pressure was low.

Cu_2O is a metal deficit p-type semiconductor and diffusion of cations is responsible for oxide growth. CuO is deficient in oxygen and oxide growth is due to anion diffusion.

The Pilling Bedworth ratio for Cu_2O is 1.64, lower than for any of the oxides of iron, but the ratio of thermal expansion coefficients of metal to oxide is high which would lead to high stresses under tribological conditions.

The significance of growth mechanisms and physical properties of the various iron and copper oxides to the formation of tribologically protective layers will be discussed in a later section of this work.

1.12 Research Programme

In this work three distinct systems will be examined where oxidational wear is the dominant equilibrium wear mode. These are:

(i) Unidirectional wear of steels at low and elevated temperatures in air.

(ii) Unidirectional wear of aluminium bronze on steel under conditions of boundary lubrication.

(iii) Reciprocating wear of steel at elevated temperature in carbon dioxide.

Experimental evidence from the three systems will be considered, theoretical models developed and analyses undertaken in order to elucidate the mechanisms of oxidational wear in each case.

From the results it will be possible to compare and contrast those mechanisms and isolate the important variables in determining the dominant wear modes.

CHAPTER 2

THE UNIDIRECTIONAL WEAR OF STEEL AT LOW AND ELEVATED TEMPERATURES IN AIR

This chapter principally describes the study of ASI 52100 steel under equilibrium mild wear conditions in the temperature range from 20 to 500^{0}C. In addition to this the wear of two other steels, a BS EN8 low alloy steel and a 9% Cr steel, is examined for unheated low ambient temperature experiments.

The study involves unidirectional sliding with measurements taken from a pin on disc apparatus.

2.1 Experimental Apparatus and Procedures

The results reported in this part of the study were gained with the aid of a conventional pin on disc machine, a detail of which is shown in figure 2.1.

Essentially the apparatus consists of a cylindrical flat faced pin mounted horizontally against the flat face of a vertical disc. The disc was driven by a 5 H.P. motor through water cooled bearings giving continually varying sliding speeds from 0.6 to 10 ms^{-1}. A 2 kW electrical resistance heater was clamped to the face of the disc opposite to the wearing surface enabling the disc to be

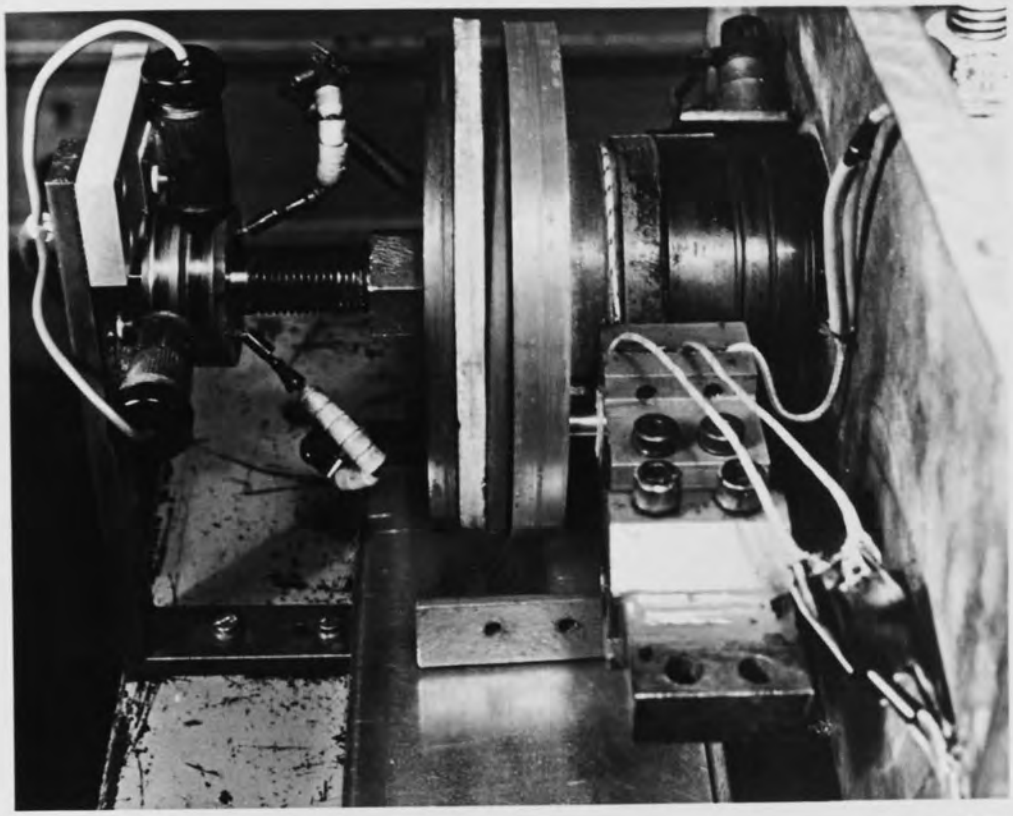

FIG. 2.1 DETAIL OF ELEVATED TEMPERATURE WEAR RIG SHOWING THE LOADING ARM WITH HORIZONTAL STEEL PIN AGAINST VERTICAL STEEL DISC.THE HEATER ELEMENT IS CLAMPED TO THE REAR OF THE DISC.THE SLIP RINGS ON THE FRONT (PIN) SIDE OF THE DISC ARE FOR THERMO-COUPLES AND THOSE AT THE REAR FEED THE HEATER.

heated to temperatures in excess of 500^{0}C. The current for the heater was supplied via slip rings and was controlled through a servo-circuit to give a disc temperature constant to ± 5^{0}C [172]. This prevented uncontrolled increases in temperature due to frictional heating.

The pin was held in a calorimeter similar to that described by Quinn[84] and temperature measurements from the calorimeter allowed heat flow into the pin to be calculated and hence the general surface temperature T_s to be evaluated by the method described by Rowson and Quinn[75]. The calorimeter was in turn held in a loading arm and the load on the pin was applied pneumatically via an air cylinder mounted axially on a shaft supporting the loading arm. Loads between 10 and 157 N were applied by this method. Loads below 10N were applied by a dead weight system loaded through a pulley.

Friction and wear were continuously monitored using a strain gauge load cell and linear displacement transducer respectively, the amplified outputs of which were displayed on a chart recorder. Temperatures of the disc and points within the calorimeter were similarly monitored using thermocouples.

More complete details of this wear test rig are given by Petraitis[172].

All pins used in the experiments were of 38 mm initial length and 6 mm diameter. They were produced from cold rolled rods and turned to a smooth finish of about 5 μm c.l.a. Discs were cut from bars and randomly ground to 0.2 μm c.l.a. The discs were 120 mm in diameter and 12.5 mm thick. To provide disc surface specimens for analysis removable taper plugs were inserted into some of the discs prior to grinding.

All pins and discs were throughly cleaned and degreased in acetone and then petroleum ether vapour prior to each experiment.

The compositions of the materials used in the experiments were nominally:

	C	Mn	Si	S	P	Cr	Mo	Ni	Fe
ASI 52100	1.0	0.2	0.3	.06	.06	1.2	-	-	Remainder
BS EN8	0.4	0.6	0.3	.06	.06	-	-	-	Remainder
9% Cr	0.1	0.4	0.6	.01	.005	9	1	0.25	Remainder

All figures are weight percentage.

The initial hardnesses of the unworn specimens are given below in VPN:

	pin	disc
ASI 52100	280 ± 10	200 ± 10
BS EN8	250 ± 10	200 ± 10
9% Cr	-	250 ± 10

Hot hardness measurements on the 52100 and BS EN8 materials used in this study were conducted by Lucas Research Laboratories and their curves of bulk hardness versus temperature are shown in figure 2.2 These results were used in the surface models to be discussed later in the chapter.

The bulk of the work to be described here concerns the wear of 52100 steel pins on discs of similar material. The experiments were conducted at a constant sliding speed of $2ms^{-1}$ and over a range of loads from 4.9 to 157 N with no external heating applied to the disc and then repeated at constant disc temperatures of 200, 300, 400 and $500^{0}C$. A new pin and fresh wear track was used for each load at each disc temperature. Before the start of an elevated temperature experiment the disc temperature was raised to the desired value and maintained at that value for a period of 15 minutes prior to loading the pin against the disc. During the running in period the servo temperature control circuit adjusted the current to the heater to compensate for the increase in frictional heating and maintain the temperature at the required level.

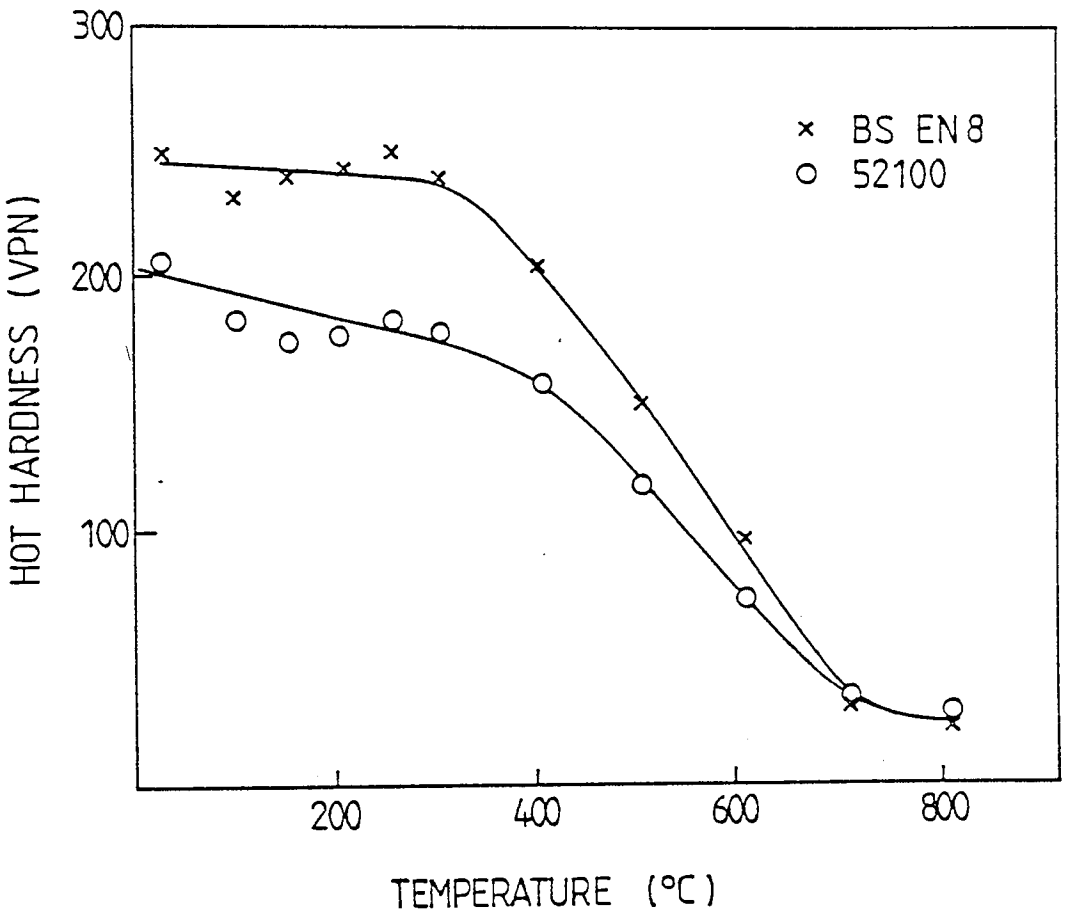

FIG. 2.2 BULK HARDNESS VERSUS SURFACE TEMPERATURE CURVES FOR 52100 AND BS EN8 STEELS.

There is still controversy over the importance of transfer in the formation of protective tribological oxide films. A further series of experiments was, therefore, conducted to investigate this. In this series a BS EN8 steel having similar physical properties to 52100, but containing no chromium, was initially slid against itself to establish that wear patterns were of the same type as for the experiments conducted on 52100. The 9% Cr steel was then introduced into the system in order to determine the role of transfer in unidirectional sliding above the T_2 transition. A limited number of experiments were conducted with BS EN8 chromium free steel pins sliding against 9% Cr steel discs. The major purpose of these experiments was to generate samples for surface analysis.

All measurements were taken after equilibrium mild wear conditions had been established

Wear debris was collected from each experiment after the initial running in period and analysed by means of X-ray powder diffraction techniques using a Debye-Scherrer camera. Cobalt K_α radiation was used throughout at a tube voltage of 40kV and current 30 mA. Average exposure times were 45 minutes. Surfaces were examined using glancing angle X-ray diffraction techniques. Similar conditions of voltage current and exposure time were employed and the glancing angle was 30^0. Under these conditions the maximum penetration depth of the X-rays was calculated to be 11 μm. This latter technique is not particularly surface sensitive,

but gives structural information about surface and subsurface layers not available from other methods.

The surfaces of worn samples, both pins and inserts taken from selected discs, were examined using scanning electron microscopy. This provided topographical information and direct measurements of oxide film thickness. Thickness measurements were made with the aid of the instrument specimen tilt control adjusted to give equal magnification in horizontal and vertical directions on the image. An average of ten thickness measurements were made on each selected worn sample and the mean value calculated. Some scanning electron micrographs were recorded for debris samples.

Auger electron spectroscopy was employed to study the nature of the tribological oxide film through the generation of oxygen, iron and some chromium depth profiles from selected surfaces. Auger spectra were recorded between successive removal of atomic layers by argon ion bombardment. Relative atomic concentrations for each spectra were calculated from spectral peak to peak heights and published elemental sensitivity factors[173] and plotted as a function of the product of ion beam current and total time of bombardment. The precise sputtering rate for anything other than simple mono elemental surfaces is difficult to assess, but calculations from the data of Carter and Colligon[174] would suggest a removal rate of about $0.5\mathring{A}$ per μA. min. for the conditions of these

experiments. For all analyses the argon beam energy was 2 keV and the beam current 30 μA. All Auger spectra were recorded for a 5 keV incident electron beam.

A limited number of surfaces were examined using X-ray photoelectron spectroscopy in order to gain chemical state information on the elements in the oxide film. In this part of the study the 0 1s and Fe 2p lines were recorded from some experiments prior to Auger electron analysis.

Finally disc surface wear track profiles were recorded using a talysurf profilimeter in a direction perpendicular to the track after the completion of a test run. From the profiles total disc wear was estimated.

2.2 Experimental Results

2.2.1 Wear and Friction

Figure 2.3 shows a series of equilibrium wear rate against load curves for the wear of 52100 pins against 52100 discs at a number of disc temperatures up to 500^0C. The graphs show clear transistions in wear rates at specific loads dependent on disc temperature. For example for the experiments conducted with no external heating two transitions occur, the first at a load of about 25 N, the second at about 80 N. Such transitions have been reported

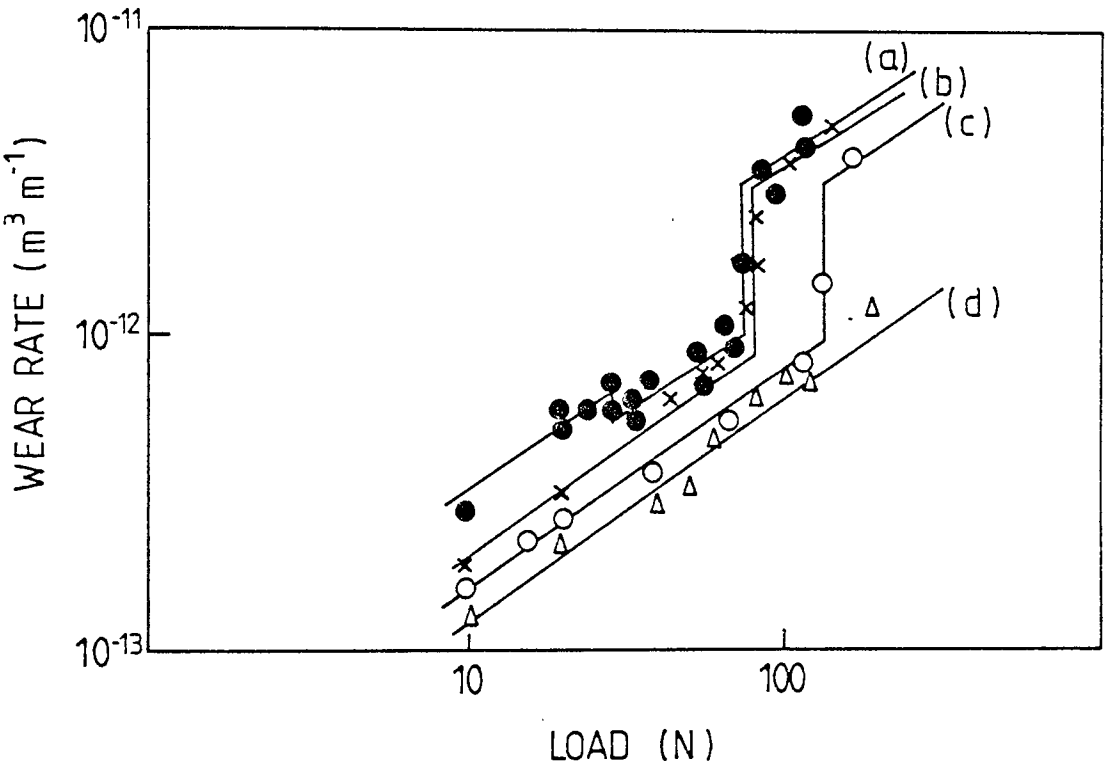

FIG. 2.3 WEAR RATE VERSUS LOAD CURVES FOR 52100 STEEL ON 52100 STEEL AT VARIOUS DISC TEMPERATURES: (a) UNHEATED DISC ● ,(b) 200 °C X ,(c) 300 °C o , (d) 500 °C Δ .

elsewhere[59,80] for similar experiments. As the disc temperature is increased the first transition disappears and the second tends to move to higher loads, a little over 80 N for 200^{0}C and 110 N for 300^{0}C. The second transition was not detected for 400^{0}C and 500^{0}C disc temperatures and if it does occur it must be at loads greater than 157 N, the load limit imposed by the apparatus used.

The log versus log representation in figure 2.3 is employed so that data from all the experiments may be easily compared, but the wear rate for any region associated with a given oxide type was found to vary linearly with load. Error bars are not included on wear data curves since the errors due to measurement were always found to be neglible compared to variations due to material properties.

Figure 2.4 shows the equilibrium wear rate versus load variation for the BS EN8 material sliding against itself. The graph shows similar transitions to those observed for the 52100 material for the experiments conducted at room temperature. In this case transitions in wear rates occur at load of about 12.5 N and 37 N. There is a linear variation in wear rate with load in each of the three regions shown in the curve.

The variation in wear rate with load for the BS EN8 steel sliding against 9% Cr steel is shown in Figure 2.5. In this case, over the limited load range investigated, no transitions were observed and again wear varied linearly

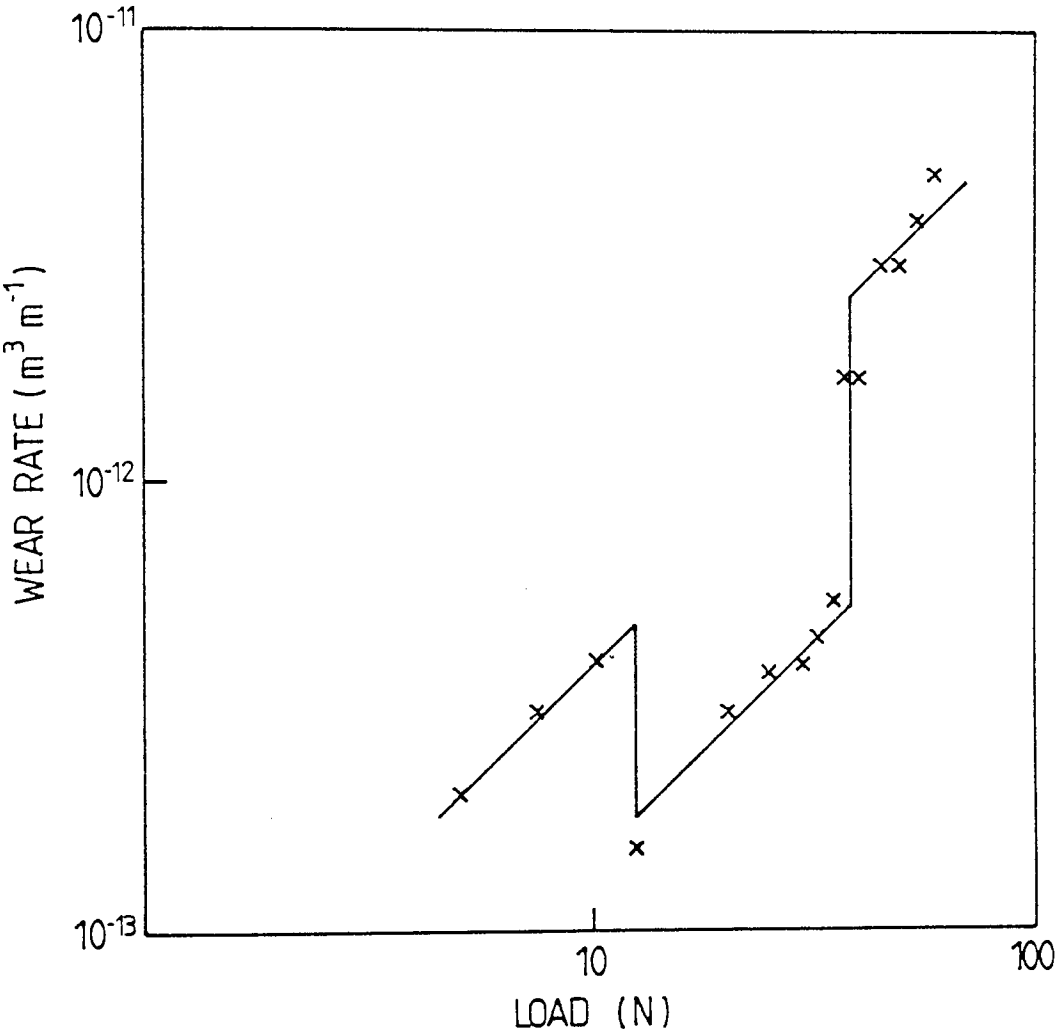

. 2.4 WEAR RATE VERSUS LOAD CURVES FOR BS EN8
EL ON BS EN8 STEEL.

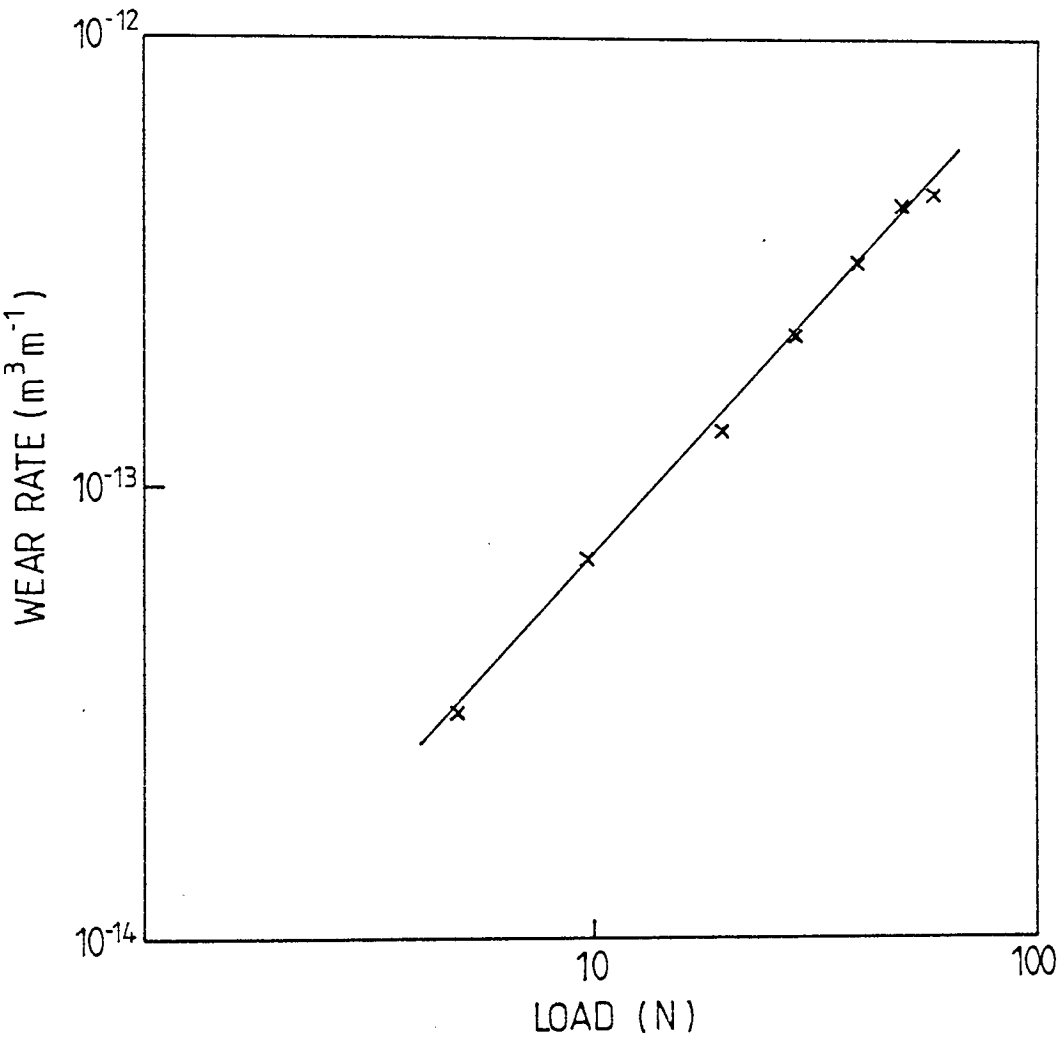

FIG. 2.5 WEAR RATE VERSUS LOAD CURVES FOR BS EN8 STEEL ON 9% Cr STEEL.

with applied load. It was not felt necessary to extend the load range since this covered both transition regions previously observed for the BS EN8 partner of the sliding pair which was the surface required for further examination.

Disc wear rates estimated from profilimetric measurements included the initial running in severe wear and hence only a semi-quantitative assessment could be made. In general, however, wear rates increased with applied load and were of the same order of magnitude as those of the pin.

Friction coefficients generally decreased with increase in load and increase in temperature. Figure 2.6 shows a variation in coefficient of friction with load which was typical of the majority of curves generated from individual experiments. In this case the friction coefficient for 52100 steel at room temperature is shown. Figure 2.7 shows the change in coefficient of friction with temperature for a series of loads.

2.2.2 X-ray Diffraction Analysis

Powder X-ray diffraction analysis of debris and glancing angle X-ray diffraction analysis of the surfaces show that the transitions in wear rate correspond to changes in oxide composition. Typical X-ray diffraction observations are shown in table 2.1 together with the identity of the compounds present, in this case for

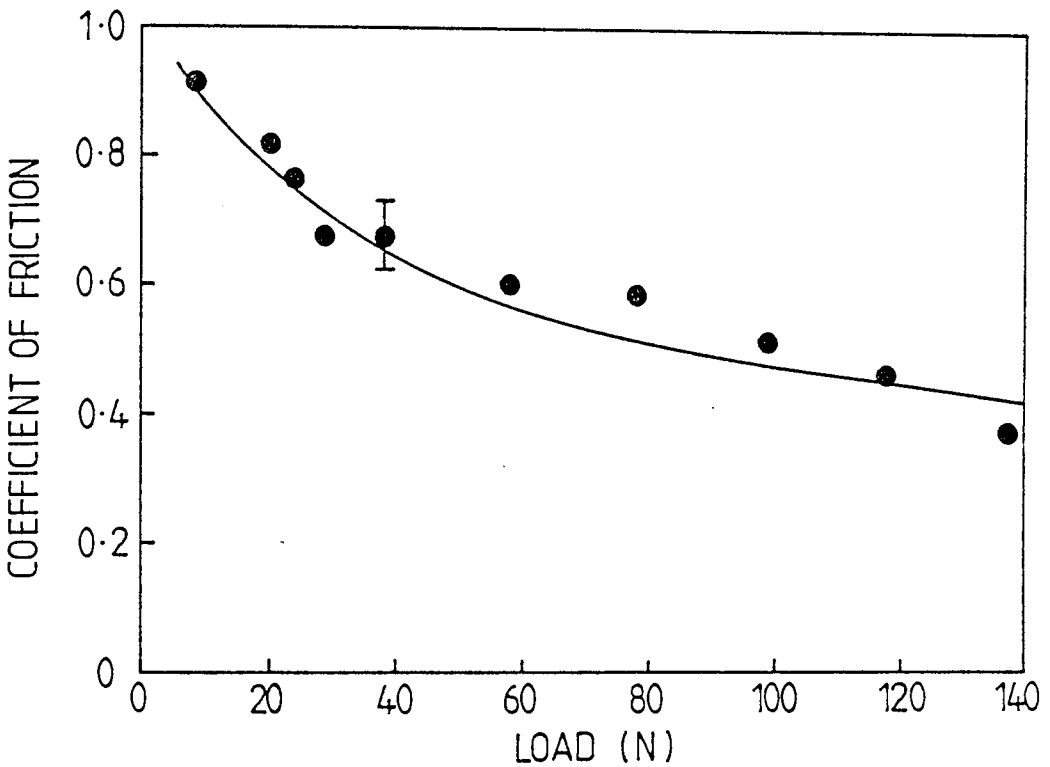

FIG. 2.6 COEFFICIENT OF FRICTION VERSUS LOAD FOR 52100 STEEL ON 52100 STEEL EXPERIMENTS AT ROOM TEMPERATURE.

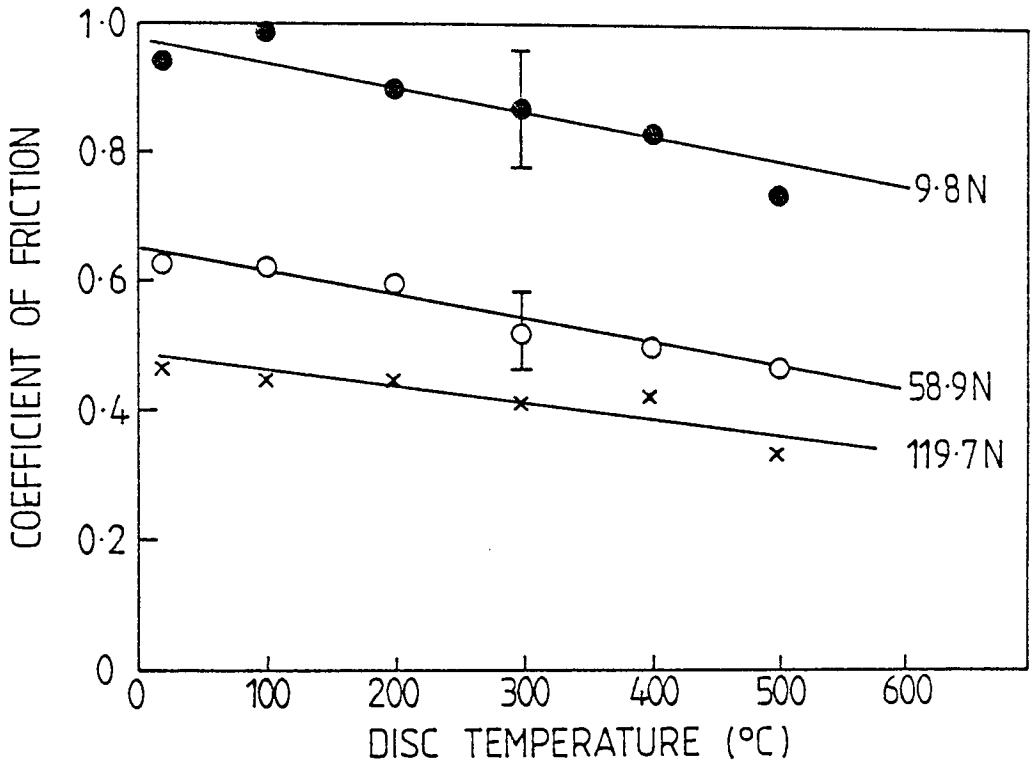

FIG. 2.7 VARIATION IN COEFFICIENT OF FRICTION WITH TEMPERATURE FOR 52100 EXPERIMENTS.

experiments conducted on 52100 steel at a load of 19.6 N and speed of $2ms^{-1}$ with no external heating.

All the data for 52100 on 52100 experiments is summarized in table 2.2. Tables 2.3 and 2.4 similarly show the summarized data for BS EN8 on itself and BS EN8 steel on 9% Cr experiments. The major constituent in the oxide is shown first in each table. In addition to the oxides, α - Fe was found in debris from all experiments.

The results in Table 2.2 clearly show that for experiments with no external heating the predominant oxide below the first transition is $\alpha - Fe_2O_3$. The first transition then corresponds to the appearance of substantial amounts of Fe_3O_4 in the oxide. After this point relative intensities of the X-ray diffraction lines corresponding to d spacings of $2.68\overset{0}{A}$ and $2.52\overset{0}{A}$ (which are the most intense lines for $\alpha - Fe_2O_3$ and Fe_3O_4 respectively) indicate that the proportion of Fe_3O_4 in the debris increases with load. The second transition corresponds to the appearance of FeO at the wearing surfaces. Similarly the transitions associated with the 200 and 300^0C experiments correspond to changes from regions of Fe_3O_4 and $\alpha - Fe_2O_3$ mixtures to regions containing FeO.

Very similar results were observed for the BS EN8 on BS EN8 experiments with similar oxide compositions corresponding to transition regions. No transition was observed for experiments involving the 9% Cr steel, although

TABLE 2.1

Powder X-ray diffraction observations of debris for 52100 steel, load 19.6N, speed $2ms^{-2}$, no external heating.

Experimental Values		Component	Diffraction file data	
2θ(deg.)	d(Å)		d(Å)	Relative Intensity I/I_o
28.0 f	3.70	α-Fe_2O_3	3.68	25
39.0 s	2.68	α-Fe_2O_3	2.69	100
41.7 m	2.51	α-Fe_2O_3, Fe_3O_4	2.51,2.53	50, 100
48.0 f	2.20	α-Fe_2O_3	2.20	20
52.3 s	2.03	α-Fe	2.03	100
58.0 f	1.84	α-Fe_2O_3	1.84	40
6.38 m	1.69	α-Fe_2O_3, Fe_3O_4	1.69,1.71	60, 10
67.5 v.f	1.61	Fe_3O_4	1.62	30
73.8 f	1.49	α-Fe_2O_3, Fe_3O_4	1.48,1.49	35, 40
76.0 f	1.45	α-Fe_2O_3	1.45	35
86.0 f	1.31	α-Fe_2O_3	1.31	20
99.4 m	1.17	α-Fe	1.17	30

S : strong, m : medium, f : faint v.f. : very faint

TABLE 2.2

Oxides identified in the debris and on worn surfaces from 52100 steel on 52100 steel experiments.

Experimental temperature	Load Range	Oxide Composition	
		Debris	Surface
Room temperature	< 25N	α-Fe_2O_3 Fe_3O_4	α-Fe_2O_3
	25N→ 80N	Fe_3O_4 α-Fe_2O_3	Fe_3O_4 α-Fe_2O_3
	80N→ 157N	FeO, Fe_3O_4 α-Fe_2O_3	FeO, Fe_3O_4
200°C and 300°C	Up to transition	Fe_3O_4 α-Fe_2O_3	Fe_3O_4 α-Fe_2O_3
	Above transition	FeO, Fe_3O_4 α-Fe_2O_3	FeO, Fe_3O_4
400°C and 500°C	All loads	α-Fe_2O_3 Fe_3O_4	α-Fe_2O_3 Fe_3O_4

TABLE 2.3.

Oxides identified in the debris and on worn surfaces from BS EN8 steel experiments

Load Range	Oxide Composition	
	Debris	Surface
5N - 10N	α-Fe_2O_3	α-Fe_2O_3
12N - 35N	Fe_3O_4 α-Fe_2O_3	Fe_3O_4 α-Fe_2O_3
35N - 60N	FeO, Fe_3O_4 α-Fe_2O_3	FeO, Fe_3O_4

TABLE 2.4

Oxides identified in the debris from 9% Cr steel on BS EN8 steel experiments

Load Range	Oxide Composition in Debris
10N - 35N	Spinel (Fe_3O_4, $FeCr_2O_4$) Rhombohedral (α-Fe_2O_3, Cr_2O_3)
40N - 60N	Spinel, Wustite (FeO), Rhombohedral

FeO was observed in the debris for loads above 35 N. Very limited data was collected however, for this series of experiments and transitions could have been missed.

In the experiments conducted at 400 and 500^{0}C the wear rate versus load curves show no transitions over the load range covered by this investigation and both debris and surface oxides consisted of Fe_3O_4 / α - Fe_2O_3 mixtures.

2.2.3 Scanning Electron Microscopy

Scanning electron microscopy was employed to gain information on topographical changes at the surfaces, but also to assess oxide film thickness. A large number of micrographs have been recorded, but only a small number representative of the major surface conditions are shown here. The micrographs in Figure 2.8 show typical surfaces generated on 52100 steel in experiments conducted without external heating. Three regions are illustrated. Figure 2.8 (a) shows the surface from a low load experiment below the first transition; the oxide is mainly α - Fe_2O_3 and the surface is covered by smooth oxide plateaux standing above relatively rough debris covered metallic areas. The second region, Figure 2.8 (b), is taken between the two transition loads in an oxide regime consisting of Fe_3O_4 with α - Fe_2O_3 . Here the plateaux have grown in size until almost the whole surface is covered with a smooth oxide film. The third region, Figure 2.8 (c), taken above the

(a)

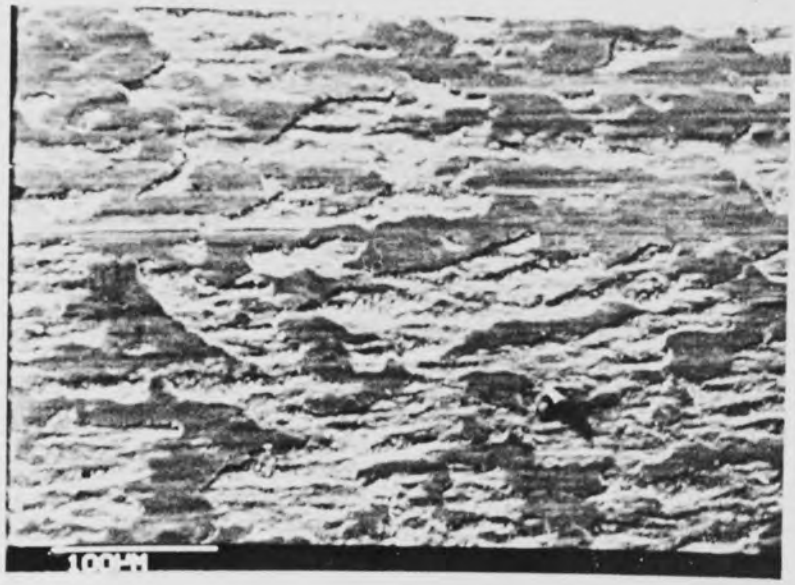

(b)

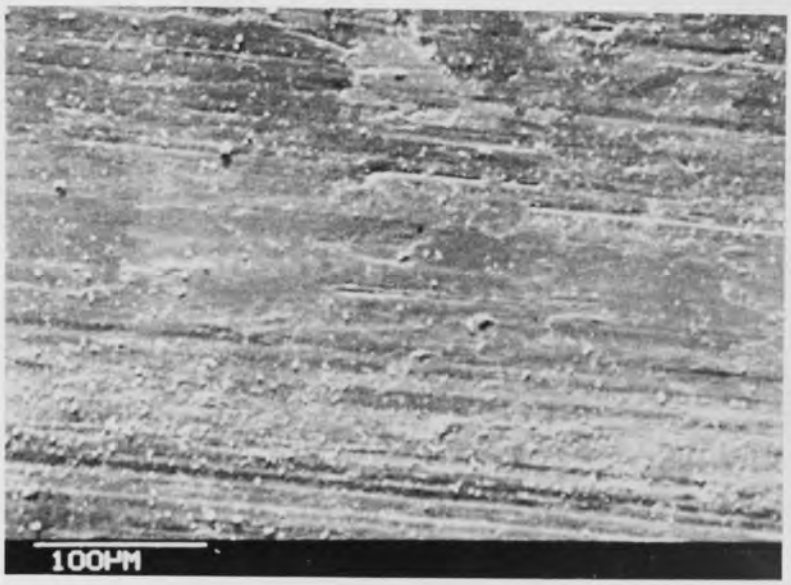

(c)

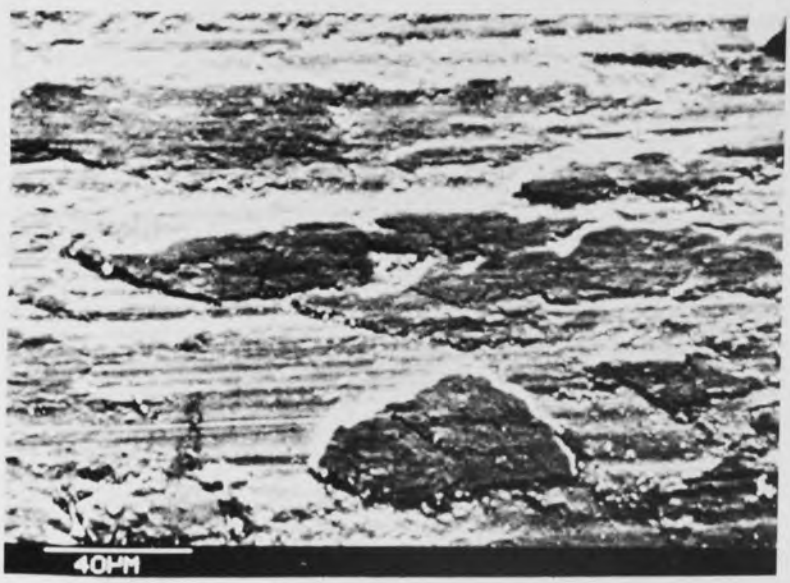

FIG. 2.8 SCANNING ELECTRON MICROGRAPHS OF SURFACES GENERATED FROM 52100 ON 52100 EXPERIMENTS WITH NO EXTERNAL HEATING AT LOADS OF ; (a) 9.8N , (b) 39N , AND (c) 98N.

second transition load, corresponds to the appearance of FeO in the debris. Here a further change in topography is evident, where at these loads surfaces have a relatively sparse covering of oxide. A similar series taken for BS EN8 experiments is shown in Figure 2.9 and the same general features are evident within a given oxide regime.

Micrographs of surfaces generated in experiments conducted at 200, 300, 400 and 500^{0}C also show remarkably similar surface characteristics for any given oxide regime. For example, Figure 2.10 shows a surface worn at 400^{0}C under a load of 59 N. This surface is smooth and heavily oxidized, but damage has occurred due to the removal of oxide flakes and the exposed metallic surface is clearly visible beneath.

Using the tilt facility on the electron microscope oxide film thickness measurements were made for both pin and disc surfaces for a range of loads and temperature conditions. Photomicrographs of typical oxide edges used in the measurements are shown in Figures 2.11 and 2.12. Examination of the edges of the oxide plateaux show them to be smooth and apparently homogeneous and not to consist of an agglomerate film. This is evidence that plateaux are due to diffusion controlled oxidation. Detailed results of these measurements on pin surfaces are shown in Table 2.5 Since only a limited number of discs contained removable inserts fewer measurements were made on disc surfaces, but where measurements were made film thicknesses on both pin

(a)

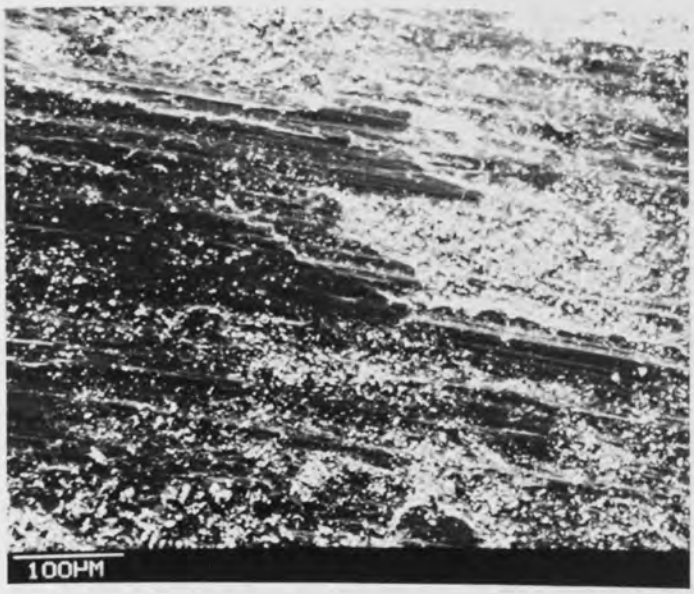

(b)

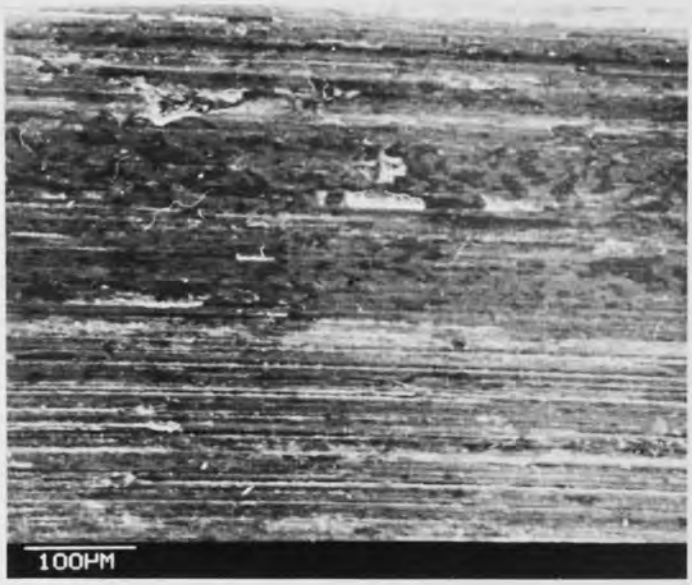

(c)

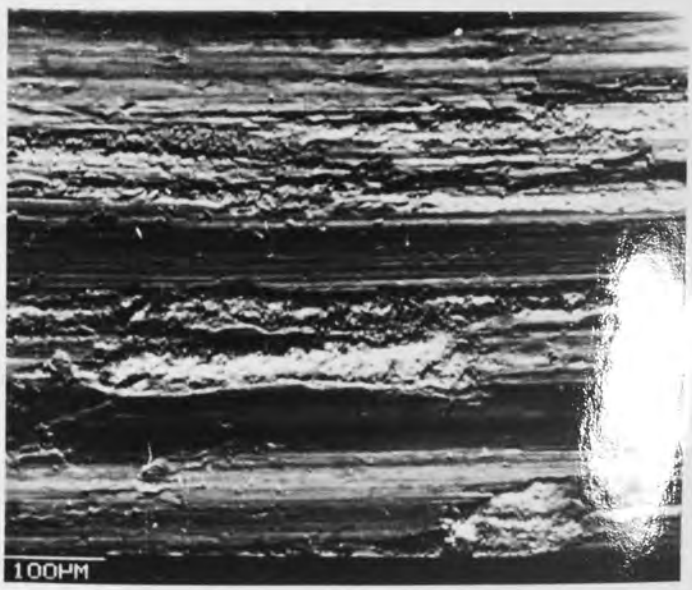

FIG. 2.9 SCANNING ELECTRON MICROGRAPHS OF SURFACES GENERATED FROM BS EN8 ON BS EN8 EXPERIMENTS WITH NO EXTERNAL HEATING AT LOADS OF ; (a) 9.8N , (b) 24.5N AND (c) 59N.

FIG. 2.10 SCANNING ELECTRON MICROGRAPH OF A 52100 STEEL PIN SURFACE WORN AT A LOAD OF 59N AND A TEMPERATURE OF 400 °C.

(a)

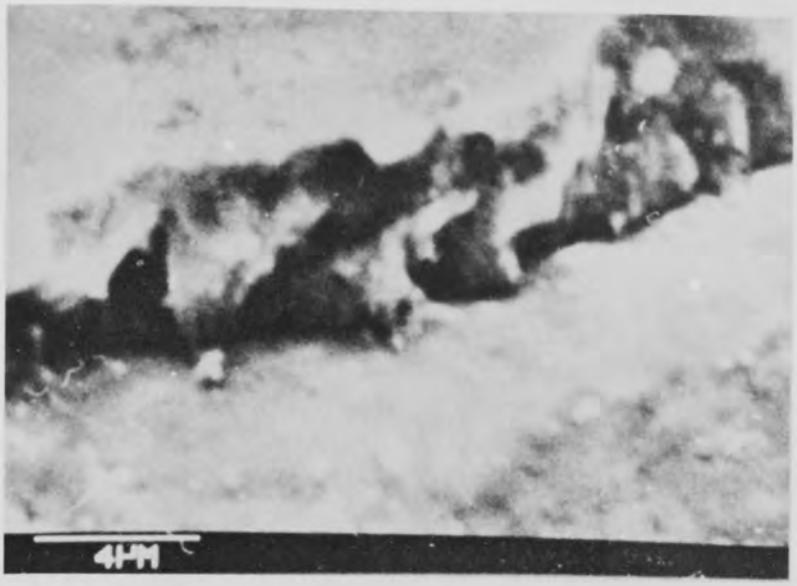

(b)

(c)

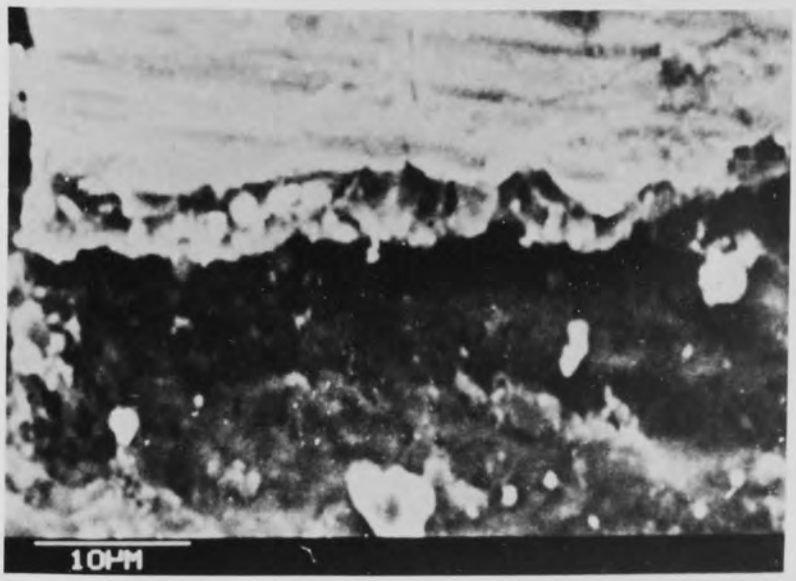

FIG. 2.11 SCANNING ELECTRON MICROGRAPH OF TYPICAL OXIDE PLATEAUX EDGES FROM 52100 ON 52100 EXPERIMENTS CONDUCTED AT ; (a) 39N LOAD,ROOM TEMPERATURE, (b) 19.6N LOAD,400 C AND (c) 49N LOAD,300 C.

(a)

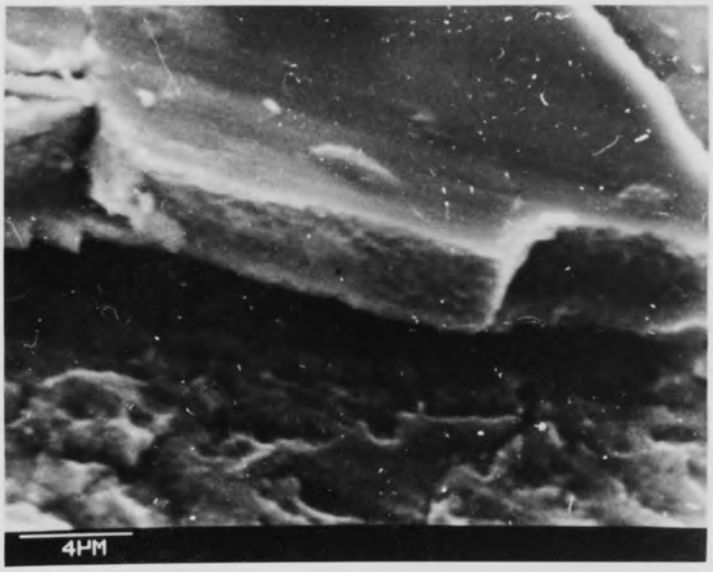

(b)

(c)

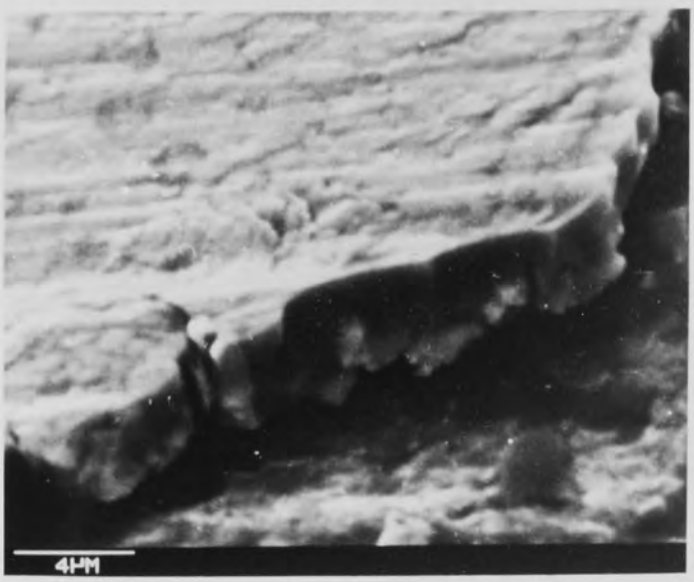

FIG. 2.12 SCANNING ELECTRON MICROGRAPHS OF TYPICAL OXIDE PLATEAUX EDGES FROM BS EN8 ON BS EN8 EXPERIMENTS CONDUCTED AT LOADS OF ; (a) 9.8N, (b) 20N AND (c) 39N.

TABLE 2.5.

Oxide film thickness measurement on pin surfaces.
(standard deviations are shown in brackets)

	Oxide Thickness					
	52100 Steel					BS.EN8
Load N \ Temp. °C	Room Temp.	200	300	400	500	Room Temp.
9.8	1.1(0.6)	1.8(0.5)	2.1(0.5)	2.3(0.7)	2.2(0.6)	3.2(0.8)
14.7	1.4(0.7)	2.5(0.5)	2.8(0.5)	2.5(0.8)	2.2(0.4)	3.9(0.7)
19.6	1.8(1.0)	2.3(0.6)	2.8(0.8)	2.8(1.1)	2.8(0.8)	4.2(0.7)
39.2	3.0(0.9)	2.7(0.4)	2.9(1.1)	2.8(0.7)	3.0(0.8)	3.5(0.4)
58.9	3.2(0.5)	2.9(0.8)	3.4(0.6)	3.9(0.7)	3.3(0.5)	3.1(0.7)
78.5	2.9(0.8)	2.6(1.0)	3.5(0.6)	3.8(1.4)	3.3(0.9)	3.0(0.5)
98.1	1.3(0.5)	2.4(0.8)	3.4(0.6)	5.1(1.8)	4.1(1.0)	-
157.0	1.3(0.6)	2.0(1.0)	3.0(1.0)	4.6(1.7)	4.7(0.8)	-

and disc were found to be similar for a given set of conditions.

2.2.4 Auger and X-ray Photoelectron Spectroscopy

In the recent past there has been some controversy about the nature of the oxide plateaux observed in experiments of this type. Questions have been raised as to whether they consist entirely of oxide or whether they are metallic with a thin oxide coating. The scanning electron micrographs shown in Figures 2.11 and 2.12 strongly suggest, not only that the layers are oxide, but that they are homogeneous and not an agglomerate layer of compacted smaller particles. The work described here using Auger electron spectroscopy confirms these findings. A typical secondary electron image of a worn surface (magnification 1000x) after argon ion etching with corresponding Auger oxygen maps is shown in Figure 2.13. It is clear from these figures that the raised regions are oxide plateaux.

Plateaux from a number of surfaces were gradually etched away by bombardment with 2keV argon ions and Auger spectra were recorded at given time intervals. Examples of the resulting oxygen concentration versus depth profiles for 52100 steel experiments are shown in Figure 2.14. The peaks used in the work were the 503 eV KLL oxygen and 703 eV LMM iron Auger peaks. The curves show the extent of the oxide film and clearly indicate that films formed in the Fe_3O_4

(a)

(b)

FIG. 2.13 (a) AUGER ELECTRON OXYGEN MAP OF PLATEAUX FORMED ON A 52100 STEEL PIN SURFACE WORN AT 39N LOAD AND AT ROOM TEMPERATURE.
(b) CORRESPONDING SECONDARY ELECTRON IMAGE.

oxide regime are thicker that those in the $\alpha - Fe_2O_3$ region. The figure further shows that the ratio of oxygen to iron remains reasonably constant throughout the oxide film.

A further series of oxygen depth profiles, in this case for BS EN8 steel sliding on itself is shown for pins in Figure 2.15 and for discs in Figure 2.16. Profiles taken from the three oxidational regimes of $\alpha - Fe_2O_3$, Fe_3O_4 and FeO predominance are shown and again it is clear that thicker oxides are produced when Fe_3O_4 is the major component.

Profiles for the BS EN8 on 9% Cr steel experiments are shown in Figures 2.17, 2.18, 2.19 and 2.20 taken at loads of 9.8, 19.6, 39.4 and 49.0 N and speed of 2 ms^{-1} . The profiles show a marked difference in concentration of Cr detected on pin and disc surfaces. The Cr concentration in the oxide on the worn disc is shown to be about 3 to 5% at the surface rising to about 9% in the bulk metal. In the case of the oxide on the worn BS EN8 pins, however, no Cr was detected in the bulk of the oxide, but a small signal corresponding to a relative concentration of no more than 1% of Cr was detected in the region of the oxide metal interface.

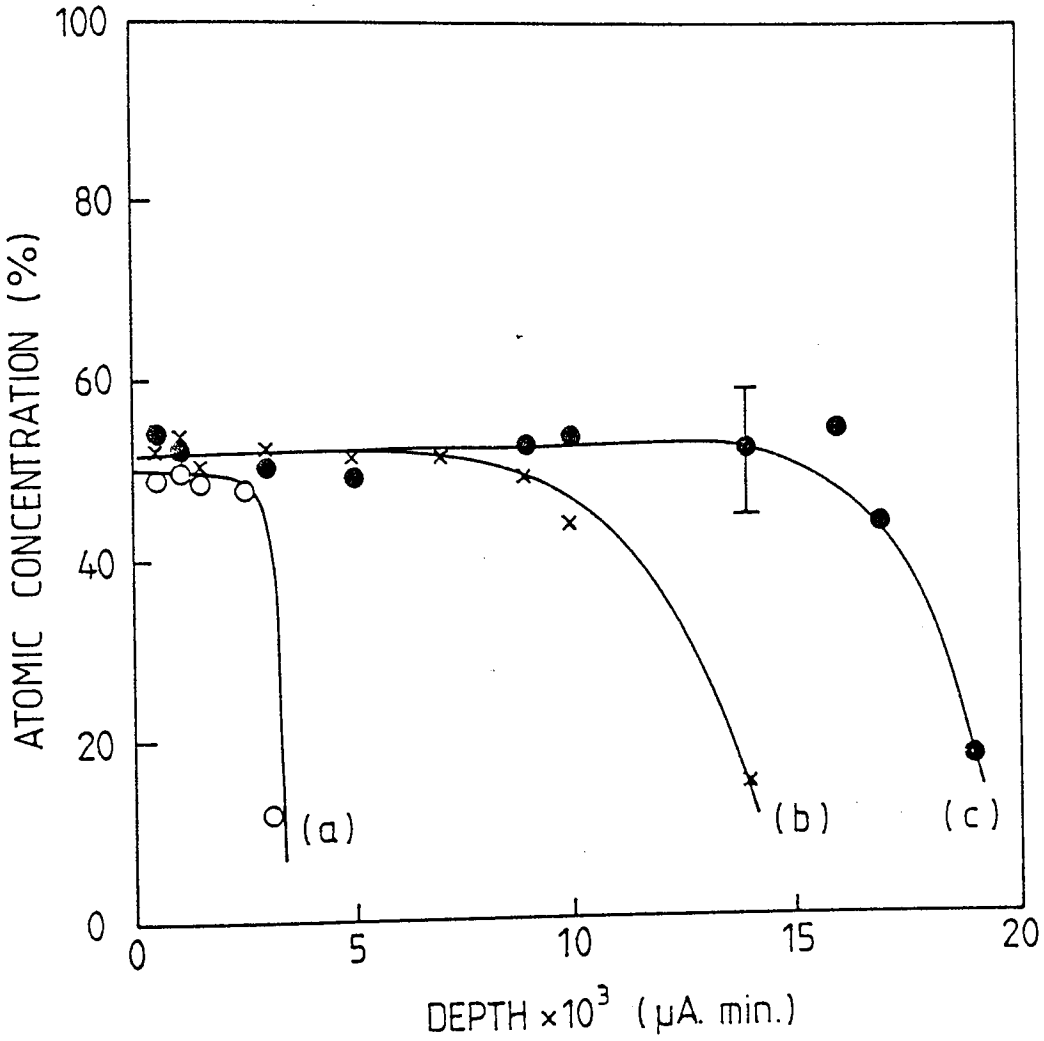

FIG. 2.14 OXYGEN CONCENTRATION VERSUS DEPTH PROFILES FOR 52100 STEEL SURFACES GENERATED AT ; (a) 15N LOAD, ROOM TEMPERATURE, o, (b) 59N LOAD, ROOM TEMPERATURE, x, AND (c) 39N LOAD, 400 °C, ●.

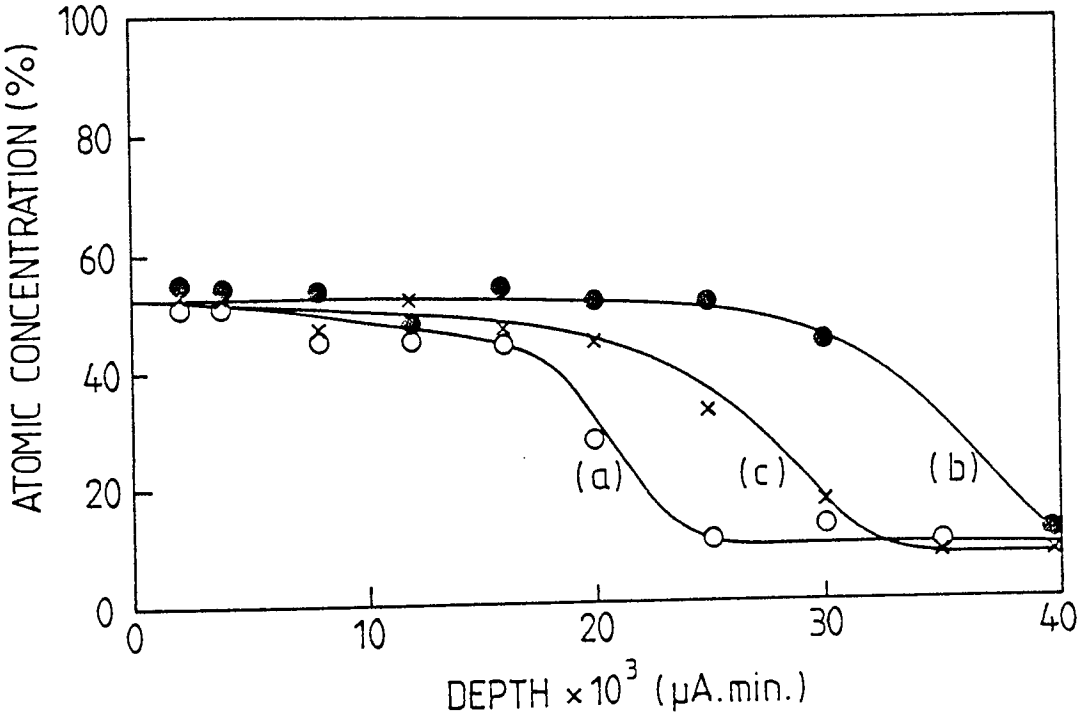

FIG. 2.15 OXYGEN CONCENTRATION VERSUS DEPTH PROFILES FOR BS EN8 PINS FROM BS EN8 ON BS EN8 EXPERIMENTS AT LOADS OF ; (a) 4.9N,o, (b) 29N,●,AND (c) 49N,x.

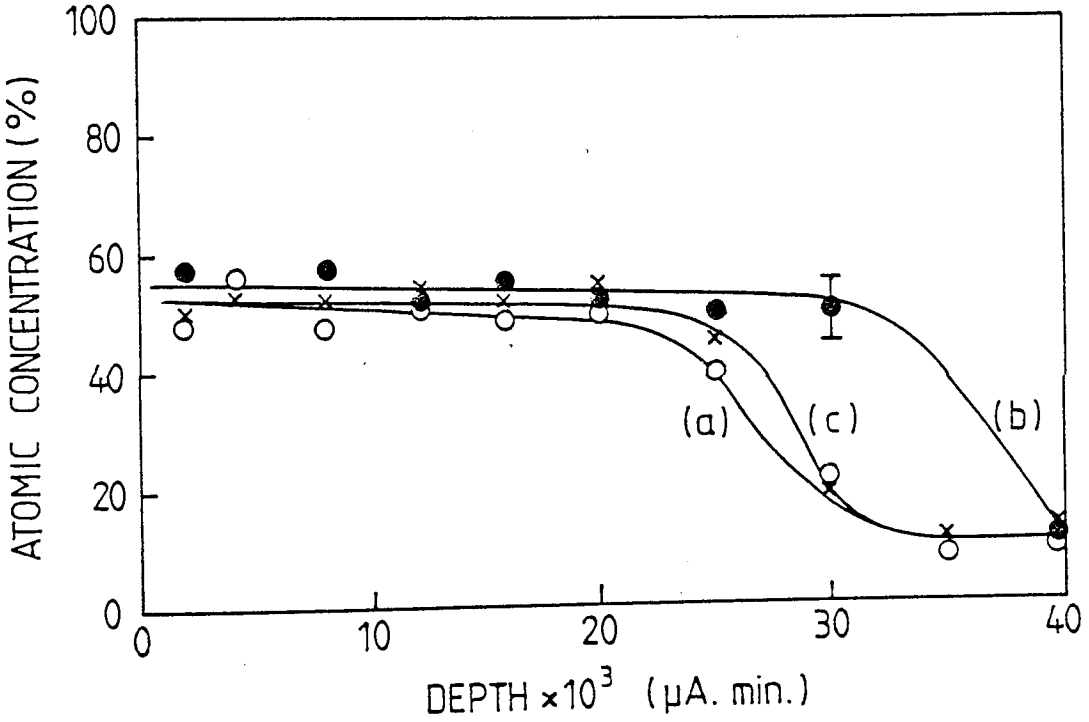

FIG. 2.16 OXYGEN CONCENTRATION VERSUS DEPTH PROFILES FOR BS EN8 DISCS FROM BS EN8 ON BS EN8 EXPERIMENTS AT LOADS OF ; (a) 4.9N,o, (b) 29N,●,AND (c) 49N,x.

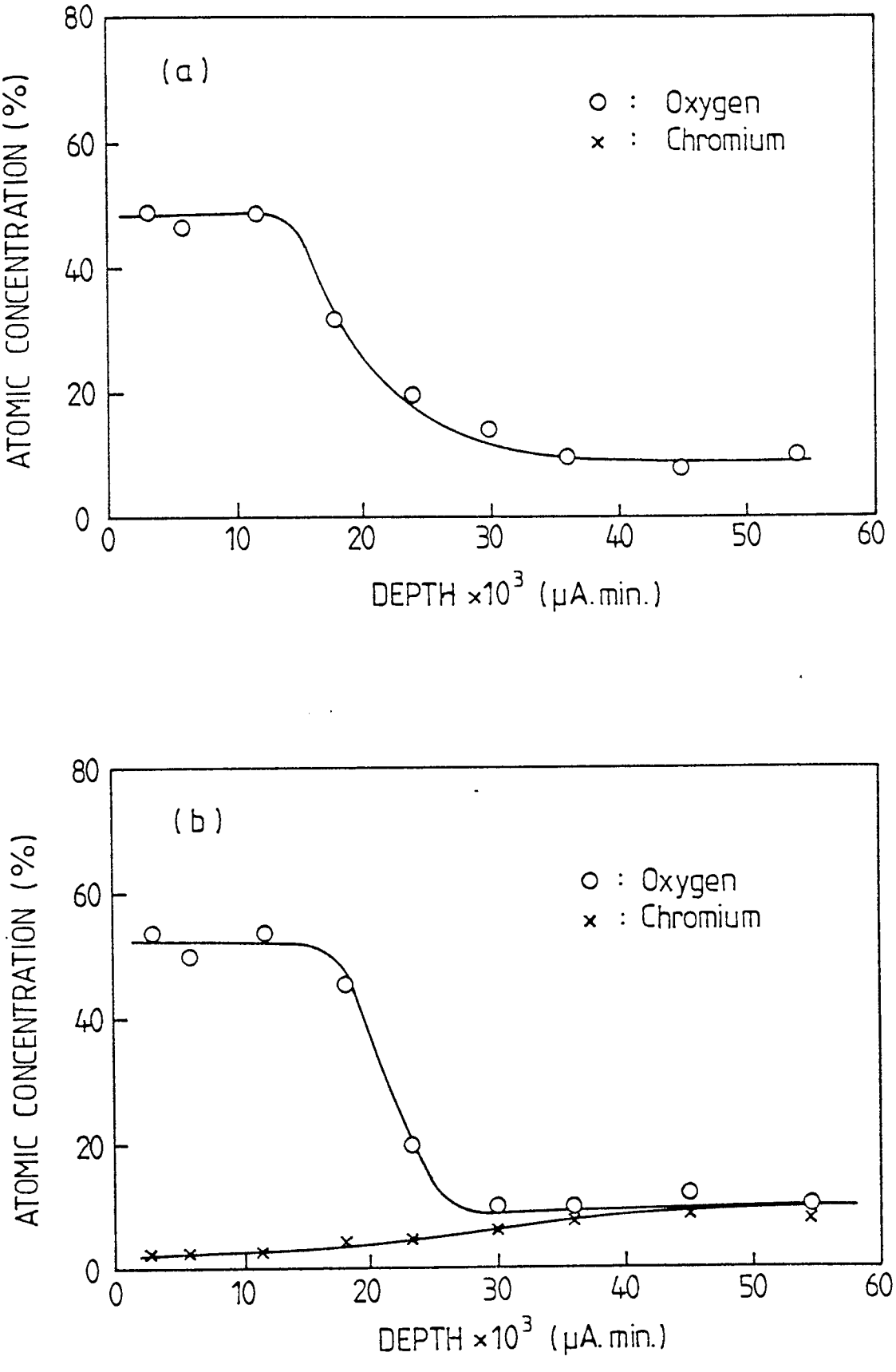

FIG. 2.17 OXYGEN AND CHROMIUM CONCENTRATION VERSUS DEPTH PROFILES FOR WORN SURFACES FROM BS EN8 ON 9% CHROMIUM EXPERIMENTS GENERATED AT A LOAD OF 9.8N. (a) BS EN8 PIN SURFACE ,(b) 9% CHROMIUM STEEL DISC SURFACE.

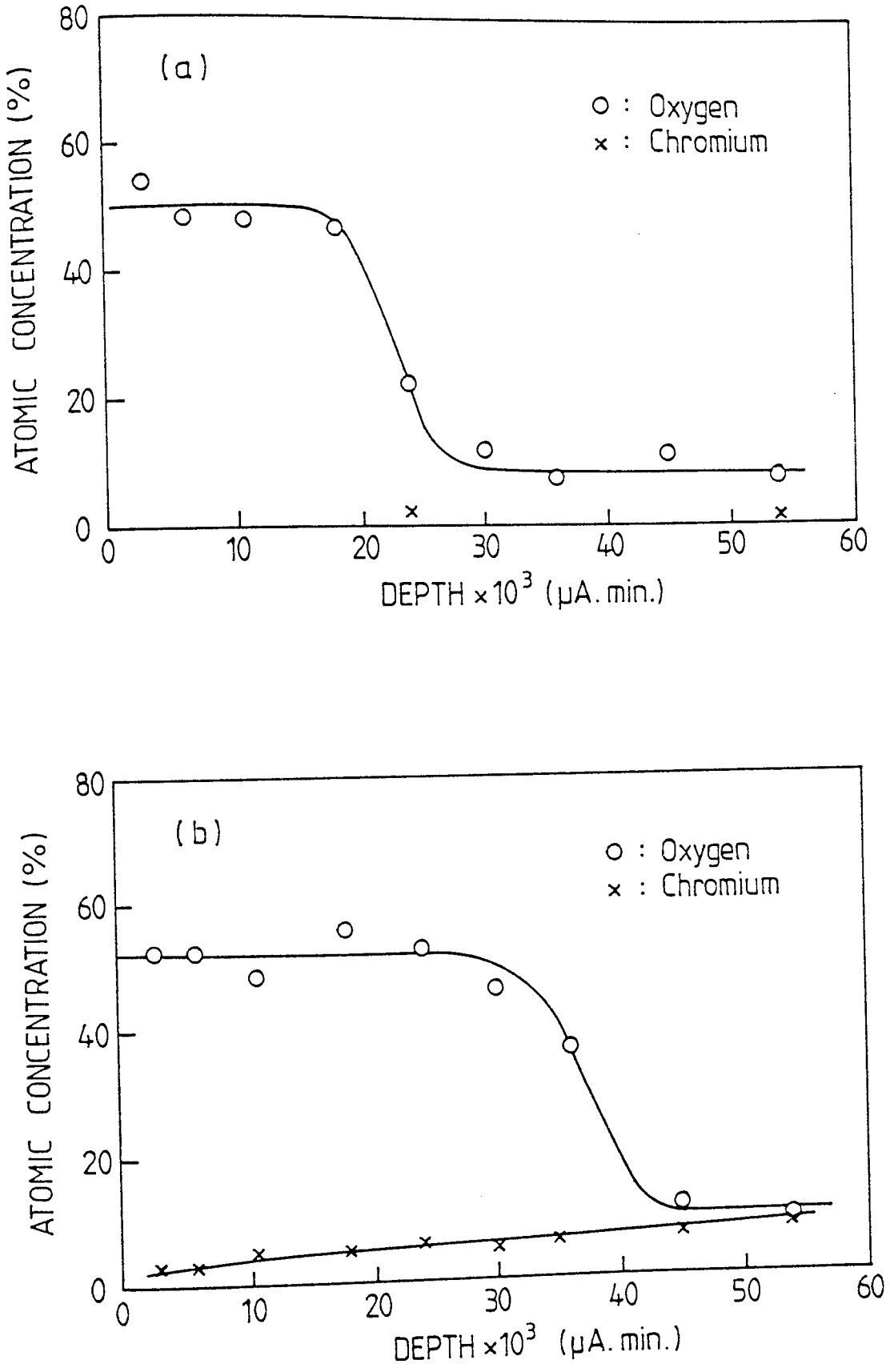

FIG. 2.18 OXYGEN AND CHROMIUM CONCENTRATION VERSUS DEPTH PROFILES FOR WORN SURFACES FROM BS EN8 ON 9% CHROMIUM EXPERIMENTS GENERATED AT A LOAD OF 19.6N. (a) BS EN8 PIN SURFACE ,(b) 9% CHROMIUM STEEL DISC SURFACE.

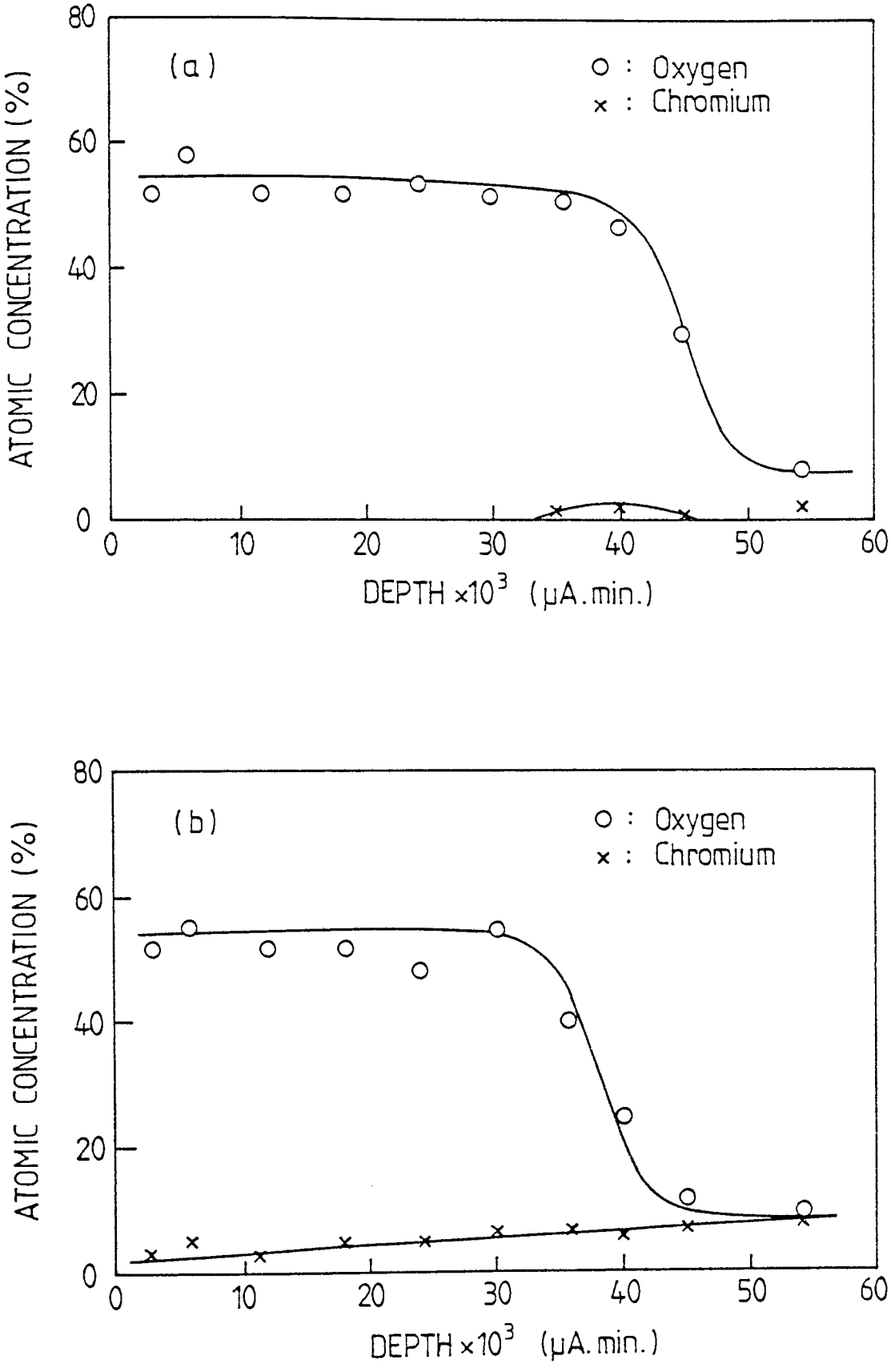

FIG. 2.19 OXYGEN AND CHROMIUM CONCENTRATION VERSUS DEPTH PROFILES FOR WORN SURFACES FROM BS EN8 ON 9% CHROMIUM EXPERIMENTS GENERATED AT A LOAD OF 39N. (a) BS EN8 PIN SURFACE ,(b) 9% CHROMIUM STEEL DISC SURFACE.

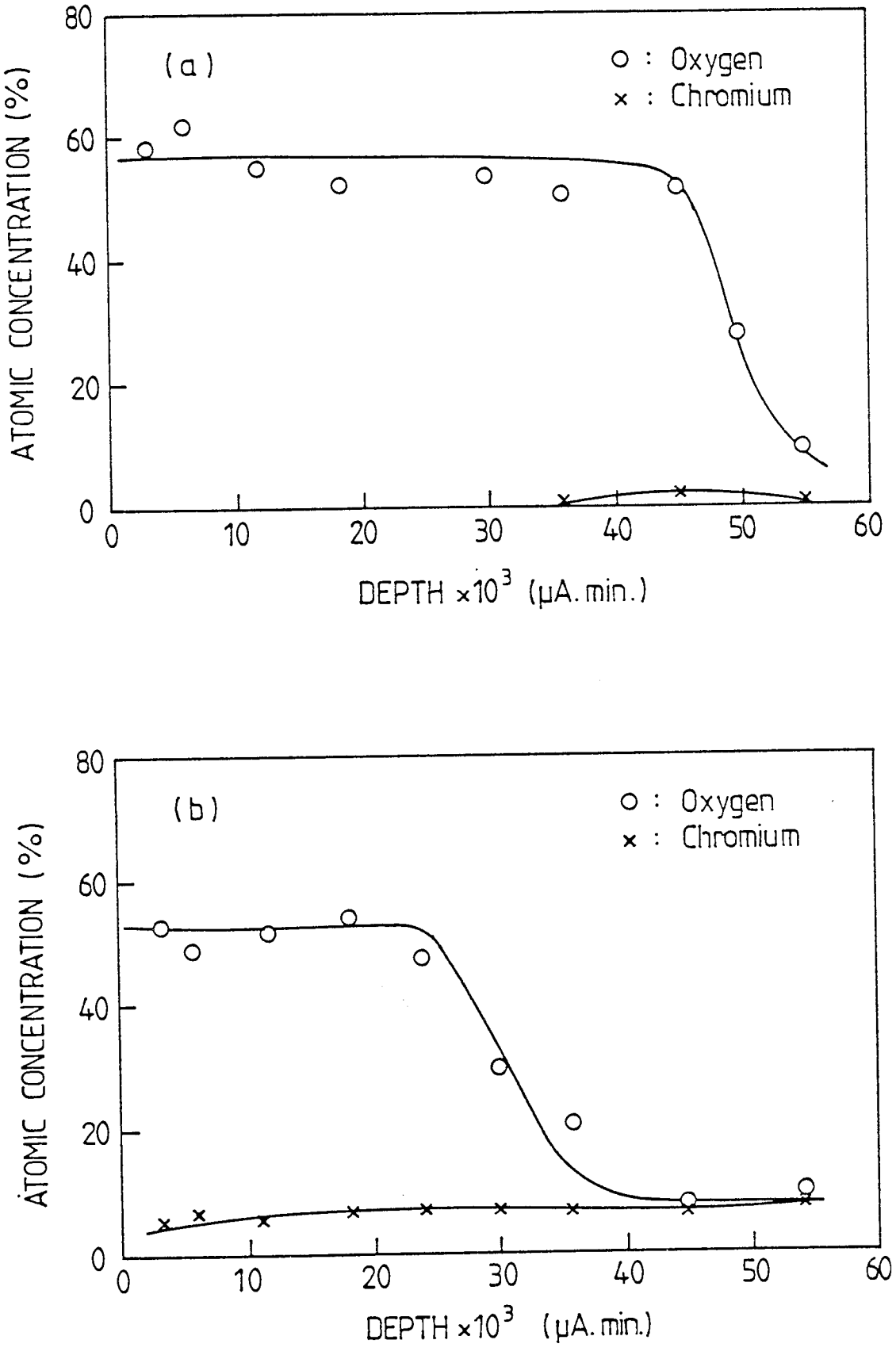

FIG. 2.20 OXYGEN AND CHROMIUM CONCENTRATION VERSUS DEPTH PROFILES FOR WORN SURFACES FROM BS EN8 ON 9% CHROMIUM EXPERIMENTS GENERATED AT A LOAD OF 49N. (a) BS EN8 PIN SURFACE ,(b) 9% CHROMIUM STEEL DISC SURFACE.

X-ray photoelectron spectroscopy is of limited use in examination of the oxides of iron for the reasons outlined by Mills and Sullivan[159], however, experiments were conducted prior to Auger analysis and revealed the presence of FeOOH on the surfaces of all oxide films examined. The compound extended to a depth of no more than a few atomic diameters and would not be observable with other techniques. This common outer layer could explain why friction is similar for the three oxide regimes with no observable transitions between oxide types.

2.2.5 Heat Flow Analysis

Heat flow into the pin and surface temperatures were calculated from heat flow data and these are reported in the next section, 2.3

2.3 Theoretical Determination of Surface Parameters

Following an approach due to Quinn[175] for a stationary pin loaded against a rotating disc, but assuming a surface model of N contacting asperities at any instant on both pin and disc, each situated on stable oxide plateaux of critical thickness ξ_p and ξ_d respectively. Then the

proportion of the frictional heat generated flowing in to the pin may be expressed as[47]:

$$\delta = \frac{\theta_d}{\theta_d + \theta_p} \qquad (2.1)$$

where θ_d is the fictitious excess temperature at a contacting asperity on the disc if it is assumed that all the frictional heat flows into the disc and θ_p the corresponding value for the pin assuming that all the heat flows into the pin.

The fictitious temperatures may be written as[175]:

$$\theta_p = \frac{H_T}{4aNK_s} + \frac{H_T\xi_p}{\pi a^2 NK_o} \qquad (2.2)$$

$$\theta_d = \frac{\beta H_T}{4aNK_s} + \frac{\beta H_T\xi_d}{\pi a^2 NK_o} \qquad (2.3)$$

where β is a dimentionless parameter related to speed and which may be written as $\beta = (0.86 - 0.10\ (Ua/2\chi_o))$ for medium speeds[47]; U = the linear velocity; a = mean radius of asperity contact; χ_o = thermal diffusivity of the oxide; K_o and K_s thermal conductivities of oxide and steel respectively; H_T = total heat per second evolved at the pin disc interface and ξ_p and ξ_d the critical oxide thickness on pin and disc respectively.

From equations (2.2) and (2.3) the asperity contact temperatures on pin and disc may be expressed as:

$$T_{c_{pin}} = T_s + \frac{H_1}{4aNK_s} + \frac{H_1 \xi_p}{\pi a^2 N K_o} \qquad (2.4)$$

and

$$T_{c_{disc}} = T_d + \frac{\beta(H_T - H_1)}{4aNK_s} + \frac{\beta(H_T - H_1)}{\pi a^2 N K_o} \xi_d \qquad (2.5)$$

where T_s and T_d are surface temperatures of the pin and disc respectively and H_1 the heat flow into the pin through the asperity contacts.

It has been assumed in previous work[85], that H_1 was equal to the total heat flow into the pin measured by the calorimeter method described by Rowson and Quinn[75]. This is probably true for experiments conducted at room temperature, but for elevated temperatures consideration must also be given to heat flow through the air gap between pin and disc. Calculations indicate that although convection and radiation effects are negligible, there is a considerable contribution to heat flow into the pin from conduction through the air gap. Hence in the experiments employing a heated disc, the measured heat flow, H_1(measured) entering the pin consists of a component due to conduction through the contacting asperities plus a

component due to conduction through the air gap. Heat flow due to conduction through the air gap may be represented to a first approximation by the equation:

$$H_{con} = \frac{K_{air}\ A\ (T_d - T_s)}{h} \qquad (2.6)$$

where K_{air} = thermal conductivity of the air at temperature T_s; A the apparent area of contact of the pin and h the mean width of the air gap estimated to be 15 μm from surface profile measurements. Hence:

$$H_1 = H_1\ (\text{measured}) - H_{con} \qquad (2.7)$$

The value of H_1 derived in this way was the one used in all calculations. As an illustration of the relative magnitude of these terms, corrected values of heat flow into the disc for experiments conducted at 500^0C disc temperature are given in Table 2.6.

Although it is obvious from the data in Table 2.6 that surface temperatures of pin and disc may be quite different the temperatures at the contacting asperities must be the same, that is, $T_{c_{pin}} = T_{c_{disc}}$. Hence equating these quantities, Equations (2.4) and (2.5), produces a quadratic in "a" of the form:

TABLE 2.6

Heat flow data at a disc temperature of 500°C.

Load N	H_l (measured) W	H_T W	T_s °C	H_{con} W	H_l (measured) - H_{con} W
9.8	10.7	13.4	410	9.7	1.0
19.6	12.7	19.5	456	5.0	7.7
39.2	13.4	29.6	449	5.7	7.7
49.1	13.5	39.6	472	3.2	10.3
58.9	14.5	43.0	473	3.2	11.2
78.5	13.9	53.7	470	4.8	9.1
98.1	14.9	65.5	486	2.6	12.3
107.9	17.3	73.9	514	-2.6	19.9
117.7	14.6	80.6	494	0.7	13.9
137.3	16.6	86.7	520	-3.0	19.6
157.0	15.7	99.1	515	-2.6	19.3

$$Aa^2 + Ba + C = 0 \qquad (2.8)$$

If we assume plastic deformation at the asperities and further assume that junction growth is negligible, then according to Bowden and Tabor[23], the real area of contact A_r may be written:

$$A_r = N\pi a^2 = \frac{W}{P_m} \qquad (2.9)$$

where W = load and P_m = the flow pressure of the underlying material.

This equation, (2.9), may then be used to eliminate N from the equation (2.8) so that the constants may be written:

$$A = \frac{0.10\ \pi\ P_m\ U\ (H_T - H_\perp)}{8\ \chi_o\ K_s\ W}$$

$$B = \frac{P_m}{W}\left\{\frac{H_\perp \pi}{4K_s} - \frac{0.86\ \pi\ (H_T - H_\perp)}{4K_s} + \frac{0.1\ U\ (H_T - H_\perp)\xi_d}{2\chi_o K_o}\right\}$$

$$C = \frac{P_m}{W}\left\{\frac{H_\perp \xi_p}{K_o} - \frac{0.86\ (H_T - H_\perp)\xi_d}{K_o}\right\} - \{T_s - T_d\}$$

Equation (2.8) has two solutions if $B^2 > 4AC$. In practice the equation generates a positive and a negative root and the positive root gives a value for the mean radius of an asperity contact. Thus providing the critical oxide thicknesses are known the equation may be solved for "a" using heat flow data, typical values of which are given in Table 2.6.

Before this calculation may be attempted, however, the temperature must be identified at which the temperature dependent parameters K_s, K_o, χ_o and P_m should be determined. It was decided that the properties of the metal, P_m and K_s, should be those corresponding to the general surface temperature while those associated with the oxide, K_o and χ_o, should be calculated at the contact temperature. The variations of P_m with temperature for the steels used in this investigation are shown in Figure 2.2. Values of K_s for low alloy steels have been published by Smithells[176] for temperatures up to 800^0C.

Molgaard and Sweltzer[177] have proposed expressions for temperature variation of the thermal conductivity K_o of the oxides α - Fe_2O_3 and Fe_3O_4 and these were used in the calculation of that quantity in the appropriate oxide regime. No such expression exists for the oxide FeO, hence in regions where this oxide predominates values appropriate to Fe_3O_4 were employed. Thermal diffusivity of the oxide χ_o was then calculated from the relation:

$$\chi_o = \frac{K_o}{\rho_o C_o}$$

where ρ_o = oxide density and C_o the specific heat capacity. No published data on temperature variation of these latter two quantities could be found, hence low temperature values were used.

Although surface temperatures were calculated from heat flow measurements, the contact temperatures are unknown. In order to determine a value for contact temperature an iteration process must be introduced into the calculations. The following procedure was adopted. A value was assumed for critical oxide thickness ξ_p on the pin. To simplify the calculations it was further assumed that ξ_p is equal to ξ_d. This assumption is not strictly valid, but scanning electron micrographs indicate that thicknesses are very similar and calculations show the results to be insensitive to changes in the values of ξ_d.

For this chosen value of ξ_d the oxide parameters K_o and χ_o were calculated[177] at the measured general surface temperature T_s. These values together with the other relevant data, were used to calculate a value for contact radius "a" from the quadratic equation (2.8). A value for the number of contacts N was determined from (2.9) and hence the contact temperature T_c calculated from Equation (2.4).

In the next step of the iteration new values of K_o and χ_o were recalculated at the new contact temmperature and the procedure was repeated to generate new values of a, N and T_c . The process was further repeated until the iteration was terminated when two subsequent contact temperatures were within 1% of each other. At this stage a value of δ was calculated from Equation (2.1) and compared with an experimentally determined value δ (expt) = $\frac{H_1}{H_T}$.

The whole iteration was repeated for different values of ξ_p and the values of ξ_p , a, N and T_c were recorded when the best comparison between δ and δ(expt) was obtained. In the computer program used to perform the iteration, oxide thicknesses were varied from 0.5 μm to 15 μm in steps of 0.1 μm.

Selected results from the computer search for experiments conducted on 52100 steel are shown in Figures 2.21, 2.22, 2.23 and 2.24. Figure 2.21 shows the variation in the number of asperity contacts with load for an unheated disc and Figure 2.22 shows the equivalent variation of mean contact radius. Number of contacts tend to increase with increased disc temperature and mean contact radii decrease. This general trend was similar for all other conditions. Figure 2.23 shows values of calculated oxide thickness with load for unheated disc experiments and for disc temperatures of 200^{0}C and 500^{0}C. Here the general trend is for an increase in oxide thickness with increased load with obvious transitions where there has been a change in oxide type.

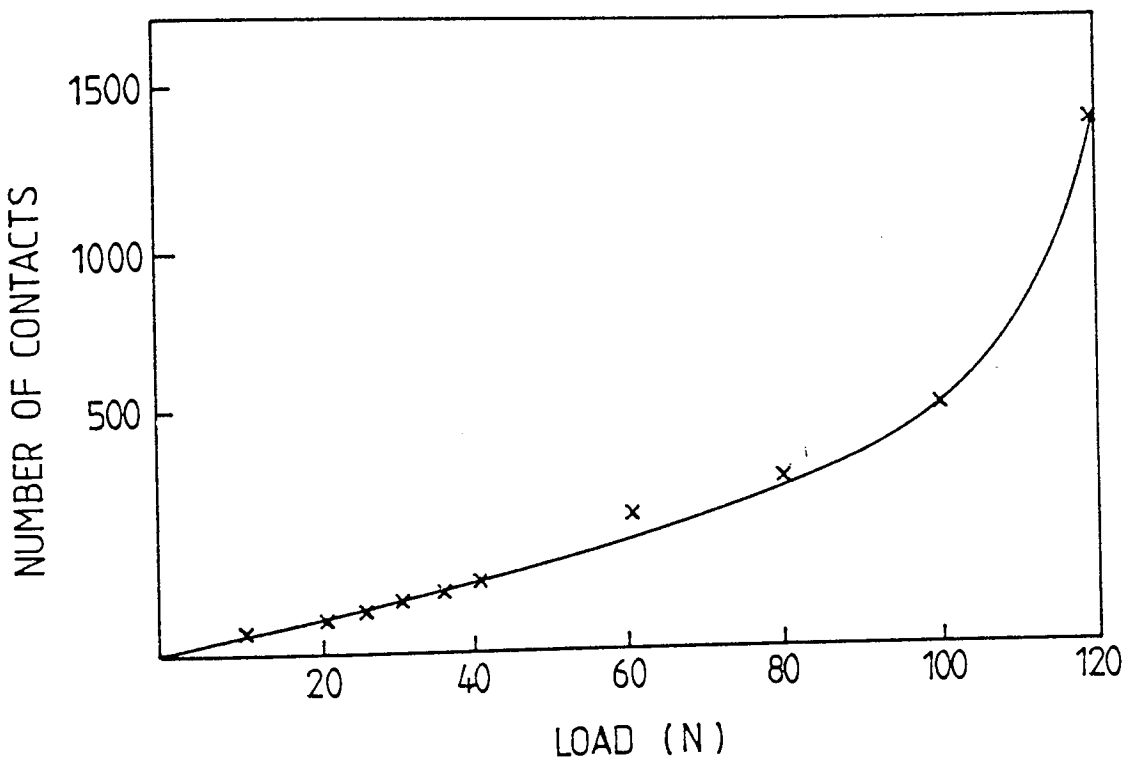

FIG. 2.21 CALCULATED NUMBER OF ASPERITY CONTACTS VERSUS LOAD FOR 52100 ON 52100 EXPERIMENTS CONDUCTED WITHOUT EXTERNAL HEATING.

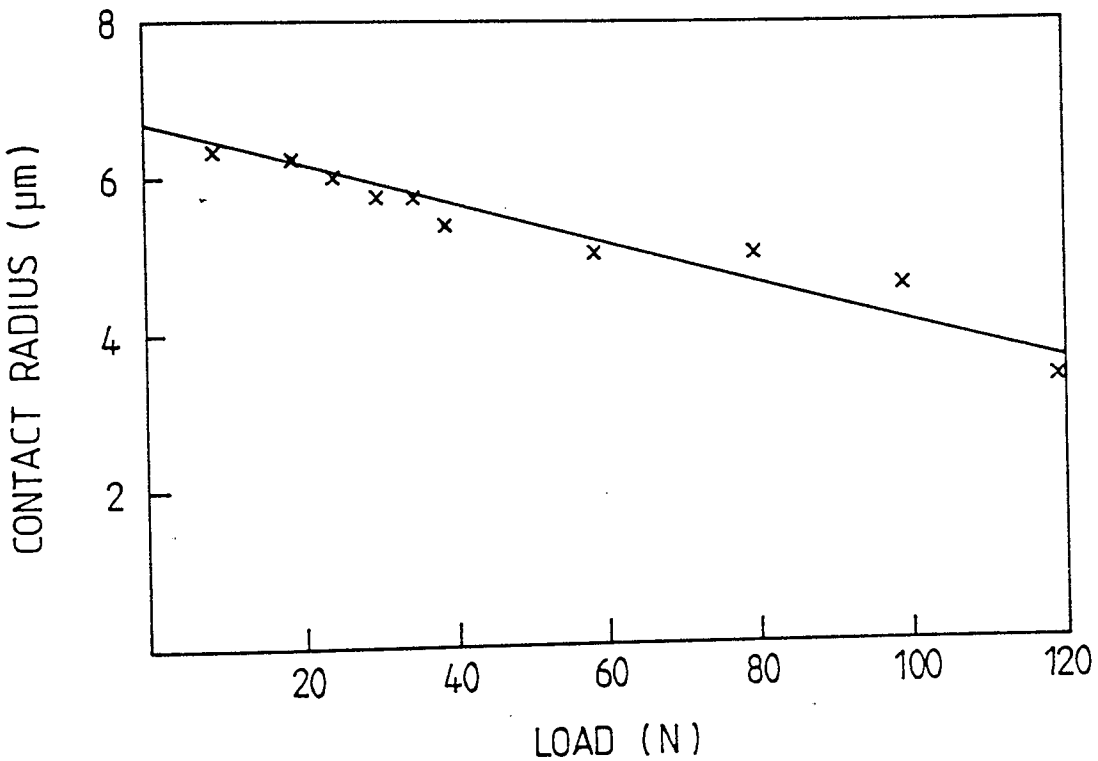

FIG. 2.22 CALCULATED MEAN CONTACT RADIUS VERSUS LOAD FOR 52100 ON 52100 EXPERIMENTS CONDUCTED WITHOUT EXTERNAL HEATING.

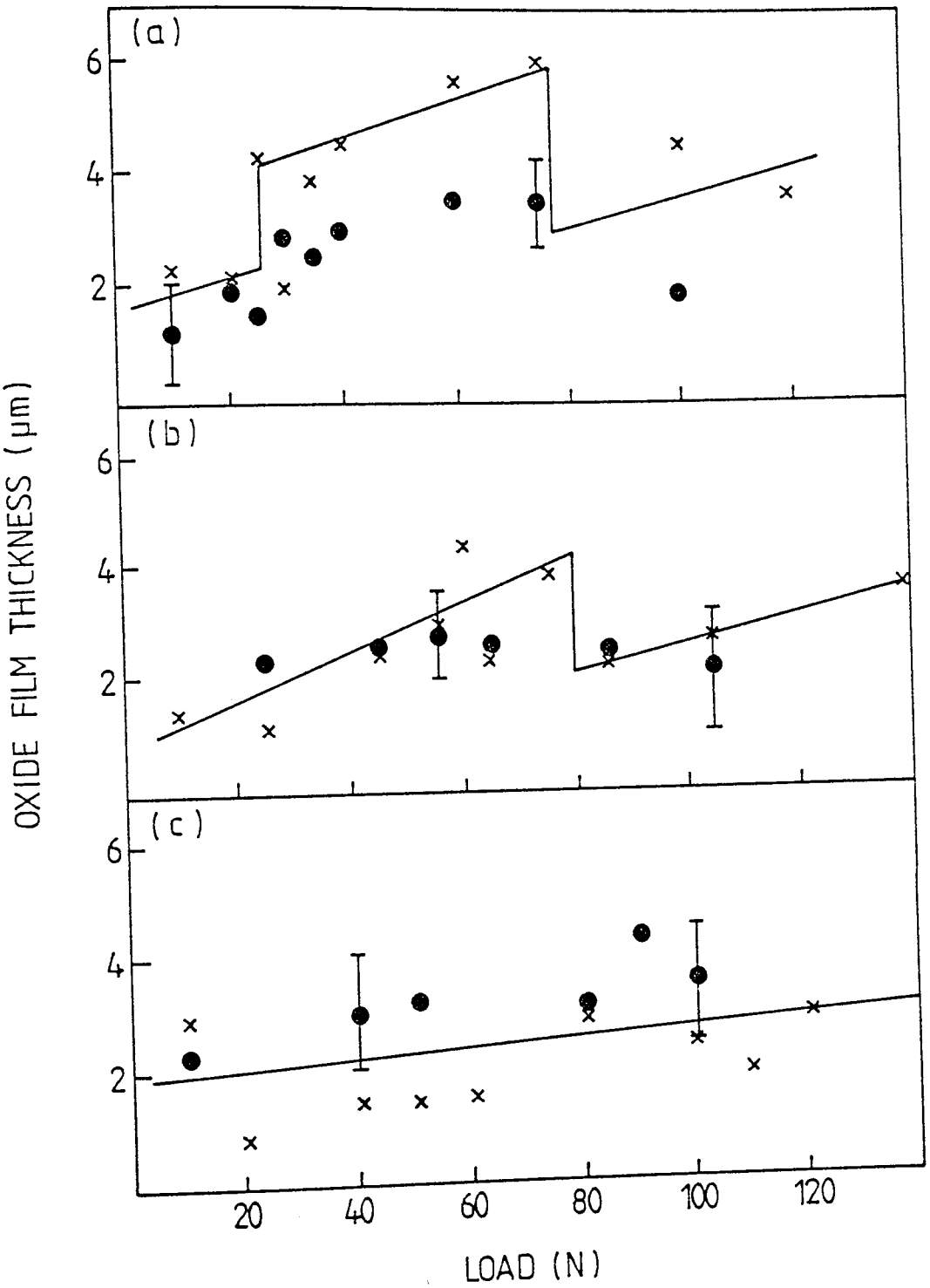

FIG. 2.23 CALCULATED OXIDE FILM THICKNESS VERSUS LOAD FOR 52100 ON 52100 EXPERIMENTS AT VARIOUS DISC TEMPERATURES ; (a) NO EXTERNAL HEATING, (b) 200°C AND (c) 500°C.(CALCULATED POINTS ARE REPRESENTED BY x ; SEM MEASURED POINTS BY • .)

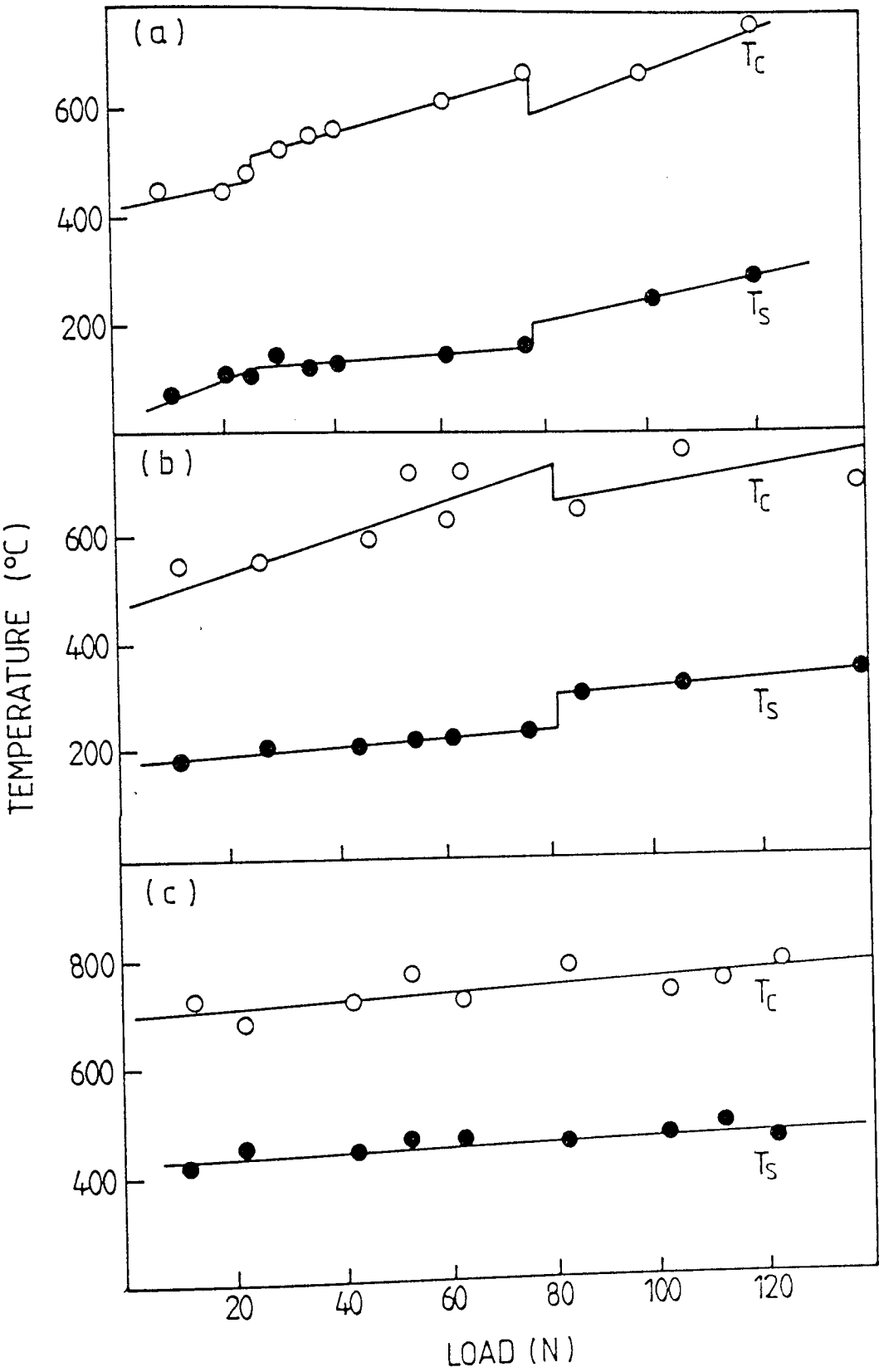

FIG. 2.24 ASPERITY CONTACT TEMPERATURE (T_c) AND GENERAL SURFACE TEMPERATURE (T_s) VERSUS LOAD FOR 52100 ON 52100 EXPERIMENTS AT VARIOUS DISC TEMPERATURES ; (a) NO EXTERNAL HEATING, (b) 200 °C AND (c) 500 °C.

Measured values of oxide thickness on pin surfaces are also shown on this figure. Considering possible errors both in computation and surface measurements, there is, remarkable agreement between these two sets of results.

Figure 2.24 shows both pin surface and contact temperature variations with load for the same conditions as for the previous figure. From these graphs it is possible to find transitions in the values of T_c corresponding to known oxide type changes. For example in experiments conducted without external heating, Figure 2.4 (a), transitions occur at about 25 N (α - Fe_2O_3 to Fe_3O_4) and 80 N (Fe_3O_4 to FeO). One can only really apply the interpretation to this set of results with prior knowledge, since it has been shown that Fe_3O_4 forms the thicker oxide with better coverage and hence slightly higher contact temperatures are to be expected in this region.

Figures 2.25, 2.26, 2.27 and 2.28 show the equivalent series of results from the computer search for experiments conducted on BS EN8 steel. It can be seen that the same pattern emerges as for the previous material and again measured oxide thickness values are very close to those calculated.

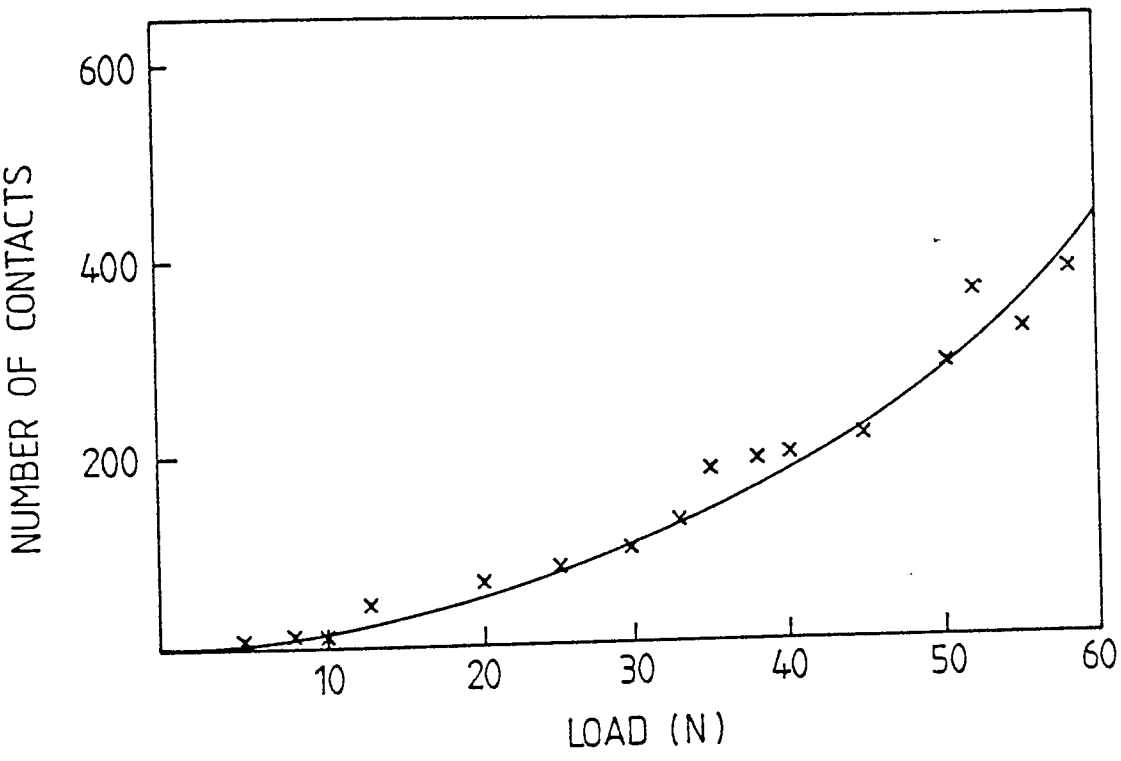

FIG. 2.25 CALCULATED NUMBER OF ASPERITY CONTACTS VERSUS LOAD FOR BS EN8 ON BS EN8 EXPERIMENTS.

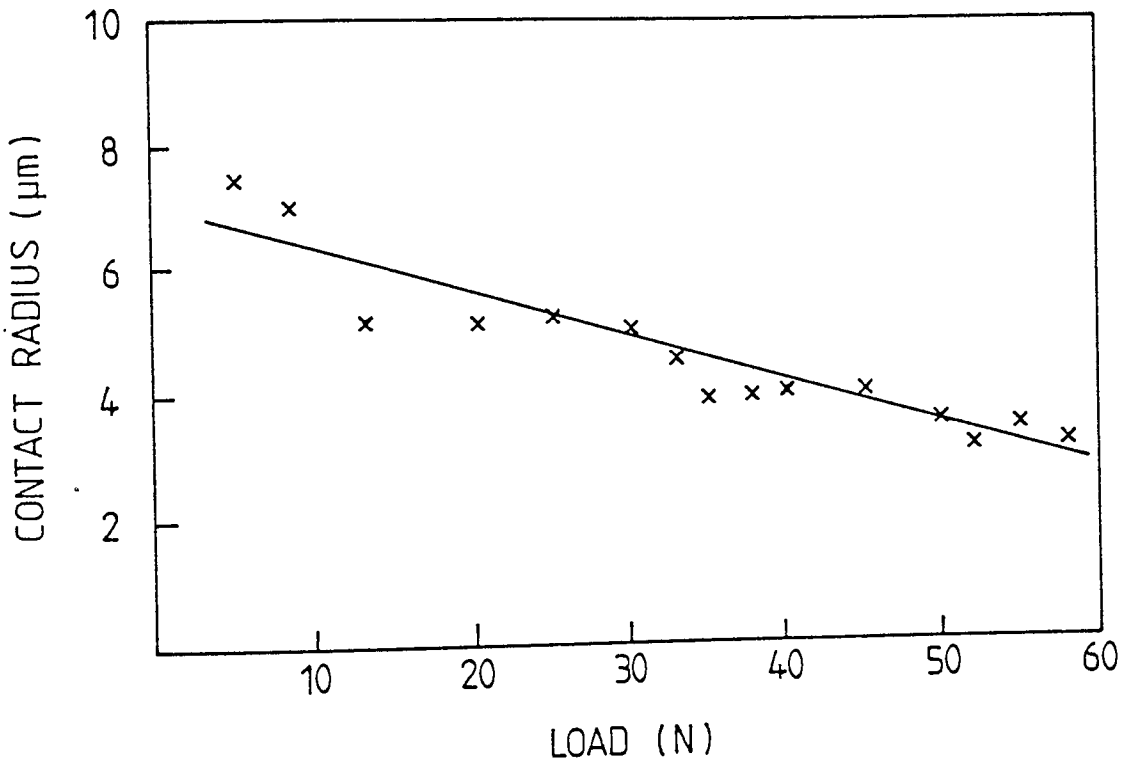

FIG. 2.26 CALCULATED MEAN CONTACT RADIUS VERSUS LOAD FOR BS EN8 ON BS EN8 EXPERIMENTS.

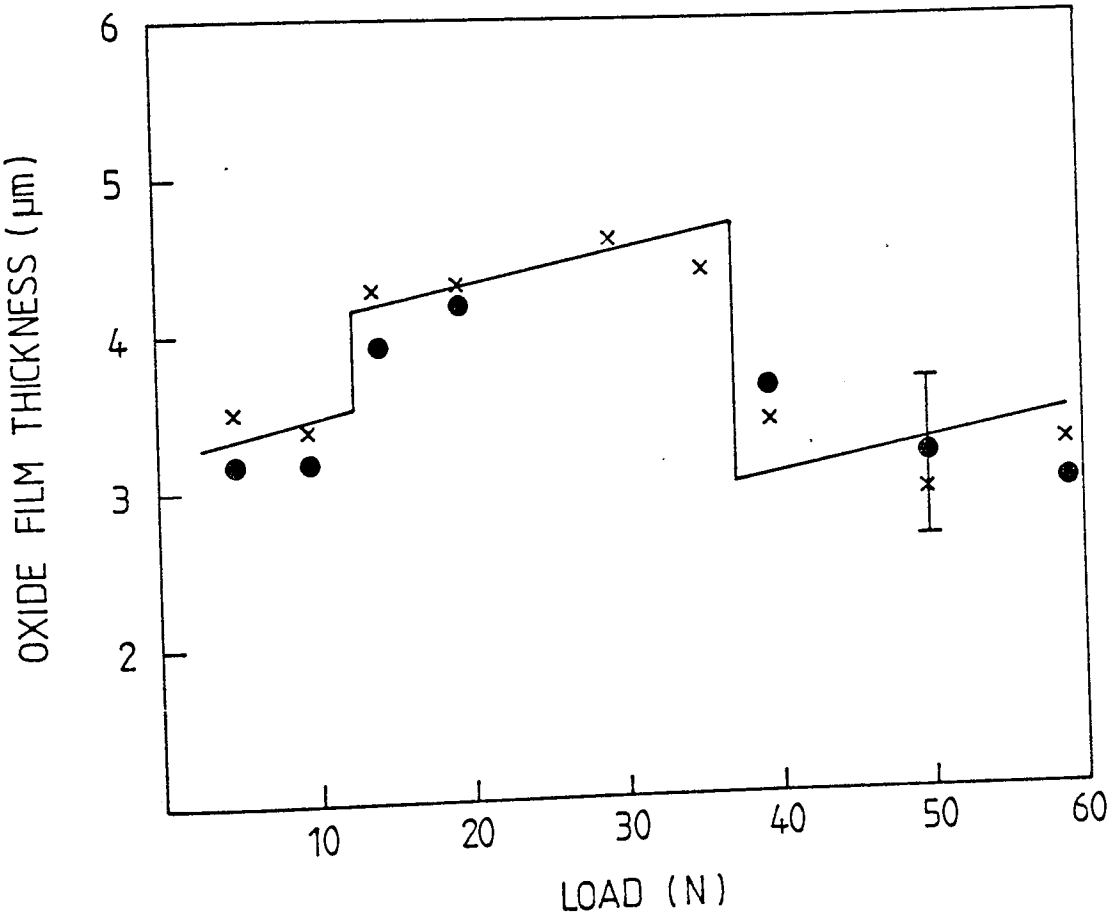

FIG. 2.27 CALCULATED OXIDE FILM THICKNESS VERSUS LOAD FOR BS EN8 ON BS EN8 EXPERIMENTS.(CALCULATED POINTS ARE REPRESENTED BY x ; SEM MEASURED POINTS BY ●.)

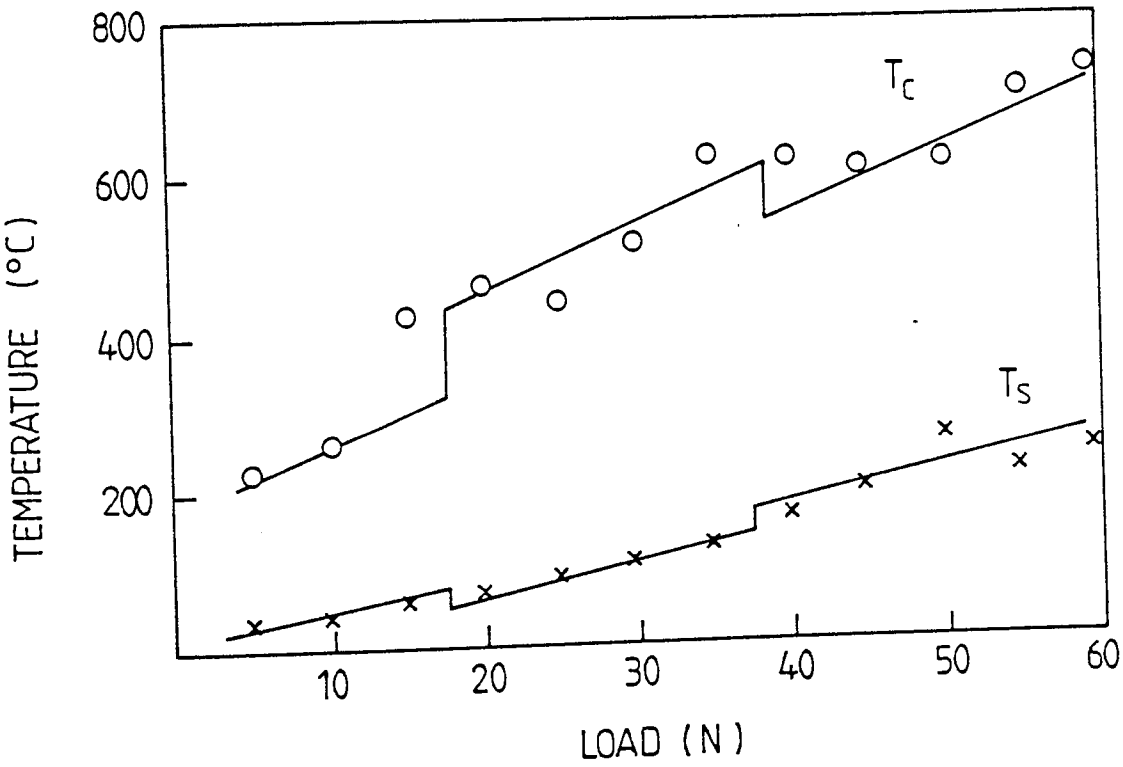

FIG. 2.28 ASPERITY CONTACT TEMPERATURE (T_c) AND GENERAL SURFACE TEMPERATURE (T_s) VERSUS LOAD FOR BS EN8 ON BS EN8 EXPERIMENTS.

2.4 Oxidational Wear at Elevated Temperatures

In the oxidational wear theory originally proposed by Quinn[84], the origins and developments of which were reviewed by Quinn, Sullivan and Rowson[85], a basic premise was that significant oxidation takes place only at the asperity contact temperatures or something close to this. There are good reasons for making this assumption for low ambient temperatures and these are outlined in Chapter 1 of this work. At elevated temperatures, however, or where contact temperatures are not too different to those of the surface, out of contact oxidation could be significant. Quinn[178], after discussions with this author, took some account of out of contact oxidation in an extension of the oxidational wear theory. In this section this basic approach is developed further.

If we assume pin on disc configuration and further assume a uniform distribution of N asperities on the pin surface for a given load W, than the number of contacts per unit area, n, is:

$$n = \frac{4N}{\pi D^2} \qquad (2.10)$$

where D = diameter of the pin.

This will also be equal to the contact density on the disc.

During rotation a given asperity will generate an annulus of width 2a on the disc wear track. Thus the number of contacts within this annulus, n_c , is

$$n_c = \frac{16a\ R\ N}{D^2} \qquad (2.11)$$

where R = mean radius of the wear track. n_c is also equal to the number of contacts made per revolution by a single contact on the pin surface.

If it is assumed that the probability of producing a wear particle per revolution is K^1 (where K^1 is analogous to the Archard K factor), then $1/K^1$ is the number of revolutions required to produce a critical oxide film thickness ξ which then becomes detached to form a wear particle.

Hence the number of encounters required to form this critical thickness is

$$\frac{1}{K} = \frac{1}{K^1}\frac{16a\ R\ N}{D^2} \qquad (2.12)$$

so that the probability of producing a wear particle per single encounter is:

$$K = \frac{K^1 D^2}{16a R N} \qquad (2.13)$$

For a single revolution the total time of oxidation, t_r, for an asperity is:

$$t_r = t_{rc} + t_{rs} = \frac{2\pi R}{U} \qquad (2.14)$$

where t_{rc} = time the asperity is in contact and t_{rs} = time the asperity is out of contact during one revolution.

$$t_{rc} = \frac{\text{Number of contacts per revolution} \times \text{distance of sliding}}{\text{Velocity}}$$

Hence from (2.11)

$$t_{rc} = \frac{32 R N a^2}{UD^2} \qquad (2.15)$$

If t_c is the total asperity contact time required to generate an oxide of critical thickness then

$$t_c = \frac{1}{K^1} t_{rc} = \frac{2a}{KU} \qquad (2.16)$$

the same result as for Quinn's original low temperature theory.

The time out of contact for one revolution:

$$t_{rs} = \frac{2\pi R}{U} - \frac{32\ RN\ a^2}{UD^2} \qquad (2.17)$$

Hence the total out of contact oxidational time, t_s , is:

$$t_s = \frac{1}{K^1} \cdot t_{rs}$$

$$= \frac{D^2}{8a\ KNU} \left\{ \pi - \frac{16\ Na^2}{D^2} \right\}$$

The second term in the brackets is negligible, hence:

$$t_s = \frac{\pi D^2}{8a\ NKU} \qquad (2.18)$$

If it is assumed that critical oxide film thickness growth is due to both in and out of contact oxidation. Then the critical thickness, ξ, may be written:

$$\xi = \xi_c + \xi_s \qquad (2.19)$$

where ξ_c = component of growth in contact

ξ_s = component of growth out of contact.

If it is further assumed that a parabolic growth rate law applies to this form of tribological oxidation, then

$$\Delta m_c^2 = k_p(T_c) \cdot t_c \qquad (2.20)$$

and

$$\Delta m_s^2 = k_p(T_s) \cdot t_s \qquad (2.21)$$

where Δm is the mass uptake of oxygen per unit area and $k_p(T)$ the parabolic growth constant at absolute temperature T.

The mass uptakes per unit area may be written in terms of the density of oxide formed in contact, ρ_c, and out of contact ρ_s; oxide thickness ξ_c and ξ_s and fraction of the film which is oxygen f_c and f_s. Hence:

$$\Delta m_c = f_c \rho_c \xi_c \qquad (2.22)$$

and

$$\Delta m_s = f_s \rho_s \xi_s \qquad (2.23)$$

From (2.19), (2.22) and (2.23)

$$\xi = \frac{\Delta m_c}{f_c \rho_c} + \frac{\Delta m_s}{f_s \rho_s}$$

or

$$\xi = \frac{(k_p(T_c)\ t_c)^{1/2}}{f_c \rho_c} + \frac{(k_p(T_s)\ t_s)^{1/2}}{f_s \rho_s} \qquad (2.24)$$

Substituting for t_c and t_s from (2.16) and (2.18).

$$\xi = \left\{ \frac{k_p(T_c)\ 2a}{U\ K} \right\}^{1/2} \frac{1}{f_c \rho_c} + \left\{ \frac{\pi k_p(T_s) D^2}{8aK\ N\ U} \right\}^{1/2} \frac{1}{f_s \rho_s}$$

(2.25)

re-arranging (2.25) in terms of K and substituting in the Archard wear law equation $w = KA_r$ gives:

$$w = \left[\frac{2ak_p(T_c)}{UP_m f_c{}^2 \rho_c^2 \xi^2} + \frac{\pi D^2 k_p(T_s)}{8P_m aNU f_s{}^2 \rho_s{}^2 \xi^2} + \frac{D\left(\frac{\pi k_p(T_c) k_p(T_s)}{N}\right)^{1/2}}{UP_m f_c \rho_c f_s \rho_s \xi^2} \right] W$$

(2.26)

If out of contact oxidation is neglected this reduces to the same equation as for Quinn's simple model.

Equation (2.26) provides a general quantitative expression for the oxidational wear rate as a function of load. The quantity in the bracket of this equation, which is equivalent to the Archard wear factor, contains a number of parameters where direct measurement is not possible. Specifically, these are N, a, T_c and the tribological growth constants $k_p(T_c)$ and $k_p(T_s)$. The surface model developed in Section 2.3 gives a completely independent estimate of N, a, T_c and ξ from heat flow measurement. The results gained from this model in the one area where

direct comparison between theoretical predictions and experimentally measured values is possible, namely oxide film thicknesses, agree so well that there can be some confidence that the other quantities represent a good approximation to real values.

The problem then is to decide which growth constants are appropriate. A substantial amount of evidence has been presented in this work to show that the oxides produced are homogeneous diffusion controlled thick films where it is known that growth is governed by a parabolic growth rate law. The growth constant may be written in Arrhenius form as:

$$k_p = A_p \exp - \left(\frac{Q_p}{RT_o}\right)$$

where A_p = Arrhenius constant, Q_p = activation energy, R = molar gas constant and T_o = oxidational temperature.

Rate constants measured under static conditions cannot in general account for tribological oxide films, where growth rates may be many orders of magnitude greater. Sullivan, Quinn and Rowson[59] have argued that the activation energy for oxidation might be expected to be similar for both static and tribo oxidation, but that Arrhenius constants will be very different and this difference accounts for the increase in rate constants. They determined values of Q_p from the data of Caplan and Cohen[102] and generated appropriate tribological values

of A_p from oxidational wear experiments on low alloy steels. The values, obtained for the different oxide regimes, are as follows:

(i) $T_o < 450^0C$, $A_p = 10^{16} kg^2 m^{-4} s^{-1}$
$Q_p = 208$ kJ. mole^{-1}

(ii) $450^0C < T_o < 600^0C$, $A_p = 10^3 kg^2 m^{-4} s^{-1}$
$Q_p = 96$ kJ mole^{-1}

(iii) $T_o > 600^0C$, $A_p = 10^8 kg^2 m^{-4} s^{-1}$
$Q_p = 210$ kJ mole^{-1}

Writing equation (2.26) in the form:

$$w = [H + I + J] W \qquad (2.27)$$

and using the above values of A_p and Q_p, together with other experimental and generated data to calculate the relative magnitudes of H, I and J for selected experiments, it is found that I and J are negligible for temperatures below 300^0C, but become dominant at temperatures greater than this. For example for an experiment conducted without external heating on 52100 steel at a load of 98 N, the calculated surface and contact temperatures were $T_s = 232^0C$

and $T_c = 675^0C$. Inserting these temperatures and all other relevant parameters in (2.27) gives:

$$H = 0.22 \times 10^{-13} \; m^3 m^{-1} N^{-1}$$

$$I = 0.002 \times 10^{-13} \; m^3 m^{-1} N^{-1}$$

$$J = 0.01 \times 10^{-13} \; m^3 m^{-1} N^{-1}$$

Comparing this with a further experiment on 52100 steel at a disc temperature of 300°C and load 98 N where the calculated temperatures were $T_s = 304^0C$ and $T_c = 580^0C$, then:

$$H = 0.17 \times 10^{-13} \; m^3 m^{-1} N^{-1}$$

$$I = 0.30 \times 10^{-13} \; m^3 m^{-1} N^{-1}$$

$$J = 1.14 \times 10^{-13} \; m^3 m^{-1} N^{-1}$$

At surface temperatures much above 300^0C I and J rapidly become very much greater than H and calculated wear rates are unrealistically high. This brief analysis shows that for low ambient temperatures, out of contact oxidation may be neglected and the reduced wear rate equation:

$$w = \left\{ \frac{2a \; A_p \exp - Q_{p/RT_o}}{U \; P_m \; (\rho_o f \; \xi)^2} \right\} W \qquad (2.28)$$

is valid and its use is justified for surface temperatures below 300^0C.

In order to examine the correctness of the Arrhenius constants proposed by Sullivan, Quinn and Rowson[59], the same values of Q_p were used, but data was taken from the room temperature experiments on both low alloy steels from this investigation and used to generate new values of A_p for the three oxide regimes using Equation (2.28). The results shown in Table 2.7 are in general agreement with those of Sullivan, Quinn and Rowson[59]. The exception is for the α - Fe_2O_3 region of 52100 steel. Here the calculated A_p values are six orders of magnitude lower. X-ray diffraction analysis of the debris from the region, reported in section 2.2, showed the presence of Fe_3O_4 (see Table 2.2). It is thus possible that although present as a minority compound in the region below the first transition, the Fe_3O_4 determines the kinetic growth rate. If this is so and the tribo-oxidation Arrhenius constant is calculated assuming an activation energy appropriate to Fe_3O_4 (that is Q_p = 96 kJ $mole^{-1}$) then a mean value of $A_p = 8.9 \times 10^2 kg^2 m^{-4} s^{-1}$ with $7.6 \times 10^2 kg^2 m^4 s^{-1}$ standard deviation is obtained, which agrees well with other measurements for the Fe_3O_4 region. The results of these calculations are also shown in Table 2.7. Some caution should be exercised when using data for α - Fe_2O_3, however, since static measurements are not reliable.

TABLE 2.7.

Calculated values of Arrhenius constants from data taken from room temperature experiments.

Load N	Tribo-oxidation Arrhenium Constants $kg^2m^{-4}s^{-1}$					
	52100			BS EN8		
	α-Fe_2O_3	Fe_3O_4	FeO	α-Fe_2O_3	Fe_3O_4	FeO
4.9				1.0×10^{17}		
7.4				4.6×10^{14}		
9.8	1.9×10^{10}	1.5×10^{2}		2.8×10^{16}		
12.3					4.7×10^{2}	
14.7					8.8×10^{2}	
19.6	6.1×10^{10}	1.5×10^{3}			1.1×10^{3}	
24.5	3.6×10^{10}	1.6×10^{3}			8.1×10^{2}	
29.4	2.5×10^{10}	3.2×10^{2}			7.0×10^{2}	
34.3		1.4×10^{3}			2.6×10^{2}	
39.2		3.2×10^{2}				
44.1						3.0×10^{8}
49.0		1.0×10^{3}				6.5×10^{7}
53.5						2.0×10^{8}
55.9						6.1×10^{7}
58.4		2.1×10^{2}				3.9×10^{7}
74.5		7.0×10^{2}				
98.1			2.2×10^{8}			
117.7			1.0×10^{7}			
Mean A_p	2.9×10^{10}	7.3×10^{2}	1.2×10^{8}	4.3×10^{16}	6.8×10^{2}	1.3×10^{8}
Standard Deviation	2.4×10^{10}	4.9×10^{2}	1.5×10^{8}	5.0×10^{16}	3.3×10^{2}	1.1×10^{8}

Using these calculated values of A_p in either equations (2.26) or (2.28) gives reasonable agreement between theoretical and experimental wear rates for surface temperatures less than 300^0C. When surface temperature exceeds this value, however, theoretical wear rates become much greater than those measured. For example taking an experiment for a disc temperature of 300^0C and load of 117.7 N where $T_s = 337^0$C and $T_c = 740^0$C, the wear rate calculated from (2.28) is $220 \times 10^{-13} m^3 m^{-1}$ and that from (2.26) $720 \times 10^{-13} m^3 m^{-1}$ but the measured wear rate from this experiment was $79 \times 10^{-13} m^3 m^{-1}$. The discrepancy was typical and its magnitude increased with increase in temperature.

It is obvious that the tribo-oxidational growth constants which produce good agreement at low ambient temperatures are not appropriate when temperatures increase beyond a certain level. Table 2.8 shows wear rates calculated from equation (2.26) for an experiment conducted at a disc temperature of 500^0C. Three separate conditions are shown the first assumes that tribo-oxidational Arrhenius constants apply to both in and out of contact oxidation and this yields wear rates which are of the order of 10^6 times too large. The second possibility, illustrated in column 2 of the table, is that tribo-oxidation constants apply to in contact oxidation, but that static constants apply to out of contact oxidation. Again it may be seen from the table that this condition yields wear rates 10^2 to 10^3 times too

TABLE 2.8.

Calculated and measured wear rates for experiments on steel at a disc temperature of 500°C.

In column 1 tribo-oxidation Arrhenius constants are assumed to apply both in and out of contact oxidation.

In column 2 tribo-oxidation Arrhenius constants are assumed to apply to in contact, but static Arrhenius constants to out of contact oxidation.

In column 3 it is assumed that static Arrhenius constants apply to both in and out of contact oxidation.

Load N	Wear rates x 10^{-13} m^3m^{-1}			
	1	2	3	Measured
9.8	2.3 x 10^6	10.9	0.2	1.5
19.6	35 x 10^6	218	5.6	2.2
39.2	43 x 10^6	327	1.6	2.9
49.1	31 x 10^6	1090	3.6	3.3
58.9	21 x 10^6	436	2.6	5.0
78.5	24 x 10^6	872	1.9	6.7
98.1	31 x 10^6	545	2.0	8.5
107.9	50 x 10^6	1090	4.2	8.6
117.7	33 x 10^6	1526	3.2	7.6
137.3	45 x 10^6	1962	4.3	13.0
157.0	31 x 10^6	1199	5.8	17.0

large. The only situation in which there is any agreement between theory and experiment is if it is assumed that static oxidation constants apply to both in and out of contact oxidation. Wear rates calculated on this basis are shown in column 3 of the table. The static Arrhenius constants used in these calculations were derived from the data of Caplan and Cohen[102] and the values were 1.5×10^{6} $kg^{2}m^{-4}s^{-1}$, for temperatures less than $450^{0}C$, $3.2 \times 10^{-2} kg^{2}m^{-4}s^{-1}$ for temperatures between 450 and $600^{0}C$ and $1.1 \times 10^{5} kg^{2}m^{-4}s^{-1}$ for temperatures greater than $600^{0}C$.

A tentative explanation for this behaviour is that at temperatures greater than $300^{0}C$ the majority of the oxidation will occur during the out of contact period where mechanical surface disruption is not as great as during contact and where oxidation does not occur during rapid transient temperature variations. Under these conditions the kinetics of growth are likely to tend to those of a statically grown film. It must then be assumed that the kinetics of in contact oxidational growth are governed by the oxide formed out of contact. Hence rapid diffusion paths will not be available and static oxidational constants will also apply. It must be realized however, that although static oxidation constants may be used to describe the growth of these tribological oxide films above $300^{0}C$ surface temperatures, the films themselves are quite different to those grown under static conditions. They are

far more tenacious and their load bearing properties are far superior.

The theoretical development discussed in this section, of a quantitative expression for wear rate when out of contact oxidation is significant is a useful aid in the understanding of the tribo-oxidation process. The brief analysis here, however, emphasises how little is known of the mechanisms involved. This is an obvious area where problems must be addressed if approaches of this type are to be exploited.

2.5 Discussion

The results presented in this chapter are concerned with mild oxidational wear and all measurements were taken after the initial severe wear running in phase, when equilibrium conditions had been established. The running in phase was not studied.

The curves showing wear rate versus load for 52100 steel for a range of temperatures, Figure 2.3 and for BS EN8 without external heating, Figure 2.4, exhibit marked transitions in wear rate when the type of oxide formed on the surface and consequently in the debris changes. The oxides associated with the various regions are listed in Tables 2.2 and 2.3.

It is obvious from the data that under any given set of circumstances wear rates are lower if Fe_3O_4 is the predominant oxide. Considering for example the wear rate versus load curves for experiments conducted without external heating. If the portion of the curves corresponding to the α - Fe_2O_3 region (below 25 N for 52100 steel and below 12 N for BS EN8) are extrapolated into the Fe_3O_4 region, wear rates of approximately twice the measured values might be expected. That is under similar conditions if it were possible to have either α - Fe_2O_3 or Fe_3O_4 as the predominant compound in the oxide, the Fe_3O_4 would be expected to have an associated wear rate half of that for α - Fe_2O_3. The same observation is true when significant amounts of FeO appear in the debris, that is after the second transition, as can be seen from the unheated, 200 and 300^{0}C curves of Figure 2.3 and from Figure 2.4, where an increase in wear rates of approximately two times is apparent.

The mechanical properties of the two steels used in the major part of this investigation are very similar, but considering the unheated experiments both transitions occur at approximately half of the value of load for the BS EN8 steel compared to the 52100 steel. The hardness of the 52100 steel was slightly the higher and this implies from Equation (2.4) a higher contact temperature at any given load. This in turn implies a lower transition load since transitions are largely temperature dependent. This is

contrary to experimental observations and hence the mechanical properties do not determine transition loads. The difference in chemical composition, however, will have an effect. The 52100 steel contains more carbon (1% compared to 0.4% for BS EN8) and contains 1% chromium. Siebert[179] has shown that iron content in the oxide is reduced with increased carbon concentration in the steel and this would tend to suppress the formation of the higher oxides, Fe_3O_4 and FeO and move the transitions to higher loads. The effect is probably less pronounced than that due to the 1% chromium in the steel, which could limit the film thickness[146]. Oxide film thicknesses measured on BS EN8 samples were greater in all oxide regimes than those on 52100 (Table 2.5) and this leads to higher contact temperatures at any given load, thus accounting for lower transition loads.

The surface scanning electron micrographs give support to the view that Fe_3O_4 is the most protective of the oxides of iron. For example, comparing the micrographs for 52100 steel in Figures 2.8 (a), (b) and (c) for loads of 9.8, 39.2 and 98.1 N respectively or expressed in terms of the predominant surface oxides, taken from regions of α - Fe_2O_3, Fe_3O_4 and FeO respectively the differences are apparent. For the oxides α - Fe_2O_3 (Figure 2.8 (a)) and FeO (Figure 2.8 (c)) the appearance of the surfaces is similar, where they consist of patchy oxide plateaux, smooth due to wear, above areas of roughened metal surface. These must be contrasted with Figure 2.8 (b) showing a surface

where the predominant oxide is Fe_3O_4 and where there is far more uniform coverage and less disruption.

A further series of photomicrographs taken from BS EN8 steel pin surfaces at loads of 9.8, 24.5 and 58.8 N is shown in Figure 2.9 (a), (b) and (c) corresponding to the three oxide regions. These are very similar to those in Figure 2.8, showing the Fe_3O_4 region to be the most protective. Scanning electron photomicrographs for some disc specimens were recorded and showed similar surface features in any given region to those of the counterpart pin.

It should be noted that the α - Fe_2O_3 region below the first transition for the unheated experiments on 52100 steel also yielded some Fe_3O_4 in the debris, although the oxide was present as a minority constituent. The transistion in this case corresponded to the point where the Fe_3O_4 became the majority component. The photomicrographs of the regions below the first transition for both steels show the same surface features. This together with the evidence of the wear data shows that the mere presence of Fe_3O_4 in the surface oxide is not sufficient to produce a wholly protective layer, but that the oxide must be the major component in the film to be effective.

Examining oxide film thicknesses both calculated from the surface model of section 2.3 and measured it can be seen that Fe_3O_4 forms a thicker oxide film than either of the other two. This better coverage and increased film

thickness undoubtedly combine to give the oxide containing a majority of Fe_3O_4 a greater protective capability.

Further evidence on the physical structure of the tribological oxide plateaux formed under the unidirectional sliding conditions of these experiments can be gained from the scanning electron micrographs of oxide plateaux edges shown in Figures 2.11 and 2.12. The figures show that the plateaux are physically homogeneous and do not consist of a layer of compacted debris. Photomicrographs of this latter type of oxide formation will be shown later in this work, but have also been published elsewhere[89]. The physical homogeneity of the oxide films in this work indicates the essential correctness of the assumption that such films grow due to a diffusion controlled mechanism similar to that responsible for thick oxide growth under static oxidizing conditions.

There have been some suggestions that such films are not oxide at all, but consist of some form of transformed metallic layer. Such suggestions have been completely refuted by the work on Auger electron spectroscopy during this investigation. The Auger elemental maps produced during argon ion removal of surface layers show them to consist wholly of oxide, as do the oxygen depth profiles which show a homogeneous distribution of oxygen with depth into the plateaux. The profiles in Figures 2.14 and 2.15 further support the evidence from electron microscopy, showing that thicker films are produced when Fe_3O_4 is

present in the debris, that thickness tends to increase with temperature and that oxide plateaux formed on both pin and disc are similar. This is important evidence since it proves that the plateaux are oxide, which is something which could only be inferred from scanning electron microscopy. A further important result in determining the nature of the oxide film and the mechanism of its formation comes from the Auger electron analysis of the system containing the 9% Cr steel, Figures 2.17 to 2.20.

Samples taken from 9% Cr disc surfaces show an oxide containing chromium with a gradation of concentration of that element varying from about 4% at the surface to about 9% at the oxide metal interface. This is consistent with diffusion controlled film growth, where after initial formation of the oxide the iron ions diffuse more rapidly through the oxide than do the chromium ions and this leads to iron rich outer layers[180]. This is particularly true if the spinel oxide is present and X-ray diffraction analyses of debris and surfaces have shown this to be a major constituent.

In contrast to the profiles from the 9% Cr disc surfaces, the depth profiles recorded for the chromium free BS EN8 pin surfaces show no chromium in the bulk of the oxide film. Low concentration of that element at levels of less than 1% were detected in some samples, but only in the region of the oxide/metal interface. Some chromium at the pin oxide/metal boundary is to be expected due to metallic

transfer during the initial severe "running in" phase. In this phase, before the production of load bearing oxide plateaux and the transition to mild wear, there is likely to be a large adhesive component of the wear mechanism and this will lead to transfer of metallic particles. It is envisaged that when oxide begins to develop such adhesive matallic wear will effectively cease and with it any transfer of material. The oxides then continue to grow by a diffusion process. If the oxide plateaux formation was due in any way to transfer, chromium would be detected by Auger spectroscopic analysis throughout the depth of the oxide.

Thus it can be concluded that for the conditions of these experiments, unidirectional sliding above the T_2 transition when debris is not entrapped at the wearing conjuction, the load bearing plateaux consist of a physically homogeneous oxide film and that they are formed due to a diffusion controlled oxidational growth mechanism. After attaining critical thickness the plateaux are then removed to form wear particles. While the analyses discussed above clearly demonstrate the mechanism of growth of the oxide film, they do not indicate which parameters govern critical thickness or the mechanism responsible for oxide removal. Various suggestions have been made for the mechanism including differential thermal expansion of oxide and metal, differential elastic moduli and thermal and mechanical stressing leading to fatigue at the oxide/metal interface[85,88]. Some of these will be examined here.

It has been shown in this investigation that one of the three oxides produced on steel surfaces, the spinel Fe_3O_4, is more protective that the other two. Thus in order to assess possible mechanisms responsible for the attainment of critical thickness and subsequent removal of the oxide film, it is instructive to consider the properties of these oxides in relation to each other.

The Pilling Bedworth[156] ratios for the three oxides FeO, Fe_3O_4 and α - Fe_2O_3 are 1.68, 2.10 and 2.14 respectively[181], hence all produce compact oxides, but compressional stresses are formed within the oxides. The higher the Pilling Bedworth ratio the greater the apparent internal stress, but this stress will also depend on the mechanism of oxide growth. α - Fe_2O_3 has the highest Pilling Bedworth ratio, but further to this, this oxide is produced by anion diffusion via vacant O^{2-} lattice sites. Thus the oxide is formed at the oxide/metal interface and expansion of the lattice is necessary to accommodate this growth. The internal compressional stresses will have a more accute effect on the mechanical integrity of the oxide under these circumstances. The stress per unit area produced in this way within the film increases with film thickness[182], thus at a particular thickness the stresses will become sufficient for loss of adhesion between film and metal substrate to occur.

FeO has a relatively low Pilling Bedworth ratio and grows at the gas/oxide interface due to diffusion of cations through the oxide. The combination of these two properties means that the internal stresses in this oxide have little effect on the mechanical stability of the film. However, when cation diffusion is responsible for oxide growth vacancies accumulate at the metal/oxide interface resulting in the formation of cavities which eventually lead to loss of adhesion. The problem may be exacerbated in the case of FeO due to the formation of point defect stresses caused by the large deviations from stoichiometry[180].

In Fe_3O_4 growth occurs by both anion and cation diffusion and hence the oxide film will not be subject to the extremes of conditions found in the other two. Thus considering the basic kinetics of formation of the three oxides, one would expect that Fe_3O_4 would be the most mechanically stable.

It has often been suggested[59,85,88] that differential thermal expansion between metal and oxide and the resulting thermally induced stresses may be in part responsible for oxide film detachment. The thermal stress is, according to Oxx[158], directly proportional to the difference in coefficients of thermal expansion and can be written for oxide grown on bulk metal as:

$$\sigma = E_o \Delta T \alpha_o \left(1 - \frac{\alpha_m}{\alpha_o}\right) \qquad (2.29)$$

where σ is the thermally induced stress

α_o and α_m the coefficient of thermal expansion for oxide and metal respectively

E_o the elastic modulus of the oxide

and ΔT the temperature difference across the oxide

The ratios of α_m/α_o for the oxides FeO, Fe_3O_4 and α - Fe_2O_3 are 1.25, 1.03 and 1.03 respectively[181]. Inserting typical values into Equation (2.9) shows that the stresses produced for Fe_3O_4 and α - Fe_2O_3 are negligible even for the large temperature differences experienced in the tribo-logical situation. For FeO stresses may be comparable with the yield stress if temperature differences across the oxide exceed about 400^0C. If these stresses are very localized high forces could be produced, but overall it is probable that differential thermal expansion is not a major factor in limiting film thickness and producing oxide detachment, particularly in the oxides Fe_3O_4 and α - Fe_2O_3 . A fact which supports this view is that oxide thickness increases with both increased load and increased surface temperature where the temperature differentials ΔT also increase.

Even under static conditions the thickness of the oxide is limited by the various factors discussed above, although films grow substantially thicker than those

obtained in tribological situations before detachment occurs. It has been shown that detachment of the oxide in tribological situations is probably not thermally induced, hence it must be due to a mechanical process. It is interesting to note that the predicted values of contact radii from the surface model in Section 2.3 of this chapter vary between about 3 and 8 μm. If it is assumed that these contacts are hemispherical, the maximum stress due to the contacts will occur at distances between 2 and 5 μm below the surface and this is very close to the thicknesses of the oxides observed. The most probable mechanism responsible for detachment of the oxide film to form laminar wear particles is a fatigue process. Continued cyclic stressing due to asperity contact leads to dislocation build up at the natural boundary between metal and oxide. This leads to delamination and removal of the oxide. The effect will be most pronounced when maximum subsurface stresses occur in a region close to the metal/oxide interface. The build up of dislocations at the interface is aided by the natural processes occuring within the oxide, thus one would expect α - Fe_2O_3 and FeO to produce thinner films with less coverage and less stability than Fe_3O_4 . With increase in temperature and/or load it might be expected that plastic flow, both within the oxide and at the metal boundary, could relax some of the internal stresses produced and so allow thicker films to form.

This suggestion of increased stress relaxation at increased temperature is supported by the variation in measured wear rate for 52100 steel with temperature. Figure 2.29 shows a wear rate versus temperature curve for a load of 39.2 N at which the predominant oxide is Fe_3O_4 . It can be seen that wear rate falls with increase in temperature. The region of α - Fe_2O_3 oxide only appears in one set of data and hence no such observation can be made for that oxide from this investigation, but the results of FeO, at a load of 117 N for example, also exhibit this trend.

Referring to the determination of surface parameters from the model in section 2.3, it is obvious that in the one area where direct comparison can be made between theoretical predictions and experimental measurements, that is for oxide film thickness, remarkable agreement is found between the two sets of data. On the basis of this success, there can be some confidence that the predicted values of contact temperature, average contact radii and numbers of contacts give a reasonable representation of the processes occuring at the real surfaces. The predicted contact temperatures are indirectly confirmed in the majority of the experiments by X-ray diffraction analysis, which shows for example the presence of FeO in the debris and on surfaces when values exceed 600^0C. It is known that FeO forms in quantity only at temperatures greater than 570^0C. An exception to this is for experiments conducted at disc temperatures of 400^0C and 500^0C when the debris consists of an Fe_3O_4

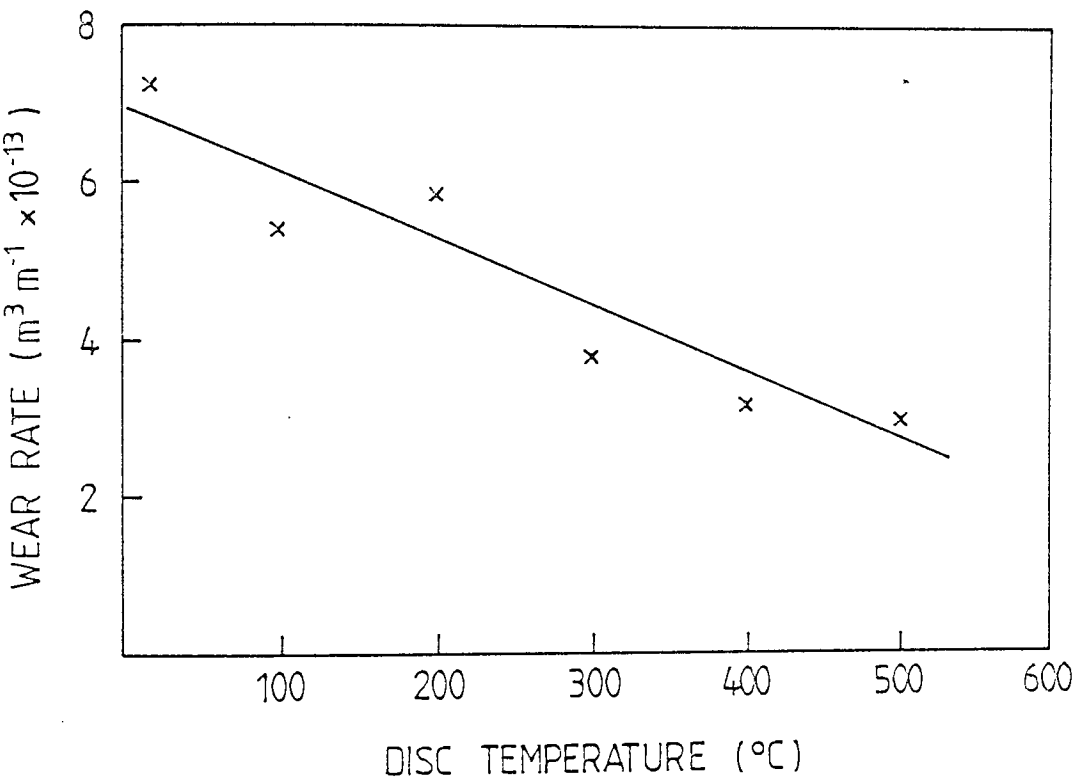

FIG. 2.29 WEAR RATE VERSUS DISC TEMPERATURE FOR 52100 ON 52100 EXPERIMENTS CONDUCTED AT A CONSTANT LOAD OF 39N.

and $\alpha - Fe_2O_3$ mixture in a region where contact temperatures indicate that significant amounts of FeO should be present. There are two possible explanations for this result. The first is that in order for the FeO to be retained it must be quenched very rapidly. If the surface temperature is low rapid quenching occurs after asperity contact and FeO is retained, but if surface temperatures are high then relatively slow cooling occurs and FeO degenerates to the lower oxides leaving only these in the debris and on the surface. If this were the process responsible for the absence of FeO the higher wear rates associated with this oxide would have been observed in the temperature range 400^0C to 500^0C, when in fact wear rates are relatively low. Thus the second explanation is the most plausible and that is that the Fe_3O_4 /$\alpha - Fe_2O_3$ mixture found in this temperature range is due to out of contact oxidation at the general surface temperature. Thus although high contact temperatures are achieved, the majority of the oxide is formed at a lower temperature giving the protective predominantly Fe_3O_4 layer and consequently low wear rates. This observation is confirmed by the analysis of the oxidational wear theory developed in section 2.4 which shows that out of contact oxidation becomes significant at surface temperatures greater than 300^0C.

Further observations which can be made concerning the values of surface parameters gained from the heat flow model are that the model predicts a large increase in the number of contacts with increase in load together with a small

decrease in the mean contact radii. The values of contact radii determined in this work are supported by Rabinowicz[183] and Kragelskii[5] has also shown that contacts increase in number to a much greater extent than does the area of a single contact.

The development of the oxidational wear theory to take account of out of contact oxidation (section 2.4) gives further insight into the nature and development of tribological oxide plateaux. Analysis of the data in terms of the quantitative expression derived from the theory shows that the assumption made in earlier work that out of contact oxidation is negligible for low ambient temperatures is essentially correct. It further shows that only when surface temperatures exceed 300^0C does out of contact oxidation become important.

At low ambient temperatures this work basically supports the ideas published by this author and colleagues[59,80,85] that the activation energy for oxidation is similar to that for static oxidation, but that Arrhenius constants will be very much larger. (This is discussed in Chapter 1 of this work). The values of Arrhenius constants calculated from this present data are in good agreement with those of Sullivan, Quinn and Rowson[59] and when employed in the quantitative expression for oxidational wear give good agreement between theory and experiment. However, no agreement is found if these values are used for surface temperatures above 300^0C when out of

contact oxidation becomes significant. In this region wear rates (or growth rates) are grossly overestimated if these low temperature tribo-oxidational constants are used. Agreement between theory and experiment is found only if statically derived values of A_p and Q_p are used for both in contact and out of contact oxidation under these conditions.

Thus it appears that if out of contact oxidation is a significant or major oxide producing process, the film grows at a rate similar to that to be expected for a film produced under non-contact conditions at the same surface temperature. This is a somewhat puzzling result, since even though the out of contact dominated films may be regarded as having grown under psudo-static conditions, it would be expected that the disruption in the film due to sliding contact would increase entropy and lead to a higher value of Arrhenius constant. It is possible that if the bulk of the oxide is maintained at a high temperature some thermal relaxation occurs which limits the degree of surface disruption.

In summary this work shows that the oxide film formed above the Welsh T_2 transition by unidirectional sliding in a system where debris cannot become entrapped at the conjunction are physically homogeneous and grow due to a diffusion controlled mechanism. A consequence of this thick film growth is that it must follow a parabolic rate law.

Of the three oxides of iron, Fe_3O_4, is found to be the most protective and this is a consequence of the kinetics of formation of the oxides.

The removal of oxide plateaux once they have attained critical thickness is probably not due to thermally induced stresses. The most probable mechanism is one of fatigue with dislocations accumulating at the metal/oxide interface leading to delamination of the oxide at this point. This mechanism is aided by the natural processes occurring within the oxides.

For sliding at low ambient temperatures oxidation takes place at the real areas of contact and at the contact temperature. Out of contact oxidation at the surface temperature is negligible. Under these conditions parabolic growth rate constants are many orders of magnitude greater than their static counterparts.

For sliding at surface temperatures greater than 300^0C out of contact oxidation becomes predominant and in this region static growth rate constants describe the oxide formation.

CHAPTER 3

OXIDATIONAL WEAR AND BOUNDARY LUBRICATION

It has been shown in Chapter 2 of this work that under unidirectional conditions of sliding where wear debris cannot be entrapped at the conjunction, the protective oxide film formed on the surfaces during mild oxidational wear is physically homogeneous and forms due to diffusion of metal ions, oxygen ions or both in a manner analagous to a statically grown thick oxide film. It is probable that oxide films formed under lubricated conditions are produced in a similar manner. There are two reasons for this suggestion. The first is that the fluid will tend to carry away debris from the contact area and thus prevent entrapment. The second is that the fluid, particularly if it contains a boundary additive, will reduce the surface energy of the debris and prevent the adhesion which is the initial prerequisite for formation of an agglomerate layer. Thus if oxide films are formed on the surface they are probably due to diffusion controlled growth.

This author has made an extensive study of one particular boundary lubricated system, that of aluminium bronze against tool steel in the presence of kerosene. In

the initial series of investigations[69,166,167,168] a boundary additive consisting of a di-linoleic acid plus 5% by volume of a phosphate ester was included in some kerosene samples at a concentration of 12 p.p.m. The materials, fluid and additive used in the investigation were chosen because of their use in modern aircraft fuel systems. The major findings of the investigations were as follows. Wear rate versus load variations were non-linear indicating that more than one wear mechanism was operative. Auger electron spectroscopic analysis and electron probe microanalysis of the bronze surfaces showed that aluminium depletion occurred during the initial stages of wear leaving a copper rich surface which oxidized to form a Cu_2O protective film. Auger electron spectroscopy further showed that overlying the oxide was an additive film of about two molecules thick. Wear debris both with and without additive in the kerosene mainly contained Cu_2O , but when the additive was present copper and aluminium phosphides and phosphates were also present. Transfer of aluminium to the steel counterface occurred in pure kerosene, but was not observed when the additive was present.

Evidence from the investigations indicated that oxidation had an important role in the wear mechanism, although the phosphate ester present at a concentration of less than 1 p.p.m. appeared to have a profound effect. It was postulated that the ester exhibited e.p. action, hence protecting surfaces under the more severe conditions.

The experiments described in this chapter are intended to extend the initial work, eliminate the effects due to the phosphate ester and isolate the dominant mechanisms of protection under conditions of boundary lubrication. It is hoped that the results of this investigation will have wider implications in explaining general modes of protection by boundary additive films.

3.1 Experimental Apparatus and Procedures

The wear test rig used in these investigations, a detail of which is shown in Figure 3.1, has been described elsewhere[166], but consists essentially of a vertical pin loaded against a horizontal rotating disc. The disc was driven by a 0.5 h.p. servo-controlled dc motor which gave continuously variable speeds from 0 to 600 r.p.m. Loads of between 5 and 200 N could be applied to the pin through a gimballed load arm by means of a spring loaded weight system, designed to reduce inertial loading. The 2mm diameter aluminium bronze pin then rested on the face of the 100mm diameter steel disc.

A peristaltic pump with flow adjustment reservior was used to pump fluid to the conjunction using a single pass, non-recovery system in order to avoid debris contamination. The rate of fluid flow could be varied to maintain pseudo-boundary conditions. Friction and wear were continuously

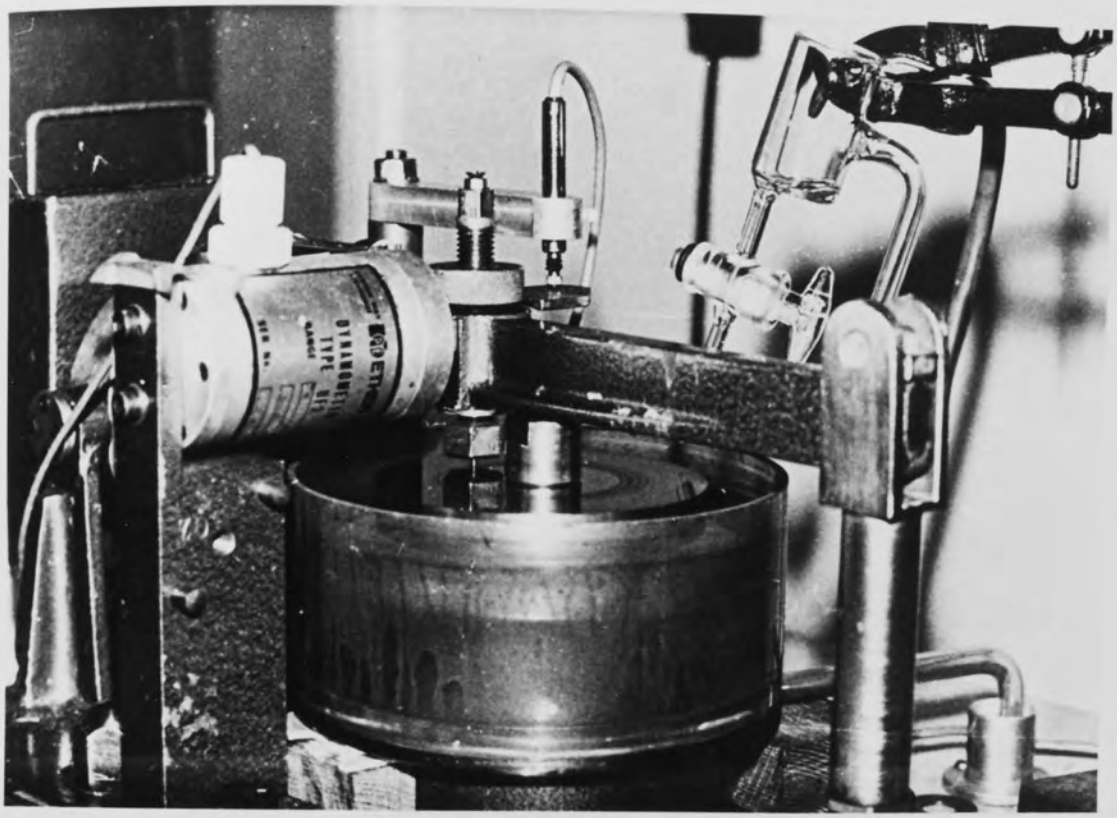

FIG. 3.1 DETAIL OF PIN ON DISC WEAR TEST RIG.

monitored using a strain gauge load cell and linear displacement transducer respectively, the amplified outputs of which were displayed on a chart recorder.

The materials used in the investigation were DTD 197A aluminium bronze and KE 180 tool steel, the weight concentration of which are:

DTD 197A: 11% Al, 4% Fe, 4% Ni, 2% Mn, remainder Cu

KE 180: 13% Cr, 1.5% C, 0.5% Mn, 0.5% Si, remainder Fe

A detailed metallographic examination of DTD 197A bronzes from various sources[184] has revealed five quite different structures. Since these would be expected to produce different wear characteristics, this could account for the lack of consistency in results reported by various workers in this area. Care was therefore taken in this study to use material of known metallurigical structure from a single supplier, although due to lack of availability this was different to the bronze used in previous investigations by this author[69,166,167,168].

The KE 180 steel discs were of hardness 700 HV and were randomly ground and lapped to a surface finish of 0.02 μm cla. The pins of hardness 240 HV were produced from rod and surfaces finished to 1 μm cla. Prior to each test all components were cleaned in a petroleum vapour at 80^{0}C for a period of one hour.

The basic fluid used in the investigation was an additive-free hydrotreated aviation kerosene. Prior to each experiment this was percolated through a one metre column of alumina catalyst to remove any polar impurities formed or taken up during storage. The additive used in the investigation consisted of dimers of ethoxylated alkyl phenol acids in a process oil and kerosene base. This was added to some of the kerosene samples at a volume concentration of 12 ppm immediately prior to the wear tests.

During initial wear tests under fully flooded conditions, friction coefficients varied erratically and were often substantially below 0.1 for all but the highest loads. This indicated a high degree of fluid film support and it was found necessary to restrict fluid flow rates to values of about 0.17 ml/min in order to maintain friction coefficients of 0.1 and ensure that boundary conditions prevailed. With these conditions established, tests were carried out at room temperature (~ 22^0C) with a new pin on a new disc track for each experiment. Equilibrium wear rates of aluminium bronze against steel were then determined as a function of load for velocities of 0.6, 2 and 4 m/s, with loads increasing from 24.5 N in increments of 24.5 N to a maximum of 196 N, or until seizure had occurred. The wear tests usually lasted for periods of between 90 and 120 minutes, all measurements being taken after an initial "running in" period when equilibrium conditions had been established. The tests were conducted in the presence of

percolated hydrofined kerosene and then repeated for kerosene plus additive. An average of five such wear tests were conducted for each load and speed combination.

Fluids used in some experiments were collected after prolonged wear tests and filtered to extract wear debris which was analysed using powder X-ray diffraction with Cu K_α radiation at 35kV and 30 μA. Samples were exposed for periods of 40 minutes and measured d values were compared with standard powder diffraction files in order to identify debris constituents.

Auger electron spectroscopy was employed to identify surface compositional changes. The analysis was conducted in a different manner to the normal mode of operation used on the steel specimens and described in Section 2.2.4 of this work. The normal mode of operation is to use a stationary electron spot and collect spectra from an area of perhaps 1 to 100 μm diameter. In these experiments information was required on the degree of coverage and mean thickness of surface films and this would have entailed a large number of spot analyses which might then not be representative. Hence, in order to overcome this, the electron beam was rastered over an area of 1 mm^2 and spectra recorded at a slow scan rate (1 $s.eV^{-1}$) . The beam energy was 3 keV with a specimen current of 2 μA. In order to gain information on changes in the concentration of elements of interest (C, O, S, Al, Cu and Fe) with depth into the surface, successive layers of the surface were

removed by periods of 0.5 keV argon ion bombardment, the Auger spectra being recorded between each successive period. Relative atomic concentrations were calculated from spectral peak to peak heights and published sensitivity factors[173] for each spectrum and the resulting depth profiles plotted.

Selected samples of pin and disc surfaces were analysed using electron probe microanalysis (15 keV beam energy, 80 μA beam current and 300 nm spot size), where spot analyses and large area elemental distribution maps of elements of interest in the surface, and on some 11^0 taper sections, were recorded. Further examination of surfaces, sub-surfaces and debris was carried out using scanning electron microscopy and X-ray energy dispersive analysis.

The dissimilar metals used in this investigation made it possible to estimate hot spot temperatures at the conjunction by means of a dynamic thermocouple method similar to that described by Furey[67]. Electrical connections were taken from the pin holder and from the disc through a carbon brush. The signals obtained were fed into a high input impedance x 30 amplifier with 1 MHz full power bandwidth, the output of which was displayed on an oscilloscope. The oscilloscope was externally triggered to allow a single shot of the output of the thermocouple amplifier to be displayed for one revolution of the disc. Calibration was achieved using aluminium bronze and steel wires spot welded together to form a junction.

3.2 Experimental Results

3.2.1. Wear

Figure 3.2 shows wear rate as a function of load for speeds of 0.6, 2 and 4 ms^{-1} for experiments conducted with kerosene and kerosene plus additive. The points lie about three straight lines. The 95% confidence interval for line (c), about which the scatter of experimental points is greatest, is $\pm$ 6.3 x 10^{-14} $m^3 m^{-1}$ at 196 N. It can be seen that the regression lines (a) and (b) lie well outside this interval, indicating statistically significant differences in the data from experiments conducted with and without additive in the kerosene. The errors in measurement of wear rates were always negligible compared with the scatter of points.

For experiments conducted in pure kerosene at speeds of 0.6 and 2 ms^{-1}, the points lie about a line (a) with 0.98 correlation coefficient. The line indicates a specific wear rate of 8.7 x 10^{-16} $m^3 m^{-1} N^{-1}$ for these experiments. Wear rates for experiments conducted at 4 ms^{-1} in pure kerosene lie about line (b) with 0.99 correlation coefficient and a significantly higher specific wear rate of 23.2 x 10^{-16} $m^3 m^{-1} N^{-1}$.

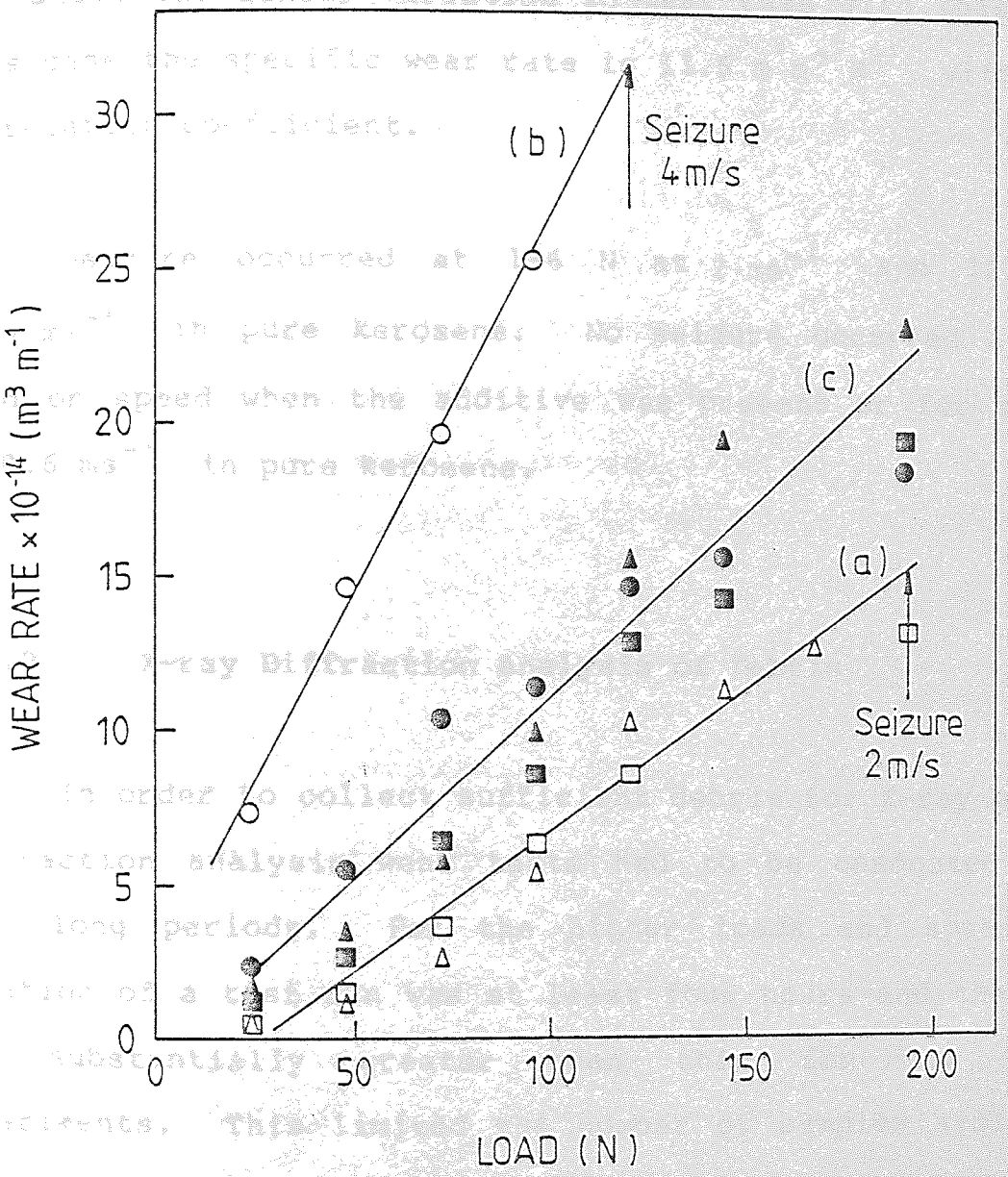

FIG. 3.2 WEAR RATE OF ALUMINIUM BRONZE VERSUS LOAD; (a) 0.6 AND 2 m/s IN PURE KEROSENE, (b) 4 m/s IN PURE KEROSENE AND (c) 0.6, 2 AND 4 m/s IN KEROSENE WITH ADDITIVE ; □ 0.6 m/s, △ 2 m/s, ○ 4 m/s - PURE KEROSENE; ■ 0.6 m/s, ▲ 2 m/s, ● 4 m/s - KEROSENE WITH ADDITIVE.

When the additive was present in the kerosene, there was no systematic variation in wear rate with speed and line (c) shows the linear variation in wear rate with load. In this case the specific wear rate is 11.5 $m^3 m^{-1} N^{-1}$ with 0.96 correlation coefficient.

Seizure occurred at 196 N at 2 ms^{-1} and 122.5 N at 4 ms^{-1} in pure kerosene. No seizure occurred at any load or speed when the additive was present or for speeds of 0.6 ms^{-1} in pure kerosene.

3.2.2 X-ray Diffraction Analysis of Debris

In order to collect sufficient debris for X-ray powder diffraction analysis wear tests had to be conducted over very long periods. For the higher loads and speed the duration of a test run was at least four hours and the time was substantially greater than this for low speed experiments. This limited the number of samples available for analysis, but a representative series of data was taken at each speed. All analyses show that the debris is similar, whether it was generated in kerosene with additive or in pure kerosene up to the point of seizure. The only constituents capable of identification were Cu_2O and Cu. No evidence of either Al or Al_2O_3 was found using this technique, although using X-ray dispersive analysis on debris samples in the scanning electron microscope revealed

levels of Al of about 2%. There is no way of determining if this is due to metallic Al or to the oxide, but later results would suggest that it is metallic and produced during the initial running in stages of wear.

The majority of powder X-ray photographs indicate that metallic copper is the major constituent in the debris, but since there was no way of separating the debris produced in the initial stages of wear from that due to the equilibrium process the majority of the Cu is probably due to the severe running in phase of wear. There was never enough debris for proper proportional analysis to be conducted, hence it was not possible to say if there was more or less oxide in the debris for any given set of conditions.

3.2.3. Auger Electron Spectroscopy

The rastering method of Auger electron spectra generation is novel, but should be considered as an alternative to "small spot ESCA" in samples where charging does not present problems, particularly in view of the more powerful techniques now available to handle N(E) spectra.

Figures 3.3 and 3.4 show typical Auger spectra produced by this method from aluminium bronze surfaces generated under relatively mild conditions, in this case a load of 73.5 N and speed of 0.6 ms^{-1} . Comparing the two figures, the spectra from experiments without additive,

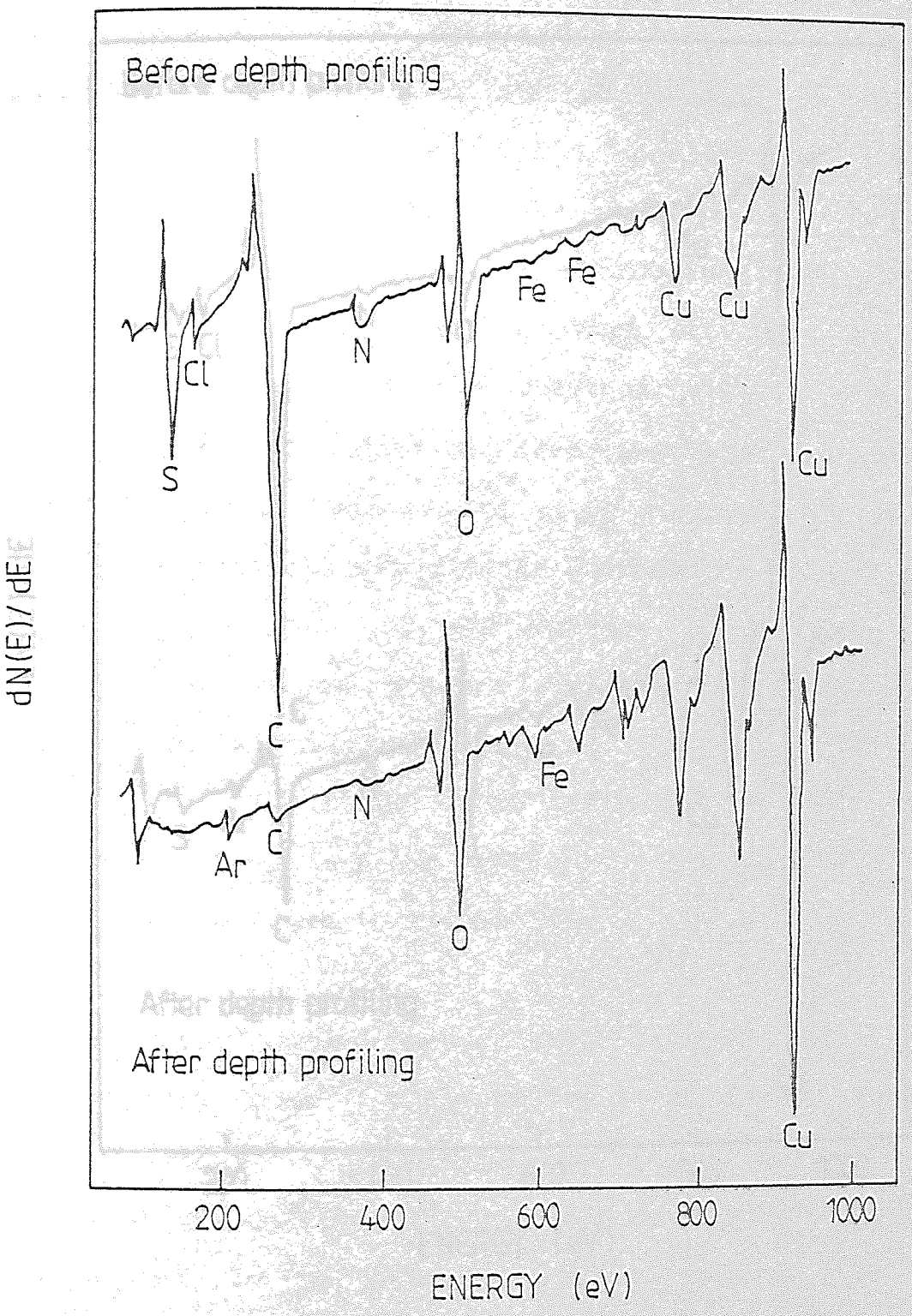

FIG. 3.3 AUGER ELECTRON SPECTRA FROM AN ALUMINIUM BRONZE PIN WORN UNDER A LOAD OF 74N AND A SPEED OF 0.6 m/s IN PURE KEROSENE , BEFORE AND AFTER A PERIOD OF 80 MINUTES OF ARGON ION ETCHING.

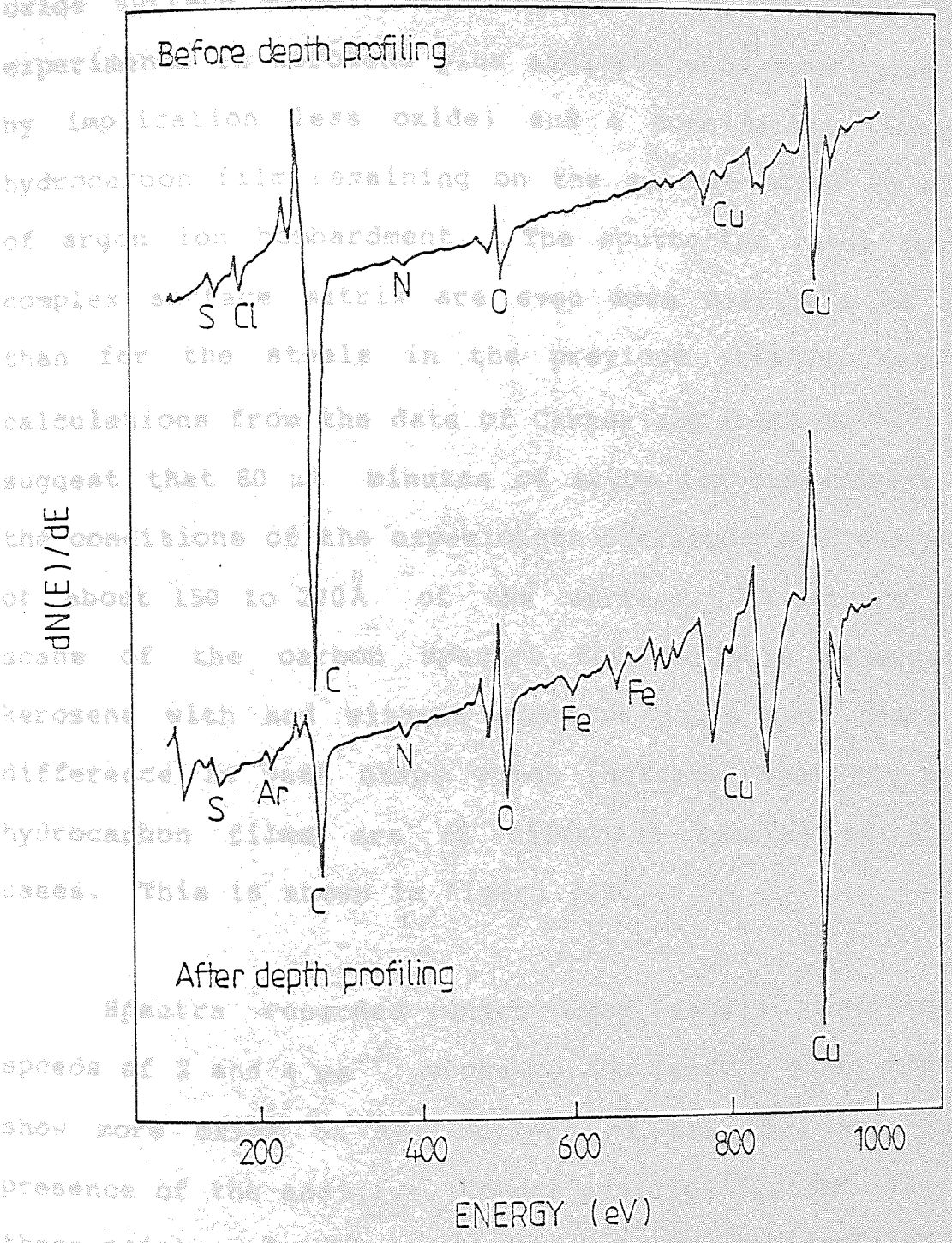

FIG. 3.4 AUGER ELECTRON SPECTRA FROM AN ALUMINIUM BRONZE PIN WORN UNDER A LOAD OF 74N AND A SPEED OF 0.6 m/s IN KEROSENE WITH ADDITIVE BEFORE AND AFTER 80 MINUTES OF ARGON ION ETCHING.

Figure 3.3, shows that the surface carbon layer is rapidly removed by argon ion bombardment leaving a mainly copper oxide surface film. In contrast to this the spectra for experiments in kerosene plus additive show less oxygen (and by implication less oxide) and a considerable amount of hydrocarbon film remaining on the surface after 80 minutes of argon ion bombardment. The sputtering rates for this complex surface matrix are even more difficult to assess than for the steels in the previous chapter, but again calculations from the data of Carter and Colligon[174] would suggest that 80 μA minutes of argon ion bombardment under the conditions of the experiments corresponds to the removal of about 150 to 200$\mathring{A}$ of the surface. Examining narrow scans of the carbon spectra for surfaces generated in kerosene with and without additive shows that there is a difference in peak shape which indicates that the surface hydrocarbon films are of different species in the two cases. This is shown in Figure 3.5.

Spectra recorded under more severe conditions at speeds of 2 and 4 ms^{-1} close to the seizure point conversly show more oxide on the surface of the pins worn in the presence of the additive. Depth profiles further illustrate these points. In the interest of clarity the profiles shown here compare carbon and oxygen concentrations only, although concentrations of all other elements of interest were recorded. All surfaces, for example, showed some sulphur and chlorine in the immediate surface layer and iron at a concentration of about 3 atomic percent throughout the

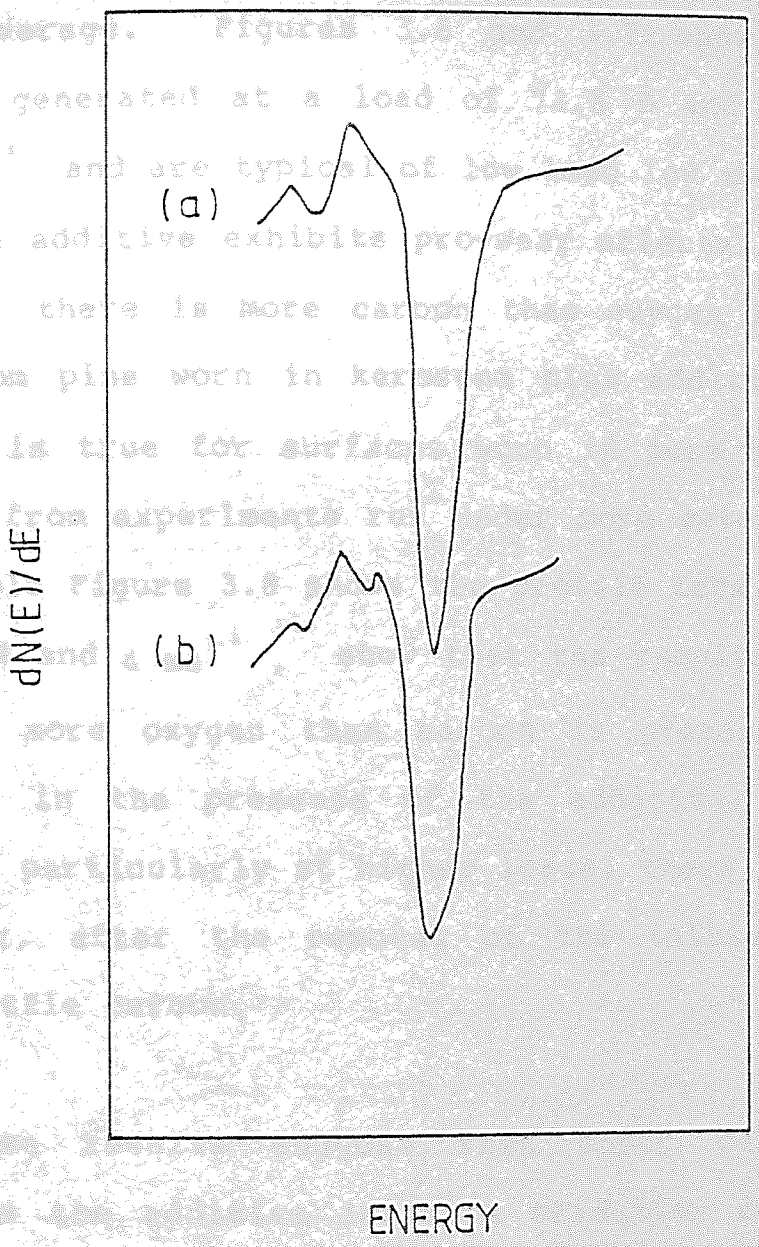

FIG. 3.5 CARBON DIFFERENTIATED AUGER PEAK SHAPES FROM ALUMINIUM BRONZE SURFACES; (a) WORN IN PURE KEROSENE, (b) WORN IN KEROSENE WITH ADDITIVE.

depth. It must be remembered that these spectra are the result of large area analysis, hence the iron signal probably comes from areas of surface material with little oxide coverage. Figures 3.6 and 3.7 show profiles for surfaces generated at a load of 74.5 N and speeds of 0.6 and 2 ms^{-1} and are typical of low load low speed conditions where the additive exhibits pro-wear effects. The profiles show that there is more carbon than oxygen in the surface films from pins worn in kerosene plus additive, while the converse is true for surfaces worn in pure kerosene. The profiles from experiments run under more severe conditions, for example Figure 3.8 shows the profile from a pin worn at 98 N load and 4 ms^{-1} , show that the results are reversed and that more oxygen than carbon is present on surfaces generated in the presence of the additive. Without the additive, particularly at higher loads, there is very little oxygen or, after the removal of the initial contaminent layer, little carbon.

These results suggest that under relatively mild conditions the additive inhibits oxidation resulting in a more patchy or perhaps thinner oxide film, but that under severe conditions the additive gives sufficient protection to the surface to allow oxidation and prevent metallic wear and seizure. These findings are summarized in Table 3.1

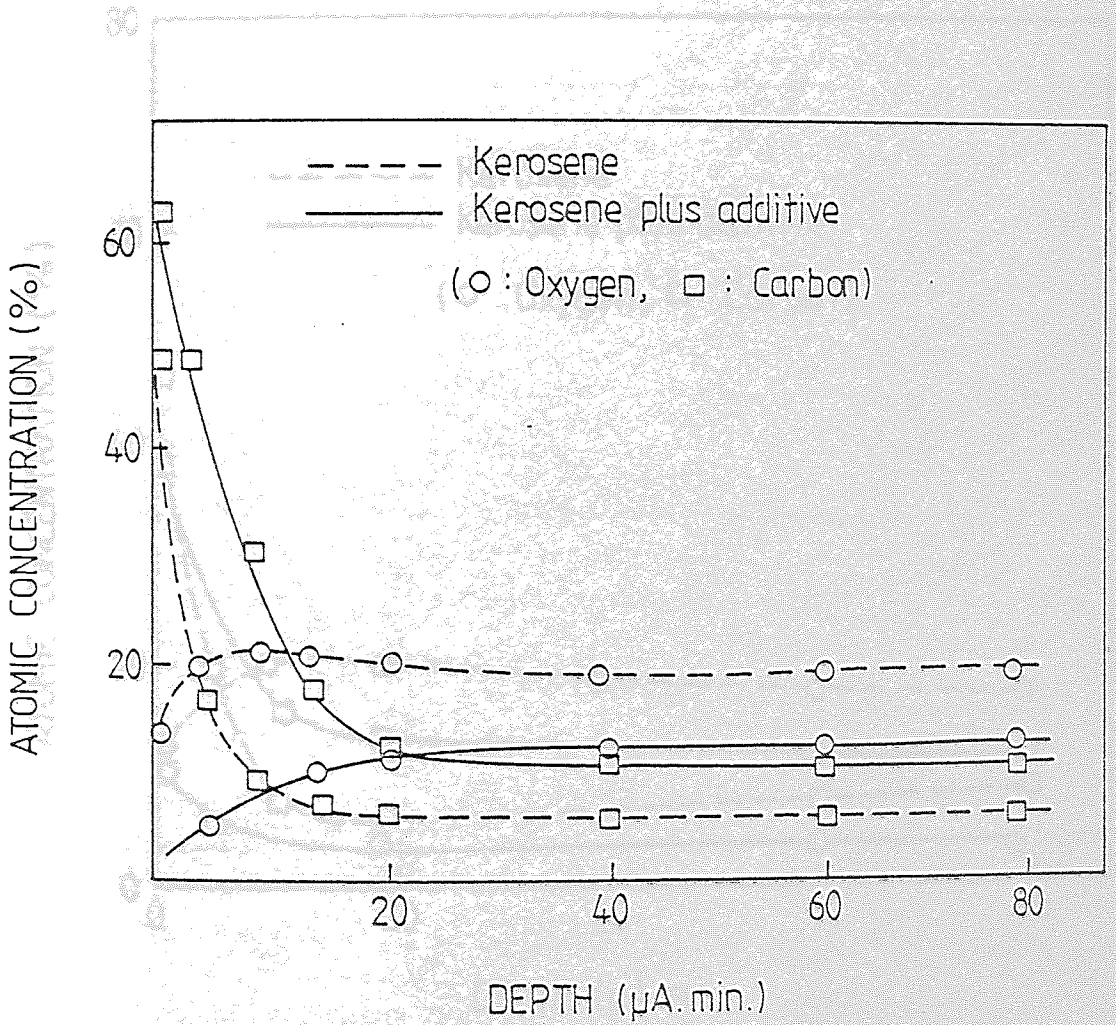

FIG. 3.6 OXYGEN AND CARBON CONCENTRATION VERSUS DEPTH PROFILES FOR AN ALUMINIUM BRONZE PIN SURFACE WORN UNDER A LOAD OF 74N AT A SPEED OF 0.6 m/s.

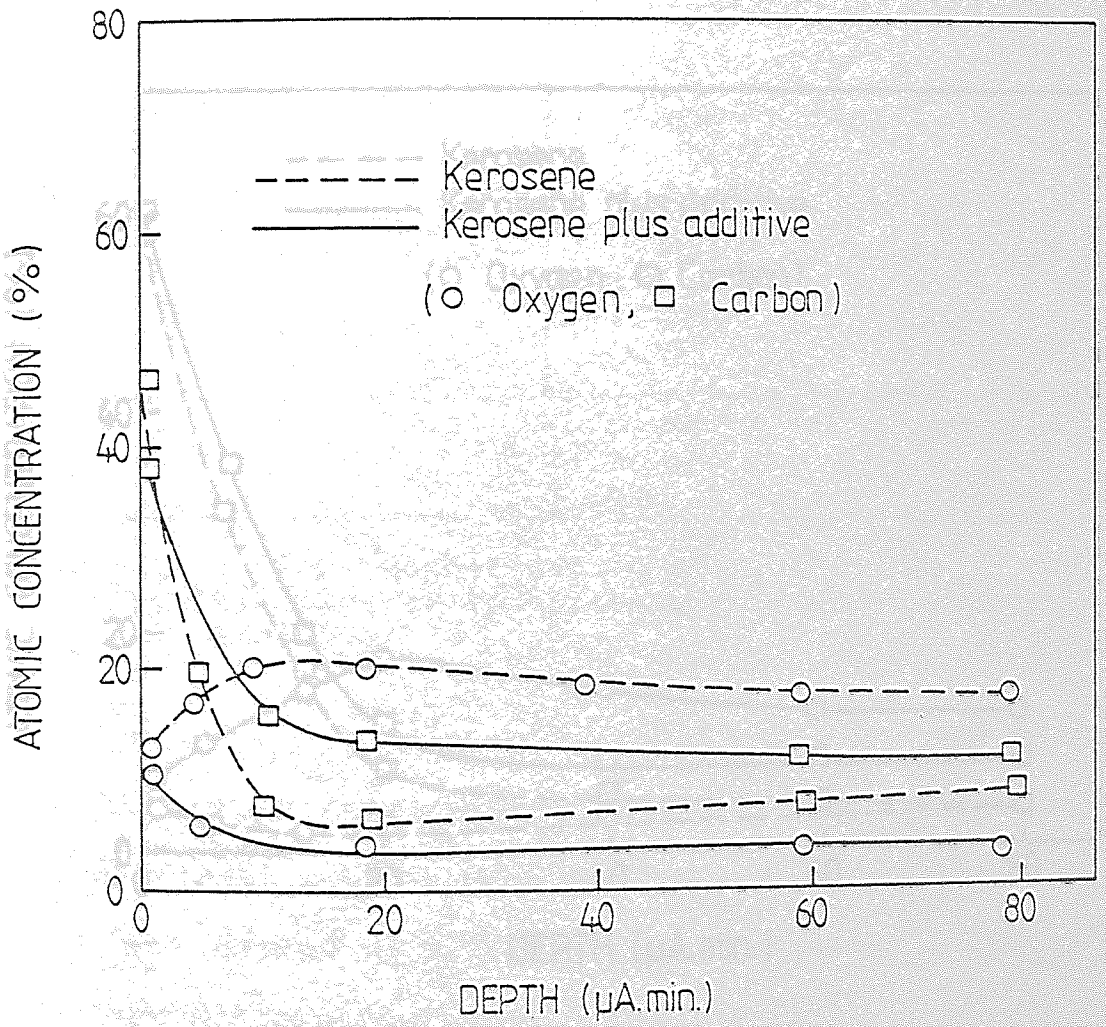

FIG. 3.7 OXYGEN AND CARBON CONCENTRATION VERSUS DEPTH PROFILES FOR AN ALUMINIUM BRONZE PIN SURFACE WORN UNDER A LOAD OF 74N AT A SPEED OF 2 m/s.

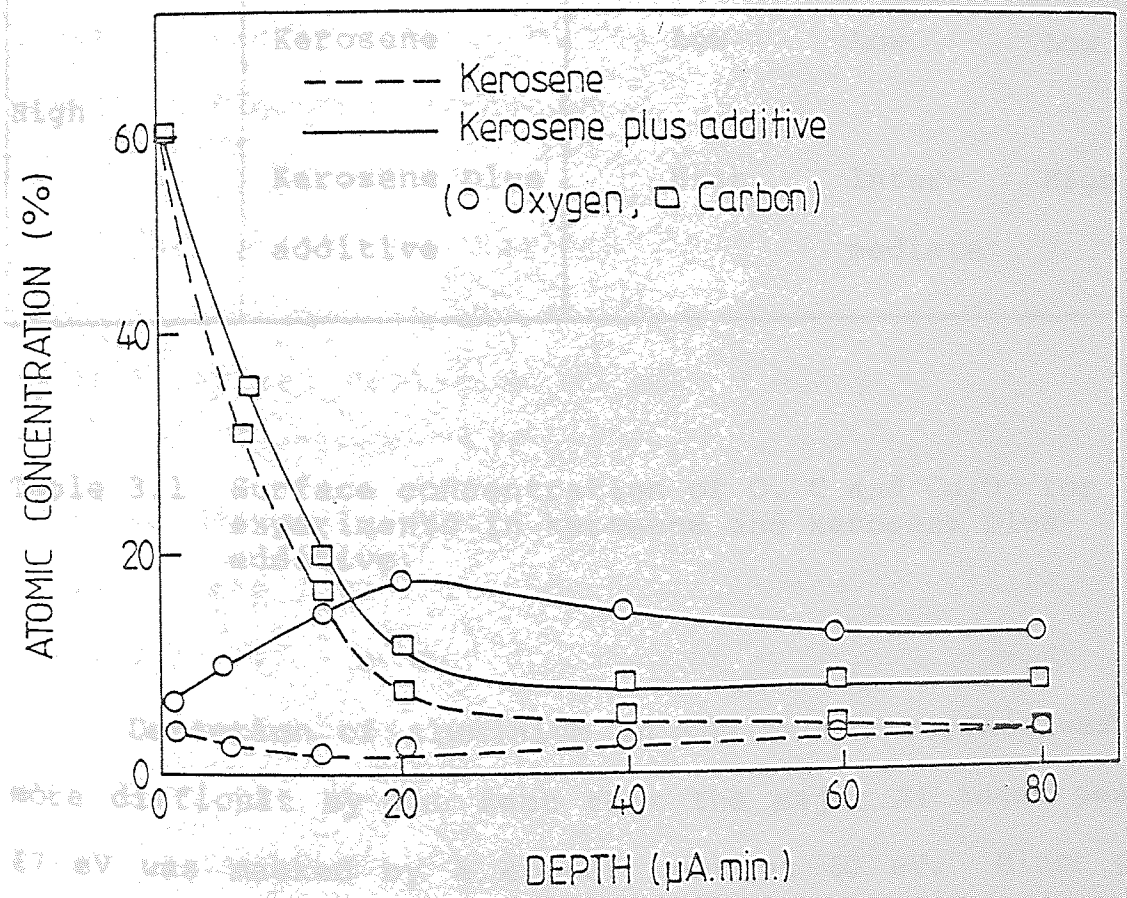

FIG. 3.8 OXYGEN AND CARBON CONCENTRATION VERSUS DEPTH PROFILES FOR AN ALUMINIUM BRONZE PIN SURFACE WORN UNDER A LOAD OF 98N AT A SPEED OF 4 m/s.

Load/Speed	Fluid	Surface Concentration		
		Oxygen	Carbon	Copper Oxide
Low	Kerosene	High	Low	High
	Kerosene plus additive	Low	High	Low
High	Kerosene	Low	Low	Low
	Kerosene plus additive	High	Inter-mediate	High

Table 3.1 Surface concentration of O, C and Cu_2O for experiments in kerosene and kerosene plus additive.

Detection of aluminium in the bronze surface was made more difficult by the fact that the major Al Auger peak at 67 eV was masked by a copper peak at 60 eV. Minor peaks were just discernable above noise levels at 42 eV, 47 eV and 54 eV with shoulders on the 60 eV copper peak at 58 eV and 67 eV. The 47 eV peak can be assigned to iron and the 58 eV shoulder to copper. This leaves peaks at 42, 47 and 67 eV. The 67 eV shoulder is a result of the main aluminium peak and those at 42 and 54 eV would appear to be the aluminium oxide plasmon loss peaks. Thus there appears to be some

aluminium or Al_2O_3 in the surface, but the fact that in the majority of cases the peak at 1396 eV was not visible above noise levels indicates that the mean aluminium concentration was low and that the oxide formed was primarily copper oxide. Aluminium at concentration close to bulk levels was detected under severe conditions close to the seizure point for some samples worn in pure kerosene.

3.2.4. Electron Probe Microanalysis and Scanning Electron Microscopy

The low concentrations of aluminium and aluminium oxide in wear debris and on the surface suggests that there is preferential depletion of that element from the bronze. This was confirmed by electron probe microanalysis on surfaces generated over the whole load range and for speeds of 0.6, 2 and 4 ms^{-1} . Concentrations were calculated from the average of a number of electron probe spot analyses on a given pin surface after correction for atomic number, absorption and fluorescence effects. For the conditions of these experiments the effective sampling depth was about 1 µm. Figure 3.9 shows curves of mean aluminium concentration versus load (a) for a speed of 0.6 ms^{-1}, (b) for 2 ms^{-1} and (c) for 4 ms^{-1}. Concentrations vary between about 4% and 8%. In the surfaces generated under relatively mild conditions the measured concentrations were greater when additive was present in the fluid. Since the measured concentration represents a mean value taken over a

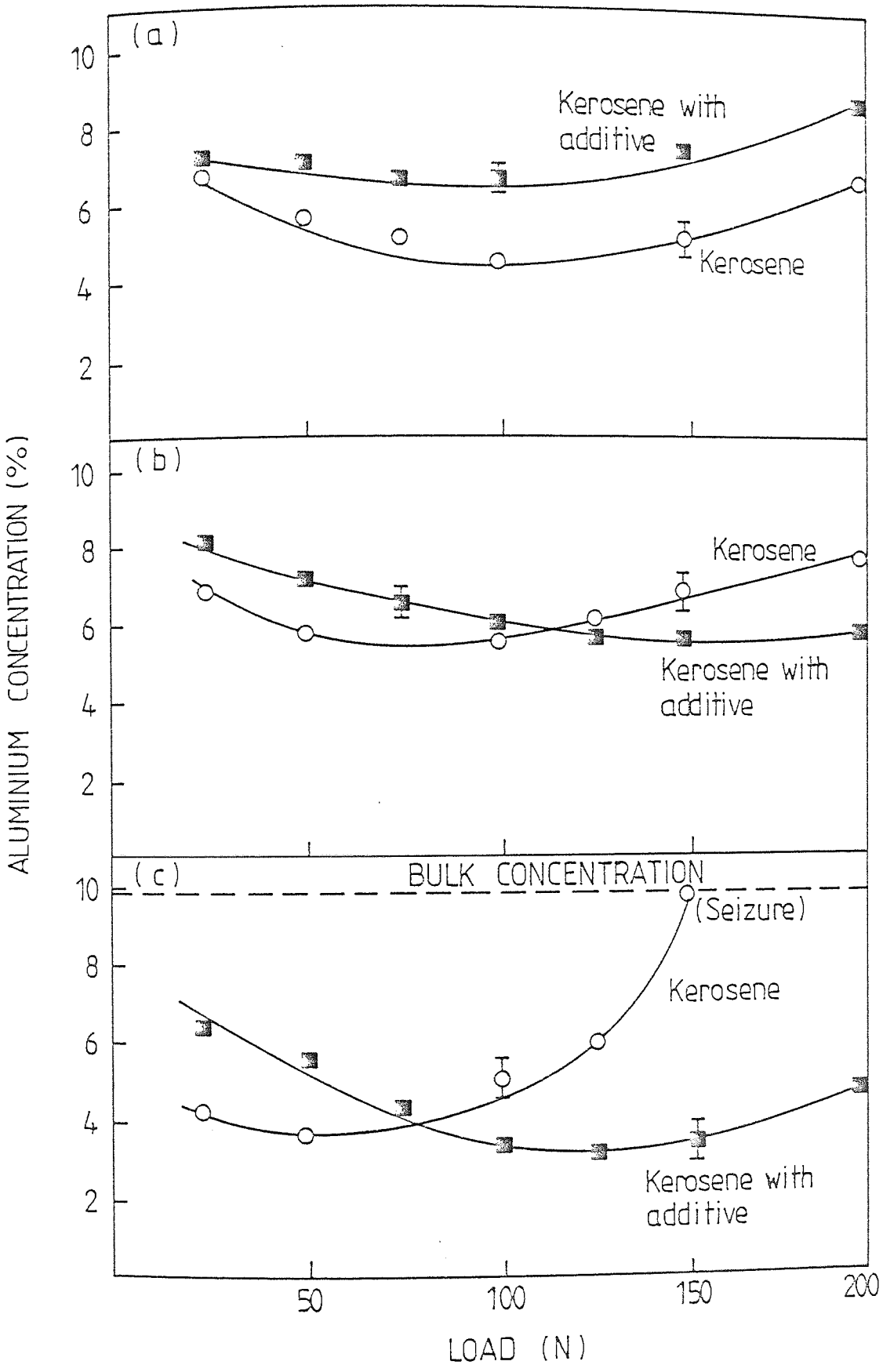

FIG. 3.9 MEAN ALUMINIUM CONCENTRATION VERSUS LOAD FOR ALUMINIUM BRONZE PINS WORN AT SPEEDS OF ; (a) 0.6 m/s, (b) 2 m/s, (c) 4 m/s.

depth of about 1 μm, if the oxide coverage is sparse one would expect the contribution from the bulk to be greater giving an apparently higher aluminium concentration.

When conditions become more severe the specimens generated in pure kerosene have no additive protection to allow oxide to grow and hence severe wear will eventually ensue with a resultant removal rate which does not allow diffusion of aluminium from surfaces to occur, hence measured concentration will be close to bulk values, see for example Figure 3.9(c). On the other hand if the additive is present then it gives sufficient protection to allow the oxide to grow and be maintained on the surface and hence give a lower apparent aluminium concentration.

Figure 3.10 shows a photomicrograph of an 11^0 taper section of a pin surface worn under relatively mild conditions (147 N load, 0.6 ms^{-1}) with corresponding copper and aluminium elemental maps. This figure is typical of the majority of worn surfaces studied and clearly shows regions of aluminium depletion near to the surface. Exceptions to this were pins worn at high loads and speeds at or near to the seizure point. In these cases depletion was not evident and in some samples areas of high aluminium concentration were found giving spot count rates of about 9000 counts s^{-1} compared with bulk rates of about 6500 counts s^{-1}.

(a)

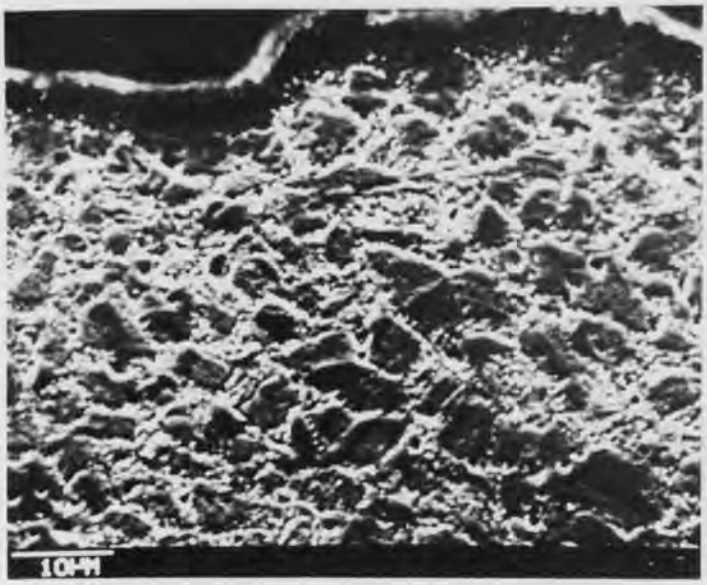

(b)

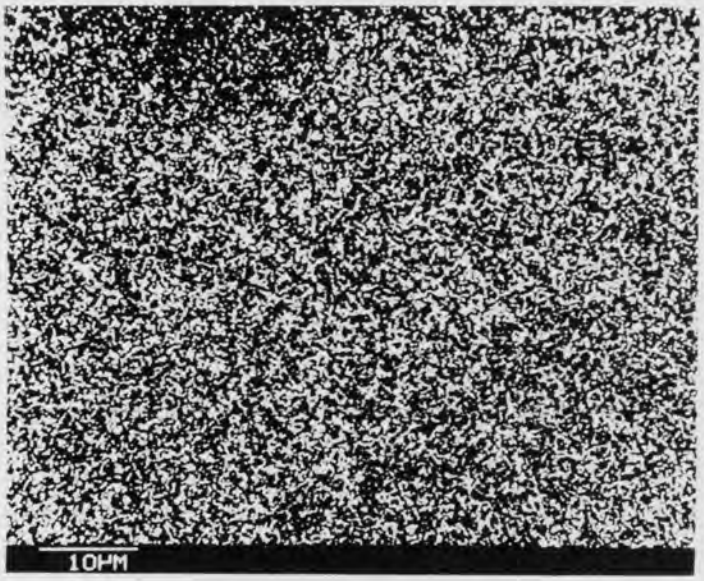

(c)

FIG. 3.10 PHOTOMICROGRAPHS OF A TAPER SECTION OF A WORN PIN SURFACE ; (a) SECONDARY ELECTRON IMAGE ,(b) COPPER X-RAY DISTRIBUTION,(c) ALUMINIUM X-RAY DISTRIBUTION.

(a)

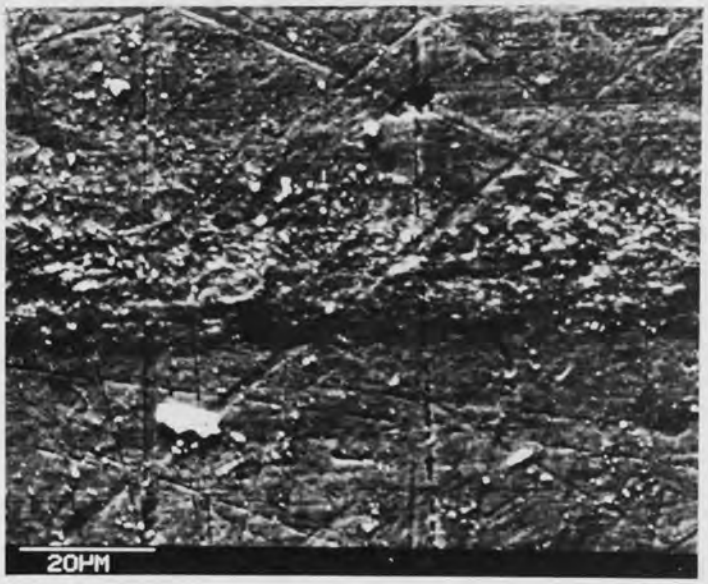

(b)

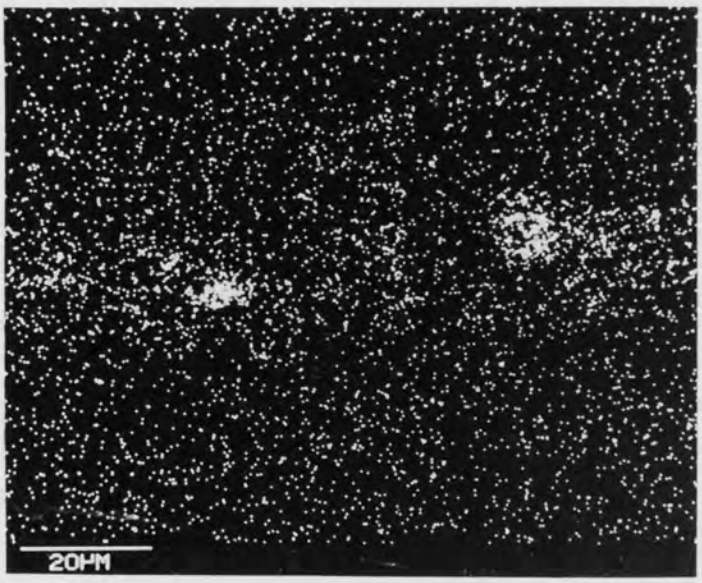

FIG. 3.11 PHOTOMICROGRAPHS OF A WEAR TRACK ON A STEEL SURFACE ; (a) SECONDARY ELECTRON IMAGE ,(b) COPPER X-RAY DISTRIBUTION.

(c)

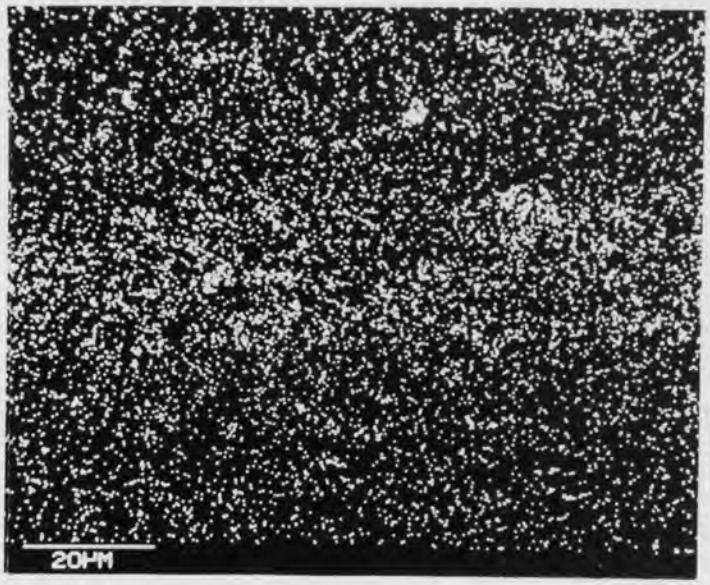

(d)

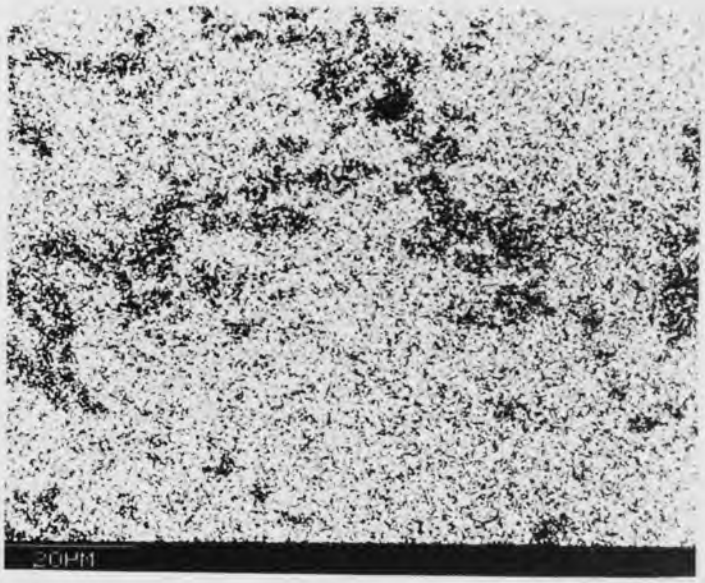

FIG. 3.11 PHOTOMICROGRAPHS OF A WEAR TRACK ON A STEEL SURFACE ; (c) ALUMINIUM X-RAY DISTRIBUTION, (d) IRON X-RAY DISTRIBUTION.

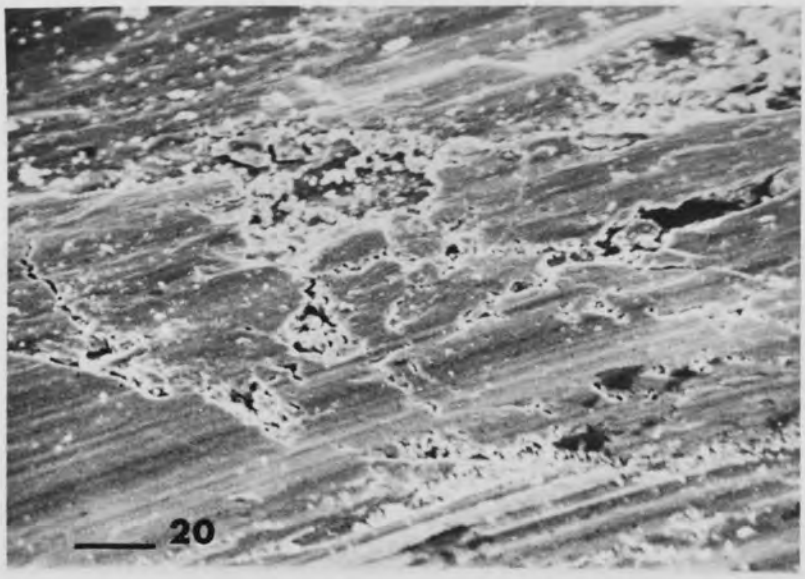

FIG. 3.12 TYPICAL SCANNING ELECTRON MICROGRAPH OF THE SURFACE OF AN ALUMINIUM BRONZE PIN WORN UNDER MILD CONDITIONS.

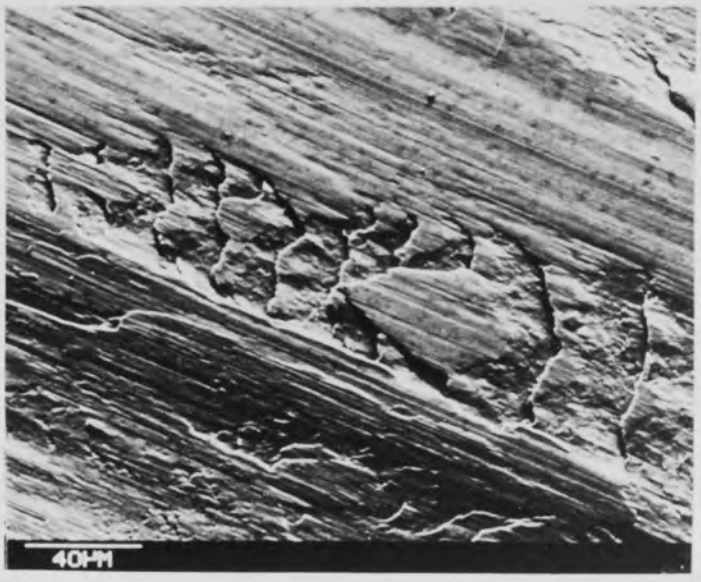

FIG. 3.13 TYPICAL SCANNING ELECTRON MICROGRAPH OF THE SURFACE OF AN ALUMINIUM BRONZE PIN WORN UNDER SEVERE CONDITIONS WITH NO ADDITIVE PRESENT IN THE KEROSENE.

Figure 3.11 shows a photomicrograph of a section of wear track from the steel couterface of an experiment conducted under similar conditions of load and speed to that of Figure 3.10. Corresponding X-ray elemental maps of copper, aluminium and iron are also included in this figure. These photomicrographs are typical of surfaces worn in the presence of pure kerosene and kerosene plus additive and clearly show that transfer from pin to disc has occurred. EPMA spot anaylses showed that the aluminium content of such transfer films on the steel surface was always higher than in the bulk bronze, usually ranging from 20 to 80% depending on postion.

Scanning electron micrographs taken from pin surfaces worn with and without additive show no apparent difference under relatively mild conditions and each surface appears smooth and oxidized, Figure 3.12 shows a typical example. The character of the surface changes, however, for high loads and speeds with no additive present in the kerosene and here considerable surface distress is seen with evidence of gross plastic flow. This is shown in Figure 3.13.

3.2.5. Contact Temperature Measurements

Temperatures at the asperity contacts on the wearing surfaces were estimated from dynamic thermocouple measurements. The results were somewhat disappointing. Temperature spikes showing flash temperatures of up to 500^{0}C were

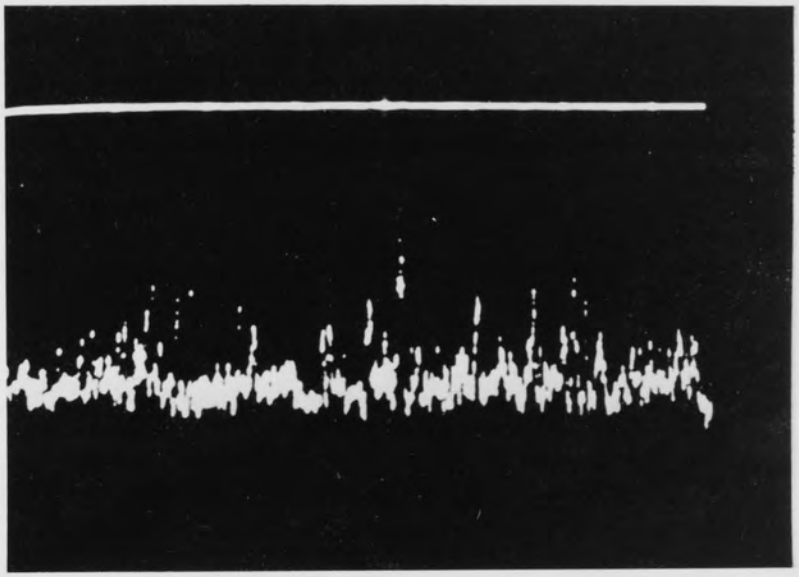

FIG. 3.14 OSCILLOCSOPE TRACE OF THE OUTPUT FROM THE DIFFERENTIAL THERMOCOUPLE AMPLIFIER FOR ONE REVOLUTION OF THE DISC.

observed, but due to the transient and intermittent nature of these spikes little systematic variation was noted with either load or speed. The measurements did indicate, however, that when asperity contacts do occur temperatures are sufficiently high to allow diffusion controlled migration mechanisms to take place and to support a considerable degree of surface oxidation. A typical oscilloscope trace from the thermocouple amplifier is shown in Figure 3.14.

3.3 Boundary Lubrication and Oxidational Wear - a Surface Model

The results presented in section 3.2 will be discussed in detail later in this chapter, but it is obvious from the evidence here that oxidation and oxidational wear have an important role in the overall wear mechanism. It is also probable that surface oxides will be physically homogeneous and grow by a diffusion controlled mechanism in a manner similar to those in the steel systems discussed in the previous chapter, since debris will be removed by the fluid.

On the basis of the above assumptions it is therefore possible to develop a model of oxidational wear under boundary lubricated conditions in order to elucidate the mechanisms of protection involved and to give some insight into methods of quantitative prediction of wear. The model may be described as follows.

When a boundary additive is present in a lubricant, contacting surfaces are separated by an adsorbed polar molecular film when loads and/or speeds are such that little or no fluid film support exists. Under ideal conditions shearing occurs wholly within the adsorbed film and this results in low friction and negligible wear. In practice, however, polar molecules continuously desorb and re-adsorb onto sites on the metal surface even at low temperatures. At the highly loaded real areas of contact the energy dissipated may generate temperatures high enough for complete molecular desorption to take place. In these circumstances asperity contact occurs leading to an increase in frictional heat generation and further increase in contact temperature. On coming out of contact the asperity temperatures so generated are too high to allow re-adsorption of the additive molecules, but oxidation occurs due to the dissolved oxygen in the fluid. After contact the asperity rapidly cools in the bulk of the fluid and polar molecules adsorb onto the oxide surface. Thus the developed equilibrium surface consists of an oxide layer over which lies the adsorbed hydrocarbon film. Wear then occurs by the oxidational wear mechanism described by Quinn, Sullivan and Rowson[85] where the oxide grows to a critical thickness when it is removed to form a wear particle. This process of the growth of a protective oxide film under boundary conditions is illustrated in Figure 3.15.

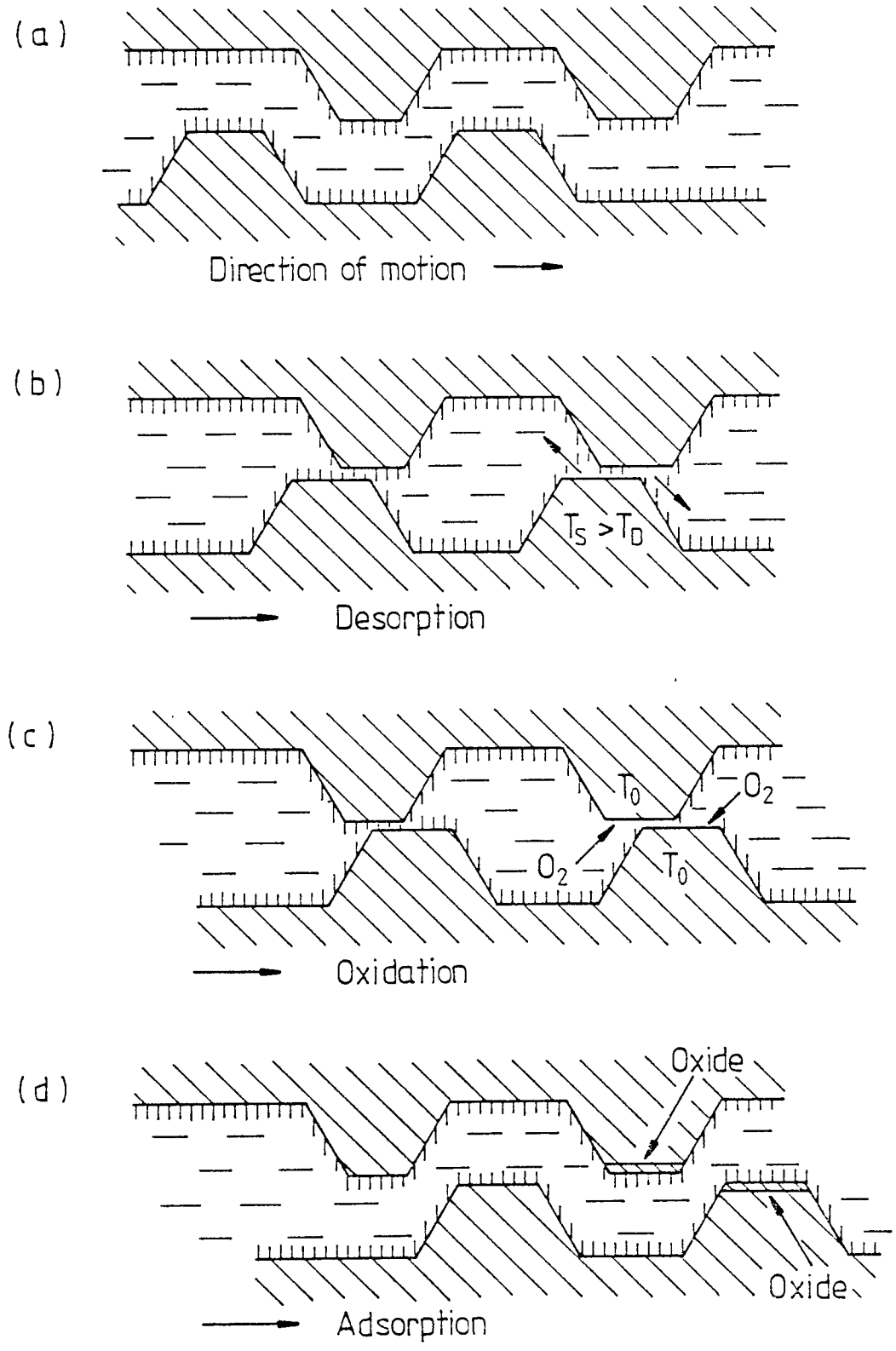

FIG. 3.15 PROCESS OF GROWTH OF A PROTECTIVE OXIDE FILM UNDER CONDITIONS OF BOUNDARY LUBRICATION. T_S IS THE GENERAL SURFACE TEMPERATURE, T_D THE MOLECULAR DESORPTION TEMPERATURE AND T_o THE OXIDATIONAL TEMPERATURE.

If the conditions of load or speed are too severe then the rate of growth of the oxide is less than the rate of surface removal and severe metallic wear and seizure ensue.

Under unlubricated conditions the real area of contact may be written[23] as

$$A_r = \frac{W}{P_m} \tag{3.1}$$

Where W is the applied load

P_m the flow pressure

Under conditions of boundary lubrication the majority of the supporting area A_r is covered by an adsorbed film and true asperity contact only occurs where desorption of the molecular film has taken place.

The fraction of the real area of contact not covered by the additive molecule at any instant is called the "fractional film defect", α, and may be defined as

$$\alpha = \frac{N_s - N_m}{N_s} \tag{3.2}$$

where N_s is the total number of sites available for the molecule and N_m is the number of occupied sites.

Thus the area of true asperity contact at any instant $A_r^{\perp}$ may be written

$$A_r^{\perp} = \alpha \frac{W}{P_m} \tag{3.3}$$

Since oxidation and hence oxidational wear can only occur at this area, then from Archard[101] we can write the wear rate w in terms of volume removed per unit distance of sliding as

$$w = K A_r^{\perp}$$

or

$$w = K \alpha \frac{W}{P_m} \tag{3.4}$$

where K is the Archard wear factor or the probability of forming a wear particle per encounter.

For oxidational wear, 1/K can be interpreted as the number of asperity encounters necessary to grow an oxide of critical thickness ξ , which then becomes detached to form a wear particle. From the oxidational wear theory[85] it has been shown that

$$K = \frac{2a A_p \exp - \frac{Q_p}{RT_o}}{U (f\rho\xi)^2} \tag{3.5}$$

where it is assumed that for thick oxide films, growth is diffusion controlled and follows a parabolic law.

In the above expression

a : mean contact radius

U : linear velocity

f : fraction of the oxide which is oxygen

ρ : density of the oxide

A_p : Arrhenius constant for parabolic oxidation

Q_p : activation energy for parabolic oxidation

R : the gas constant

T_o : temperature at which oxides are formed at the real areas of contact

Kingsbury[185,186] proposed a relationship between fractional film defect and the ratio of the time, t_x, for an asperity to travel a distance, X, equivalent to the diameter of an absorbed molecule to the periodic time of vibration of that molecule, t_r, such that

$$(1 - \alpha) = \exp - \frac{t_x}{t_r} \qquad (3.6)$$

where

$$t_x = \frac{X}{U} \qquad (3.7)$$

and according to Frenkel[187]

$$t_r = t_o \exp \frac{E}{RT_s} \tag{3.8}$$

t_o : fundamental periodic time of vibration of the molecule at the adsorbed site

E : molecular heat of adsorption

and T_s : the temperature of the surface film

Thus from (3.6), (3.7) and (3.8)

$$(1 - \alpha) = \exp - \left\{ \frac{X}{Ut_o \exp \frac{E}{RT_s}} \right\} \tag{3.9}$$

Rowe[188] showed that even for a poor boundary lubricant α is seldom greater than 10^{-2}, hence to a good approximation $\log_e (1 - \alpha) \simeq (- \alpha)$ and equation (3.9) becomes:-

$$\alpha = \frac{X}{Ut_o \exp \frac{E}{RT_s}} \tag{3.10}$$

combining equations (3.4), (3.5) and (3.10) gives:

$$w = \left\{ \frac{2a\ X \exp - \frac{E}{RT_s}\ A_p \exp - \frac{Q_p}{RT_o}}{U^2\ f^2\ \rho^2\ \xi^2\ t_o} \right\} \frac{W}{p_m} \tag{3.11}$$

If complete desorption of surface boundary molecules and hence asperity contact occurs when the surface temperature T_s reaches the molecular desorption temperature T_d, then

$$w = \left\{ \frac{2a \; X \; A_p \exp - \frac{E}{RT_d} \quad \exp - \frac{Q_p}{RT_o}}{U^2 \; f^2 \; \rho^2 \; \xi^2 \; t_o} \right\} \frac{W}{P_m} \qquad (3.12)$$

The quantity enclosed in the brackets in the equation (3.12) is the Archard wear factor for boundary lubricated oxidational wear.

3.4 Discussion

The results show that under relatively mild conditions the additive produces a pro-wear effect similar to that observed for first generation additives with this material combination by this author[166, 167] and by other workers[189]. The inclusion of the additive results in reduced wear rates only at the higher speed of 4 ms^{-1} and this is due rather to the wear rates for aluminium bronze in pure kerosene showing a significant increase. The high wear rate at higher speeds is somewhat unexpected, but can be explained in terms of the surface model proposed in Section 3.3 and the properties of the oxide film. This will be discussed in more detail later in this section.

All wear rate versus load curves shown in Figure 3.2 are linear and this linearity indicates a single dominant wear mechanism. For the majority of loads and speeds studied, however, there is only a small difference in wear rates whether the additive was present or not and the major function of the additive appears to be to prevent metal to metal contact and seizure under severe conditions.

In all cases both with and without the additive where seizure had not occurred, the wear debris consisted of Cu_2O and Cu and in the light of other evidence it may be surmised that the majority of the copper was due to the initial severe wear running in phase.

Electron probe microanalysis showed that there was transfer of material from the bronze surface to the steel counterface and that this film was rich in aluminium. It must be concluded that once formed, this transfer film was extremely adherent to the steel surface since the amount of aluminium in the debris was below the detection limit of XRD. Hence equilibrium debris could not have been generated from this layer, but must have originated from the pin surface. It is possible that the adherence of the film could be due to the formation of aluminium/iron intermetallic compounds similar to those observed by Dzhavaga and Lebeder [190].

The mechanism of aluminium depletion from the bronze surface and transfer to the steel is not fully understood, but Sury and Oswald[191] and Schussler and Napolitan[192] have shown preferential removal of aluminium and formation of Cu_2O on the surface of similar bronzes. Transfer of aluminium to the steel surface could occur due to the Kirkendall effect[193].

The fact that aluminium concentration in the transfer layer was high, but that in the debris low, suggests that depletion and preferential transfer occurs mainly in the initial stages of wear and subsequently only during film breakdown. This process leaves a copper rich surface on the bronze which oxidises to form a Cu_2O protective layer. The elastic moduli of Cu_2O and Cu (aluminium bronze) are very close and this would encourage the formation of a stable wear resistant film of Cu_2O . Al_2O_3, however, has a much higher elastic modulus that either Cu or Cu_2O and due to this mismatch any brittle aluminium oxide formed on the surface during the initial stages of film formation would be easily removed. This results was confirmed by the Auger spectra such as those shown in Figures 3.3 and 3.4, which show little trace of aluminium in the extreme surface region of the bronze. The results for the surface and debris analyses discussed above show little difference whether the additive was present in the kerosene or not. Further to this, the topo-graphies of surfaces worn with and without additive, as revealed by scanning electron microscopy, were

very similar showing smooth oxidized surfaces. Surface distress and plastic flow was only evident in those scanning electron micrographs taken from pin surfaces worn at high load and speed and worn in pure kerosene. The results indicate that both with and without additive present in the kerosene, the dominant mechanism is one of oxidational wear. It is only when the outermost layers are analysed using Auger electron spectroscopy that differences become apparent. The Auger depth profiles shown in Figure 3.6 and 3.7 show that surfaces generated in the presence of the additive under mild boundary conditions have less oxide and more hydrocarbon than those generated in pure kerosene. For surfaces at higher speeds and loads when wear trends are reversed, the profiles, Figure 3.9, show a very sparse coverage of both oxide and hydrocarbon for surfaces generated in pure kerosene, but a relatively thick oxide film for those worn in the presence of additive.

From the evidence discussed above from the mechanical measurements and the data from the complementary physical methods of analysis used, it is now possible to understand the mechanisms of boundary film formation and protection of the aluminium bronze surfaces in this system. The initial stages of formation depend on preferential surface depletion of aluminium and transfer to the steel counterface to produce a stable aluminium rich transfer layer. Subsequently the copper rich surface of the bronze oxidizes to form a thick protective film of Cu_2O. The extent of coverage of the film and the degree of protection afforded

then depends on whether the additive is present or not and on the severity of the conditions. The results show that under relatively mild conditions the additive slightly inhibits oxidation compared with the pure kerosene and this leads to less complete oxide coverage and higher wear rates. Under more severe conditions the additive still provides sufficient protection to allow surface oxidation and prevent catastrophic metallic wear and seizure.

These basic mechanisms of film formation and protection are essentially the same whether the additive is present in the kerosene or not and the only difference is in the degree of protection afforded. To understand why this is so it must be realized that the kerosene used here is not a pure single hydrocarbon. Vere[189] has shown that even after hydrofining and filtering to remove polar impurities, there are components within the kerosene which give the fluid some boundary action. Thus the presence of the dimeric acid additive provides an additional component having more effective boundary action, this probably being due to a combination of higher desorption temperature and higher heat of adsorption than the inherent boundary constituents in the base fluid.

All these results support the model proposed in Section 3.3 of this work and the model may now be used to further elucidate the phenomena associated with the wear of this and other boundary lubricated systems. Further considering this system in terms of the model. For the

kerosene without additive the boundary active components will desorb more readily from the surface than the dimeric acid additive molecules. Thus from the model, this will lead to greater oxide coverage and more oxide surface protection than when the dimeric acid is present, provided that conditions do not become too severe. The hypothesis here is that the oxide component in the complete boundary film is the major protecting element. Considering Equation (3.12) somewhat uncritically a reduction in desorption temperature, T_d , results in a reduction in wear rate. One factor should not be considered in isolation, however, as many parameters are inter-related, for example reduction in desorption temperature might also be expected to increase oxide thickness and this would also decrease wear rate. Thus for a poorer boundary lubricant under relatively mild conditions, it would be expected that the increase in surface oxide film protection over that for a good boundary lubricant would lead to lower wear rates and this is what has been found for the 0.6 and 2 ms^{-1} experiments reported here.

There will obviously be a limit to this effect. If surface active molecules are too easily removed, then attrition rates will always be greater than oxidational growth rates and the system will remain in a severe wear mode. In the case of these experiments for kerosene alone, then as conditions become more severe, boundary action breaks down, the wear rate becomes greater than the oxide growth rate and severe wear ensues. This is shown in the 2

and 4 ms^{-1} experiments at loads of 196 and 122.4 N respectively. With the additive present under these conditions its greater tenacity and boundary effectiveness give sufficient protection to the surface to allow the oxide film to grow and be maintained, thus preventing seizure and severe wear. If the load had been increased in these experiments to values exceeding the limit imposed by the apparatus, it is expected that seizure would eventually have occurred.

From the wear rate versus load graphs shown in Figure 3.2, there is also an effect due to speed. This is connected both with surface temperature and the nature of the oxide film produced. Increase in speed leads to an increase in contact temperature and Equation (3.12) predicts that such an increase should lead to an increase in wear rate. For a good boundary additive or where the temperatures are not too high this effect is obviously secondary to the better protection provided by increased surface oxide coverage. It will be shown later in this section, however, that an increase in speed from 2 to 4 ms^{-1} gives rise to a relatively large predicted temperature increase, such that contact temperatures at the lowest load at 4 ms^{-1} are as high as those at the highest load at 2 ms^{-1}. In the case where the boundary action is relatively weak, that is for kerosene without additive, the higher temperatures lead to more asperity contact, more rapid attainment of critical oxide thickness and hence more rapid production of oxide wear debris.

There is a further effect on wear due to the nature of the oxide Cu_2O . If the possible mechanisms of removal of the oxide after attainment of critical thickness are considered Cu_2O has a relatively low Pilling Bedworth[156] ratio of 1.64 and further to this is a metal deficit semiconductor, which grows due to cation diffusion. Thus stress produced within the oxide due to growth will be small, but voids will accumulate at the metal/oxide boundary thus favouring laminar removal. The ratio of thermal expansion coefficients of metal and oxide, α_m/α_o , is high and equal to 4.32 (compared for example to a ratio of 1.03 for Fe/Fe_3O_4). Calculation from the Equation (2.29), derived from the formula due to Oxx[158], show that thermally induced stresses of the order of ten times the yield stress could be produced within the oxide by transient contact temperatures of 500^0C. These thermally induced stresses will become particularly significant at higher surface temperatures and with thicker oxides. Thus at higher speeds with weak boundary lubricants the combination of higher oxidational growth rates leading to more rapid attainment of critical thickness plus the greater effect of thermally induced stresses on oxide stability leads to higher wear rates. With the dimeric acid additive present it is still effective in limiting growth rate under these conditions and hence minimizing both of the above effects. For optimum conditions there appears to be a fine balance to be maintained.

In all cases for kerosene both with and without additive surface effects can be explained in terms of competing interactions between the surface active molecules from the fluid and oxygen also originating from the fluid. The differences in magnitudes in wear rates are simply due to the relative boundary effectiveness of the polar molecules. The oxygen giving rise to surface oxidation is in this case probably due to dissolved oxygen in the fluid, but it is possible as suggested by Newley, Spikes and Macpherson[131] that metal oxidation takes place by reaction with peroxy radicals which form as intermediates due to oxidation of the lubricant. The source of the oxygen ions is probably not a rate determining factor and hence does not affect the basic mechanisms proposed in this chapter.

Summarizing the findings of this investigation, therefore, in this boundary lubricated system oxidational wear is the dominant mode and the experimental observations support the theory of boundary lubrication and oxidational wear developed in Section 3.3 The surface model has proved useful in developing a better understanding of boundary lubricated systems, but the theoretical relationship derived from the model, Equation (3.12), contains a number of ill-defined parameters. Probably the most difficult of these parameters to determine is the temperature at the real areas of contact, T_o , although dynamic thermocouple measurements indicate that temperatures in the region of 500^0C were attained. Hence in order to test the quantitative validity

of the theory for the experiments with kerosene plus additive, the measured values of wear rates for different loads and speeds will be used together with other parameters, to calculate values of T_o from Equation (3.12). Insufficient is known of the properties of the polar components in the kerosene to conduct a similar exercise for the experiments in kerosene without additive.

It is first necessary to assign values to the other quantities in Equation (3.12).

Direct measurement of the contact radius "a" is not possible, however, from the surface model proposed in Section 2.3 an equation may be derived describing the variation in mean contact radius with change in applied load. From Equations (2.4), (2.5) and (2.9), the asperity contact temperatures of the pin and disc respectively may be expressed as:

$$T_{o_p} = T_{s_p} + \frac{\delta H_T \pi a P_{m_p}}{4 W K_{m_p}} + \frac{\delta H_T P_{m_p} \xi_p}{W K_{o_p}} \qquad (3.13)$$

and

$$T_{o_d} = T_{s_d} + \frac{\beta(1-\delta) H_T \pi a P_{m_d}}{4 W K_{m_d}} + \frac{\beta(1-\delta) H_T P_{m_d} \xi_d}{W K_{o_d}} \qquad (3.14)$$

where

T_o, T_s : contact and surface temperatures respectively

H_T : total heat generated at contacts

δ : the proportion of that heat which flows into the pin

β : a factor to account for the moving heat source

K_m, K_o : thermal conductivities of metal and oxide respectively

P_m : flow pressure

a : mean contact radius

W : load

the subscripts "p" and "d" refer to pin and disc materials respectively.

The temperatures at the contacting asperities must be the same for both pin and disc, that is $T_{o_p} = T_{o_d}$. Hence if a number of simplifying assumptions are made, for example that

oxide thickness and division of heat do not change significantly with load and that the effect of "a" on the speed dependent parameter β is negligible, then equating (3.13) and (3.14) produces a linear equation in "a" of the form:

$$a = R + SW \qquad (3.15)$$

Many of the parameters required for the evaluation of the constants R and S in Equation (3.15) are not available for the present experiments. However, considering the results of the previous chapter, where graphs of "a" versus "W" are plotted for two different steels of similar hardness to the bronze used in this part of the investigation. Then Figures 2.22 and 2.26 show linear reductions in the mean contact radius with load. Taking the data of Figure 2.22 since the load range in this figure is closer to that of this investigation, then mean values of the constants may be calculated such that $R = 6.8 \times 10^{-6}$ m and $S = -0.03 \times 10^{-6}$ m N^{-1}. Inserting these values into Equation (3.15) gives:

$$a = (6.8 - 0.03W) \times 10^{-6} \qquad (3.16)$$

The steels used in the investigations described in Chapter 2 of this work were of similar surface roughness to the bronze and load and speed ranges were also similar. Hence it may be assumed that the size and distribution of

contact spots will depend only on material hardness and that the author is justified in applying this relationship to the present results.

The molecular diameter "X", must be at least equal to the width of the ring structure of the acid additive and this imposes a lower limit on the value of X of 6.85 x 10^{-10} m . Calculations due to a formula proposed by Beerbower[194] give a value of X equal to 1.5 x 10^{-9} m. For the purpose of this calculation a mid value of X = 1 x 10^{-9} m was assumed.

The fundamental periodic time of vibration "t_o" was shown by Lindemann[195] to be given by the equation:

$$t_o = 1.54 \times 10^{-9} \left\{ \frac{MV_m^{2/3}}{T_m} \right\}^{1/2} \text{ seconds}$$

where

M is the molecular weight of the additive

V_m is the molecular volume

and T_m is the melting temperature

inserting appropriate values gives $t_o = 3 \times 10^{-12}$ s .

The heat of absorption "E" was taken as E = 55kJ mole $^{-1}$ (Allen and Drauglis,[196]) and desorption temperature "T_d" as T_d = 353K (Dakre, Savory and Wheeler[197]).

Scanning electron micrographs, for example Figure 3.12, indicate that the mean critical oxide thickness "ξ" was about 1μm and no significant variation was found in this value over the range of loads and speeds employed. The mean measured flow pressure immediately below the oxide surface was 2×10^{9} Nm^{-2}. The fraction of the oxide Cu_2O which is oxygen is 0.11 and the density of the copper oxide is 6×10^{3} kg m^{-3}.

For a thick oxide grown under the conditions of these experiments, oxidation may be assumed to be diffusion controlled and to obey a parabolic growth rate law. Tylecote[169] has reported values for the parabolic oxidation constants for copper oxide grown under static conditions in the temperature range up to 500^{0}C. The activation energy for low temperature oxidation is reported as Q_p = 84 kJ $mole^{-1}$ and although there was considerable variation in reported values of Arrhenius constant, the theoretical and experimental work of Valensi [170] suggests that A_p 1.6×10^{-3} kg^{2} m^{-4} s^{-1}. Sullivan, Quinn and Rowson[59] have shown, however, that "tribo-oxidational" growth rates are very different to those measured under static conditions, the difference in growth rates being due to large variations in Arrhenius constants. This point has been discussed at length in both Chapters 1 and 2 of this work.

If the static values of A_p reported by Velensi are used together with other parameters in Equation (3.12), the calculated values of T_o are either excessively high or no valid solution is found.

Following this argument the static values of Q_p (Tylecote[169]) are used in the calculations, but the static values of A_p are not appropriate. Poole[198] has shown that the most probable value of Arrenhius constant for the "tribo-oxidation" of copper measured under similar conditions to the experiments described here is $A_p = 1.3 \times 10^6$ kg^2 m^{-4} s^{-1} and it is this value which has been employed in the calculations. An order of magnitude variation in this value of A_p produces a 20% variation in the calculated value of T_o under the most severe conditions.

Rearranging Equation (3.12) in terms of T_o gives:

$$T_o = \frac{Q_{p/R}}{\log_e \left\{ \frac{2a \times A_p \exp - E/RT_d}{U^2 f^2 \rho^2 \xi^2 t_o \cdot w/W P_m} \right\}}$$

and inserting the values of the parameters discussed above into this equation, we have:

$$T_o = \frac{1.01 \times 10^4}{\log_e \left\{ \frac{7.0 \times 10^{-9} \ (6 - 0.03W)}{U^2 . \ w/W} \right\}}$$

Further, if values of wear rate are inserted for each load and speed combination, then corresponding oxidational temperatures T_o can be calculated. Figure 3.16 is derived from these calculated values and shows contact temperature expressed in degrees Celcius as a function of load, for speeds of 0.6, 2.0 and 4.0 ms^{-1}.

The figure shows a calculated temperature range from 300^0C to 500^0C which is in agreement with the rough estimates of contact temperatures determined from dynamic thermocouple measurements.

It is realized that the model proposed in this work does not account for all of the complex processes which must be occuring at the real areas of contact during boundary lubrication and many simplifying assumptions have had to be made. However, the closeness of the agreement between the contact temperatures calculated on the basis of the model and those to be expected in practice together with the fact that the model coincides with physical experimental observations indicates that the approach is essentially correct.

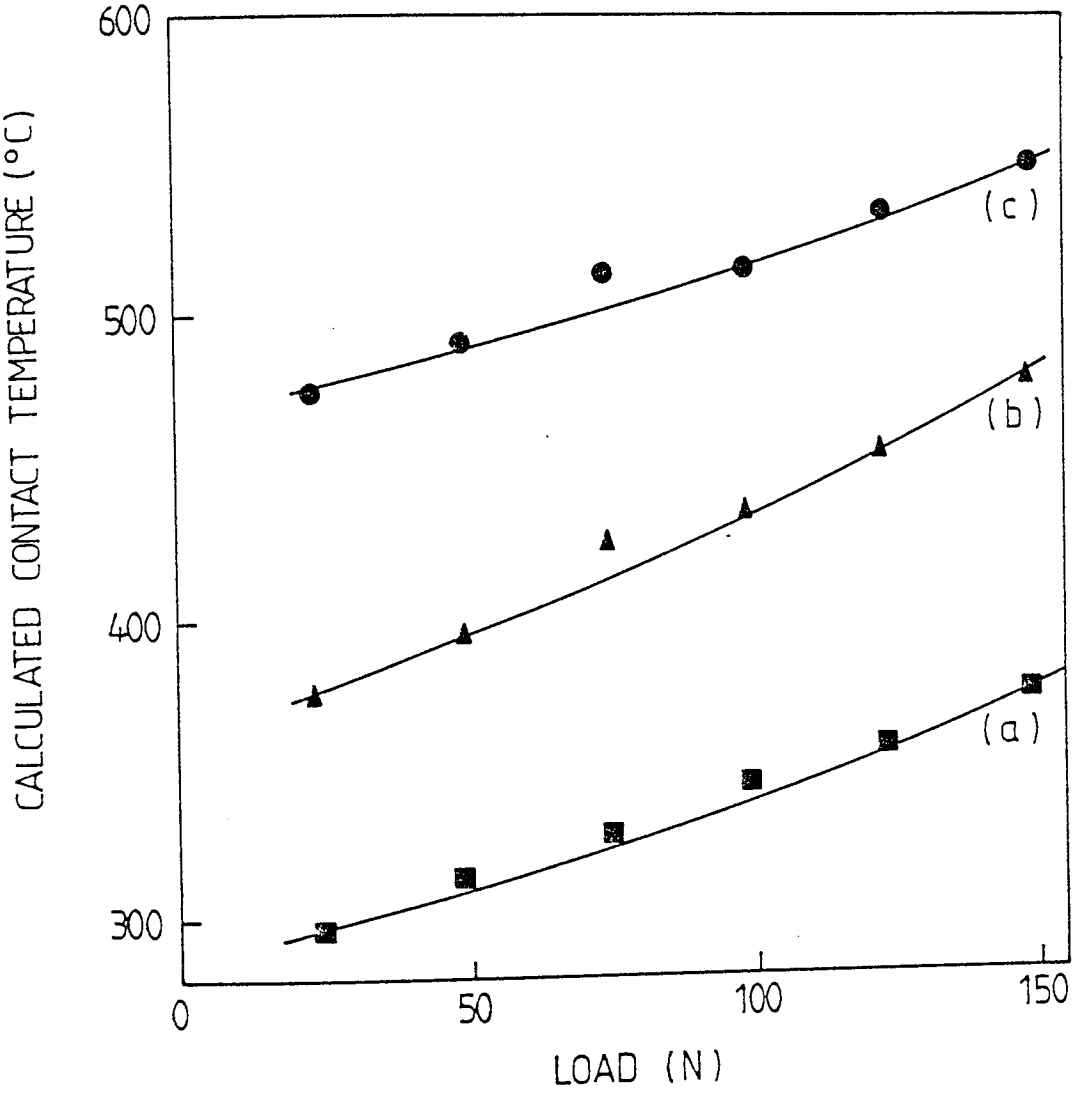

FIG. 3.16 CALCULATED ASPERITY CONTACT TEMPERATURES VERSUS LOAD FOR EXPERIMENTS CONDUCTED WITH KEROSENE PLUS ADDITIVE AT SPEEDS OF ; (a) 0.6 m/s, (b) 2 m/s, (c) 4 m/s.

CHAPTER 4

RECIPROCATING WEAR OF STEEL IN CO_2 AT HIGH TEMPERATURE

In Chapters 1 and 2 two different systems have been described, one dry and one lubricated, where oxidational wear is the dominant mode and where the load bearing oxide plateaux consist of physically homogeneous oxide film, which grow due to a diffusion controlled mechanism. There are a number of reasons for this particular type of oxide growth and these include system geometry, material properties and environment.

In order to provide a contrast the experiments described in this chapter would be expected to produce a quite different type of protective oxide film. The experiments were conducted in carbon dioxide where gas-metal phase boundary interactions may be important, on a slow speed reciprocating sliding test rig which encouraged debris accumulation and at elevated temperature which would promote agglomeration.

Because of the very long time periods taken for the tests under the conditions described in this chapter mild equilibrium wear was not studied in detail, but it was felt more appropriate to examine the mechanisms leading to the formation of stable supportive oxide films. The 9% chromium steel used in the study was chosen for its practical applications in the nuclear power industry where it has been used in boiler components subject to large amplitude vibrations[199].

4.1 Experimental Apparatus and Procedures

All wear tests described in this study were carried out on a reciprocating wear test rig a diagram of which is shown in Figure 4.1 In this apparatus a flat specimen 32 mm x 13 mm x 3 mm, was mounted on the lower driven beam and was subject to reciprocating sliding against a specimen with a domed end of 12 mm diameter and 13 mm length mounted on the upper loading beam. A detail of this arrangement is shown in Figure 4.2. Loads of either 22 or 41 N were then applied to this upper beam by means of a pulley with dead weight loading. The lower reciprocating beam was driven by a variable speed 1 h.p. motor through a crank. For these experiments the crank was adjusted to give a constant stroke length of 9 mm and the speed varied to give reciprocating frequencies between 1 and 8 Hz. The mean sliding speed referred to later in this chapter, is then the product of twice the stroke length and the reciprocating frequency.

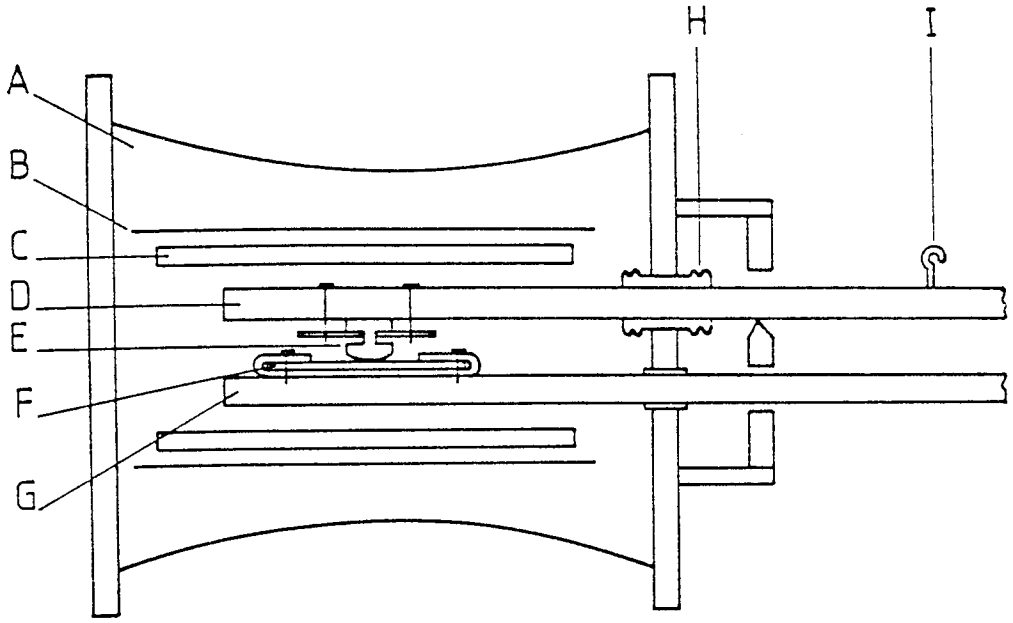

KEY

A. Air-tight specimen chamber.
B. Metal heat shield.
C. One of the ten 300W heaters.
D. Upper, or loading, beam.
E. Pin specimen.
F. Flat specimen.
G. Lower, or sliding, beam.
H. Bellows allowing vertical movement of the loading beam.
I. Point at which load is applied.

FIG. 4.1 SCHEMATIC DIAGRAM OF THE RECIPROCATING WEAR TEST RIG.

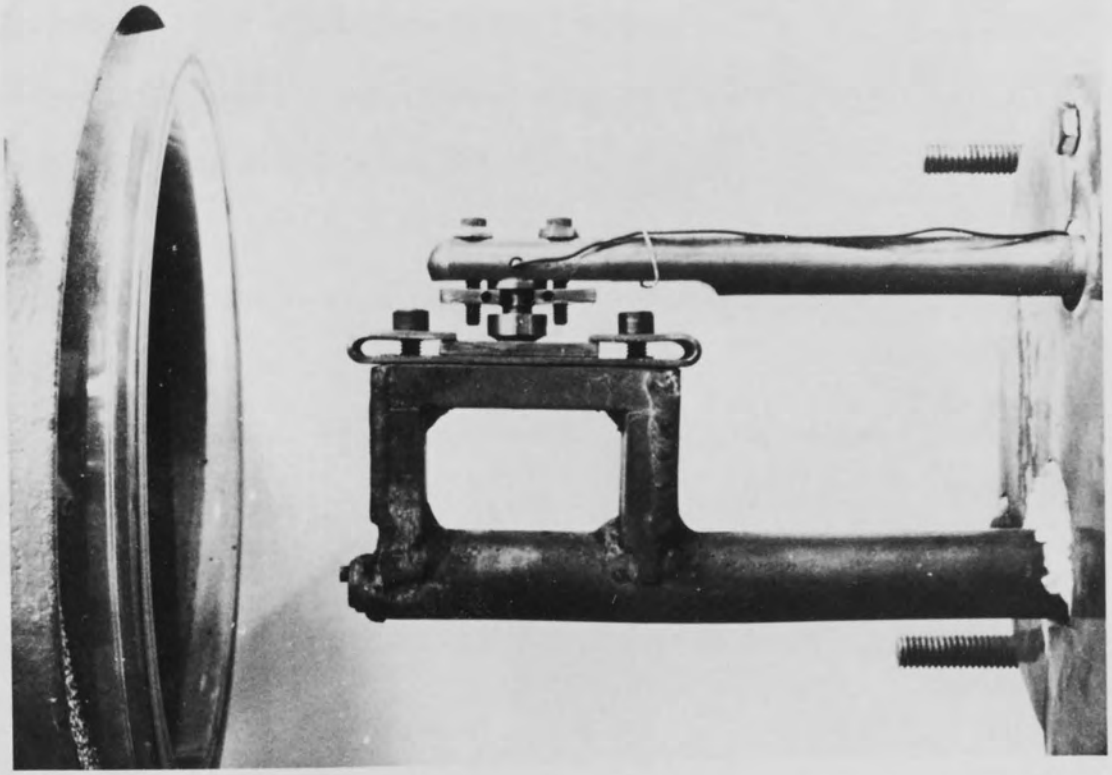

FIG. 4.2 DETAIL OF PIN AND FLAT SPECIMEN LOCATION.

The specimens were contained in an air-tight chamber, of which the temperature inside could be maintained at values up to 600^{0}C by means of ten 300W heater elements. The temperature could be held constant to $\mp$ 1^{0}C over the whole range. The atmosphere within the specimen chamber was pure carbon dioxide held at a positive pressure of 1.5 bar and admitted at a constant rate of $8 \times 10^{-5} m^3 min^{-1}$ in order to ensure that metal oxidation did not alter gas composition and that no back diffusion of air into the chamber occurred.

The specimens were produced from 9% Cr steel and were thoroughly cleaned in a petroleum vapour bath prior to use. A new pin and flat specimen were used for each experiment. The 9% Cr steel was of the same composition as that used in some of the unidirectional sliding wear experiments described in Chapter 2 of this work and its composition is given in Section 2.1.

Friction was measured using a strain gauge dynomometer located at the end of the loading beam and due to the length of many of the experiments was recorded intermittently on the ultraviolet recorder. Overall wear rates were determined by specimen weight loss, but this, if an experiment was run to its conclusion, gave no indication of the proportions of the material removed in the various wear modes encountered. A linear voltage differential transducer was employed with the object of remedying the situation, but since the wear rates were low and the transducer necessarily

had to be located remote from the wearing surface where it was subject to considerable vibration, the results from this source proved unreliable. The transducer did, however, prove useful in confirming when a transition from severe to mild wear had occurred, since at that point overall vibration was reduced and the trace became less noisy.

Wear test runs were conducted in carbon dioxide at 275^{0}C, 290^{0}C, 300^{0}C and 450^{0}C with a load of 22 N and at 300^{0}C with a load of 41 N. Mean reciprocating sliding speeds were varied from 18 mm s^{-1} to 144 mm s^{-1} and the number of cycles required for the system to reach the severe/mild wear transition (N_T) was noted. From the value of N_T, the total sliding distance to reach such a transition, D_T, was calculated. For comparison a small number of experiments were also conducted in air.

In addition to these wear tests, experiments were conducted at a sliding speed of 36 mm s^{-1} and a load of 22 N for temperatures between 200^{0}C and 550^{0}C in order to establish a relationship between D_T and temperature, and a further series conducted to investigate the effects of static oxidation on the establishment of stable oxidational wear conditions. In the first of this latter series, specimens were mounted on the apparatus in the usual way and pre-heated to a temperature of 290^{0}C for 750 h. After this period, the wear test was continued as previously described until a severe/mild wear transition occurred when the value of D_T was noted and compared with values obtained from

similar experiments conducted without the extended period of pre-heating. Three tests were then carried out under various conditions where the specimens were worn for several thousand reciprocating cycles and then the motion stopped when the specimens were left at the operating temperature for a "dwell period" where static oxidation took place. The dwell period was then followed by a further period of sliding, the whole process being repeated several times until a transition occurred, when the value of D_T was noted. Two of these dwell tests were carried out at 290^{0}C and 300^{0}C with dwell periods of 96 h and loads of 22 N and 41 N and one at 450^{0}C with a 4 h dwell period and a load of 22 N. The dwell periods were chosen to be about 5 times the expected time required for a transition to occur without dwell. A further series of tests was conducted to determine relative weight gains and losses in successive periods of dwell and wear.

Debris was collected after some experiments and analysed by means of X-ray powder diffraction techniques using similar apparatus and conditions to those described in Section 2.1. The surfaces of some specimens were also examined using glancing angle X-ray diffraction in the same Debye-Scherrer camera. Taper sections of some selected specimens were produced in order that micro-hardness versus depth measurements might be made. Scanning electron microscopy was employed to study surface topography and to give some insight into the nature and thickness of oxide plateaux and a limited number of Auger depth profiles were

recorded on oxide plateaux in order to gain further information on the nature of the protective oxide film through a study of the oxygen, iron and chromium concentration with depth.

4.2 Experimental Results

4.2.1. Wear and Wear Transitions

Due to the fact that the system was totally enclosed and that it was not possible to locate a wear transducer close to the wearing contact it was generally not possible to determine accurately wear rates for the various wear modes experienced during these experiments. It was obvious, however, from the limited data recorded from extensive surface examination and from careful monitoring of friction traces that three types of wear were occurring:

(i) running-in severe wear

(ii) equilibrium severe wear

(iii) equilibrium mild (oxidational) wear.

In all experiments described here running-in severe wear was encountered initially, before the system settled into one of the two other modes. For the conditions of these experiments, the type of equilibrium wear mode was determined by the ambient temperature. For temperatures

of 290^{0}C and above, a transition from severe to mild wear occurred for all sliding speeds after a prolonged period of sliding. For temperatures below this value, no such transition occurred and the system settled into an equilibrium severe wear mode at all sliding speeds.

Severe/mild wear transitions were indicated by the friction trace, an example of which is shown in Figure 4.3 and also by a substantial reduction in the noise on the LVDT output trace. Figure 4.3 shows a gradual fall in friction coefficient from an initial value of 1.5 to a value of 0.7 over a sliding distance of 1000 m, followed by a rapid fall to a value of 0.3 over a further sliding distance of 1.8 m. The data shown were recorded for an experiment conducted at 290^{0}C with a load of 22 N and mean sliding speed of 36 mm s^{-1}, but the general pattern was typical of all experiments in which severe/mild wear transitions were observed. Experiments conducted in air under similar conditions of load, speed and temperature showed similar variations, but the distance of sliding required to reach the transition was about two orders of magnitude lower, that is about 10 m. Wilson, Stott and Wood[91] observed similar behaviour for experiments on a 9.2% Cr steel run in air at elevated temperature. In the small number of experiments run on after the wear transition, the friction coefficient was observed to increase to an equilibrium value of between 0.4 and 0.6 after a sliding distance of the order of $2D_T$.

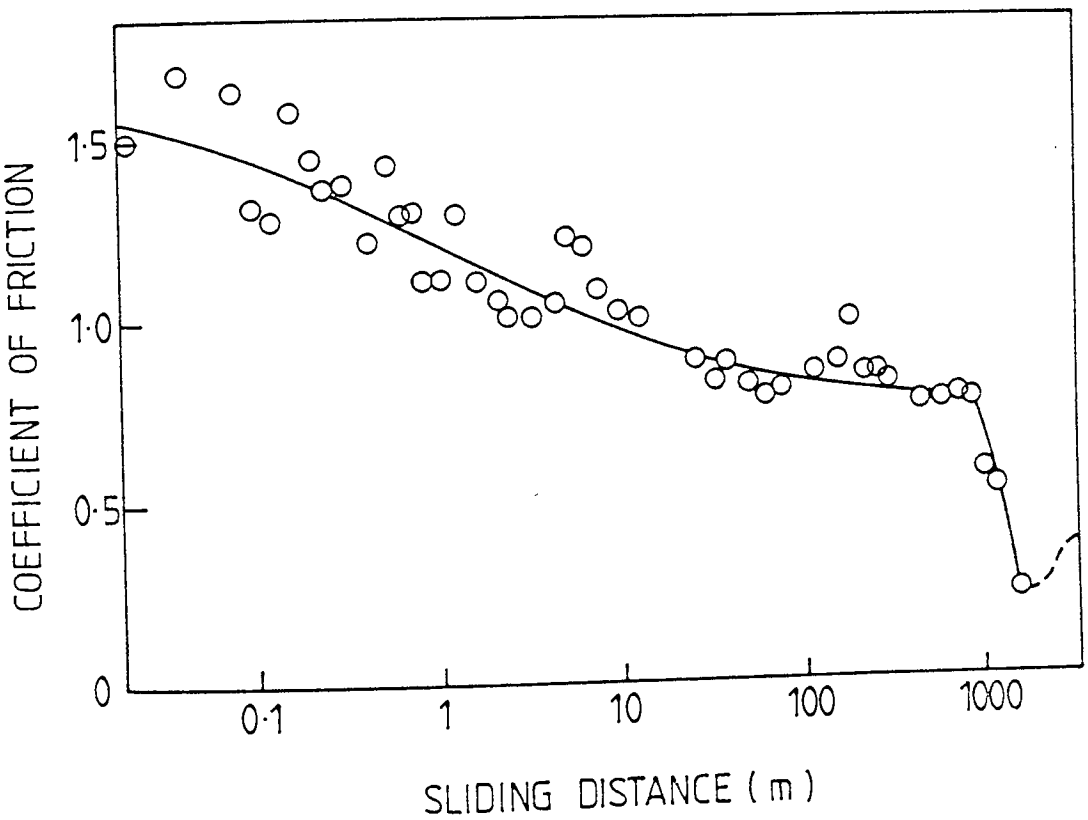

FIG. 4.3 COEFFICIENT OF FRICTION VERSUS SLIDING DISTANCE FOR EXPERIMENTS CONDUCTED AT A MEAN SLIDING SPEED OF 36 mm/s, LOAD OF 22N AND TEMPERATURE 290 °C .

Experiments conducted at 275^{0}C gave initial friction traces similar to that shown in Figure 4.3, but these levelled out to a value of 0.7 and showed no transition.

In the majority of experiments conducted at 290^{0}C and above during this investigation, the run was terminated soon after the severe/mild wear transition occurred and the sliding distance required to produce the transition, D_T , noted. Figure 4.4 shows the variation of D_T with ambient temperature recorded for a load of 22 N and speed of 36 mm s^{-1}. In this particular series additional experiments were conducted at temperatures of 200^{0}C and 550^{0}C, but the same general trend was exhibited for all other load and speed combinations. The decrease in D_T was due to the increasing rate of oxide production with increasing temperature. At temperatures below 290^{0}C the rate of oxide growth was clearly always less than its rate of removal and hence no transition occurred.

Figure 4.5 shows the variation in D_T with mean sliding speed at 290, 300 and 450^{0}C with 22 N load and at 300^{0}C with 41 N load. The lower temperature curves show the same general pattern; an increase in D_T to a maximum at a mean speed of about 120 mm s^{-1} followed by a fall with further increase in speed. The initial slope of the curves shows that D_T is directly proportional to speed which implies that the time taken to reach the transition is constant for any given combination of load and temperature

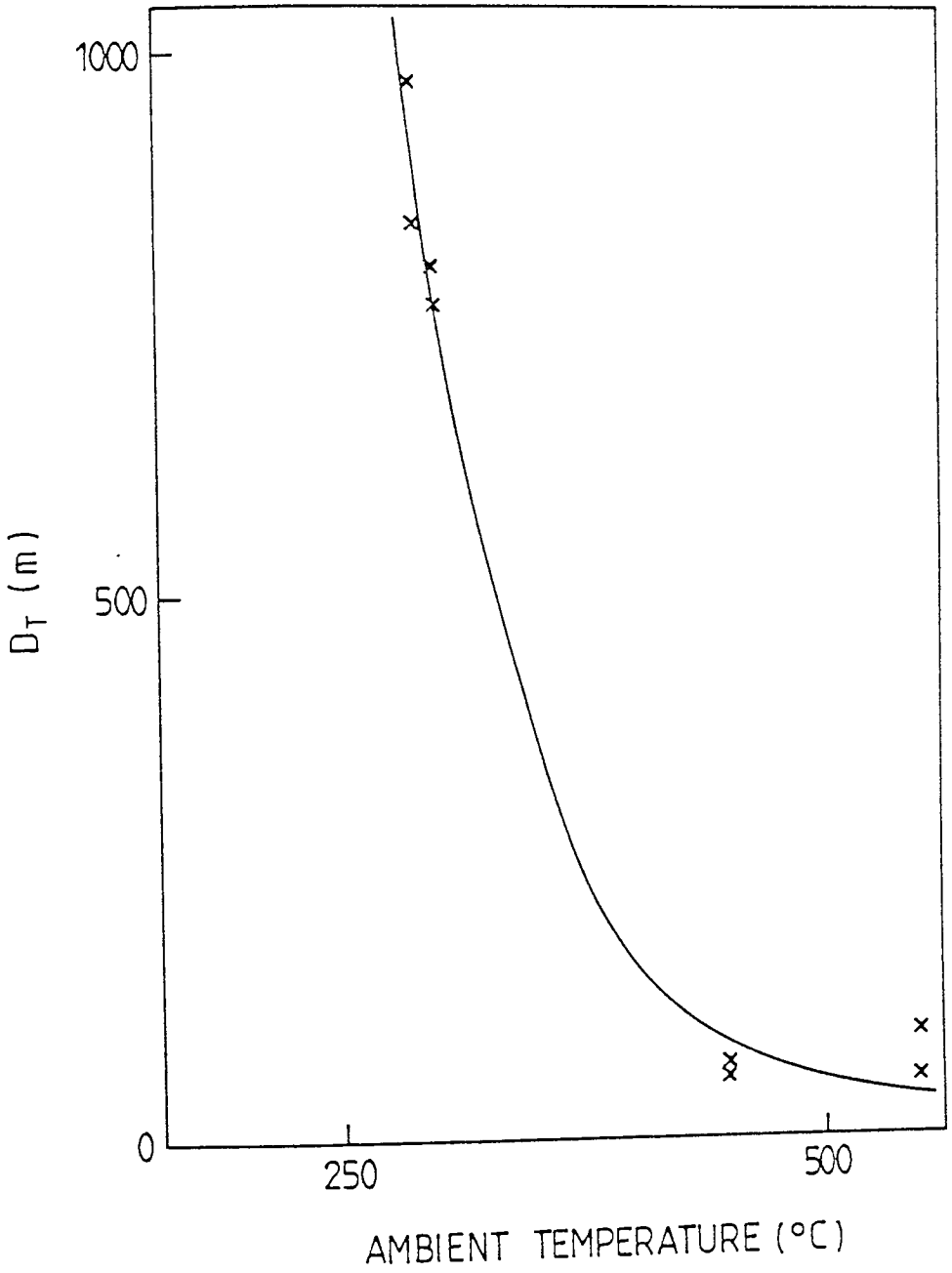

FIG. 4.4 DISTANCE OF SLIDING TO THE TRANSITION, D_T, VERSUS AMBIENT TEMPERATURE FOR EXPERIMENTS CONDUCTED AT A MEAN SLIDING SPEED OF 36 mm/s AND LOAD OF 22N.

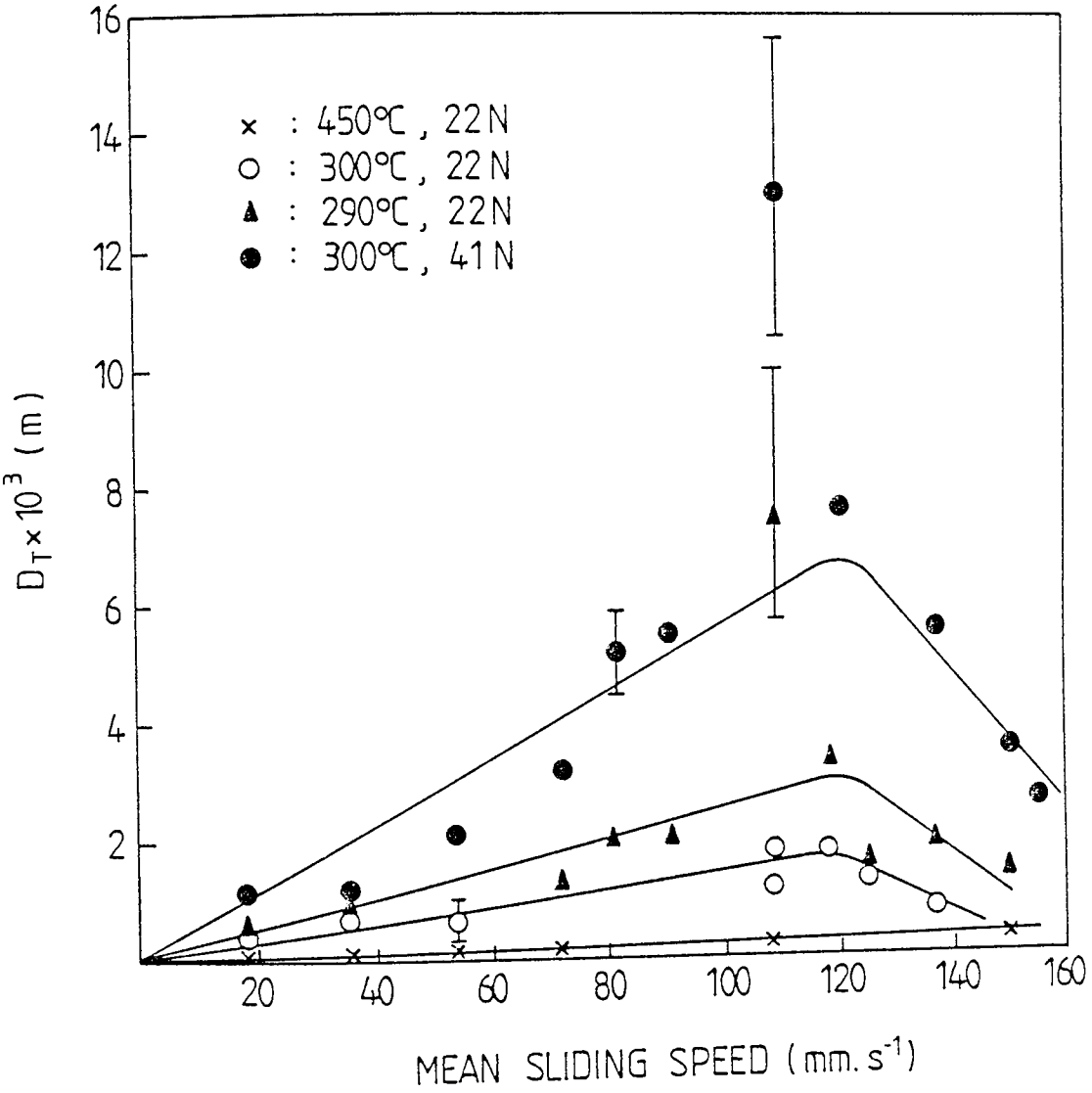

FIG. 4.5 DISTANCE OF SLIDING TO THE TRANSITION, D_T, VERSUS MEAN SLIDING SPEED AT DIFFERENT AMBIENT TEMPERATURES.

and is independent of sliding speed up to a velocity of approximately 120 mm s^{-1}. The time taken to reach a transition was not specifically measured in any experiments. At speeds in excess of 120 mm s^{-1} the time taken to reach the transition decreases for the experiments conducted at 290 and 300^{0}C. The graph of D_T versus speed for the experiments at 450^{0}C is linear over the whole speed range indicating a constant time to transition independent of speed. Variations from linearity were observed at speeds of about 110 mm s^{-1} where non-typically large values of D_T were recorded. It is possible that this was due to machine resonance at the oscillating frequency, 6 Hz, corresponding to this speed.

Mean specific wear rates for these experiments calculated from total weight loss up to the point of transition were recorded. There was a great deal of experimental scatter in these values, but generally they showed that the overall mean specific wear rate up to the point of transition increased with increasing temperature. This is opposite to the observations in Chapter 2 of this work, where mild wear rates for a unidirectional sliding system were found to decrease with temperature. This point illustrates that material removal during the running-in phase in this system is dominated by severe metallic wear. These values of average specific wear rate taken over the whole of the pre-transition period are not particularly informative since they give no indication of the variation in instantaneous wear rates throughout a test run. Such a

variation in specific wear rate is indicated in Figure 4.6 which shows the cumulative volume removed with time of sliding. In the series of experiments represented in this figure, test runs were stopped after 100, 1000, 5000, 15000, 30000, 45000, 75000 and 100000 reciprocating cycles and weight loss for both pin and flat recorded. A new set of specimens was used for each run. The curves in Figure 4.6 show a continuously falling wear rate with time (or distance) for both pin and flat. The running-in severe wear on the flat was the greater of the two, but mild wear rates estimated from the slope of the curves after the transition, were probably about the same. Also included in this figure is a theoretically derived curve from the surface model proposed in the next section.

It was difficult to measure mild wear rates because of the closed system and of wear rate being determined primarily by weight loss, the majority of which was due to the severe running-in period. It typically took about 8 hours of sliding for a 290^{0}C temperature experiment to produce a severe/mild wear transition. If it is assumed that mild wear rates are two orders of magnitude lower than severe rates it would take 800 hours or almost five weeks to remove an equivalent amount of material.

Two attempts were, however, made to calculate mild wear rate. The first used the results from two experiments run under similar conditions at a load of 22 N, speed 36 mm s^{-1} and 300^{0}C. It was assumed that the total weight

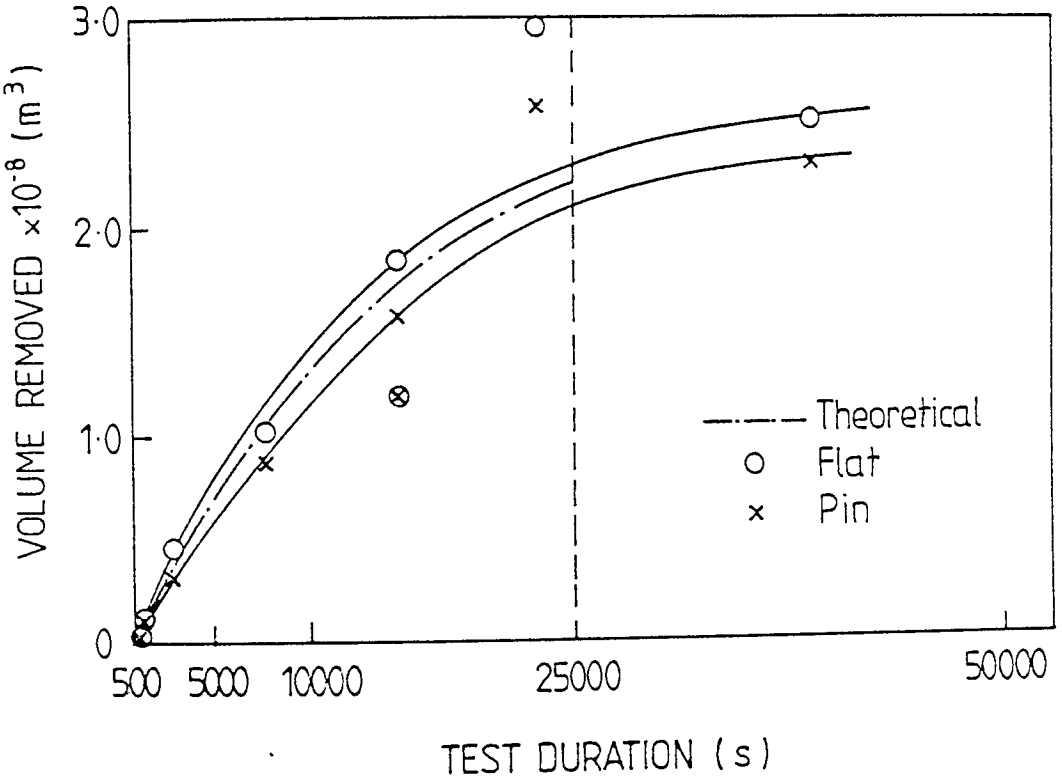

FIG. 4.6 VOLUME REMOVED VERSUS TIME OF SLIDING FOR EXPERIMENTS CONDUCTED AT A MEAN SLIDING SPEED OF 36 mm/s, LOAD 22N AND TEMPERATURE 290 °C.

loss was equal to the sum of a severe wear and mild wear component such that:

$$\text{Total weight loss} = w_s \rho_s D_T + w_m \rho_c (D - D_T)$$

where w_s and w_m are mean severe and mild wear rates respectively

ρ_s and ρ_o are densities of steel and oxide respectively

D_T the distance of sliding to the transition

D total distance of sliding.

The data from the two experiments is:

		Experiment 1	Experiment 2
D	(m)	1.15×10^3	49.7×10^3
D_T	(m)	0.76×10^3	0.85×10^3
Total weight loss	(kg)	86.6×10^{-6}	128.4×10^{-6}

Solving the simulaneous equations gives:

mean severe specific wear rate = $7 \times 10^{-13} \text{ m}^3 \text{N}^{-1} \text{m}^{-1}$

mean mild specific wear rate = $4 \times 10^{-15} \text{ m}^3 \text{N}^{-1} \text{m}^{-1}$

A second estimate of the mild wear rate was obtained using the output from the LVDT from experiment 2 and this gave a mild wear rate of 5×10^{-15} $m^3 N^{-1} m^{-1}$.

All attempts to measure mild wear rates by stopping the experiment just after the transition, weighing the samples and replacing and restoring them, yeilded much higher apparent wear rates. This was due to the fact that it was not possible to re-locate the samples exactly and this led to a further period of running-in.

4.2.2. Static Oxidational "Dwell Tests".

The results of "dwell tests" to investigate the effects of static oxidation on the development of the protective oxide film are summarized in Table 4.1.

In the series of experiments designed to assess weight gains and losses the gains during dwell periods were always very much less than weight losses due to wear in the shorter intervening sliding periods. For example, for an experiment carried out at 290^0C, 22 N load and a mean sliding speed of 110 mm s^{-1} , the weight gain of the pin over the 96 hour dwell periods averaged 0.1 mg, indicating an increase in oxide mass of a little over 0.3 mg. The oxide grown in this period is, however, distributed over the whole surface area of the pin and hence the increase at the wearing surface will be very much smaller than this. Weight gains on the

TABLE 4.1

Results of dwell test conducted to investigate the effects of static oxidation.

Sliding speed, mms^{-1}	Load, N	Temperature, ^{o}C	Initial sliding distance, m	Dwell period, h	Transition distance, m
110	22	290	0	750 *	5400(6100)
	22	290	180	96	585(6100)
	41	300	180	96	960(9000)
	22	450	36	4 **	225(216)

* In this experiment, specimens were heated for 750h prior to sliding, which was then continuous until a transition occurred.

** In this experiment, the initial sliding distance was followed by one 4h dwell period. The test was then run continuously to the transition. Transition distances for experiments conducted under the same conditions but with no dwell periods are shown in brackets in the last column.

flat during the same period were a little lower.

In contrast to this weight losses in the 27 minute sliding periods varied from 57 mg in the severe wear dominated first 180 m period to 0.8 mg in the mild wear dominated last period of sliding.

4.2.3. Microhardness Measurements

In Section 4.2.1 the results of a series of experiments to determine cumulative weight loss with sliding distance are shown in Figure 4.6. After weighing, selected samples were taken from this series, taper sections were prepared and microhardness measurements made at various depths into the specimens. Figure 4.7 shows a typical hardness versus depth curve, each plotted point is the mean value taken from five indentations. In all cases there was a hardened layer near to the surface, the depth being fairly constant at about 30 μm for all specimens run between 1000 and 100,000 reciprocating cycles. The wear scar produced on the specimen run for 100 cycles was too small for any meaningful data to be obtained. Maximum hardness of the subsurface region for speciemens taken from the severe wear region varied between 400 and 650 HV, but not in any systematic way. Hardnesses as high as 1500 HV were recorded on samples measured after the mild wear transition very close to the surface, but these were almost certainly due to the surface oxide film.

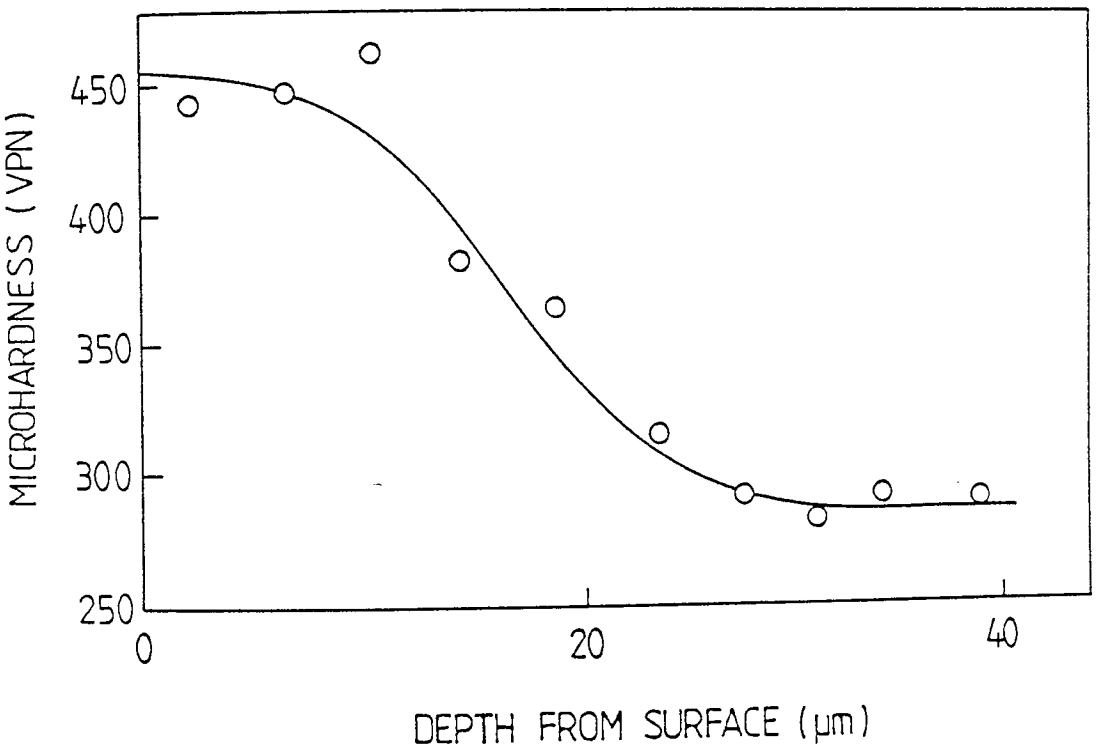

FIG. 4.7 MICROHARDNESS VERSUS DEPTH INTO THE SURFACE OF A WORN FLAT SPECIMEN FROM AN EXPERIMENT CONDUCTED AT A MEAN SLIDING SPEED OF 36 mm/s, LOAD OF 22N AND TEMPERATURE 290 °C. THE TEST DURATION WAS 15000 s OR 540 m.

4.2.4. X-ray Diffraction Analysis

X-ray powder diffraction photographs were taken of debris samples collected after the completion of a number of test runs. These revealed only metal Fe(Cr) diffraction lines. This is not unexpected since the majority of wear occurs during the severe running-in period and the detection limit of the technique is only about 4% by volume. Thus since mean severe wear rates are typically two orders of magnitude greater than mild wear rates, the experiment would have to run for a post transition period of at least four times that of the time up to the transition, for a detectable amount of debris to be produced.

In a small number of experiments conducted at 290^0C, the test run was stopped after the transition and the debris collected. The experiment was then restarted and run for a period of about 50 times the time taken to reach the transition, when the debris was again collected. In this way it was possible to obtain representative samples of debris from both pre-transition (severe wear) and post-transition (mild wear) regions. The method suffered the disadvantage, however, that the system had to be disturbed and returned to an atmospheric environment between the two parts of the wear test run. Typical X-ray diffraction observations are shown in Tables 4.2 and 4.3 with the identity of the compounds present, in this case for an experiment conducted at 36 mm s^{-1} speed and 22 N load.

TABLE 4.2.

Powder diffraction observations of debris from the pre-transition region of an experiment conducted on 9% Cr steel at a speed of 36mms^{-1}, load of 22N and temperature 290°C.

Experimental Values		Compound	Diffraction file date	
2.θ(deg)	d(Å)		d(Å)	Relative Intensity I/I_o
52.5 s	2.02	α-Fe(Cr)	2.03(2.04)	100(100)
79.0 f	1.44	α-Fe(Cr)	1.43(1.44)	20(16)
101.5 m	1.17	α-Fe(Cr)	1.17(1.18)	30(30)
125.0 f	1.02	α-Fe(Cr)	1.01(1.02)	10(18)

s = strong, m = medium, f = faint

TABLE 4.3.

Powder X-ray diffraction observations of debris from the post-transition region of an experiment conducted on 9% Cr steel at a speed of 36 mms^{-1}, load of 22N and temperature 290°C.

Experimental Values		Compound	Diffraction file data	
2θ (deg)	d(Å)		d(Å)	Relative Intensity I/I_o
28.5 m	3.67	Rhombohedral oxide	3.68	25
35.3 f	2.96	Spinel oxide	2.97	30
38.8 s	2.70	Rhombohedral oxide	2.69	100
41.8 s	2.51	Rhombohedral, Spinel oxide	2.51,2.53	50,100
48.0 m	2.20	Rhombohedral oxide	2.20	20
50.5 f	2.09	Spinel	2.10	20
52.5 m	2.02	α-Fe(Cr)	2.03(2.04)	100(100)
58.3 m	1.84	Rhombohedral	1.84	40
64.0 s	1.69	Rhombohedral, Spinel oxide	1.69,1.71	60, 10
74.3 m	1.49	Rhombohedral, Spinel oxide	1.48,1.49	35, 40
76.2 m	1.45	Rhombohedral oxide, α-Fe(Cr)	1.45,1.43	35, 20
84.3 f	1.35	Rhombohedral oxide	1.31	20
99.5 f	1.17	α-Fe(Cr)	1.17(1.18)	30(30)

s = strong, m = medium, f = faint

TABLE 4.4

Glancing angle X-ray observations of 9% Cr pin surface taken from an experiment conducted at a speed of 36 mms^{-1}, load 22N and temperature 290°C.

Experimental Values		Compound	Diffraction file data	
2θ(deg)	d(Å)		d(Å)	Relative Intensity I/I_o
38.7 f	2.71	Rhombohedral oxide	2.79	100
41.8 f	2.51	Rhombohedral, Spinel oxide	2.51,2.53	50,100
52.3 s	2.03	α-Fe(Cr)	2.03(2.04)	100(100)
79.0 f	1.44	α-Fe(Cr)	1.43(1.44)	20(16)
99.3 m	1.17	α-Fe(Cr)	1.17(1.18)	30(30)
123.5 f	1.01	α-Fe(Cr)	1.01(1.02)	10(18)

s = strong, m = medium, f = faint

For debris collected in the region up to the severe/-mild wear transition the analysis showed only metallic particles to be present. For debris collected in the mild wear region after the transition, the major component was a rhombohedral oxide, of the type α - $Fe,Cr)_2O_3$ with some spinel oxide, $Fe\ Fe_{(2-x)}\ Cr_xO_4$, and some metallic debris, α - Fe(Cr) . This mixture was typical for the limited number of conditions investigated over the whole speed range.

Glancing angle X-ray diffraction analysis was made more difficult by the rough surfaces generated in the wear tests. Where oxides were identified, however, results such as those shown in Table 4.4 were typical. In this technique there will obviously be a large contribution from the bulk metal, but rhombohedral oxides were clearly observed on the surface. It is possible that spinel oxides may also have been present, but at lower concentrations.

4.2.5. Scanning Electron Microscopy and Auger Electron Spectroscopy

Scanning electron microscopy was employed to study the surface topography of selected samples taken from all the series of tests.

Figure 4.8 shows a typical surface generated in the severe running-in region, in this case for an experiment stopped at about a quarter of the way to an expected transition. A great deal of surface distress is visible and severe plastic deformation has obviously occurred. In contrast to this Figure 4.9 (a) shows a region of a surface generated after mild wear had been established under the same conditions of load, speed and temperature as those used to generate the surface shown in Figure 4.8.

Large smooth oxide plateaux, such as that shown in Figure 4.9 (a), are typical of surfaces examined after mild wear conditions had been established. The plateaux were generally observed to cover about half of the wearing surface.

Figure 4.9 (b) shows a detail of the edge of a crack in the plateaux shown in 4.9 (a) and visible to the upper left of centre in that photomicrograph. Examination of this and other edges, for example those shown in Figure 4.10 (a) and (b), suggest that the plateaux are formed by quite a different mechanism to those for the unidirectional sliding experiments described in Chapter 2 of this work. Here the plateaux are seen to consist largely of compacted debris and are very different to those shown, for example, in Figures 2.11 and 2.12 where the plateaux edges are smooth and apparently homogeneous. From examination of plateaux edges thicknesses varied between about 6 μm and 10 μm , although exceptionally thicknesses of up to 20 μm were observed.

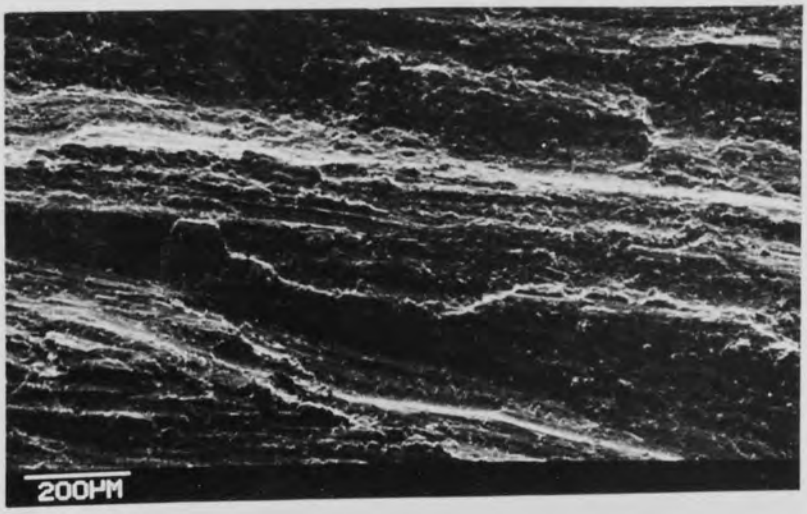

FIG. 4.8 SCANNING ELECTRON MICROGRAPH OF TYPICAL SEVERE WEAR SURFACE.

(a)

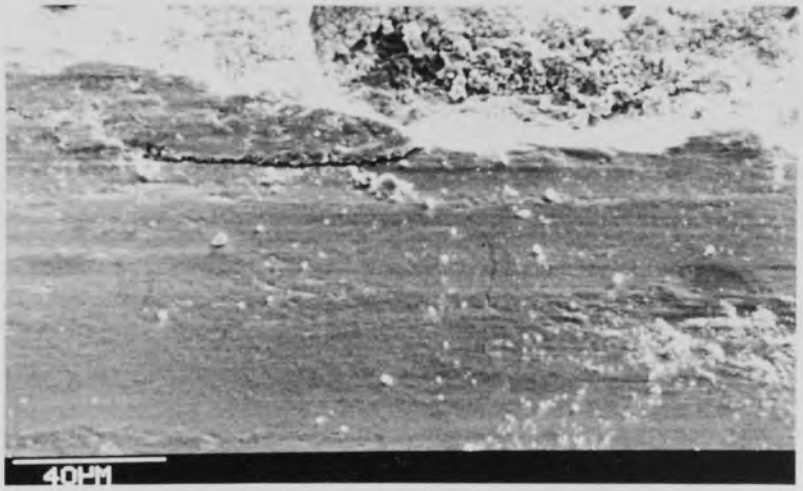

(b)

FIG. 4.9 SCANNING ELECTRON MICROGRAPHS OF SURFACES AFTER THE ESTABLISHMENT OF MILD WEAR CONDITIONS IN THIS CASE FOR AN EXPERIMENT CONDUCTED AT 120 mm/s, 22N LOAD AND TEMPERATURE OF 300 C.
(a) OXIDE PLATEAU
(b) DETAIL OF THE EDGE OF A CRACK VISIBLE IN THE PLATEAU.

(a)

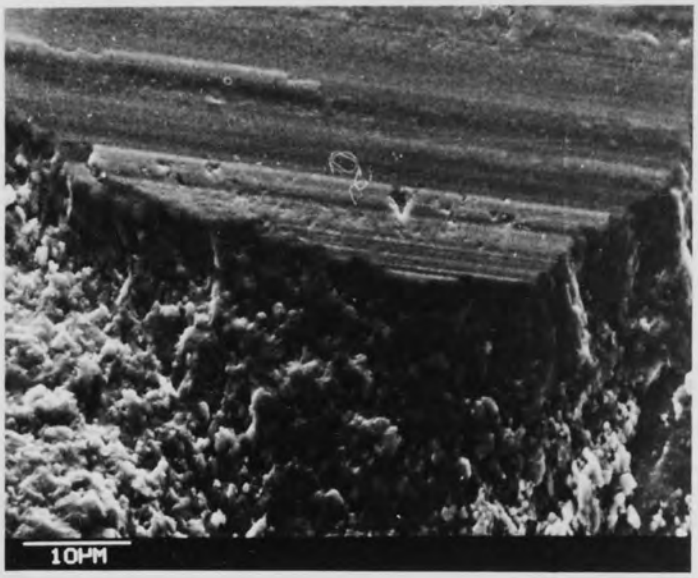

(b)

FIG. 4.10 SCANNING ELECTRON MICROGRAPHS OF PLATEAUX EDGES ; (a) 120 mm/s, 41N LOAD, 300 C, (b) 36 mm/s, 22N LOAD, 300 C.

(a)

(b)

FIG. 4.11 SCANNING ELECTRON MICROGRAPHS OF OXIDE DEBRIS; (a) SURFACE DEBRIS, (b) AGGLOMERATE DEBRIS PARTICLE.

Oxide debris collected from the reciprocating sliding experiments was generally of two types, small particles of between 2 μm and 4 μm diameter often found on the surface between plateaux, Figure 4.11 (a), and plate like fragments up to about 20 μm long and consisting of agglomerates of smaller particles, Figure 4.11 (b).

Auger electron spectroscopic examination of some plateaux was carried out in order to gain evidence on the nature of the protective load bearing oxide films. In a manner similar to that described for the technique in Chapter 2 of this work, spot analyses were conducted while the plateaux were gradually etched away by bombardment with 2 keV argon ions at a specimen current of 20 μA. The conditions used in the analysis were similar to those described in 2.1. Auger spectra of oxygen, iron and chromium were recorded at specific time intervals during the bombardment. The relative atomic concentrations were then calculated from peak to peak heights and published elemental sensitivity factors[173]. Typical resultant concentration versus depth profiles are shown in Figure 4.12. Unlike the Auger depth profiles shown in Figures 2.14, 2.15 and 2.16 plotted for unidirectional sliding experiments in air, Figure 4.12 clearly shows a decreasing oxygen to iron ratio with depth into the sample. Calculations indicate that a total ion dose of 40×10^3 μA minutes is equivalent to the removal of a depth of about 5 μm of this surface.

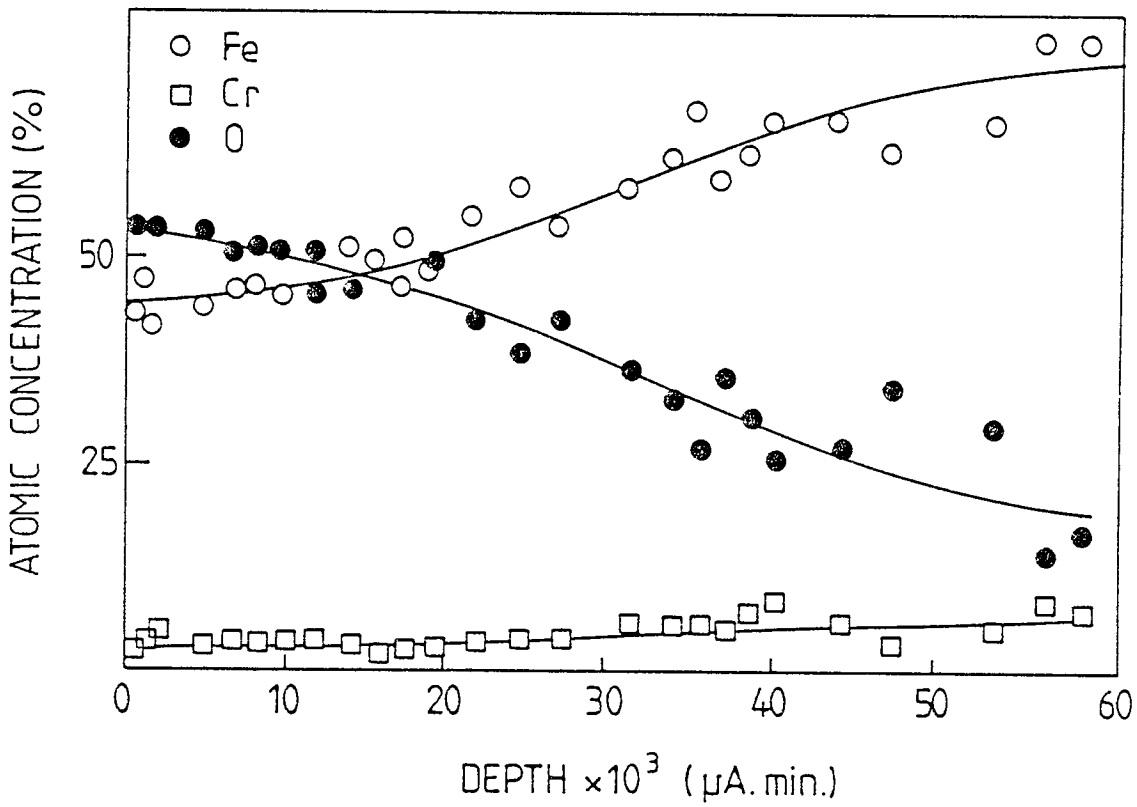

FIG. 4.12 OXYGEN, IRON AND CHROMIUM CONCENTRATION VERSUS DEPTH PROFILES FOR A FLAT SPECIMEN FROM AN EXPERIMENT CONDUCTED AT A MEAN SPEED OF 36 mm/s, 22N LOAD AND TEMPERATURE OF 300 °C.

4.3 Transition from Severe to Mild Wear - a Surface Model

During sliding at elevated temperatures, oxidation of the whole of the two contacting surfaces will occur out of contact at the ambient temperature T_A and at the real areas of contact at or near to the hot-spot temperature T_c. If the ambient temperature or the speed of sliding (or both) are too low, the rate of formation of protective oxide film will always be less than the rate of material removal and the system will operate in a continual severe wear mode. No severe/mild wear transition will occur. If the rate of oxide growth is sufficiently high, then oxide plateaux begin to form and the area of these plateaux increases with sliding until full support and hence oxidational wear occurs. This is probably equivalent to coverage of the majority of the two contacting surfaces by a stable oxide film of critical thickness ξ. In a reciprocating system where debris cannot easily escape, it is proposed that the following film formation mechanism applies.

Oxidation occurs over the whole surface at the ambient temperature T_A, but particularly initially around nucleation sites, probably at the contact temperature T_c. Most of this oxide is then removed with some metal by the reciprocating sliding motion. When all the debris is not allowed to escape, some oxide (and metal) particles become entrapped and form agglomerate plateaux around some of the

initial nucleation sites. These then become major load bearing areas where further oxidation takes place together with further particle agglomeration, resulting in a growth of area of the plateaux. Much experimental work in this and many other studies suggests that the thickness of the plateaux stabilizes at a critical value. The area of the plateaux continues to increase, however, until contacts are mainly oxide-oxide and mild wear ensues.

Let us consider the system at some time t after the start of a run. Let ΔV be the volume of material removed from the surface in time t to t + Δt.

Then,

$$\Delta V = \Delta V_{m-m} + \Delta V_{m-o} + \Delta V_{o-o} - \frac{1}{2} \Delta V_{ox} \qquad (4.1)$$

where

ΔV_{m-m} = volume removed due to metal-metal contact

ΔV_{m-o} = volume removed due to metal-oxide contact

ΔV_{o-o} = volume removed due to oxide-oxide contact

ΔV_{ox} = volume of oxide produced.

The factor of 1/2 in the last term of Equation (4.1) accounts for the fact that the Pilling Bedworth ratio[156] for both rhomboheral and spinel oxides is approximately 2.

If γ is the fraction of the apparent contact area covered by oxide plateaux at time t, then[91]:

probability of a metal-metal contact, $P_{m-m} = (1 - \gamma)^2$

probability of a metal-oxide contact, $P_{m-o} = 2\gamma\ (1 - \gamma)$

and

probability of an oxide-oxide contact, $P_{o-o} = \gamma^2$

If it is assumed that the major proportion of the wear particles which compact and agglomerate to form load bearing plateaux are produced in the region between these plateaux. Then the area associated with this region decreases as sliding progresses with a subsequent decline in the rate of oxide build up. The volume rate of oxide production will be proportional to the area $(1 - \gamma)$ [93] and if it assumed that the plateaux attain critical thickness then the area growth rate of the plateaux will also be proportional to this factor. Hence

$$\frac{d\gamma}{dt} = (1 - \gamma)$$

or

$$\log (1 - \gamma) = -Gt \qquad (4.2)$$

where G is a constant.

If γ is small

$\log (1 - \gamma) \quad - \gamma$

and (4.2) reduces to

$$\gamma = Gt \qquad (4.3)$$

In the experiments the maximum value of γ was estimated from scanning electron micrographs to be of the order of 0.5. Hence for the maximum value of γ close to the transition the assumption that γ is small could introduce errors of a little over 30%. However, for the majority of the test run the linear relationship in (4.3) is adequate.

Thus if a linear relationship such as that in (4.3) is assumed then:

$$\gamma = \frac{\varepsilon t}{t_T} \tag{4.4}$$

where ε is the fraction of the contact area covered for equilibrium mild wear conditions and t_T is the time taken to reach the severe mild wear transition.

The volume of material removed due to metal-metal contacts in time Δt may be written[101]:

$$\Delta V_{m-m} = K_{m-m} P_{m-m} A_r \Delta d$$

or

$$\Delta V_{m-m} = K_{m-m}(1 - \frac{\varepsilon t}{t_T})^2 \frac{W}{P_m} U \Delta t \tag{4.5}$$

where

K_{m-m} = wear constant for metal-metal contacts

A_r = real area of contact

Δd = distance of sliding in time Δt

W = load

P_m = hardness

U = mean sliding velocity.

Similarly for metal-oxide and oxide-oxide contacts in the same time, one can write:

$$\Delta V_{m-o} = K_{m-o} \frac{2\varepsilon t}{t_T} \left(1 - \frac{\varepsilon t}{t_T}\right) \frac{W}{P_m} U\Delta t \qquad (4.6)$$

and

$$\Delta V_{o-o} = K_{o-o} \left(\frac{\varepsilon t}{t_T}\right)^2 \frac{W}{P_m} U\Delta t \qquad (4.7)$$

where K_{m-o} and K_{o-o} are wear constants for the metal-oxide and oxide-oxide contacts respectively.

If one assumes a continual process of oxide attrition and subsequent agglomeration to form load bearing plateaux, the development of thick diffusion controlled oxide films is unlikely and this is confirmed by the evidence presented in the previous section, 4.2. In the system described in this chapter, where wear occurs in a carbon dioxide atmosphere, gas/metal phase boundary interactions are probably the rate determining factor and oxidational growth rate may then be described by the linear relationship $\Delta m = k\Delta t$, where Δm is

the mass uptake of oxygen per unit area and k is the linear oxidational rate constant. For similar experiments conducted in air one would expect a direct logarithmic relationship to hold of the form:

$$\Delta m = k_1 \log_e (k_2 t + 1) \qquad (4.8)$$

where k_1 and k_2 are constants.

For an oxidation - scrape - oxidation mechanism where t is small, then with regard to the possible magnitude of k_2 the relationship (4.8) also reduces to linear form.

The total oxide produced in time Δt is due to the sum of that produced out of contact at temperature T_A and that due to tribo-oxidation in the contact region at temperature T_C . Thus:

$$\Delta m_{total} = \Delta m_{out\ of\ contact} + \Delta m_{tribo\text{-}oxidation}$$

Written in terms of volume of oxide, this becomes

$$\Delta V_{ox} = k_{T_A} \left(\frac{A}{\rho f}\right) \Delta t + k_{T_C} \left(\frac{A_r}{\rho f}\right) \Delta t \qquad (4.9)$$

where

k_{T_A} = oxidational rate constant for out-of-contact oxidation at T_A

k_{T_C} = oxidational rate constant for tribo-oxidation at T_C

ρ = density of the oxide

f = mass fraction of the oxide which is oxygen

A = apparent area of contact

Substituting for Equations (4.5), (4.6), (4.7) and (4.9) in (4.1):

$$\Delta V = \left(P\left(\frac{\varepsilon t}{t_T}\right)^2 - Q\,\frac{\varepsilon t}{t_T} + R\right)\Delta t \qquad (4.10)$$

where

$$P = \left(K_{m-m} + K_{o-o} - 2K_{m-o}\right)\frac{WU}{P_m}$$

$$Q = 2\left(k_{m-m} - K_{m-o}\right)\frac{WU}{P_m}$$

and

$$R = K_{m-m}\,\frac{WU}{P_m} - \frac{1}{2}\left\{k_{T_A}\,\frac{A}{\rho f} + k_{T_C}\,\frac{W}{P_m \rho f}\right\}$$

In the limit when $\Delta t \to 0$, the total volume removed in time t is given by

$$V = \int_0^t \left(P\left(\frac{\varepsilon t}{t_T}\right)^2 - Q\,\frac{\varepsilon t}{t_T} + R\right) dt$$

or

$$V = \left\{\frac{P}{3}\left(\frac{\varepsilon t}{t_T}\right)^2 - \frac{Q}{2}\,\frac{\varepsilon t}{t_T} + R\right\} t \qquad (4.11)$$

and the instantaneous wear rate w (in $m^3 m^{-1}$) is given by:

$$w = \frac{1}{U}\left(P\left(\frac{\varepsilon t}{t_T}\right)^2 - Q\,\frac{\varepsilon t}{t_T} + R\right) \qquad (4.12)$$

Equations (4.11) and (4.12) are vaild only up to the wear transition.

Considering one series of wear tests described in section 4.2.1, conducted at 290^0C, 22 N load and a speed of 36 mm s^{-1}, for which the experimental values of cummulative volume removed versus time are given in Figure 4.6. Then if the above theoretical relationship derived from this surface model (Equation 4.11) is applied to these conditions, the values of P and Q in (4.11) reduce to:

$$P = K_{m-m}\,\frac{WU}{P_m}$$

$$Q = 2K_{m-m} \frac{WU}{P_m}$$

since the measured value of K_{m-m} for initial severe wear (estimated from the first 100 seconds of sliding) is about two orders of magnitude greater than the value of K_{o-o} estimated from the mild wear region after the transition. Although there is no way of determing the value of K_{m-o}, it is thought that this will be close to the value of K_{o-o}. The measured value of severe wear rate for these conditions was $5.4 \times 10^{-11} m^3 m^{-1}$ and this produced a calculated value of K_{m-m} of 5.6×10^{-3}. In two separate experiments the transitions occurred after 23×10^3 s and 26.4×10^3 s respectively, hence t_T was taken as 24.7×10^3 s. The subsurface hardness P_m was 2.8×10^9 Nm^{-2}.

During mild oxidational wear, the volume of oxide produced per unit time (both out of contact and tribo-oxide) may be determined directly from the wear rate, since it is assumed in this wear mode that the rate of production of the oxide must be equal to its rate of removal. Hence the volume produced per unit time, $V_{ox} = w_m U$, where w_m is the mild wear rate in units of $m^3 m^{-1}$. If we assume further that the processes of oxide production are similar in the period of sliding wear leading up to the transition to mild oxidational wear, then the value of V_{ox} can replace the term

$k_{T_A} A/\rho f + k_{T_c} W/P_m \rho f$ in Equation (4.11).

For the conditions of the experiments described in Figure 4.6 the mild wear rate was $1.1 \times 10^{-13} m^3 m^{-1}$. Thus $V_{ox} = 4 \times 10^{-15} m^3 s^{-1}$.

Inserting the values of the various parameters into Equation (4.11) gives:

$$V = 8.4 \times 10^{-22} \varepsilon^2 t^3 - 6.5 \times 10^{-17} \varepsilon t^2 + 1.6 \times 10^{-12} t \qquad (4.13)$$

Different values of ε were tried in Equation (4.13) to give a best fit to the experimentally derived curves ub Figure 4.6. The theoretical curve plotted for a value of $\varepsilon = 0.5$ on that figure gives very good agreement between experiment and theory. This theoretical result suggests that one half of each surface must be covered with a stable supportive oxide film for a transition from severe to equilibrium mild oxidational wear to occur. Visual observations of the surfaces just after mild wear has been established show that a little over half of the surface is covered by oxide plateaux. These results strongly suggest that the model is a good representation of the processes occurring during the initial stages of sliding of the surfaces.

A further test of the validity of the theory, however, is its ability to predict wear volumes for experiments conducted outside the range for which the constants in Equation (4.13) were derived. The total wear volume, V_T, up to the severe/mild wear transition may be calculated by substituting $t = t_T$ in Equation (4.13), which then becomes:

$$V_T = 1.2 \times 10^{-12} WUt_T - 1.9 \times 10^{-14} t_T \qquad (4.14)$$

or writing this in terms of M_T, the mean total weight loss up to the transition, then:

$$M_T = 6.3 \times 10^{-3} WUt_T - 9.9 \times 10^{-5} t_T \qquad (4.15)$$

where V_T is in m^3 and M_T in mg.

Taking the experiments conducted at 450^0C, Figure 4.13 shows a curve of the predicted weight losses (calculated from Equation (4.15) using transition times derived from the product of the number of cycles to the transition, N_T, and the reciprocal of the oscillating frequency) as a function of speed. The mean measured weight losses for the series of experiments are also shown on the graph. It can be seen that there is good agreement between theoretical and experimental data, which further strengthens confidence in the essential correctness of the model.

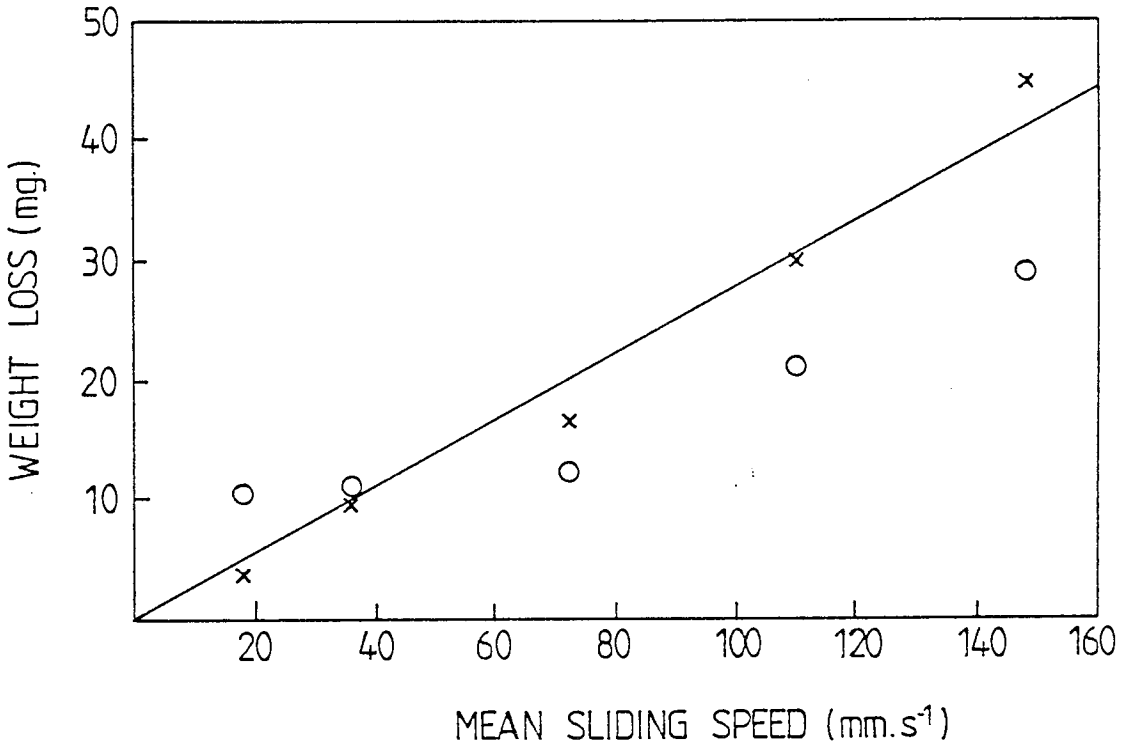

FIG. 4.13 CALCULATED PRE-TRANSITION WEIGHT LOSS VERSUS MEAN SLIDING SPEED FOR EXPERIMENTS CONDUCTED AT 22N LOAD AND AMBIENT TEMPERATURE OF 450 C ; x THEORETICAL POINTS , o EXPERIMENTALLY MEASURED VALUES.

4.4 Discussion

Large area scanning electron micrographs of worn surfaces show that for a transition from severe to mild wear to occur about half the wearing surface must be covered with stable load bearing oxide plateaux, which for the conditions of these experiments are between 6 and 10 μm thick. The vast majority of contact then takes place between the plateaux of opposing surfaces, with minimal metal-metal contact occurring. Microhardness measurements have shown that the oxide layers are supported by transformed or work hardened metallic layers of maximum hardness between 400 and 650 HV, which extend to a depth of about 30 μm into the sample surfaces. The hard layers were formed very early during sliding and neither the hardness nor depth of the layers changed significantly after 1000 seconds of sliding in a series of experiments where the severe/mild wear transition occurred after about 25,000 seconds. Skinner[95] using a similar experimental arrangement, but austenitic stainless steel specimens, found that sub-surface hardness of 750 HV were achieved after only 50 seconds of sliding. He attributed his results to oxide formation and incorporation into a highly disrupted surface layer, but there is no evidence of such a process occurring in these experiments. It is thus more probable that the layer is due to work hardening. The hard surface is probably important in establishing the conditions necessary to promote the growth of oxide plateaux, but since there is such a long

time period between the formation of the hard sub-surface layer and the transition to a mild wear mode, its influence is likely to be secondary.

Evidence of the composition and mechanisms of growth of plateaux was gained from further surface examination. Scanning electron micrographs of the edges of the plateaux, for example those shown in Figures 4.9 (b) and 4.10 (a) and (b), strongly suggest that they consist of agglomerate layers of sub-micron particles of wear debris. This suggestion is reinforced by the photomicrographs of debris, such as that of Figure 4.11 and further strengthened by comparison with photomicrographs of plateaux edges which are thought to be physically homogeneous and produced by diffusion controlled growth mechanisms such as those shown in Figures 2.11 and 2.12 of this work.

The Auger electron spectroscopy depth profiles, such as that shown in Figure 4.12, further show that these plateaux are quite different to those produced in the unidirectional sliding experiments described in Chapter 2. As explained in previous chapters it is impossible to accurately assess the depth of material removed for such a complex surface, but calculations indicate that the maximum depth removed from the plateaux in the case of Figure 4.12 was about 5 μm, a depth commensurate with the thickness of the oxide layer. In this region, oxygen concentrations fell from 55% $\pm$ 10% at the surface to 20% $\pm$ 10% close to the plateaux/metal interface. Since analyses were conducted at

the centre of plateaux, this shows that the plateaux do not consist wholly of oxide, but are composed of metal and oxide mixtures. X-ray powder diffraction analyses indicate that oxide in the wear debris is mainly the rhombohedral oxide α - $(Fe, Cr)_2O_3$ in which one would expect an oxygen concentration of 60%. Thus the profile indicates that the plateau consists almost entirely of oxide at its surface, with a gradation of oxide with depth into the surface and a final oxide of metal ratio of about 1 : 3 at or near the oxide/metal interface.

The Auger depth profile provides a history of the build up of the plateaux, but there are two possible explanations for the observations. It has been postulated that the layer is formed by the sintering of wear particles, it may then be assumed either that the particles consist initially mainly of metal debris with the amount of oxide in that debris increasing with sliding distance or that the ratio of oxide to metal particles included in the agglomerate remains constant at about 1 : 3 during the formation of the load bearing plateaux, but that further surface oxidation takes place during and after build up to critical thickness. Both explanations appear plausible and it is therefore probable that a combination of the two mechanisms is responsible for the plateaux in their final form.

At the lower speeds of sliding and high ambient temperatures used in these experiments, it is not unreasonable to assume that out of contact oxidation is primarily responsible for oxide production via an oxidation-scrape-oxidation mechanism. (There is no evidence of thick primary oxide layer production). For the reciprocating motion in these experiments, the time between contacts at any given area, t_r , will be:

$$t_r = \frac{\text{reciprocating stroke length } (d_r)}{\text{velocity } (U)}$$

Assuming linear oxidation kinetics or even logarithmic kinetics where oxidation occurs over a short time period. Then the mass uptake of oxygen per unit area, Δm , in the time period between contacts is:

$$\Delta m = k \left(\frac{d_r}{U}\right) \qquad (4.16)$$

or in terms of volume of oxide produced, ΔV_r , at the real area of contact A_r :

$$\Delta V_r = \frac{k}{f\rho_o} \left(\frac{d_r}{U}\right) A_r \qquad (4.17)$$

where f is the fraction of the oxide which is oxygen

ρ_o is the oxide density

and k the oxidational growth constant

If an oxidation-scrape-oxidation mechanism is assumed, the whole of this volume is removed at the next encounter. Thus the volume of oxide produced per unit distance of sliding may be written as:

$$\left(\frac{\Delta V_r}{d_r}\right) = \frac{kA_r}{f\rho_o U} \qquad (4.18)$$

and the total volume produced up to the transition in the sliding distance, D_T , as:

$$V_T = \frac{kA_r}{f\rho_o U} D_T \qquad (4.19)$$

but $D_T = Ut_T$, hence

$$V_T = \frac{kA_r}{\rho_o f} t_T \qquad (4.20)$$

It has been shown that for a transition to occur about half of the apparent surface area is covered with oxide plateaux of approximately constant thickness, hence under any given set of conditions the volume of oxide required to produce mild oxidational wear conditions is constant and must be directly related to V_T . Hence V_T may be regarded as constant and therefore t_T is constant.

This is consistent with the observations for 450^{0}C experiments at all speeds and for the 290^{0}C and 300^{0}C experiments at speeds up to 110 - 120 mm s^{-1} , where Figure 4.5 shows a linear relationship between D_T and U for these conditions.

Taking data from the mild wear rate measurements from experiments conducted at 300^{0}C, 22 N load and speed of 36 mm s^{-1} described in Section 4.2.1 and assuming as in Section 4.3 that for mild wear the rate of removal is equal to the rate of oxide production then the quantity $(kA_r/\rho_o f)$ in Equation (4.20) is equal to 4 x 10^{-15} m^3 s^{-1} . Further, taking a typical pin wear scar of 2 mm diameter and typical plateaux thickness of 10 μm and assuming that at the transition 0.5 of the total area is oxide plateaux, then inserting these quantities into equation (4.20) gives a value of t_T = 3.9 x 10^3 s . From Figure 4.5 the mean value of t_T for the 300^{0}C experiments in the initial speed range is about 16 x 10^3 seconds.

This approach neglects the experimental observations that a substantial proportion of the total volume of the load bearing plateaux is metal; the plateaux contains about 60% by volume oxide. The total volume of debris produced up to the transition is given by Equation (4.14) which is dominated by the metal-metal wear term. If a constant proportion of this debris were used in the formation of plateaux, this would imply a falling value of t_T with

increase in velocity, where the experimental results show that t_T is constant, at least for relatively low velocities. Thus it is the production of oxide debris which is the plateaux growth rate determining factor even though a far greater amount of metallic debris will be produced and some of that debris is included in the plateaux. It must be assumed that transfer or adhered metallic particles are removed in the same manner and at the same rate as the virgin metal surface and that it is the oxide in the growing plateaux which changes the relative proportions of metal-metal, metal-oxide and oxide-oxide contacts and leads to the onset of mild wear.

As one would expect the curve in Figure 4.5 corresponding to experiments conducted at 300^0C and 41 N load exhibits longer transition distances and a corresponding longer transition time, due to the increased attrition rates at the higher load, the rate of production of oxide not being particularly affected by load.

At speeds greater than 110 ~ 120 mm s^{-1} for 290^0C and 300^0C experiments there is a marked fall in transition distance and hence also transition time with increase in velocity. From the limited X-ray diffraction data collected, there is no evidence of oxide type change, hence this fall is probably due to an increase in the amount of oxide formed due to tribo-oxidation at the contact temperatures. A constant value of transition time t_T suggests that tribo-oxidation is negible up to this point. Calculations based

on the equations due to Archard[47], indicate that the maximum excess contact temperature is about 250^{0}C at 22 N loads and 120 mm s^{-1} speed, although in practice, considering multiple contacts, the temperature would be somewhat lower than this. At 450^{0}C surface temperature is high enough to completly dominate oxide growth and no effect due to tribo-oxidation is observed. At temperatures below 290-^{0}C, the rate of material removal is clearly always greater than the rate of oxide production necessary to form load bearing plateaux in the speed range considered here and transitions to mild wear will never occur.

Further evidence on the importance of out of contact oxidation in the formation of protective oxide layers in the circumstances of these experiments was provided by the results of the "dwell tests". Static pre-oxidation of surfaces had no significant effect on formation. The experiment conducted at 290^{0}C with a load of 22 N where a 750 hour heated pre-sliding dwell period was employed, showed no statistically significant reduction in the time of sliding required to reach a transition. There could be a number of reasons for this, but it appears that a tribo-logically disturbed surface might be necessary for the formation of an oxide layer capable of giving protective regenerative properties. The fact that prior to the dwell period, no hard sub-surface layer had been formed to support an oxide would undoubtedly also have affected its protective properties.

Conversely the experiments conducted at 290^{0}C and 300^{0}C, where sliding periods were interspersed by dwell periods, showed a significant effect of static oxidation. Here transition sliding distances were reduced by an order of magnitude. The measured amounts of oxide produced during these 96 hour dwell periods were insignificant compared with the amount of material removed during the intervening periods of sliding wear. Hence the attainment of the transition to mild wear cannot simply be due to a greater volume of oxide being made available for agglomeration to form plateaux once sliding is re-commenced. There must, therefore, be a substantial effect due to oxidation and consolidation of partially formed plateaux which would then effectively increase the relative proportion of oxide-oxide contacts. It is not clear why dwell did not have a similar effect on the 450^{0}C experiments, but it must be assumed that consolidation by further oxidation of plateaux was not necessary in the formation process at this high temperature.

The limited number of experiments conducted in air showed that the process of plateaux formation is exactly similar to that in carbon dioxide, with the exception that the transition from severe to mild wear occurred more rapidly. The ultimate equilbrium mild wear rates were, however, very similar. This indicates that more oxygen is required to initiate mild wear than to sustain it. The oxygen necessary to produce oxidation and hence support mild wear may be in the form of O_2 molecules or O atoms. Van

Wylen and Sonntag[200] have shown that only 1 in 10^{16} oxygen molecules dissociates at 750 K in the gaseous phase. Hence it is unlikely that mild wear in any environment is initiated by free oxygen from this source; it is much more probable that dissociation takes place at the gas/metal interface and is assisted by the more reactive highly disturbed metal surface. Similar calculations for carbon dioxide atmospheres at 750 K[200] show that 1 in 10^{11} molecules of CO_2 dissociate in the gaseous phase in equilbrium according to the reaction:

$$CO_2 = CO + \frac{1}{2} O_2$$

It is again probable that such dissociation occurs to a far greater extent at or near to the gas/metal interface. This then releases O_2 molecules which may then further dissociate and produce metal oxidation. This two stage dissociation process results in less rapid production of oxide and a delay to the initiation of mild wear.

Two other sources of oxygen molecules must not be neglected in these experiments. One is due to water where it is known that one molecule in 10^9 of H_2O dissociates to form $H_2 + \frac{1}{2} O_2$ at room temperature and the other source is the possible leakage of oxygen from the atmosphere back into the chamber in spite of the positive pressure of CO_2 .

In summary, the oxide plateaux formed in these experiments and leading to oxidational mild wear, consist of agglomerate layers of sub-micron particles. The layers have a volume composition of three metal to one oxide at the metal/plateaux boundary with oxide concentration increasing with thickness until the plateaux is almost entirely oxide at their outer surface. The plateaux are supported by a work hardened sub-surface layer of about 30 μm thick.

The oxide debris, which agglomerates to form the plateaux, is probably formed by an oxidation-scrape-oxidation mechanism and it is the rate of production of this oxide which is the rate determing factor in plateaux growth, even though plateaux contain a substantial proportion of metal fragments. The majority of the oxide growth occurs out of contact and is governed by the ambient temperature, but for high speeds at temperatures of 290 and 300^{0}C, the combination of increased contact temperature and increase frequency of contact results in significant additional tribo-oxidation and a more rapid transition to mild wear.

Out of contact oxidation has the further effect of oxidation and consolidation of the growing oxide plateaux with a resultant reduction in metal-metal contact. Pre-oxidation without sliding has no effect in the promotion of mild wear.

CHAPTER 5

CONCLUDING DISCUSSION - COMPARISON OF SLIDING SYSTEMS

The results and theoretical analyses from each of the three sliding systems which form the basis of this study on oxidational wear have been discussed in great detail in appropriate preceding chapters. Repetition of those discussions is therefore superfluous, but before formally stating the conclusions of this work, it is worth spending some time on a comparison of the various mechanisms involved in producing oxidational wear modes in these quite different systems. This will necessarily involve reiteration of some of the salient points.

For the unidirectional dry wear experiments described in Chapter 2, all the evidence shows that oxides are physically homogeneous and grow to produce load bearing plateaux by a diffusion controlled mechanism similar to that responsible for the growth of thick oxide films under static conditions. Both electron microscopy and electron spectroscopy support this hypothesis. Electron spectroscopy further shows that transfer or back transfer has no part to play in the formation of the plateaux. At low ambient temperatures the growth of the oxide occurs at temperatures close to the contact temperatures with negligible out of

contact oxidation. Under these circumstances the oxidational growth constants are quite different to those measured for static oxide growth. This latter result should be expected both for the reasons discussed in earlier sections of this work and from consideration of power dissipation at the real areas of contact during sliding. If for example an experiment is considered where the load is 100N, speed 2 ms^{-1} giving rise to a friction coefficient of 0.7, the power dissipation at the real areas of contact is of the order of 400$kWcm^{-2}$. The magnitude of this power input is quite outside normal experience and, therefore, it should not be surprising that oxidation and other surface changes in tribological systems can not easily be explained in terms of bulk or static parameter values.

At ambient temperatures above 300^0C, the role of in-contact oxidation becomes less significant and out of contact oxidation at the general surface temperature becomes the dominant mode of growth. An observation which is somewhat surprising here is that statically derived oxidation constants appear to govern growth under these conditions.

The reasons for the growth of such thick physically homogeneous diffusion controlled oxide films in these circumstances, rather than the development of any other form of load bearing protective oxide layer (such as an agglomerate layer, or oxide included layer) may now be examined. The physical geometry of the wear test rig

undoubtedly has some influence on the type of oxide formed. In the experiments described in Chapter 2 a wear test rig was used with a vertical disc and horizontal pin and relatively high rotational disc speeds were employed. Under these conditions the combination of gravitational and centrifugal forces ensure that very little debris remains on the surface to become entrapped and form an agglomerate layer. Yahata and Hayama[201] have demonstrated the influence of surface debris in their experiments where mild wear of steel was rapidly induced by the introduction of iron oxide to the conjunction.

The influence of mechanical system geometry and entrapped debris have been demonstrated for quite different materials by Dickens, Sullivan and Lancaster[202]. In a series of experiments where polymers were slid against steel surfaces, they showed, using different wear test rigs, that transfer or back transfer layers were produced only in circumstances where the mechanical configuration of the test pieces was such that debris became easily entrapped. The different test rigs were operated under similar conditions of load and speed. This work has other important implications for lubricated sliding and these will be mentioned in a later paragraph.

System geometry is not all important, however. Using the same test rig as that described in Chapter 2, Sullivan and Petraitis[203] in a study of the wear of tool steel against a sintered WC-11%Co material showed that for

temperatures over 400^0C a complex tungsten and cobalt transfer film was produced on the steel counterface. The transfer film reduced both friction and wear and here perhaps is a clue to the success or otherwise of transfer layers. In the case of the Sullivan and Petraitis study [203] the transfer layer would be encouraged to develop due to this low friction and wear. In the case of a steel on steel system, however, as long as there are not copious amounts of debris present any transferred metal formed on a surface would be removed in the same manner and at the same rate as the original surface. Hence such a layer will not survive and will be replaced by the eventual growth of a diffusion controlled oxide film if the rate of material removal is not greater than the rate of oxide production.

The transition from severe to mild wear through the running-in period may be described by a model similar to that developed in Section 4.3 in terms of changing relative proportions of metal-metal, metal-oxide and oxide-oxide contacts.

The removal of oxide plateaux once they attain critical thickness is probably due, in this system, to mechanical cyclic stressing leading to dislocation accummulation and delamination at the oxide metal interface. An asperity will be subject to alternate compressional and tensional stresses at each contact. The physical properties and mechanisms of formation of the three primary oxides of iron would suggest that Fe_3O_4 is the most

mechanically stable and this is supported by the evidence of this and other studies. The relative thermal expansion coefficients of oxides and metal make differential thermal expansion an unlikely process for removal even at the high transient temperatures experienced during sliding contact.

For the boundary lubricated system described in Chapter 3, it is shown that oxidational wear is the dominant equilibrium mode, although in this sytem the mechanisms are somewhat more complex due to initial preferential removal and transfer of aluminium from the bronze to the steel surface. Thus it appears that in the initial stages direct transfer of mainly metallic material occurs from one body to the other, but that when equilibrium conditions are established physically homogeneous diffusion controlled oxide growth occurs on the bronze surface and this oxide is the major protecting element in the boundary layer. This process must of course be cyclic on a local scale.

The initial transfer of metallic material must take place by direct asperity interaction and not by any debris compaction mechanism. The system would preclude this latter possibility. There are two reasons for this; the fluid will carry away debris from the contact area and hence prevent entrapment and surface active molecules in the fluid will reduce the surface energy and prevent particle adhesion. This latter effect has been demonstrated by Dickens, Sullivan and Lancaster[202] in experiments on the polymer PEEK. Thus under equilibrium conditions the oxide

grows on the bronze surface in a similar manner to that described for the unlubricated steel on steel system in Chapter 2. The function of the boundary additives in this system is to give the surface sufficient protection for the oxide film to grow and be maintained. Such oxide films have been reported in quite different systems. Wheeler[204] reported that for mild wear conditions in steel worn in oil containing dibenzyle disulphide, thick oxides were developed with no evidence of sulphide or mercaptide and Sullivan and Middleton[205] have similarly reported the development of thick oxide films on rolling/sliding steel systems under conditions of boundary lubrication in aqueous lubricants.

A further similarity between this boundary lubricated system and the unlubricated system described in Chapter 2 is the temperature responsible for oxide growth. For low ambient temperatures in the dry steel on steel system it has been shown that oxide growth occurs at or near to the contact temperature. In this boundary lubricated system surface temperatures were governed by the temperature of the fluid and were about 22 to25^{0}C. This temperature could not possibly account for the thicknesses of oxide observed and hence growth must have occurred at contact temperatures which were measured to be up to 500^{0}C. The model developed for boundary lubrication also suggests that growth constants under tribological conditions are not the same as statically measured values.

The mechanism of oxide removal is again probably primarily due to continued cyclic stressing, but in this case the Cu_2O and Cu surfaces have widely different thermal expansion coefficients and hence additional stresses would be introduced at the interface due to differential thermal expansion. The Cu_2O grows by cation diffusion hence new oxide is formed at the fluid/oxide boundary which means that internal stresses are low, but the process produces voids at the oxide/metal interface. The production of voids and the stresses due to differential thermal expansion eventually aid the laminar removal of the oxide film. The latter two effects will also serve to limit critical oxide thickness and indeed thicknesses estimated for the boundary lubricated aluminium bronze are substantially less than those observed in the steel on steel study.

The final system described in Chapter 4, exhibits quite a different mechanism of protective oxide film formation. In this reciprocating sliding study speeds are low, debris cannot easily escape from the contact area and temperatures are high, all of which are ingredients for the formation of agglomerate layers. Physical analysis of the surfaces shows that such agglomerate layers are indeed formed. The experimental results do not entirely resolve the question of how these agglomerate layers are formed, but there are strong indications of the important mechanisms. Kerridge[26] suggested that such layers were formed by metallic transfer with subsequent oxidation of the metallic

transfer layer to form a hard protective film. The results of the Auger depth profile examinations given in Chaper 4 could support this suggestion, since they indicate a gradation of oxide (oxygen) through the layer with concentrations varying from 100% oxide at the outer surface to about 30% oxide at the oxide/metal boundary. From the arguments advanced in Section 4.4, however, if this mechanism were operative it would be expected that the time taken to establish mild wear would depend on the rate of metallic debris production. This in turn is directly proportional to speed and hence the transition time t_T should fall with speed. In fact in the majority of the experiments t_T is independent of speed and is only reduced when, it is proposed, tribo-oxidation becomes important.

If it is assumed that oxide is produced by an oxidation-scrape-oxidation mechanism, the volume rate of production of oxide is independent of speed. Hence it appears that the rate of production of the oxide is the rate determining factor in the growth of plateaux even though the plateaux contain a considerable proportion of metallic debris. Further oxidation of the layers during and after formation will also undoubtedly occur.

One further point to consider is that if pure metallic transfer occurs there is no reason to assume that this layer is not removed in the same manner and at the same rate as the original surface and hence oxidation of such a layer is no more probably than oxidation of the original

surface. From the above argument, the agglomerate layer requires the incorporation of oxide in order that the relative proportion of contacts changes from mainly metal-metal, to mainly oxide-oxide. The model developed in Section 4.3 shows that it is such a change in the nature of the contact which is responsible for the transition from severe to mild wear.

The study also demonstrates the importance of out of contact oxidation. Oxide production is governed for the majority of conditions by out of contact oxidation at the ambient temperature. When surface temperatures fall below 290^{0}C,oxide production, under these starved oxygen conditions, is insufficient to promote oxidational wear even at the highest sliding speeds employed.

As with the previous systems laminar removal of plateaux was observed and hence the processes leading to this removal are probably similar; that is fatigue at the film/metal boundary due to repeated cyclic stressing. Since in this case the plateaux are not wholly oxide and are not produced by a diffusion controlled growth process the discontinuities at the metal boundary are not so abrupt. Hence it might be expected that these films would be thicker than physically homogeneous diffusion controlled films and this in general is what is observed. If differential thermal expansion does play some part in the generation of internal stresses, then the effect would be reduced by the gradation of oxide throughout the film. A further factor is

thermal conductivity where this quantity is greater in the case of the metal/metal oxide agglomerate layers than for oxide layers, hence temperature differences across plateaux are likely to be smaller.

Finally there should be some mention of the surface models and theoretical relationships developed throughout the study. It must be recognized that these necessarily contain simplified interpretations of the very complex processes occurring at the real surfaces during sliding contact. In each case, however, with the appropriate assumptions they provide remarkable agreement between theoretically derived and experimentally measured values of various parameters. This gives some confidence in the essential correctness of the models. The major value of the models, however, is not the quantitative expressions in themselves, but the insight and understanding of the real processes occurring at the sliding contact which the development and application of these expressions affords.

CHAPTER 6

CONCLUSIONS

The major conclusions of this work may be summarized as follows:

6.1. Unidirectional Sliding

(i) For the unidirectional sliding of steels above the Welsh T_2 transition load and under conditions where debris is not retained on the wearing surface, protective load bearing oxide films grow by a diffusion controlled mechanism similar to that responsible for the growth of thick oxide films under static conditions.

(ii) These films are physically homogeneous and transfer or back transfer is not involved in the formation process.

(iii) At low ambient temperatures (below 300^0C) the majority of film growth occurs at the real areas of contact at a temperature close to the "hot spot" or contact temperature.

(iv) For such low ambient temperature growth, the oxidational growth constants are very much higher than values measured statically at temperatures corresponding to estimated "hot spot" temperatures. This is due to greatly increased Arrhenius constants under tribological conditions.

(v) At temperatures above 300^0C, out of contact oxidational growth at the general surface temperature becomes rapidly dominant.

(vi) At these high ambient temperatures statically derived oxidational constants may be used to account for growth both in and out of contact.

(vii) Oxide films formed at low and high ambient temperatures grow to form load bearing plateaux of critical thickness, before becoming detached to form wear debris.

(viii) Of the three oxides of iron, Fe_3O_4 forms the thickest, most adherent plateaux with the greatest degree of surface coverage and the measured wear rates for Fe_3O_4 are lower than if $\alpha - Fe_2O_3$ or FeO had been present. The greater wear resistance of Fe_3O_4 is explained in terms of the kinetics of formation of the oxides and the subsequent physical properties.

(iv) For such low ambient temperature growth, the oxidational growth constants are very much higher than values measured statically at temperatures corresponding to estimated "hot spot" temperatures. This is due to greatly increased Arrhenius constants under tribological conditions.

(v) At temperatures above 300^0C, out of contact oxidational growth at the general surface temperature becomes rapidly dominant.

(vi) At these high ambient temperatures statically derived oxidational constants may be used to account for growth both in and out of contact.

(vii) Oxide films formed at low and high ambient temperatures grow to form load bearing plateaux of critical thickness, before becoming detached to form wear debris.

(viii) Of the three oxides of iron, Fe_3O_4 forms the thickest, most adherent plateaux with the greatest degree of surface coverage and the measured wear rates for Fe_3O_4 are lower than if α - Fe_2O_3 or FeO had been present. The greater wear resistance of Fe_3O_4 is explained in terms of the kinetics of formation of the oxides and the subsequent physical properties.

(ix) Removal of the oxide plateaux to form wear debris is probably due to a cyclic fatigue mechanism which leads to the accumulation of dislocations at the metal/oxide boundary with subsequent delamination of the oxide film. (This mechanism should not be confused with the Suh[103] delamination mechanism). Voids produced at the metal/oxide boundary during the formation of the oxide FeO assists this process as do the internal stresses produced in α - Fe_2O_3 due to oxide growth at the boundary with a Pilling Bedworth ratio[156] of 2.03. Differential thermal expansion is not an important factor in the removal of the oxides α - Fe_2O_3 or Fe_3O_4 and probably not in FeO, but stresses may be produced in this latter oxide at very high transient excess contact temperatures.

(x) The surface models developed and the theoretical expressions derived for contact temperatures and oxidational wear rates give good agreement between theoretically derived parameters and experimental measurements.

6.2. Boundary Lubricated Sliding

(i) The studies of the wear of aluminium bronze on steel in kerosene and kerosene with boundary additive conducted under conditions of boundary lubrication, show that oxidational wear is the dominant mechanism in the majority of conditions employed in this investigation.

(ii) The major protecting element in the boundary layer formed both with and without additive is a thick copper oxide (Cu_2O) film.

(iii) The initial mechanism of formation of load bearing oxide plateaux is complex and involves depletion of aluminium from the surface of the bronze and preferential transfer to the steel counterface leaving a copper rich bronze surface.

(iv) The initial transfer of aluminium rich material is due to direct asperity interaction and does not involve debris production and agglomeration.

(v) The copper oxide then grows on the bronze surface due to a diffusion controlled oxidational growth mechanism similar to that described for the unlubricated steel on steel systems of Chapter 2, producing plateaux of critical thickness.

(vi) Oxide growth occurs during hydrocarbon film breakdown at the real areas of contact and at temperatures close to the "hot spot" temperatures.

(vii) Parabolic oxidational growth constants govern this thick film formation.

(viii) The function of the boundary active additive is to afford sufficient protection to the surface to allow the growth and maintenance of the oxide plateaux and prevent metallic contact and seizure.

(ix) A consequence of the competing interaction between oxygen molecules from the fluid and the surface active hydrocarbon molecules with the surface is that a thinner or less extensive oxide film is formed in the presence of molecules with the greatest degree of surface activity. This results, in these experiments, in the dimeric acid additive producing slight pro-wear effects under mild conditions.

(x) The mechanism of production of wear debris by the removal of plateaux once they have attained critical thickness is probably similar to that suggested for the unidirectional steel on steel systems. Cyclic stressing produces a fatigue induced accumulation of dislocations at the oxide/metal boundary which leads to delamination of the oxide. Cu_2O grows due to

cation diffusion, hence voids will develop at the oxide/metal boundary and this will assist the delamination process. In addition to this there is a large difference between the thermal expansion coefficients of oxide and metal substrate. Hence thermally induced stresses due to high transient excess contact temperatures probably limit critical thickness and further assist in detachment of the oxide plateaux. These latter two effects combine to produce oxide critical thicknesses which are less than those observed in steel on steel systems.

(xi) A model to explain oxidational wear under boundary conditions has been proposed and from that model a relationship developed to give wear rate as a function of load. Contact temperatures derived from the relationship are in agreement with the range suggested by the limited experimental data obtained.

6.3. Reciprocating Sliding

(i) For the reciprocating sliding experiments conducted in CO_2 at elevated temperatures, it is found that when a transition from running-in severe wear to equilibrium mild wear occurs, the majority of the sliding surfaces are covered by stable, load bearing, mainly oxide plateaux of between 6 and 10μm thickness.

(ii) The plateaux consist of a sintered agglomerate of particles of wear debris, the composition of which varies from mainly metallic particles at the boundary between plateau and substrate to mainly oxide at the outer plateau surface. They are quite different to the physically homogeneous plateaux formed in the other two sliding systems considered in this study.

(iii) Subsurface examination shows that beneath the plateaux is a supportive work hardened layer extending to about 30μm into the bulk.

(iv) In the majority of conditions where a severe/mild wear transition is observed in the temperature range 290 to 450^{0}C, the time taken to reach the transition is independent of speed at any given temperature. This suggests that the majority of oxidation takes place out of contact at the general surface temperature.

(v) Tribo oxidation at the real area of contact does occur for temperatures of 290^{0}C and 300^{0}C at speeds greater than 120mms^{-1} and this results in a reduction of the transition time.

(vi) The oxide debris which agglomerates to partially form the plateaux is probably produced by an oxidation-scrape-oxidation mechanism and it is the rate of production of this oxide which is the rate determining factor in plateau growth, even though the plateaux contain a substantial proportion of metal fragments.

(vii) Static oxidation of the surface has a substantial beneficial effect once plateaux have been initiated by tribological action, but there is no effect due to pre-oxidation of an unworn surface.

(viii) At temperatures of $275^{0}C$ and below the rate of oxide production is always insufficient to initiate or sustain the growth of oxide plateaux and the system settles into an equilibrium severe wear mode, with no transition to mild wear.

(ix) Limited experimental evidence suggests that similar mechanisms are operative when this system is run in air, but that the time to the transition is very much shorter. This implies that it requires less oxygen to sustain oxidational wear then to initiate the condition.

(x) The evidence suggests that under equilibrium conditions wear debris originates from the removal of plateaux fragments once the plateaux have attained critical thickness. Again the most probable mechanism is delamination due to fatigue at the plateaux/metal interface caused by cyclic stressing.

(xi) The surface model developed to explain the processes of material removal and oxide growth leading to the establishment of mild wear gives good agreement between theoretically predicted values of volume removed and the experimentally determined values.

6.4. General Conclusions

(i) The type of protective load bearing oxide formed leading to mild wear conditions is very dependent on system geometry and system environment. If geometry or oxidized debris is not retained in the contact area, then oxidational growth, if it occurs, will be due to diffusion controlled thick oxide films. Debris retained on a surface would, due to its abrasive nature, discourage such growth and under these conditions agglomerate layer production is probably the preferred mechanism.

(ii) A major part of this work has been concerned with the development of surface models and quantitative theoretical expressions. In the models many simplifying assumptions are made, but there is still very good agreement between theoretical predictions and experimental values of the various parameters. The major value of the models, however, is not simply this agreement, but the elucidation of the mechanisms and processes occurring at the contacts which the application of the models affords.

6.5. Further work

Buckley[206] stated that oxygen is natures best lubricant, but even after many years of study oxidation under tribological conditions is not understood. In this study this author has attempted to add to the knowledge of oxidation in different tribological systems, but many questions remain unanswered. In order to provide some of these answers this author is initiating further study in four areas. These are:

(i) A study of oxidational wear below the Welsh T_1 transition under dry and lubricated conditions. This work will take place on the wear test rig described in Chapter 3 of this work consisting of a horizontal disc and vertical pin. The combination

of specimen configuration and very slow speeds used could results in the formation of agglomerate layers.

(ii) A study of the factors affecting the transition to mild oxidational wear of steels at low ambient temperatures in air. This study is concerned with the region around and above the Welsh T_2 transition and will be conducted on the wear test rig, described in Chapter 2. The work is similar in some ways to that described in Chapter 4 of this work, in that the history of the development of protective oxidational plateaux will be studied. The fact that test specimens are unheated and open to the atmosphere will make this task very much easier, however.

(iii) A study of the wear of steels in different partial pressures of oxygen and in other atmospheres. This work is concerned with a region above the T_2 transition and is intended to provide further information on oxidation processes and oxidation kinetics at reduced oxygen pressures under sliding conditions.

(iv) A further study of boundary lubrication and oxidational wear. This work will examine and extend some of the ideas developed in Chapter 3 of this work, but with a much simpler system. The base test

fluid will be a highly refined white spirit with negligible amounts of polar impurities. A number of boundary active components will then be added from the simple fatty acids to the more complex e.p. additives.

In all these studies extensive use of physical methods of analysis will be employed and it is envisaged that more attention will be paid to sub-surface changes than has been the practice in previous studies.

REFERENCES

1. ARCHARD, J.F. and HIRST, W., "The wear of metals under unlubricated conditions", Proc.Roy.Soc., A236 (1956) 397 - 410.

2. SULLIVAN, J.L. and CHOUDHURY, T., "The wear of steels at low partial oxygen pressures" to be published.

3. BURWELL, J.T. and STRANG, C.D., "On the empirical law of adhesive wear," J.Appl.Phy., 23 (1952) 18 - 28.

4. BURWELL, J.T., "Survey of possible wear mechanisms" Wear 1 (1957) 119 - 141.

5. KRAGELSKII, I.V., "Friction and Wear", Butterworths, (1965), Washington D.C.

6. BOWEN, E.R. and WESTCOTT, V.C., "Wear Particle Atlas" Final Report on Contract N-156-74-C-1982, Naval Air Engineering (1976) Lakehurst, N.J.

7. TABOR, D., "Wear - a crytical synoptic view," Proc.Int.Con. on Wear of Materials, St.Louis (1977) 1 - 11.

8. PATTERSON, M.B., "Source Book of Wear Control" Ed.by RIGNEY, D.A., and GLAESER, W.C., ASME (1978) Ohio.

9. FINK, M., "Wear oxidation - a new component of wear", Am.Soc. for Steel Treating, 18 (1930) 1026 - 1034.

10. ROSENBERG, S.J. and JORDAN, L., "The influence of oxide films on the wear of steels," Trans.Am.Soc.Metals, 23 (1935) 577 - 598.

11. THUM, A. and WUNDERLICH, W., "Frictional oxidation at metal-metal joints and its importance in fatigue," Z.Metallkunde, 27 (1935) 277 - 289.

12. MAILANDER, R. and DIES, K., "Contribution to the study of wear phenomena," Archiv. fur Eisenhuttenw., 16 (1943) 385 - 398.

13. DIES, K., "Processes taking place during wear in conditions of pure sliding," Archiv fur Eisenhuttenw., 16 (1943) 399 - 407.

14. SIEBEL, E. and KOBITZSCH, R., "Verschleisscheinungen bei Gleitender Trocker Reibung," VKI Verlag (1941) Berlin.

15. WHITEHEAD, J.R., "Surface deformation and fracture of metals at light loads," Proc.Roy.Soc., A201 (1950) 109 - 124.

16. WILSON, R.W., "Influence of oxide films on metallic friction," Proc.Roy.Soc., A212 (1952) 450 - 452.

17. WILSON, R.W., "The contact resistance and mechanical properties of surface films on metals," Proc.Phy.Soc., B68 (1955) 625 - 641.

18. COCKS, M., "The effect of compressive and shearing forces on the surface films present in metallic contacts," Proc.Roy.Soc. B67 (1954) 238 - 248.

19. COCKS, M., "The role of atmospheric oxidation in high speed sliding phenomena - I" J.Appl.Phy., 28 (1957) 835 - 843.

20. COCKS, M., "The role of atmospheric oxidation in high speed sliding phenomena - II," Trans.ASLE, 1 (1958) 101 - 107.

21. ARCHARD, J.F., "Contact and rubbing of flat surfaces," J.Appl.Phy., 24 (1953) 981 - 988.

22. HOLM, R., "Electrical Contacts Handbook," Springer-Verlag (1958) Berlin.

23. BOWDEN, F.P. and TABOR, D., "The Friction and Lubrication of Solids," Clarendon Press (1954) Oxford.

24. HIRST, W. and LANCASTER, J.K., "Surface film formation and metallic wear," J.Appl.Phy., 27 (1956) 1057 - 1065.

25. MOORE, A.J.W. and TEGART, W.J.M., "The effect of induced oxide films on the structure of the Beilby layer," Proc.Roy.Soc., A212 (1952) 458 - 459.

26. KERRIDGE, M., "Metal transfer and the wear process," Proc.Phy.Soc.(London), B68 (1955) 400 - 407.

27. ARCHARD, J.F. and HIRST, W., "An examination of a mild wear process," Proc.Roy.Soc., A238 (1957) 515 - 528.

28. RABINOWICZ, E. and TABOR, D., "Metallic transfer between sliding metals," Proc.Roy.Soc., A208 (1951) 455 - 474.

29. RABINOWICZ, E., "A quantitative study of the wear process," Proc.Phy.Soc.(London), B66 (1953) 929 - 936.

30. GREEN, A.P., "Friction between unlubricated metals: a theoretical analysis of the junction model," Proc.Roy.Soc., A228 (1955) 191 - 204.

31. GREENWOOD, J.A. and TABOR, D., "Deformation properties of friction junctions," Proc.Phy.Soc.(London), B68 (1955) 609 - 619.

32. KERRIDGE, M., and LANCASTER, J.K., "The stages in a process of severe metallic wear," Proc.Roy.Soc., A236 (1956) 250 - 264.

33. LANCASTER, J.K., "The influence of temperature on metallic wear," Proc.Phy.Soc.(London), B70 (1957) 112 - 118.

34. LANCASTER, J.K., "The formation of surface films and the transition between mild and severe wear," Proc.Roy.Soc., A273 (1963) 466 - 483.

35. HIRST, W. and LANCASTER, J.K., "The influence of speed on metallic wear," Proc.Roy.Soc., A259 (1960) 228 - 241.

36. WELSH, N.C., "Frictional heating and its influence on the wear of steels." J.Appl.Phy., 28 (1975) 960 - 968.

37 WELSH, N.C., "The dry wear of steels. Part I - the general pattern of behaviour," Phil.Trans.Roy.Soc., 257A (1964) 31 - 50.

38. WELSH, N.C., "The dry wear of steels. Part II - interpretation and special features," Phil.Trans.Roy.Soc. 257A (1964) 51 - 70.

39. ARCHARD, J.F. and ROWNTREE, R.A., "Metallurgical phase transformations in the dry wear of steels," Proc. 6th Leeds-Lyon Symposium on Tribology (1979) 168 - 174.

40 DEARNALEY, G., "The alteration of oxidation and related properties of metals by ion implantation," Nucl.Inst. and Methods, 182-183 (1981) 899 - 914.

41 BLAU, P.J., "Interpretations of the friction and wear break-in behaviour of metals in sliding contact," Wear, 71 (1981) 29 - 43.

42. EYRE, T.S., "Wear characteristics of metals," Tribology International, 9 (1976) 203 - 212.

43. FARRELL, R.M., and EYRE, T.S., "The relationship between load and sliding distance in the initiation of mild wear in steels," Wear, 15 (1970) 359 - 372.

44. EYRE, T.S. and MAYNARD, D., "Surface aspects of unlubricated metal to metal wear," Wear, 18 (1971) 301 - 310.

45. EYRE, T.S. and BAXTER, A., "The formation of white layers at rubbing surfaces," Metals and Materials, 6 (1972) 435 - 439.

46. TRENT, E.M., "The formation and properties of martensite on the surface of rope wire," J.Iron Steel Inst., 143 (1941) 401 - 412.

47. ARCHARD, J.F., "The temperature of rubbing surfaces." Wear, 2 (1959) 438 - 448.

48. QUINN, T.F.J., "The role of oxidation in the mild wear of steel." B.J.Appl.Phy., 13 (1962) 33 - 37.

49. ATHWAL, S.S., Ph.D.Thesis, The University of Aston (1983) Birmingham.

50 BISSON, E.F., JOHNSON, R.L. and SWIKERT, M.A., "Friction, wear and surface damage: a review of NASA research." Proc.I.Mech.E. Conf. on Lubrication and Wear, London (1958) 384 - 391.

51. PIGGOTT, M.R. and WILAMN, H., "Nature of wear and friction of mild steel on mild steel and effect of surface oxide and sulphide layers," Proc. I.Mech.E. Conf. on Lubrication and Wear, London (1958) 613 - 619.

52. GODFREY, D., "Fretting corrosion of steels," National Advisory Committee for Aeronautics Technical Note 2039 (1950) Washington D.C.

53. WRIGHT, K.H.R., "An investigation of fretting corrosion" Proc. I.Mech.Eng. 1B (1953) 556 - 563.

54. HALLIDAY, J.S. and HIRST, W., "The fretting corrosion of mild steel," Proc.Roy.Soc., A236 (1956) 411 - 425.

55. CLARK, W.T., PRITCHARD, C. and MIDGLEY, J.W., "Mild wear of unlubricated hard steels in air and carbon dioxide," Proc.I.Mech.E., 182 (1967) 97 - 105.

56. RAZAVIZADEH, K. and EYRE, T.S., "Oxidative wear of aluminium alloys," Wear, 87 (1983) 261 - 271.

57 SEXTON, M.D., "A study of wear in Cu-Fe systems," Wear, 94 (1984) 275 - 294.

58. ARCHARD, J.F., "A review of wear studies," Proc. NASA Symposium on Interdisciplinary Approach to Friction and Wear (1967) 267 - 334.

59. SULLIVAN, J.L., QUINN, T.F.J. and ROWSON, D.M., "Developments in the oxidational theory of mild wear," Tribology International, 13 (1980) 153 - 158.

60. TAO, F.F., "A study of oxidational phenomena in corrosive wear," ASLE TRANS., 12 (1969) 97 - 105.

61. MOLGAARD, J. and SRIVASTAVA, V.K., "The activation energy of oxidational wear," Wear, 41 (1977) 263 - 270.

62. MOLGAARD, J. and SRIVASTAVA, V.K., "Apparatus for the study of oxidative wear of unlubricated surfaces," Wear, 33 (1975) 179 - 188.

63. SULLIVAN, J.L. and ATHWAL, S.S., "Mild wear of low alloy steel at temperatures up to 500^0C," Tribology International, 16 (1983) 123 - 131.

64. SULLIVAN, J.L. and GRANVILLE, N.W., "Reciprocating sliding wear of steel in carbon dioxide at elevated temperatures," Triboloty International, 17 (1984) 63 - 71.

65. STOTT, F.H., GLASCOTT, J. and WOOD, G.C., "Models for the generation of oxides during sliding wear," Proc.Roy.Soc., A402 (1985) 167 - 186.

66. BOWDEN, F.P. and RIDLER, K.E.W., "The surface temperature of sliding metals," Proc.Roy.Soc., A154 (1936) 640 - 656.

67. FUREY, M.J., "Surface temperatures in sliding contact," ASLE Trans., 7 (1964) 133 - 156.

68. GLASCOTT, J., STOTT, F.H. and WOOD, G.C., "Thermoelectric voltage measurements and the determination of surface flash temperatures during sliding contact," Phil.Mag., A52 (1958) 811 - 832.

69. SULLIVAN, J.L. and POOLE, W., "The role of surface temperature in the wear of aluminium bronze on steel," Proc. Leeds-Lyon Symposium on Thermal Effects in Tribology, (1980) 316 - 321.

70. MEINDERS, M.A., WILCOCK, D.F. and WINER, W.O., "Infra red temperature measurements of a reciprocating seal test," Proc. Leeds-Lyon Symposium, (1982) 321 - 328.

71. QUINN, T.F.J. and WINER, W.O., "Thermal aspects of oxidational wear," Wear, 102 (1985) 67 -80.

72. EARLES, S.W.E. and POWELL, D.G., "Stability of self generated oxide films on unlubricated EN1A steel surfaces," Proc.I.Mech.E., 182 (1968) 167 - 179.

73. EARLES,S.W.E., HAYLER, M.G. and POWELL, D.G., "A comparison of surface temperature theories and experimental results for high speed dry sliding," Trans ASLE, 14 (1971) 135 - 143.

74. POWELL, D.G. and EARLES, S.W.E., "An assessment of surface temperature predictions in the high speed sliding of unlubricated SAE 1113 steel surfaces," Trans.ASLE, 15 (1972) 103 - 112.

75. ROWSON, D.M. and QUINN, T.F.J., "Frictional heating and the oxidational wear theory," J.Phy.D., 13 (1980) 209 - 219.

76. BLOK, H., "A Theoretical study of temperature rise at surfaces of actual contact under oiliness lubricating conditions," Proc.,I.Mech.E., 2 (1937) 222 - 243.

77. JAEGER, J.C., "Moving sources of heat and the temperature at sliding contacts," Proc.Roy.Soc (NSW) 56 (1942) 203 - 224.

78. GROSBERG, P. and MOLGAARD, J., "Aspects of the wear of spinning travellers: the division of heat at the rubbing surface," Proc.I.Mech.E., 181 (1966) 16 - 24.

79. QUINN, T.F.J., "The division of heat and surface temperatures at sliding steel surfaces and their relation to oxidational wear," Trans.ASLE, 21 (1978) 78 - 86.

80. QUINN, T.F.J., ROWSON, D.M. and SULLIVAN, J.L., "Application of the oxidational theory of mild wear to the sliding wear of low alloy steel," Wear, 65 (1980) 1 - 20.

81. QUINN, T.F.J., SULLIVAN, J.L. and ROWSON, D.M., "New developments in the oxidational wear theory," Proc.Int.Con. on Wear of Materials (1979) 1 - 11.

82. QUINN, T.F.J., SULLIVAN, J.L. and ROWSON, D.M., "Application of the oxidational theory of the mild wear of metals," Proc. 4th International Tribology Conference, Paisley, (1979) 163 - 183.

83. YOSHIMOTO, G. and TSUKIZOE, T., "On the mechanism of wear between metal surfaces," Wear, 1 (1957) 472 - 490.

84. QUINN, T.F.J., "The effect of hot-spot temperatures on the unlubricated wear of steel," Trans.ASLE, 10 (1967) 158 - 168.

85. QUINN, T.F.J., SULLIVAN, J.L. and ROWSON, D.M., "Origins and developments of oxidational wear at low ambient temperatures," Wear, 94 (1984) 175 - 192.

86. ALLEN, C.B., SULLIVAN, J.L. and QUINN, T.F.J., "The wear of valve-valve seat materials at elevated temperatures," Proc.Leeds Lyon Tribology Symposium (1982) 279 - 286.

87. ALLEN, C.B., QUINN, T.F.J. and SULLIVAN, J.L., "The oxidational wear of high chromium ferritic steel on austenitic stainless steel," Trans.ASME J.of Trib., 107 (1985) 172 - 212.

88. ARONOV, V., "Kinetic characteristics of the transformation and failure of the surface layers of metal under dry friction," Wear, 41 (1977) 205 - 212.

89. STOTT, F.H. and WOOD, G.C., "The influence of oxides on the friction and wear of alloys, "Tribology International, 11 (1978) 211 - 218.

90. STOTT, F.H., LIN, D.S. and WOOD, G.C., "The structure and mechanism of formation of the glaze oxide produced on nickel based alloys during wear at high temperatures," Cor.Sci., 13 (1973) 449 - 469.

91. WILSON, J.E., STOTT, F.H. and WOOD, G.C., "The development of wear protective oxides and their influence on sliding friction," Proc.Roy.Soc. A369 (1980) 557 - 574.

92. SASADA, T., NOROSE, S. and MISHINA, H., "The behaviour of adhered fragments interposed between sliding surfaces and the formation process of wear particles," Trans. ASME J.Lub.Tech., 103 (1981) 195 - 202.

93. STOTT, F.H., GLASCOTT, J. and WOOD, G.C., "Factors affecting the progressive development of wear protective oxides on iron based alloys during sliding at elevated temperatures," Wear, 97 (1984) 93 - 106.

94. RABINOWICZ, E., DUNN, L.A. and RUSSELL, P.G., "A study of abrasive wear under three body conditions," Wear, 4 (1961) 345 - 355.

95. SKINNER, J.,"Friction and wear transitions of an austenitic stainless steel in high temperature carbon dioxide," C.E.G.B. Report RD/B/5220/81 (1981).

96. SMITH, A.F., "The friction and sliding wear of unlubricated 316 stainless steel at room temperature in air," Wear, 96 (1984) 301 - 318.

97. WATERHOUSE, R.B. and WHARTON, M.H., "Titanium and tribology," Ind.Lub.Trib., 26 (1974) 20 - 23.

98. KOSTETSKII, B.I. and FILIPCHUCK, I.K., "Surface wear due to oxidizing in rolling friction conditions," Rus.Eng.J., 42 (1962) 23 - 25.

99. TOTH, L., "The investigation of the steady stage of steel fretting," Wear, 20 (1972) 277 - 286.

100. TENWICK, N. and EARLES, S.W.E., "A simplified theory of oxidative wear, "Wear, 18 (1971) 381 - 391.

101. ARCHARD, J.F., "Single contacts and multiple encounters," J.Appl.Phy., 32 (1961) 1420 - 1425.

102. CAPLAN, D. and COHEN, M., "The effect of cold work on the oxidation of iron from 100 to 650^{0}C," Corr.Sci., 6 (1966) 321 - 335.

103 SUH, N.P., "The delamination theory of wear," Wear, 25 (1973) 111 - 124.

104. SUH, N.P., "An overview of the delamination theory of wear," Wear, 44 (1977) 1 - 16.

105. ENGEL, P.A., "Impact Wear of Materials," Elsevier (1978) Amsterdam.

106. JAHANMIR, S., SUH, N.P. and ABRAHAMSON, E.P., "Microscopic observations of the wear sheet formation by delamination wear," Wear, 28 (1974) 235 - 249.

107 CHILDS, T.H.C., "The sliding wear mechanisms of metals, mainly steels," Tribology International, 13 (1980) 285 293.

108. PAMIES-TEIXEIRA, J.J., SAKA, N. and SUH, N.P., "Wear of copper based solid solutions," Wear, 44 (1977) 65 - 75.

109. SAKA, N., PAMIES-TEIXEIRA, J.J. and SUH, N.P., "Wear of two phase metals," Wear, 44 (1977) 77 - 86.

110. SAKA, N. and SUH, N.P., "Delamination wear of dispersion hardened alloys," Trans.ASME J. Eng. Ind., 99 (1977) 289 - 294.

111. SAKA, N., ELEICHE, A.M. and SUH, N.P., "Wear of metals at high sliding speeds," Wear, 44 (1977) 109 - 125.

112. HIRTH, J.P. and RIGNEY, D.A., "Crystal plasticity and the delamination theory of wear," Wear, 39 (1976) 133 - 141.

113. RIGNEY, D.A. and GLAESER, W.A., "The significance of near surface microstructure in the wear process", Wear,. 46 (1978) 241 - 250.

114. HSU, K.L., AHN, T.M. and RIGNEY, D.A., "Friction wear and microstructure of unlubricated austenitic stainless steel," Wear, 60 (1980) 13 - 37.

115. HABIG, K.J., KIRSCHKE, K., MAENNIG, W. and TISCHER, H., "Friction and wear properties of Fe, Co, Cu, Ag, Mg and Al in oxygen nitrogen mixtures at pressures between 760 and 2 x 10^{-7} torr", Wear, 22 (1972) 373 - 397.

116. PRUTTON, C.F., FREY, D.R., TURNBULL, D. and DLOUHY, G., "Corrosion of metals by organic acids in hydrocarbon solvents," Ind.Eng.Chem. 37 (1945) 90 - 100.

117. TINGLE, E.D., "Influence of water on the lubrication of metals." Nature, 160 (1947) 710 - 711.

118. BOWDEN, F.P. and YOUNG, J.E., "Friction of clean metals and the influence of adsorbed films," Proc.Roy.Soc., A208 (1951) 311 - 325.

119. BOWDEN, F.P., GREGORY, J.N. and TABOR, D., "Lubrication of metal surfaces by fatty acids," Nature, 156 (1945) 97 - 101.

120. HIRST, W. and LANCASTER, J.K., "The influence of oxide and lubricant films on the friction and surface damage of metals," Proc.Roy.Soc., A223 (1954) 324 - 338.

121. FENG, I.M. and CHALK, H., "Effects of gases and liquids in lubricating fluids on lubrication and surface damage," Wear, 4 (1961) 257 - 268.

122. TOYOGUCHI, M. and TAKAI, Y., "The extreme pressure lubricating properties of some sulphur compounds in mineral oils and the effects of dissolved oxygen," Bul.Japan Pet.Inst., 3 (1961) 63 - 70.

123. GODFREY, D., "Boundary lubrication," Proc.Int.Symposium on Lubrication and Wear, Houston (1963) 283 - 299.

124. GODFREY, D., "Boundary lubrication," Interdisciplinary Approach to Friction and Wear, NASA SP-181, (1968) 335 - 384.

125. TOMARU, M., HIRONAKA, S. and SAKURAI, T., "Effects of oxygen on the load carrying action of some additives," Wear, 41 (1977) 117 - 140.

126. BJERK, R., "Oxygen - an extreme pressure agent," Trans.ASME, 16 (1973) 97 - 106.

127. BEGELINGER, A. and DEGEE, A.J.W., "On the mechanism of lubricant film failure in sliding concentrated steel contacts," Trans ASME J.Lub.Tech., 98 (1976) 575 - 579.

128. KLAUS, E.E. and BIEBER, H.E., "Effect of some physical and chemical properties of lubricants on boundary lubrication," Trans.ASLE, 7 (1964) 1 - 10.

129 FEIN, R.S. and KREUZ, K.L., "Chemistry of boundary lubrication of steel by hydrocarbons," Trans.ASLE, 8 (1965) 29 - 38.

130. NAKAYAMA, K. and OKAMOTO, J., "Effect of dissolved oxygen on friction and wear of copper under boundary lubrication," Trans.ASLE, 23 (1980) 53 - 60.

131. NEWLEY, R.A., SPIKES, H.A. and MACPHERSON, P.B., "Oxidative wear in lubricated contact," Trans.ASME J.Lub.Tech., 102 (1980) 539 - 544.

132. SULLIVAN, J.L. and WONG, L.F., "Wear of aluminium bronze on steel under conditions of boundary lubrication," Tribology International, 18 (1985) 275 - 281.

133. SULLIVAN, J.L. and WONG, L.F., "The influence of surface films on the protection of metal surfaces under boundary lubrication," Surface and Interface Analysis, 9 (1986) 493 - 499.

134. SULLIVAN, J.L., "Boundary lubrication and oxidational wear," J.Phy.D., 19 (1986). 1500 - 1510.

135. SULLIVAN, J.L., "A theoretical model for boundary lubricated wear," Z.Schmierungstechnick, (1986).

136. KOMVOPOULOS, K., SUH, N.P. and SAKA, N., "Wear of boundary lubricated metal surfaces," Wear, 107 (1986) 107 - 123.

137. LAWLES, K.R., "The oxidation of metals," Rep.on Prog.in Phy., 37 (1974) 231 - 316.

138. BERNARD, J., "The oxidation of metals and alloys," Metallurgical Reviews, 9 (1964) 473 - 482.

139. CABRERA, N. and MOTT, N.F., "Theory of the oxidation of metals," Rep.on Prog.in Phy., 12 (1948-49) 163 - 184.

140. HAUFFE, K., in "The Surface Chemistry of Metals and Semiconductors," Ed.by GATOS, H.C., John Wiley and Sons (1960) N.Y.

141. FROMHOLD, A.T. and COOK, E.L., Kinetics of oxide film growth on metal crystals : electron tunnelling and ionic diffusion," Phy.Rev., 158 (1967) 600 - 612.

142. FEHLNER, F.P. and MOTT, N.F., "Low temperature oxidation", Oxid. Metals, 2 (1970) 59 - 99.

143. LANDSBERG, P.T., "On the logarithmic rate law in chemisorption and oxidation," J.Chem.Phy., 23 (1955) 1079 - 1087.

144. RITCHIE, I.M. and HUNT, G.L., "The kinetics and pressure dependence of surface controlled metal oxidation reactions," Surf.Sci., 15 (1969) 524 - 534.

145. DAVIES, D.E., EVANS, U.R. and AGAR, N.J., "The oxidation of iron at 175 to 350^{0}C ," Proc.Roy.Soc., A225 (1954) 443 - 462.

146. KUBACHEWSKI, O. and HOPKINS, B.E., "Oxidation of Metals and Alloys," (2nd edition) Butterworths (1932) London.

147. ENGELL, H.J., HAUFFE, K. and ILSCHNER, B., "Kinetics of the oxidation of nickel at 400^{0}C", Z. Electrochem., 58 (1954) 478 - 491.

148. WAGNER, C., "Theoretical analysis of the diffusion processes determining the oxidation rate of alloys," J.Electrochem.Soc., 99 (1952) 369 - 380.

149. DUNN, J.S., "The high temperature oxidation of metals," Proc.Roy.Soc., A111 (1926) 203 - 209.

150. DARRAS, R., LECLERCQ, D. and BUNARD, C., "Oxidation of steel heated in carbon dioxide under pressure," Proc. of the 2nd Int.Con. on Peaceful Uses of Atomic Energy, U.N., 5 (1958) 261 - 265.

151. SULLIVAN, J.L., "The diffusion of compensating impurities in single crystal cadmium sulphide," J.Electrochem.Soc., 123 (1976) 1251 - 1254.

152. SULLIVAN, J.L., "An ultrasonic identification of diffusion mechanisms in cadmium sulphide," Trans.IEEE, SU-32 (1985) 71 - 75.

153. DIENES, G.J., "Frequency factor and activation energy for the volume diffusion of metals," J.Appl.Phy., 21 (1960) 1189 - 1192.

154. DIENES, G.J., "On the volume diffusion of metals," J.Appl.Phy., 22 (1951) 848 - 849.

155. BOLTACKS, B.I., "Diffusion in Semiconductors," Infosearch (1963) London.

156. PILLING, N.B. and BEDWORTH, R.E., "The oxidation of metals at high temperatures," J.Inst.Metals, 29 (1923) 529 - 538.

157. SHOTTKY, W., "Reaktionsstypen bei der oxydation von legierungen," Z.Electrochem., 632 (1959) 784 - 788.

158. OXX, G.D., "Which coating at high temperature," Prod.Eng., 29 (1958) 61 - 63.

159. MILLS, P. and SULLIVAN, J.L., "A study of the core level electrons in iron and its three oxides," J.Phy.D., 16 (1983) 723 - 732.

160. MOLGAARD, J., "A discussion of oxidation, oxide thickness and oxide transfer in wear," Wear, 40 (1976) 277 - 291.

161. GOOD, J.N. and GODFREY, D., "Changes found on run in scuffed surfaces of steel, chrome plate and cast iron," NASA Tech.Note 1432 (1947).

162. BISSON, E.F., JOHNSON, R.L. and SWIBERT, M.A., "Friction, wear and surface damage of metals as affected by solid films," NASA Tech.Note 3444 (1955).

163. CORNELIUS, D.F. and ROBERTS, W.H., "Friction and wear of metals in gases up to 600^0C ," Trans.ASLE, 4 (1961) 20 - 32.

164. TSUJI, E., "Research on the wear of carbon steel from 200^0C to 500^0C ," Trans.NRIM, 9 (1967) 301 - 308.

165. HURRICKS, P.L., "The fretting wear of mild steel from 200^0C to 500^0C ," Wear, 30 (1974) 189 - 212.

166. POOLE, W. and SULLIVAN, J.L., "The wear of aluminium bronze on steel in the presence of aviation fuel," Trans.ASLE, 22 (1979) 154 - 161.

167. POOLE, W. and SULLIVAN, J.L., "The effects of the addition of corrosion inhibitors on the wear of aluminium bronze on steel in kerozene," Proc. Eurotrib. 77 (1977) 189 - 196.

168. POOLE, W. and SULLIVAN, J.L., "The role of aluminium segregation in the wear of aluminium bronze on steel under conditions of boundary lubrication," Trans.ASLE, 23 (1980) 401 - 408.

169. TYLECOTE, R.F., "Review of published information on the oxidation and scaling of copper and copper base alloys," J.Inst.Met., 78 (1950) 259 - 300.

170. VALENSI, G., "Theoretical and experimental investigations on the simultaneous formation of several layers during oxidation," Proc.Int.Con. on Surface Reactions, Pittsburgh, (1948) 156 - 161.

171. CRUZAN, C.G. and MILEY, H.A., "Cuprous-cupric oxide films on copper," J.Appl.Phy., 11 (1940) 631 - 634.

172. PETRAITIS, S.J., Ph.D. Thesis, The University of Aston (1983) Birmingham.

173. DAVIS, L.E., MACDONALD, N.C., PALMBERG, P.W., RIACH, G.E. and WEBER,R.E., "Handbook of Auger Electron Spectroscopy, Perkin Elmer, (1976) Eden Prairie, MN.

174. CARTER, G. and COLLIGON, J.S., "Ion Bombardment of Surfaces," Heineman (1968) London.

175. QUINN, T.F.J., "An experimental study of the thermal aspects of sliding and their relation to the unlubricated wear of steels," Proc.I.Mech.E., 183 (1968) 131 - 142.

176. SMITHELLS, C.J., "Metals Reference Handbook - Volume 3," 4th Edition, Butterworths (1967) London.

177. MOLGAARD, J. and SMELTZER, W.W., "Thermal conductivity of magnetite and hematite," J.Appl.Phy., 42 (1971) 3644 - 3647.

178. QUINN, T.F.J., "The effect of out of contact oxidation on the oxidational wear of steels," Proc.3rd Trib.Congress, Warsaw (1980) 192 - 201.

179. SIEBERT, C.A., "Effect of carbon content on the rate of oxidation of steel in air at high temperature", Trans. Am. Soc.Met., 27 (1939) 752 - 757.

180. BIRKS, N. and MEIER, G.H., "Introduction to High Temperature Oxidation of Metals," Edward Arnold, (1983) London.

181. HANCOCK, P. and HURST, R.C., "The mechanical properties and breakdown of surface oxide films at elevated temperatures," Ad.in Corr.Science and Technology, Ed. by STAEHLE, R.W. and FONTANA, M.G., Plenum Press (1974) N.Y.

182. EVANS, U.R., "The Corrosion and Oxidation of Metals," Edward Arnold (1960) London.

183. RABINOWICZS, E., "Friction and Wear of Materials," John Wiley and Sons (1965) N.Y.

184. WONG, L.F., Ph.D.Thesis, The University of Aston (1982) Birmingham.

185. KINGSBURY, E.P., "Some aspects of thermal desorption of a boundary lubricant," J.Appl.Phy., 29 (1958) 888 - 891.

186. KINGSBURY, E.P., "The heat of adsorption of a boundary lubricant," Trans.ASLE, 3 (1960) 30 - 33.

187. FRENKEL, J.,"Theorie der adsorption und verwandter erscheinungen," Z.Physik, 26 (1924) 117 - 130.

188. ROWE, C.N., "Some aspects of the heat of adsorption in the function of a boundary lubricant," Trans.ASLE, 9 (1966) 100 - 111.

189. VERE, R.A., ASKWITH, T.C. and HARDY, P.J., "Second report of the findings of the M.O.D. fuels lubricity panel," M.O.D.(P.E.) AX/395/014 (1976).

190. DZHEVAGA, I.I. and LEBEDEV, Y.M., "Research into the fusion zones of welded joints between carbon steel and aluminium bronze," Aut.Svarka, 8 (1970) 11 - 15.

191. SURY, P. and OSWALD, H.R., "On the corrosion behaviour of individual phases present in aluminium bronzes," Corr.Sci., 12 (1972) 77 - 90.

192. SCHUSSLER, M. and NAPOLITAN, D.S., "Dealuminization of aluminium bronze," Corrosion, 12 (1955) 25 - 30.

193. SMIGELSKAS, A.D. and KIRKENDALL, E.O., "The mutual diffusion of copper and brass," Trans. AIME, 171 (1947) 130 - 141.

194. BEERBOWER, A., "A critical survey of mathematical models for boundary lubrication," Trans.ASLE, 14 (1971) 90 - 104.

195. LINDEMANN, F.A., "Calculation of molecular vibration frequencies," Z.Physik., 11 (1910) 609 - 614.

196. ALLEN, C.M. and DRAUGLIS, E., "Boundary layer lubrication : monolayer or multilayer," Wear, 14 (1969) 363 - 384.

197. DACRE, B., SAVORY, B. and WHEELER, P.A., "Adsorption of lubricity additives," Tech.Report AC/R/13, RMCS, Shrivingham (1977).

198. POOLE, W., Ph.D.Thesis, The University of Aston, (1979) Birmingham.

199. NEWELL, J.E., "Corrosion of 9% Cr steel in AGR boilers," Nucl.Eng.Int., 17 (1972) 637 - 639.

200. VAN WYLEN, G.J. and SONNTAG, R.E., "Fundamentals of Classical Thermodynamics," 2nd Edition, John Wiley and Sons (1976) N.Y.

201. YAHATA, N. and HAYAMA, F., "The relation between wear characteristics of mild steel and the worn surface layer," J.Jap.Inst.Met., 39 (1975) 1254 - 1260.

202. DICKENS, P.M., SULLIVAN, J.L. and LANCASTER, J.K., "Speed effects on the dry and lubricated wear of polymers," Wear, (1986).

203. SULLIVAN, J.L. and PETRAITIS, S.J., "The wear of martensitic stainless steel against tungsten carbide at temperatures up to $500^{0}C$," Wear, 75 (1982) 87 - 104.

204. WHEELER, D.R., "X-ray photoelectron spectroscopic study of the surface chemistry of dibenzyle disulphide on steel under mild and severe wear conditions," Wear, 47 (1978) 243 - 254.

205. SULLIVAN, J.L. and MIDDLETON, M.R., "The effect of water based fire resistant lubricants on the pitting of steel," Proc.Leeds-Lyon Symposium (1984) 164 - 170.

206. BUCKLEY, D.H., "Definition and effect of chemical properties of surfaces in friction, wear and lubrication," Fundamentals of Tribology, ed. by SUH, N.P. and SAKA, N., M.I.T. Press (1980) Cambridge, MA.

PUBLICATIONS

The author of this thesis has published 38 refereed papers in learned journals plus many more in conference proceedings.

18 of these papers deemed relevant to the work presented here are included with this thesis in support of the candidates submission for the degree of Ph.D.